

1. Report No. FHWA/TX-04/0-1405-7		2. Government Accession No.		3. Recipient's Catalog No.	
4. Title and Subtitle Long-Term Post-Tensioned Beam Exposure Test Specimens: Final Evaluation				5. Report Date August 2003	
				6. Performing Organization Code	
7. Author(s) R. M. Salas, A. L. Kotys, J. S. West, A. J. Schokker, J. E. Breen, and M. E. Kreger				8. Performing Organization Report No. Research Report 0-1405-7	
9. Performing Organization Name and Address  Center for Transportation Research The University of Texas at Austin 3208 Red River, Suite 200 Austin, TX 78705-2650				10. Work Unit No. (TRAIS)	
				11. Contract or Grant No. Research Study 0-1405	
12. Sponsoring Agency Name and Address  Texas Department of Transportation Research and Technology Implementation Office P.O. Box 5080 Austin, TX 78763-5080				13. Type of Report and Period Covered Research Report (9/93-8/03)	
				14. Sponsoring Agency Code	
15. Supplementary Notes  Project conducted in cooperation with the U.S. Department of Transportation, Federal Highway Administration, and the Texas Department of Transportation.					
16. Abstract  In the last few years, the effectiveness of cement grout in galvanized or polyethylene ducts, the most widely used corrosion protection system for multistrand bonded post-tensioned concrete tendons, has been under debate, due to significant tendon corrosion damage, several reported failures of individual tendons as well as a few collapses of non-typical structures. While experience in the USA has been generally good, some foreign experience has been less than satisfactory.  This report is part of a comprehensive research program started in 1993, which has the objectives to examine the use of post-tensioning in bridge substructures, identify durability concerns and existing technology, develop and carry out an experimental testing program, and conclude with durability design guidelines.  Three experimental programs were developed: A long term macrocell corrosion test series, to investigate corrosion protection for internal tendons in precast segmental construction; a long term beam corrosion test series, to examine the effects of post-tensioning on corrosion protection as affected by crack width; and, a long term column corrosion test series, to examine corrosion protection in vertical elements.  Preliminary design guidelines were developed previously in the overall study by the initial researchers, after an extensive literature review.  This report documents the final evaluation of the long-term post-tensioned beam exposure test specimens, after comprehensive autopsies of selected beams and updating the durability design guidelines based on the exposure testing and autopsy results.  After autopsies were performed, overall findings indicate negative durability effects due to the use of mixed reinforcement, galvanized steel ducts, and industry standard or heat-shrink galvanized duct splices. The width of cracks was shown to have a direct negative effect on specimen performance. Grout voids were found to be detrimental to the durability of both galvanized ducts and strand. On the other hand, very positive effects were found with the use of high performance concrete, high post-tensioning levels, and plastic ducts.					
17. Key Words  corrosion, grout, post-tensioned concrete tendons, post-tensioning ducts, mixed reinforcement, duct splicer, concrete cracking, high performance concrete			18. Distribution Statement  No restrictions. This document is available to the public through the National Technical Information Service, Springfield, Virginia 22161.		
19. Security Classif. (of report) Unclassified		20. Security Classif. (of this page) Unclassified		21. No. of pages 222	22. Price

# **LONG-TERM POST-TENSIONED BEAM EXPOSURE TEST SPECIMENS: FINAL EVALUATION**

by

*R. M. Salas, A. L. Kotys, J. S. West, A. J. Schokker,  
J. E. Breen, and M. E. Kreger*

**Research Report 1405-7**

*Research Project 0-1405*

*DURABILITY DESIGN OF POST-TENSIONED  
BRIDGE SUBSTRUCTURE ELEMENTS*

conducted for the

**Texas Department of Transportation**

in cooperation with the

**U.S. Department of Transportation**

**Federal Highway Administration**

by the

**CENTER FOR TRANSPORTATION RESEARCH**

**BUREAU OF ENGINEERING RESEARCH**

**THE UNIVERSITY OF TEXAS AT AUSTIN**

August 2003

**Research performed in cooperation with the Texas Department of Transportation and the U.S. Department of Transportation, Federal Highway Administration.**

## **ACKNOWLEDGMENTS**

We greatly appreciate the financial support from the Texas Department of Transportation that made this project possible. We are grateful for the active support of the project director, Bryan Hodges (TYL), and the support of program coordinator, David Hoffman (BRG), and project advisor, Ronnie VanPelt (BMT), is also very much appreciated. We thank Project Monitoring Committee members, Jim Craig (FHWA), Susan Lane (FHWA), and Bob Stanford (FHWA).

## **DISCLAIMER**

The contents of this report reflect the views of the authors, who are responsible for the facts and the accuracy of the data presented herein. The contents do not necessarily reflect the view of the Federal Highway Administration or the Texas Department of Transportation. This report does not constitute a standard, specification, or regulation.

**NOT INTENDED FOR CONSTRUCTION,  
PERMIT, OR BIDDING PURPOSES**

J.E. Breen, P.E., TX #18479

M.E. Kreger, P.E., TX #65541

*Research Supervisors*

The United States Government and the State of Texas do not endorse products or manufacturers. Trade or manufacturer's names appear herein solely because they are considered essential to the object of this report.

# TABLE OF CONTENTS

<b>CHAPTER 1: INTRODUCTION.....</b>	<b>1</b>
1.1 PROBLEM STATEMENT .....	1
1.2 PROJECT OBJECTIVES, SCOPE, AND REPORTS .....	1
1.2.1 <i>Project Objectives</i> .....	1
1.2.2 <i>Project Scope</i> .....	2
1.2.3 <i>Project Reports</i> .....	4
<b>CHAPTER 2: EXPERIMENTAL PROGRAM .....</b>	<b>7</b>
2.1 TEST SPECIMEN .....	7
2.1.1 <i>Specimen Description</i> .....	7
2.1.2 <i>Specimen Design</i> .....	8
2.2 VARIABLES.....	12
2.2.1 <i>Control Variables</i> .....	12
2.2.2 <i>Phase I Variables</i> .....	12
2.2.3 <i>Phase II Variables</i> .....	14
2.3 SPECIMEN TYPES .....	16
2.4 MATERIALS .....	16
2.5 EXPERIMENTAL SET-UP.....	18
2.6 SPECIMEN FABRICATION.....	21
2.7 SPECIMEN LOADING.....	22
2.8 BLOCK SPECIMENS .....	22
2.9 BEAM DRIPPER SYSTEM .....	23
<b>CHAPTER 3: MEASUREMENTS DURING EXPOSURE TESTING .....</b>	<b>25</b>
3.1 VISUAL INSPECTION.....	25
3.2 CRACK WIDTH MEASUREMENTS.....	25
3.3 HALF-CELL READINGS.....	25
3.4 CORROSION RATE READINGS .....	27
3.5 CHLORIDE PENETRATION MEASUREMENTS .....	30
3.6 LIMITED AUTOPSY .....	32
<b>CHAPTER 4: EXPOSURE TEST RESULTS.....</b>	<b>33</b>
4.1 CRACK WIDTH MEASUREMENTS.....	33
4.1.1 <i>Crack Widths during Initial Loading</i> .....	33
4.1.2 <i>Crack Widths at the End of Testing for Autopsy Beams</i> .....	36
4.2 HALF-CELL POTENTIAL READINGS.....	38
4.2.1 <i>Phase I Beam Specimens</i> .....	39
4.2.2 <i>Phase II Beam Specimens</i> .....	45
4.3 CORROSION RATE MEASUREMENTS .....	49
4.3.1 <i>Phase I Beam Measurements</i> .....	50
4.3.2 <i>Phase II Beam Measurements</i> .....	52
4.4 CHLORIDE CONTENT ANALYSIS.....	53
4.4.1 <i>Phase I Concrete Block Specimens</i> .....	54

4.4.2	<i>Phase II Concrete Block Specimens</i> .....	55
4.4.3	<i>Phase I Autopsy Beam Specimens</i> .....	57
4.4.4	<i>Phase II Autopsy Beam Specimens</i> .....	61
<b>CHAPTER 5: FORENSIC EXAMINATION .....</b>		<b>65</b>
5.1	<b>AUTOPSY PROCEDURE</b> .....	65
5.1.1	<i>Specimen Selection for Forensic Examination</i> .....	65
5.1.2	<i>Specimen Condition at End of Testing</i> .....	67
5.1.3	<i>Crack Measurements</i> .....	67
5.1.4	<i>Concrete Powder Samples for Chloride Analysis</i> .....	67
5.1.5	<i>Saw Cuts and Concrete Removal</i> .....	67
5.1.6	<i>Exposure and Removal of Ducts</i> .....	69
5.1.7	<i>Splice Condition Examination</i> .....	70
5.1.8	<i>Duct Opening and Grout Condition Examination</i> .....	70
5.1.9	<i>Grout Samples for Chloride Analysis</i> .....	70
5.1.10	<i>Grout Removal and Strand Exposure</i> .....	70
5.1.11	<i>Mild Steel Exposure and Removal</i> .....	70
5.2	<b>EVALUATION AND CORROSION RATING SYSTEM USED DURING FORENSIC EXAMINATION</b> .....	70
5.2.1	<i>Mild Steel Reinforcement</i> .....	71
5.2.2	<i>Galvanized Steel Duct/Duct Splice</i> .....	73
5.2.3	<i>Prestressing Strand</i> .....	74
5.2.4	<i>Duct Splices</i> .....	75
5.2.5	<i>Grout</i> .....	75
5.3	<b>FORENSIC EXAMINATION RESULTS FOR PHASE I BEAMS</b> .....	75
5.3.1	<i>Beam Specimen 1.1 - Non-PS, Unloaded</i> .....	75
5.3.2	<i>Beam specimen 1.3 - Non-PS, Constant Service Load</i> .....	76
5.3.3	<i>Beam Specimen 2.3 – 2/3 PS, Service Load</i> .....	78
5.3.4	<i>Beam Specimen 2.11 – 2/3 PS, Service Load, Fly Ash Grout</i> .....	82
5.3.5	<i>Beam Specimen 3.1 – 100%U PS, Unloaded</i> .....	84
5.3.6	<i>Beam Specimen 3.2 – 100%U PS, Service Load</i> .....	87
5.3.7	<i>Beam Specimen 3.3 – 100%U PS, Overload</i> .....	90
5.3.8	<i>Beam Specimen 4.2 – 100%S PS, Service Load</i> .....	93
5.4	<b>FORENSIC EXAMINATION RESULTS FOR PHASE II BEAMS</b> .....	97
5.4.1	<i>Beam Specimen 1.5 – Non-PS, Fly Ash Concrete</i> .....	97
5.4.2	<i>Beam Specimen 1.6 – Non-PS, High Performance Concrete</i> .....	98
5.4.3	<i>Beam Specimen 2.5 – 2/3 PS, Fly Ash Concrete</i> .....	100
5.4.4	<i>Beam Specimen 2.6 – 2/3 PS, High Performance Concrete</i> .....	103
5.4.5	<i>Beam Specimen 3.6 – 100%U PS, Fly Ash Concrete</i> .....	106
5.4.6	<i>Beam Specimen 3.7 – 100%U PS, High Performance Concrete</i> .....	109
5.5	<b>CORROSION RATING SUMMARY</b> .....	112
5.5.1	<i>Stirrup Corrosion Ratings</i> .....	113
5.5.2	<i>Rebar Corrosion Ratings</i> .....	114
5.5.3	<i>Galvanized Steel Duct Ratings</i> .....	115
5.5.4	<i>Prestressing Strand Ratings</i> .....	117
<b>CHAPTER 6: ANALYSIS AND DISCUSSION OF RESULTS.....</b>		<b>119</b>
6.1	<b>OVERALL PERFORMANCE</b> .....	119

6.2	EFFECT OF CRACKING .....	123
6.2.1	<i>Crack Density</i> .....	123
6.2.2	<i>Crack Width</i> .....	127
6.2.3	<i>Longitudinal Cracking</i> .....	131
6.2.4	<i>Loading Levels</i> .....	132
6.2.5	<i>Prestressing Levels</i> .....	132
6.3	EFFECT OF CONCRETE TYPE .....	132
6.4	EFFECT OF SPLICE TYPE .....	132
6.5	EFFECT OF SPLICE DAMAGE .....	133
6.6	EFFECT OF GROUT TYPE.....	133
6.7	SPECIAL AUTOPSY FINDINGS.....	133
6.8	EXPOSURE TESTING MEASUREMENTS VERSUS FORENSIC EXAMINATION RESULTS .....	134
6.8.1	<i>Half-Cell Potential Readings versus Forensic Examination Results</i> .....	134
6.8.2	<i>Corrosion Rate Measurements versus Forensic Examination Results</i> .....	140
6.8.3	<i>Chloride Penetration versus Forensic Examination Results</i> .....	145
6.9	FINAL FULL AUTOPSIES.....	151
<b>CHAPTER 7: SUMMARY AND CONCLUSIONS.....</b>		<b>153</b>
7.1	OVERALL PERFORMANCE .....	153
7.2	LOAD/PRESTRESS LEVEL VERSUS CORROSION: THE EFFECT OF CRACKING.....	154
7.3	FLY ASH IN CONCRETE .....	154
7.4	DUCT SPLICES FOR GALVANIZED STEEL DUCT .....	154
7.5	HIGH PERFORMANCE FLY ASH GROUTS .....	155
7.6	EXPOSURE TESTING RESULTS .....	155
<b>CHAPTER 8: RECOMMENDATIONS FOR FUTURE TESTING .....</b>		<b>157</b>
<b>CHAPTER 9: IMPLEMENTATION OF RESULTS.....</b>		<b>159</b>
<b>APPENDIX: SUPPLEMENTARY MATERIAL .....</b>		<b>161</b>
A.	DETAIL BEAM CONSTRUCTION DRAWINGS.....	161
B.	SURFACE CRACK PATTERNS AND WIDTHS PRIOR TO AUTOPSY .....	172
C.	HALF-CELL POTENTIALS (LINE GRAPHS) .....	179
D.	HALF-CELL POTENTIALS (CONTOUR MAPS).....	187
E.	HALF-CELL POTENTIALS (OUTLIERS).....	188
F.	CORROSION RATE READINGS.....	189
G.	BLOCK CHLORIDE PENETRATION GRAPHS.....	192
H.	BEAM CHLORIDE PENETRATION GRAPHS.....	195
<b>REFERENCES.....</b>		<b>203</b>



## LIST OF TABLES

Table 1.1	Proposed Project 0-1405 Reports.....	4
Table 1.2	Project 0-1405 Theses and Dissertations, The University of Texas at Austin.....	5
Table 2.1	Summary of Section Details <sup>12</sup> .....	11
Table 2.2	Control Variables (Adapted from Reference 2).....	13
Table 2.3	Planned Crack Widths, Prestress Amounts and Loading <sup>2</sup> .....	13
Table 2.4	Beam Specimen Types and Variables <sup>2</sup> .....	16
Table 2.5	Construction Material Details: Phase I Beam Specimens <sup>2</sup> .....	19
Table 3.1	Common Reference Electrode Potentials versus SHE18.....	26
Table 3.2	Interpretation of Half-Cell Potentials for Uncoated Reinforcing Steel, Based on ASTM C876-91 <sup>2</sup> .....	26
Table 3.3	PR Monitor Corrosion Severity Based on Current Density <sup>24</sup> .....	29
Table 4.1	Time to Initiation of Corrosion for Phase I Autopsy Beams.....	43
Table 4.2	Time to Initiation of Corrosion for Phase II Autopsy Beams.....	48
Table 4.3	Phase I Autopsy Beam Corrosion Current Density Measurements <sup>6</sup> .....	51
Table 4.4	Phase II Autopsy Beam Corrosion Current Density Measurements <sup>6</sup> .....	53
Table 4.5	Phase I Ponded Block Chloride Penetration Measurements <sup>6</sup> .....	54
Table 4.6	Phase II Ponded Block Chloride Penetration Measurements <sup>6</sup> .....	57
Table 4.7	Phase I Autopsy Beam Chloride Penetration Measurements <sup>6</sup> .....	60
Table 4.8	Phase II Autopsy Beam Chloride Penetration Measurements <sup>6</sup> .....	64
Table 5.1	Phase I Beams Selected for Forensic Examination <sup>7</sup> .....	66
Table 5.2	Phase II Beams Selected for Forensic Examination <sup>7</sup> .....	66
Table 5.3	Evaluation and Rating System for Corrosion Found on Mild Steel Bars <sup>28</sup> .....	72
Table 5.4	Evaluation and Rating System for Corrosion Found on Galvanized Steel Duct /Duct Splice <sup>28</sup> .....	73
Table 5.5	Evaluation and Rating System for Corrosion Found on Prestressing Strand <sup>28</sup> .....	74
Table 6.1	Summary of Forensic Examination Corrosion Rating Results <sup>6</sup> .....	122
Table 6.2	Summary of Exposure Test Results <sup>6</sup> .....	135
Table 6.3	Main Variables to be Analyzed During Final (Future) Autopsy of Beam Specimens.....	152





## LIST OF FIGURES

Figure 1.1	TxDOT Project 0-1405 Scope, Researchers and Technical Reports .....	3
Figure 2.1	Linear Rectangular Beam Specimens (on Top of Reaction Beams).....	8
Figure 2.2	Specimen Dimensions .....	8
Figure 2.3	100%S PS Section Tendon Profile and Allowable Limits <sup>3</sup> .....	9
Figure 2.4	Section Reinforcement Details <sup>2</sup> .....	10
Figure 2.5	Moment Curvature Behavior for All Sections with Class C Concrete <sup>2</sup> .....	11
Figure 2.6	Applied Moment- Estimated Crack Width Behavior for All Sections with Class C Concrete <sup>2</sup> .....	12
Figure 2.7	Duct Splices <sup>2</sup> .....	14
Figure 2.8	Locations of Intentional Damage to Epoxy-Coated Strand <sup>3</sup> .....	15
Figure 2.9	VSLAB+™ System <sup>3</sup> .....	15
Figure 2.10	Phase I Beam Specimens <sup>2</sup> .....	17
Figure 2.11	Phase II Beam Specimens <sup>3</sup> .....	18
Figure 2.12	Test Setup <sup>2</sup> .....	20
Figure 2.13	Beam Test Setup at North End of Ferguson Laboratory <sup>2</sup> .....	20
Figure 2.14	Reinforcing Cage, End Detail for PT Beam, and Formwork <sup>2,3</sup> .....	21
Figure 2.15	Staged Post-Tensioning Sequence <sup>2</sup> .....	22
Figure 2.16	Beam Loading System.....	22
Figure 2.17	Concrete Blocks for Beam Chloride Analysis <sup>2</sup> .....	23
Figure 2.18	Beam End Dripper System <sup>3</sup> .....	23
Figure 3.1	Crack Width Measurement Locations <sup>2</sup> .....	25
Figure 3.2	Grid for Half-Cell Potential Readings Non-Prestressed Beams and Half-Cell Reading Locations for other beams <sup>2</sup> .....	26
Figure 3.3	Polarization Resistance Apparatus (Schematic) <sup>2</sup> .....	28
Figure 3.4	3LP Equipment and Setup .....	30
Figure 3.5	Non-PS and 2/3 PS Beam Concrete Sample Locations (Adapted from Reference 6).....	31
Figure 3.6	100%U PS (and 100%S PS) Beam Concrete Sample Locations (Adapted from Reference 6).....	31
Figure 4.1	Phase I Beam Specimens Crack Patterns <sup>2</sup> .....	34
Figure 4.2	Calculated Cracking Behavior <sup>3</sup> .....	35
Figure 4.3	Measured Maximum Crack Widths <sup>3</sup> .....	35
Figure 4.4	Non-PS Section – Crack Patterns and Measurements .....	36
Figure 4.5	2/3 PS Section – Crack Patterns and Measurements .....	37
Figure 4.6	100%U PS Section – Crack Patterns and Measurements .....	37
Figure 4.7	Crack Widths – Phase I Beams <sup>6</sup> .....	38
Figure 4.8	Crack Widths – Phase II Beams <sup>6</sup> .....	38
Figure 4.9	Half-Cell Potential Readings for Phase I Autopsy Beams.....	40
Figure 4.10	Half-Cell Potential Readings for Non-PS Specimens in Phase I Autopsy Beams.....	40
Figure 4.11	Half-Cell Potential Readings for 2/3 PS Specimens in Phase I Autopsy Beams.....	41
Figure 4.12	Half-Cell Potential Readings for 100%U PS Specimens in Phase I Autopsy Beams.....	41
Figure 4.13	Half-Cell Potential Readings for Unloaded Specimens in Phase I Autopsy Beams.....	42
Figure 4.14	Half-Cell Potential Readings for Service Load Specimens in Phase I Autopsy Beams .....	42

Figure 4.15	Greatest Negative Half-Cell Potential Reading at 1594 Days (End of Testing) for Phase I Autopsy Beams.....	43
Figure 4.16	Half-Cell Potential Contour Maps at 1594 Days for All Phase I Beams.....	44
Figure 4.17	Half-Cell Potential Readings for Phase II Autopsy Beams.....	45
Figure 4.18	Half-Cell Potential Readings for Non-PS Specimens in Phase II Autopsy Beams.....	45
Figure 4.19	Half-Cell Potential Readings for 2/3 PS Specimens in Phase II Autopsy Beams.....	46
Figure 4.20	Half-Cell Potential Readings for 100%U PS Specimens in Phase II Autopsy Beams.....	46
Figure 4.21	Half-Cell Potential Readings for Fly Ash Concrete Specimens in Phase II Autopsy Beams.....	47
Figure 4.22	Half-Cell Potential Readings for High Performance Concrete Specimens in Phase II Autopsy Beams.....	47
Figure 4.23	Greatest Negative Half-Cell Potential Reading at 1235 Days (End of Testing) for Phase II Autopsy Beams.....	48
Figure 4.24	Half-Cell Potential Contour Maps at 1235 Days for All Phase II Beams.....	49
Figure 4.25	Maximum Corrosion Rate Readings Using PR Monitor for Phase I Autopsy Beams <sup>6</sup> .....	50
Figure 4.26	Maximum Corrosion Rate Readings Using 3LP for Phase I Autopsy Beams <sup>6</sup> .....	51
Figure 4.27	Comparison of Corrosion Rate Measurement Equipment <sup>6</sup> .....	52
Figure 4.28	Corrosion Rate Readings Using 3LP for Phase II Autopsy Beams <sup>6</sup> .....	53
Figure 4.29	Acid-Soluble Chloride Content for Phase I Poned Block Specimens <sup>6</sup> .....	55
Figure 4.30	Acid-Soluble Chloride Content for Phase II Poned Block Specimens <sup>6</sup> .....	56
Figure 4.31	Beam and Block Chloride Penetration at 1594 Days for Phase I – Poned Region on Beams <sup>6</sup> .....	58
Figure 4.32	Beam and Block Chloride Penetration at 1594 Days for Phase I – Unponed Region on Beams <sup>6</sup> .....	59
Figure 4.33	Acid-Soluble Chloride Content at Bar and Top-of-Duct Level for Phase I Beams <sup>6</sup> .....	60
Figure 4.34	Beam and Block Chloride Penetration at 1235 Days for Phase II – Poned Region on Beams <sup>4,5</sup> .....	62
Figure 4.35	Beam and Block Chloride Penetration at 1235 Days for Phase II – Unponed Region on Beams <sup>6</sup> .....	63
Figure 5.1	Selected Beams for Forensic Examination <sup>7</sup> .....	67
Figure 5.2	Beam Section Removed for Investigation <sup>6</sup> .....	68
Figure 5.3	Concrete Saw used in Autopsy <sup>6</sup> .....	68
Figure 5.4	Concrete Removal to Expose Duct and Mild Steel <sup>7</sup> .....	69
Figure 5.5	Partial Autopsied Beam <sup>7</sup> .....	69
Figure 5.6	Mild Steel Reinforcement Cage.....	70
Figure 5.7	Intervals for Corrosion Rating on Mild Steel.....	71
Figure 5.8	Intervals for Corrosion Ratings on Galvanized Steel Duct/Splice <sup>7</sup> .....	73
Figure 5.9	Specimen 1.1 - Condition Prior to Autopsy.....	75
Figure 5.10	Specimen 1.1 - Mild Steel Bar and Stirrup.....	76
Figure 5.11	Specimen 1.1 Crack Pattern and Specimen Corrosion Rating Graphs.....	77
Figure 5.12	Specimen 1.3 Condition Prior to Autopsy.....	77
Figure 5.13	Specimen 1.3 Mild Steel Bar and Stirrup.....	78
Figure 5.14	Specimen 1.3 Crack Pattern and Specimen Corrosion Rating Graphs.....	78
Figure 5.15	Specimen 2.3 – Condition Prior to Autopsy.....	79
Figure 5.16	Specimen 2.3 – Duct Splices.....	79

Figure 5.17	Specimen 2.3 – Reinforcing Elements.....	80
Figure 5.18	Specimen 2.3 – Crack Pattern and Specimen Corrosion Rating Graphs .....	81
Figure 5.19	Specimen 2.11 – Condition Prior to Autopsy .....	82
Figure 5.20	Specimen 2.11 – Duct Splices .....	83
Figure 5.21	Specimen 2.11 – Reinforcing Elements.....	83
Figure 5.22	Specimen 2.11 – Crack Pattern and Specimen Corrosion Rating Graphs .....	84
Figure 5.23	Specimen 3.1 – Condition Prior to Autopsy .....	85
Figure 5.24	Specimen 3.1 – Duct Splices .....	86
Figure 5.25	Specimen 3.1 – Reinforcing Elements.....	86
Figure 5.26	Specimen 3.1 – Crack Pattern and Specimen Corrosion Rating Graphs .....	87
Figure 5.27	Specimen 3.2 – Condition Prior to Autopsy .....	88
Figure 5.28	Specimen 3.2 – Grouted Duct.....	88
Figure 5.29	Specimen 3.2 – Duct Splices .....	89
Figure 5.30	Specimen 3.2 – Reinforcing Elements.....	89
Figure 5.31	Specimen 3.2 – Crack Pattern and Specimen Corrosion Rating Graphs .....	90
Figure 5.32	Specimen 3.3 – Condition Prior to Autopsy .....	91
Figure 5.33	Specimen 3.3 – North Duct Splice.....	92
Figure 5.34	Specimen 3.3 – Reinforcing Elements.....	92
Figure 5.35	Specimen 3.3 – Crack Pattern and Specimen Corrosion Rating Graphs .....	93
Figure 5.36	Specimen 4.2 – Condition Prior to Autopsy .....	94
Figure 5.37	Specimen 4.2 – Duct Splices .....	94
Figure 5.38	Specimen 4.2 – Reinforcing Elements.....	95
Figure 5.39	Specimen 4.2 – Crack Pattern and Specimen Corrosion Rating Graphs .....	96
Figure 5.40	Specimen 1.5 – Condition Prior to Autopsy .....	97
Figure 5.41	Specimen 1.5 – Mild Steel Bar and Stirrup .....	97
Figure 5.42	Specimen 1.5 – Crack Pattern and Specimen Corrosion Rating Graphs .....	98
Figure 5.43	Specimen 1.6 – Condition Prior to Autopsy .....	99
Figure 5.44	Specimen 1.6 – Mild Steel Bar and Stirrup .....	99
Figure 5.45	Specimen 1.6 – Crack Pattern and Specimen Corrosion Rating Graphs .....	100
Figure 5.46	Specimen 2.5 – Condition Prior to Autopsy .....	101
Figure 5.47	Specimen 2.5 – Duct Splices .....	101
Figure 5.48	Specimen 2.5 – Reinforcing Elements.....	102
Figure 5.49	Specimen 2.5 Crack Pattern and Specimen Corrosion Rating Graphs .....	103
Figure 5.50	Specimen 2.6 – Condition Prior to Autopsy .....	104
Figure 5.51	Specimen 2.6 – Duct Splices .....	105
Figure 5.52	Specimen 2.6 – Reinforcing Elements.....	105
Figure 5.53	Specimen 2.6 – Crack Pattern and Specimen Corrosion Rating Graphs .....	106
Figure 5.54	Specimen 3.6 – Condition Prior to Autopsy .....	107
Figure 5.55	Specimen 3.6 – Duct Splices .....	107
Figure 5.56	Specimen 3.6 – Reinforcing Elements.....	108
Figure 5.57	Specimen 3.6 – Crack Pattern and Specimen Corrosion Rating Graphs .....	109
Figure 5.58	Specimen 3.7 – Condition Prior to Autopsy .....	110
Figure 5.59	Specimen 3.7 – Duct Splices .....	111
Figure 5.60	Specimen 3.7 – Reinforcing Elements.....	111

Figure 5.61	Specimen 3.7 – Crack Pattern and Specimen Corrosion Rating Graphs .....	112
Figure 5.62	Generalized Stirrup Corrosion Ratings <sup>6,7</sup> .....	113
Figure 5.63	Localized Stirrup Corrosion Ratings <sup>6,7</sup> .....	114
Figure 5.64	Generalized Bar Corrosion Rating <sup>6,7</sup> .....	115
Figure 5.65	Localized Bar Corrosion Ratings <sup>6,7</sup> .....	115
Figure 5.66	Generalized Duct Corrosion Ratings <sup>6,7</sup> .....	116
Figure 5.67	Localized Duct Corrosion Ratings <sup>6,7</sup> .....	116
Figure 5.68	Generalized Strand Corrosion Ratings <sup>6,7</sup> .....	117
Figure 5.69	Localized Strand Corrosion Ratings <sup>6,7</sup> .....	118
Figure 6.1	Generalized Stirrup Corrosion Ratings for Phase I Autopsy Beams Ordered According to Performance .....	119
Figure 6.2	Generalized Stirrup Corrosion Ratings for Phase II Autopsy Beams Ordered According to Performance .....	120
Figure 6.3	Generalized Rebar Corrosion Ratings for Phase I Autopsy Beams Ordered According to Performance .....	120
Figure 6.4	Generalized Rebar Corrosion Ratings for Phase II Autopsy Beams Ordered According to Performance .....	121
Figure 6.5	Generalized Corrosion Ratings for Phase I Autopsy Beams Ordered According to Performance .....	121
Figure 6.6	Generalized Corrosion Ratings for Phase II Autopsy Beams Ordered According to Performance .....	122
Figure 6.7	Effect of Crack Density on Stirrup and Rebar Corrosion for Phase I Autopsy Beams <sup>7</sup> .....	124
Figure 6.8	Effect of Crack Density on Duct and Strand Corrosion for Phase I Autopsy Beams <sup>7</sup> .....	125
Figure 6.9	Effect of Crack Density on Stirrup and Rebar Corrosion for Phase II Autopsy Beams <sup>7</sup> .....	126
Figure 6.10	Effect of Crack Density on Duct and Strand Corrosion for Phase II Autopsy Beams <sup>7</sup> .....	127
Figure 6.11	Localized Stirrup and Rebar Corrosion Rating versus Maximum Crack Width for Phase I Autopsy Specimens <sup>7</sup> .....	128
Figure 6.12	Localized Duct and Strand Corrosion Rating versus Maximum Crack Width for Phase I Autopsy Specimens <sup>7</sup> .....	129
Figure 6.13	Localized Stirrup and Rebar Corrosion Rating versus Maximum Crack Width for Phase II Autopsy Specimens <sup>7</sup> .....	130
Figure 6.14	Localized Duct and Strand Corrosion Rating versus Maximum Crack Width for Phase II Autopsy Specimens <sup>7</sup> .....	131
Figure 6.15	Duct Splice Performance .....	132
Figure 6.16	Effect of Grout Cracking <sup>7</sup> .....	133
Figure 6.17	Bleed Water Void and Duct Corrosion <sup>7</sup> .....	134
Figure 6.18	Half-Cell Potential at 1594 Days (End of Testing) for Phase I Autopsy Beams .....	134
Figure 6.19	Time to Initiation of Corrosion for Phase I Autopsy Beams .....	134
Figure 6.20	Half-Cell Potential at 1594 days (end of testing)for Phase II Autopsy Beams.....	136
Figure 6.21	Time to Initiation of Corrosion for Phase II Autopsy Beams .....	136
Figure 6.22	Half-Cell Readings at the End of Testing versus Stirrup and Rebar Corrosion Ratings for Phase I Autopsy Specimens <sup>7</sup> .....	137
Figure 6.23	Half-Cell Readings at the End of Testing versus Duct and Strand Corrosion Ratings for Phase I Autopsy Specimens <sup>7</sup> .....	138
Figure 6.24	Half-Cell Readings at the End of Testing versus Stirrup and Rebar Corrosion Ratings for Phase II Autopsy Specimens <sup>7</sup> .....	139

Figure 6.25	Half-Cell Readings at the End of Testing versus Duct and Strand Corrosion Ratings for Phase II Autopsy Specimens <sup>7</sup> .....	140
Figure 6.26	Final Corrosion Rate Measurements Using 3LP Equipment for Phase I Autopsy Beams ..	141
Figure 6.27	Final Corrosion Rate Measurements Using 3LP Equipment for Phase II Autopsy Beams	141
Figure 6.28	Corrosion Rate Measurements (using 3LP equipment) after 47 Months of Exposure versus Stirrup and Rebar Corrosion Ratings for Phase I Autopsy Specimens <sup>7</sup> .....	142
Figure 6.29	Corrosion Rate Measurements (using 3LP equipment) after 47 Months of Exposure versus Duct and Strand Corrosion Ratings for Phase I Autopsy Specimens <sup>7</sup> .....	143
Figure 6.30	Corrosion Rate Measurements (using 3LP equipment) after 35 Months of Exposure versus Stirrup and Rebar Corrosion Ratings for Phase II Autopsy Specimens <sup>7</sup> .....	144
Figure 6.31	Corrosion Rate Measurements (using 3LP equipment) after 35 Months of Exposure versus Duct and Strand Corrosion Ratings for Phase II Autopsy Specimens <sup>7</sup> .....	145
Figure 6.32	Beam Chloride Content at Bar Level – 3 in. Offset for Phase I Autopsy Beams .....	146
Figure 6.33	Beam Chloride Content at Bar Level – 18 in. Offset for Phase I Autopsy Beams .....	146
Figure 6.34	Beam Chloride Content at Bar Level – 3 in. Offset for Phase II Autopsy Beams.....	147
Figure 6.35	Beam Chloride Content at Bar Level – 18 in. Offset for Phase II Autopsy Beams <sup>7</sup> .....	147
Figure 6.36	Acid-Soluble Chloride Content versus versus Stirrup and Rebar Corrosion Ratings for Phase I Autopsy Specimens <sup>7</sup> .....	148
Figure 6.37	Acid-Soluble Chloride Content versus versus Duct and Strand Corrosion Ratings for Phase I Autopsy Specimens <sup>7</sup> .....	149
Figure 6.38	Acid-Soluble Chloride Content versus Stirrup and Rebar Corrosion Ratings for Phase II Autopsy Specimens <sup>7</sup> .....	150
Figure 6.39	Acid-Soluble Chloride Content versus Duct and Strand Corrosion Ratings for Phase II Autopsy Specimens <sup>7</sup> .....	151



## SUMMARY

In the last few years, the effectiveness of cement grout in galvanized or polyethylene ducts, the most widely used corrosion protection system for multistrand bonded post-tensioned concrete tendons, has been under debate, due to significant tendon corrosion damage, several reported failures of individual tendons as well as a few collapses of non-typical structures. While experience in the USA has been generally good, some foreign experience has been less than satisfactory.

This report is part of a comprehensive research program started in 1993, which has the objectives to examine the use of post-tensioning in bridge substructures, identify durability concerns and existing technology, develop and carry out an experimental testing program, and conclude with durability design guidelines.

Three experimental programs were developed: A long-term macrocell corrosion test series, to investigate corrosion protection for internal tendons in precast segmental construction; a long term beam corrosion test series, to examine the effects of post-tensioning on corrosion protection as affected by crack width; and, a long term column corrosion test series, to examine corrosion protection in vertical elements.

Preliminary design guidelines were developed previously in the overall study by the initial researchers, after an extensive literature review.

This report documents the final evaluation of the long-term post-tensioned beam exposure test specimens, after comprehensive autopsies of selected beams and updating the durability design guidelines based on the exposure testing and autopsy results.

After autopsies were performed, overall findings indicate negative durability effects due to the use of mixed reinforcement, galvanized steel ducts, and industry standard or heat-shrink galvanized duct splices. The width of cracks was shown to have a direct negative effect on specimen performance. Grout voids were found to be detrimental to the durability of both galvanized ducts and strand. On the other hand, very positive effects were found with the use of high performance concrete, high post-tensioning levels, and plastic ducts.



# CHAPTER 1: INTRODUCTION

The use of post-tensioning in flexural members can provide many advantages. The improvement in crack control and the precompression applied to the concrete suggest that moisture and chloride penetration would be reduced, impacting positively on durability. However, when post-tensioning systems are used, new durability concerns arise, since new hardware is incorporated within the elements.

The durability concern increases when mixed reinforcement (i.e., a combination of non-prestressed and prestressed reinforcement as the main flexural tension element) is used. Mixed reinforcement has received much attention in the last few years, since fully prestressed members may not always lead to an optimum design, from a strength and economic perspective.<sup>1,2</sup> The limitation of concrete tensile stresses in fully prestressed members below cracking, can lead to large prestress requirements, resulting in very unconservative designs, excessive creep deflections and the requirement for stage prestressing as construction progresses. Mixed reinforcement may increase ductility in comparison to fully prestressed members, have less congestion than reinforced concrete elements, reduce creep and excessive camber, produce a more efficient design, and the reinforcement can be tailored to control deflections, cracking, and cracking moment.<sup>2</sup> Also, from recent research in Europe, it seems that a better fatigue resistance is also attained. However, all these benefits could be outweighed by the increased corrosion risk, since prestressed concrete members with mixed reinforcement are likely to crack under service load levels.

## 1.1 PROBLEM STATEMENT

This report presents a portion of the results of the Texas Department of Transportation Research Project 0-1405: “Durability Design of Post-Tensioned Bridge Substructure Elements.” The research is being performed at the Phil M. Ferguson Structural Engineering Laboratory and is sponsored by the Texas Department of Transportation and Federal Highway Administration. The title of Project 0-1405 involves two main aspects:

- Durability of Bridge Substructures, and
- Post-Tensioned Bridge Substructures.

The durability emphasis is in response to the deteriorating condition of bridge substructures in some areas of Texas. While considerable research and design effort has been given to bridge deck design to prevent corrosion damage, substructures had historically been more overlooked. Often superstructure drainage details result in substructures having a high exposure to aggressive agents such as deicing salts. Also, substructures are often in direct contact with salt water and damaging soils.

The second aspect of the research is post-tensioned substructures. Relatively few post-tensioned substructures have been used in the past. There are many possible applications in bridge substructures where post-tensioning can provide structural and economical benefits, and can possibly improve durability. Post-tensioning is now being used in Texas bridge substructures, and it is reasonable to expect the use of post-tensioning to increase in the future as precasting of substructure components becomes more prevalent and as foundation sizes increase. This is expected, even though some problems have been encountered in post-tensioned bridges throughout the world.

The problem that bridge engineers face is that there are few comprehensive durability design guidelines for post-tensioned concrete structures. Durability design guidelines should provide information on how to identify possible durability problems, how to improve durability using post-tensioning, and how to ensure that the post-tensioning system does not introduce new durability problems.

## 1.2 PROJECT OBJECTIVES, SCOPE, AND REPORTS

### 1.2.1 *Project Objectives*

The overall research objectives for TXDOT Project 0-1405 are as follows:

1. To examine the use of post-tensioning in bridge substructures,

2. To identify durability concerns for bridge substructures in Texas,
3. To identify existing technology to ensure durability or improve durability,
4. To develop experimental testing programs to evaluate protection measures for improving the durability of post-tensioned bridge substructures, and
5. To develop durability design guidelines and recommendations for post-tensioned bridge substructures.

A review of literature has indicated that while a few problems have been encountered in some bridges in Europe, Japan, and the U.S.A., damage has been limited to a very small percentage of post-tensioned bridges. In general, post-tensioning systems have been successfully used in bridge designs. However, as these bridges age and increase in cumulative exposure, more problems are being noted. New practices and materials are required to guarantee the safety and design life of these structures.

The initial literature review performed by West<sup>2</sup> identified a substantial amount of relevant information that could be applied to the durability of post-tensioned bridge substructures. This existing information allowed the scope of the experimental portion of the project to be narrowed. The final objective represents the culmination of the project. All of the research findings are to be compiled into the practical format of comprehensive durability design guidelines.

The research objectives for the portion of TxDOT Project 0-1405 reported in this document that relate to the large-scale beam corrosion test series, are as follows:

1. To determine the effect of post-tensioning on durability (corrosion protection) through crack control, and
2. To evaluate the relative performance of a broad scope of corrosion protection variables for multistrand posttensioning systems, including:
  - a. different levels of prestress and load, producing different crack widths and patterns
  - b. different post-tensioning hardware: duct types, duct splices, strand types and anchorage systems
  - c. different concrete and grout mixes
  - d. different grout injection procedures

### ***1.2.2 Project Scope***

The subject of durability is extremely broad, and as a result a broad scope of research was developed for TXDOT Project 0-1405. Based on the project proposal and an initial review of relevant literature, the project scope and necessary work plan were defined. The main components of TXDOT Project 0-1405 are:

1. Extensive Literature Review
2. Survey of Existing Bridge Substructures Inspection Reports (BRINSAP)
3. Long-Term Corrosion Tests with Large-Scale Post-Tensioned Beam and Column Elements
4. Investigation of Corrosion Protection (near joints) for Internal Prestressing Tendons in Precast Segmental Bridges
5. Development of Improved Grouts for Post-Tensioning
6. Development of recommendations and design guidelines for durable bonded post-tensioned bridge substructures

Components 1 and 2 (literature review and survey of Brinsap report) were performed initially by West<sup>2</sup>, Schokker<sup>3</sup>, Koester<sup>4</sup> and Larosche<sup>5</sup> and findings up to 1998 were published in references 2 and 3. The literature review process was continued by Kotys<sup>6</sup> and Salas<sup>7</sup> and is published in References 6 and 7.

Component 3 was divided into Large Scale Column Corrosion Tests and Large Scale Beam Corrosion Tests. The column tests were started by Larosche<sup>5</sup> and West.<sup>2</sup> Column exposure testing began in July 1996.

Full autopsies were performed by Salas<sup>7</sup> in 2003 and were reported in Reference 7. The beam tests were implemented in two phases: the first phase was implemented by West,<sup>2</sup> and exposure testing began in December 1997. The second phase was implemented by Schokker,<sup>3</sup> and exposure testing begun in December 1998. Comprehensive autopsies of around half of these specimens, at the end of their exposure testing period were performed in 2002 by Kotys<sup>6</sup> and Salas<sup>7</sup> and are reported herein.

Component 4 (corrosion protection at joints of segmental bridges) was developed and implemented by Vignos<sup>8</sup> under TxDOT Project 0-1264. This testing program was transferred to TxDOT Project 0-1405 in 1995 for long-term testing. Although this aspect of the research was developed under Project 0-1264 to address corrosion concerns for precast segmental bridge superstructures, the concepts and variables are equally applicable to precast segmental substructures, and the testing program fits well within the scope of Project 0-1405. Half of the macrocell laboratory specimens were autopsied at four and a half years of exposure testing by West.<sup>2</sup> Final autopsies of the remaining specimens were performed by Kotys<sup>6</sup> and Salas,<sup>7</sup> and findings were reported in References 7 and 29.

Component 5 (Development of Improved Grouts for Post-Tensioning) was developed and implemented by Schokker<sup>4</sup> based on previous work published by Hamilton<sup>9</sup> and Koester<sup>4</sup>. The accelerated corrosion testing was performed and conclusions were drawn and published.<sup>3,10</sup> Under this portion of the research, high-performance grouts for bonded post-tensioning were developed through a series of fresh property tests, accelerated corrosion tests, and large-scale field trials. These grouts have become widely used in practice.

Component 6 (Development of recommendations and design guidelines for durable bonded post-tensioned bridge substructures) refers to the most important implementation directed aspect of the research program. Interim design guidelines were developed and published by West and Schokker<sup>11</sup> based on research results up to 1999. Updated Guidelines based on final autopsy results from the macrocell, column and beam tests are reported by Salas in Reference 7 and will be reported in CTR Report 1045-9.

The project scope is outlined in Figure 1.1. This figure shows the cooperative effort performed by all graduate research assistants during the length of the project. In Figure 1.1 the years in brackets show the actual or expected publication dates for each Technical Report, published under TxDOT Project 0-1405.

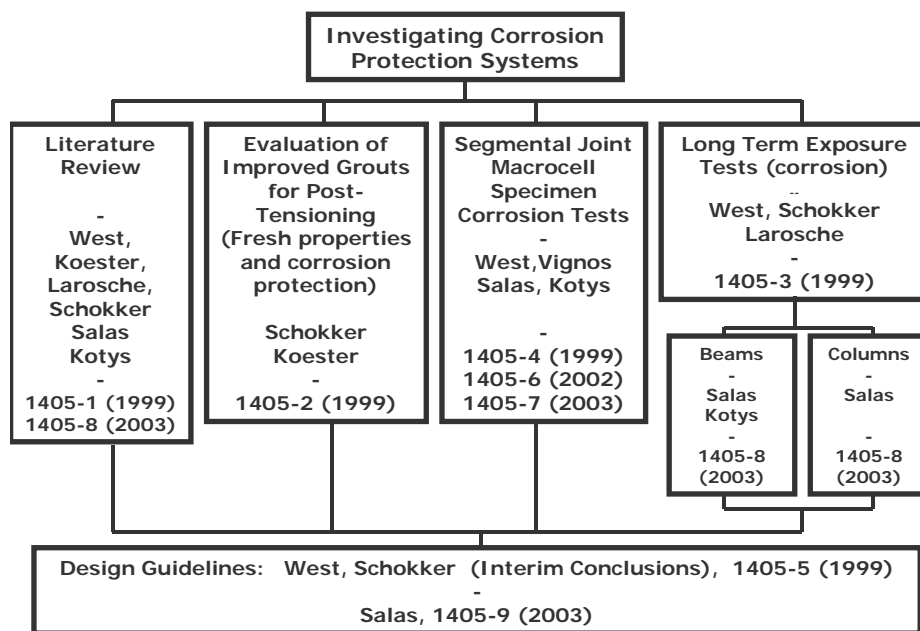


**Figure 1.1 TxDOT Project 0-1405 Scope, Researchers and Technical Reports**

### 1.2.3 Project Reports

Nine reports are schedule to be developed from Project 0-1405 as listed in Table 1.1. This report is the seventh in this series.

**Table 1.1 Proposed Project 0-1405 Reports**

<b>Number</b>	<b>Title</b>	<b>Estimated Completion</b>
1405-1	State of the Art Durability of Post-Tensioned Bridge Substructures	1999
1405-2	Development of High-Performance Grouts for Bonded Post-Tensioned Structures	1999
1405-3	Long-term Post-Tensioned Beam and Column Exposure Test Specimens: Experimental Program	1999
1405-4	Corrosion Protection for Bonded Internal Tendons in Precast Segmental Construction	1999
1405-5	Interim Conclusions, Recommendations and Design Guidelines for Durability of Post-Tensioned Bridge Substructures	1999
1405-6	Final Evaluation of Corrosion Protection for Bonded Internal Tendons in Precast Segmental Construction	2002
1405-7	Long-term Post-Tensioned Beam Exposure Test Specimens: Final Evaluation	2003
1405-8	Long-term Post-Tensioned Column Exposure Test Specimens: Final Evaluation	2003
1405-9	Conclusions, Recommendations and Design Guidelines for Durability of Post-Tensioned Bridge Substructures	2003
1405-S	Corrosion Protection of Post-Tensioned Bridge Elements	2003

Report 1405-1 provides a detailed background on the topic of durability design of post-tensioned bridge substructures. The report contains an extensive literature review on various aspects of the durability of post-tensioned bridge substructures and a detailed analysis of bridge substructure condition rating data in the State of Texas.

Report 1405-2 presents a detailed study of improved and high-performance grouts for bonded post-tensioned structures. Three testing phases were employed in the testing program: fresh property tests, accelerated corrosion tests and large-scale pumping tests. The testing process followed a progression of the three phases. A large number of variables were first investigated for fresh properties. Suitable mixtures then proceeded to accelerated corrosion tests. Finally, the most promising mixtures from the first two phases were tested in the large-scale pumping tests. The variables investigated included water-cement ratio, superplasticizer, antibleed admixture, expanding admixture, corrosion inhibitor, silica fume and fly ash. Two optimized grouts were recommended depending on the particular post-tensioning application.

Report 1405-3 describes the development of two long-term, large-scale exposure testing programs, one with beam elements, and one with columns. A detailed discussion of the design of the test specimens and selection of variables is presented. Preliminary experimental data is presented and analyzed, including cracking behavior, chloride penetration, half-cell potential measurements and corrosion rate measurements. Preliminary conclusions are presented.

Report 1405-4 describes a series of macrocell corrosion specimens developed to examine corrosion protection for internal prestressing tendons in precast segmental bridges. This report briefly describes the test specimens and variables, and presents and discusses four and a half years of exposure test data. One-half (nineteen of thirty-eight) of the macrocell specimens were subjected to a forensic examination after four

and a half years of testing. A detailed description of the autopsy process and findings is included. Conclusions based on the exposure testing and forensic examination are presented.

Report 1405-5 contains a summary of the conclusions and recommendations from the first four reports from Project 0-1405. The findings of the literature review and experimental work were used to develop preliminary durability design guidelines for post-tensioned bridge substructures. The durability design process is described, and guidance is provided for assessing the durability risk and for ensuring protection against freeze-thaw damage, sulfate attack and corrosion of steel reinforcement. These guidelines were refined and expanded as more experimental data became available and will be reported in Report 1405-9.

Report 1405-6 describes a series of macrocell corrosion specimens developed to examine corrosion protection for internal prestressing tendons in precast segmental bridges. This report briefly describes the test specimens and variables, and presents and discusses eight years of exposure test data. One-half (nineteen of thirty-eight) of the macrocell specimens were subjected to a forensic examination after four and a half years of testing, and were reported in Report 1405-4. A detailed description of the autopsy process for the remaining macrocell specimens and findings is included. Final conclusions and recommendations based on the exposure testing and forensic examination are presented.

Report 1405-7 (this document) describes a series of beam corrosion specimens developed to examine corrosion protection for bonded internal prestressing tendons in linear flexural bridge elements. This report briefly describes the test specimens and variables, and presents and discusses the results after approximately one-half of the beam specimens were autopsied after three and a half years and four and a half years of exposure testing. A detailed description of the autopsy process and findings is included. Final conclusions based on the exposure testing and forensic examination are presented. The report concludes with recommendations for materials and implementation measures.

Several dissertations and theses at The University of Texas at Austin were developed from the research from Project 0-1405. These documents may be valuable supplements to specific areas in the research and are listed in Table 1.2 for reference.

**Table 1.2 Project 0-1405 Theses and Dissertations, The University of Texas at Austin**

<b>Title</b>	<b>Author</b>	<b>Date</b>
<i>Master's Theses</i>		
Evaluation of Cement Grouts for Strand Protection Using Accelerated Corrosion Tests”	Bradley D. Koester	12/95
“Durability Examination of Bonded Tendons in Concrete Beams under Aggressive Corrosive Environment”	Andrea L. Kotys	5/03
“Test Method for Evaluating Corrosion Mechanisms in Standard Bridge Columns”	Carl J. Larosche	8/99
“Test Method for Evaluating the Corrosion Protection of Internal Tendons Across Segmental Bridge Joints”	Rene P. Vignos	5/94
<i>Ph.D. Dissertations</i>		
“Accelerated Corrosion Testing, Evaluation and Durability Design of Bonded Post-Tensioned Concrete Tendons”	Ruben M. Salas	8/03
“Improving Corrosion Resistance of Post-Tensioned Substructures Emphasizing High-Performance Grouts”	Andrea J. Schokker	5/99
“Durability Design of Post-Tensioned Bridge Substructures”	Jeffrey S. West	5/99



## CHAPTER 2: EXPERIMENTAL PROGRAM

Beam specimen exposure testing includes combination of structural loading with aggressive exposure, by means of cyclic wetting and drying with a 3.5% NaCl solution to promote accelerated corrosion. The effect of prestressing levels is investigated for a range of systems, from nonprestressed (reinforced concrete) to partially prestressed (mixed reinforcement) to fully prestressed. Variables in the research program include the influence of crack width, type of concrete (normal and high performance concrete), prestressing strand coatings, duct splices, high performance grout, and encapsulated post-tensioning systems.

Two phases were implemented as part of the experimental program. Phase I was developed to investigate the influence of prestressing levels, cracking, high performance grout and post-tensioning duct splices. This phase was designed and implemented by West.<sup>2</sup> Phase II was developed to investigate high performance concrete, high performance grout, prestressing strand coatings and an encapsulated post-tensioning system. This phase was implemented by Schokker.<sup>3</sup> Both researchers, West and Schokker, built series of beam specimens and initiated exposure testing in the early part of the experimental program. Both phases used the same overall beam specimen design and loading.

Chapter 2 and Chapter 3 include a summary of the work done by West and Schokker. For a detailed description of their experimental program and description of measurements during exposure testing, refer to References 3 and 4. TxDOT Report 1405-3<sup>12</sup> also contains a detailed summary of West's and Schokker's work.

Chapter 4 through Chapter 9 include all exposure testing results and final autopsy results, conclusions and recommendations for the selected specimens. Exposure testing was performed as a cooperative effort by West and Schokker in the first stages, and Kotys and Salas in the final stages of the specimens selected for full autopsy. Full autopsies were performed by Kotys and Salas. Approximately half of the specimens have been transferred to Project 0-4562 and remain under exposure for future autopsy.

### 2.1 TEST SPECIMEN

#### 2.1.1 Specimen Description

The specimens used in this experimental program are not patterned after a prototype structure. Linear rectangular flexural elements, as shown in Figure 2.1, were chosen for the following reasons:

- results can be applied to bent cap and beam elements directly and some results may be qualitatively applied to other elements such as pile caps.
- all desired variables can be readily incorporated into design
- ease of construction, handling and placement
- simplicity of controlling and maintaining loading

The beams subjected to combined structural loading are tested outside the Ferguson Structural Engineering Laboratory and are exposed to cyclic wetting and drying with a 3.5% NaCl solution to provide and highly aggressive corrosive environment.

Specimen dimensions and details were selected to provide concrete covers, reinforcement sizes, post-tensioning hardware and crack widths of a similar order of magnitude as in practical applications, with consideration for handling and loading of the specimens. Prestressed specimens used a minimum of two tendons (multistrand) to represent applications typical of post-tensioned bridges.

The Type E multistrand anchorage hardware manufactured by VSL Corporation was selected because it is available in tendon configurations with as few as three strands. The 18" x 24" concrete section, accommodating up to eight strands in two tendons, was chosen to provide the most flexibility in the design of mixed reinforced sections. For practical reasons, a nominal beam length of 15 feet was chosen. Specimen dimensions are shown in Figure 2.2.



Figure 2.1 Linear Rectangular Beam Specimens (on Top of Reaction Beams)<sup>7</sup>

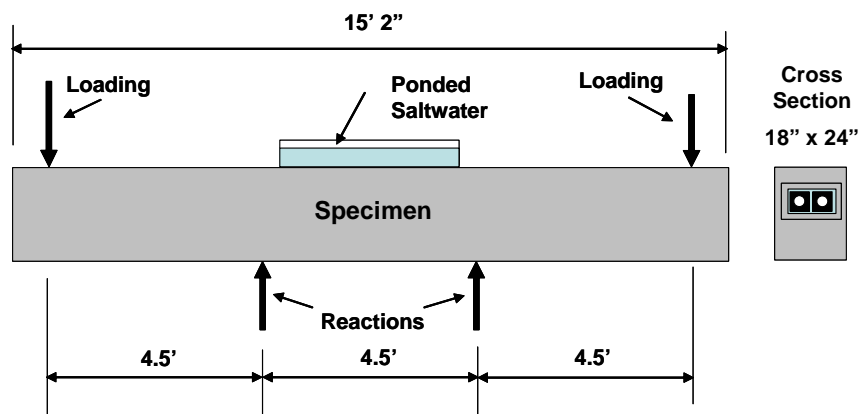


Figure 2.2 Specimen Dimensions<sup>7</sup>

## 2.1.2 Specimen Design

### 2.1.2.1 Levels of Prestress

To examine a broad range of prestressing, section reinforcement was proportioned for the following prestressing levels:

- non-prestressed (Non-PS)
- mixed reinforcement with nominal prestress amount between 50% and 75% of total tensile force (2/3 PS).
- 100% prestressed based on ultimate (nominal) strength (100 %U PS)
- 100% prestressed based on service load/allowable stress design (100% S PS)

The amount of prestress in percent, is defined as the tensile force component provided by prestressing steel at the nominal flexural capacity of the section. Only 100% S PS specimens would not be expected to crack under service loading. The selected specimen dimensions and requirement for two tendons dictated



the use of 8 strands for the 100%S PS section, 6 strands for the 100%U PS section, and 4 strands for the 2/3 PS (mixed reinforcement) section.

### 2.1.2.2 Design Loading

Reinforcement was proportioned based on the total allowable service load moment (dead load plus live load) computed for the 100%S PS section. Assuming a ratio of dead load to live load of 1.5, the calculated permissible total service load moment was used to compute the dead and live load moments. The factored moment was then computed and used to proportion the reinforcement for the non-prestressed sections as well as the mixed reinforcement and the 100%U PS post-tensioned sections.

The 100%S PS section was design to meet the stress limits according to Clause 5.9.4 of AASHTO LRFD<sup>13</sup>(Clause 18.4 of ACI 318<sup>14</sup>). The sections with eight post-tensioning strands in two tendons were analyzed with the following assumptions:

- Gross section properties, elastic stresses
- $f'_c = 5$  ksi
- $A_{ps} =$  eight 12.7 mm (0.5 in.) 7-wire prestressing strands,  $f_{pu} = 270$  ksi
- $f_{pi} = 0.65f_{pu}$
- Long term losses = 15% ( $f_{pe} = 0.55f_{pu}$ )
- Maximum tendon eccentricity,  $e = 8$  in. based on clear cover to duct of 2.5 in.
- Computation of the total allowable moment assumed that the governing stress in the concrete (tensile or compressive) is at least 75% of the corresponding allowable value. (i.e., either  $0.75f_{callow} \leq f_{cmax} \leq f_{callow}$  or  $0.75f_{tallow} \leq f_{tmax} \leq f_{tallow}$ )
- Self weight of the beam could be neglected (self weight is very small in comparison to applied forces)

The section was analyzed for stresses in the concrete immediately after prestress transfer and under maximum applied loading. Calculated stresses and moments are included in Reference 2. The service load moment, with  $f_t = 0.75f_{tallow}$  governing, was calculated as 2750 k-in. To meet stress limits at the member ends a draped profile was chosen for the tendons. Figure 2.3 shows the tendon profile and the allowable limits for the steel center of gravity (cgs).

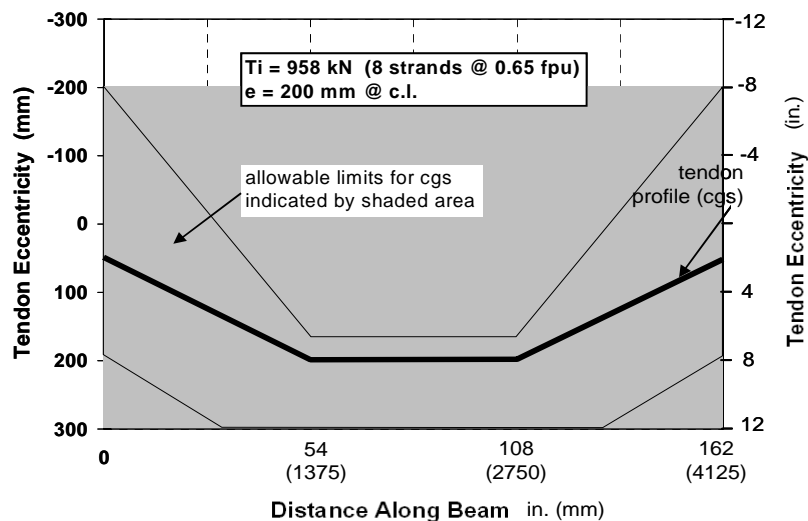


Figure 2.3 100%S PS Section Tendon Profile and Allowable Limits<sup>3</sup>

Based on the calculated service load moment, the dead and live load moments, factored moments and nominal moments were calculated as follows:

$$M_{\text{service}} = 2750 \text{ k-in. (based on 100\%S PS section)}$$

$$M_D/M_L = 1.5 \quad (\text{assumed})$$

Therefore,

$$M_D = 1650 \text{ k-in.}$$

$$M_L = 1100 \text{ k-in.}$$

$$M_{\text{factored}} = 4180 \text{ k-in.}$$

$$M_{\text{nominal}} = 4650 \text{ k-in. (for } \phi = 0.9)$$

### 2.1.2.3 Section Reinforcement

The required nominal flexural capacity,  $M_n$ , was used for the strength design of the remaining sections. The 100% U PS section required the use of six strands. Mixed reinforced sections (50% to 75% prestress) required the use of four strands, for an effective prestress level of 66.7% (2/3 PS). Reference 2 describes in detail the procedure followed to select the appropriate amounts of reinforcement, based on AASHTO LRFD (1998) and ACI 318-95. Figure 2.4 shows the final reinforcement details for each section. Detailed construction drawings, from Reference 2, have been included in Appendix A. Table 2.1 includes a summary of Section Details.

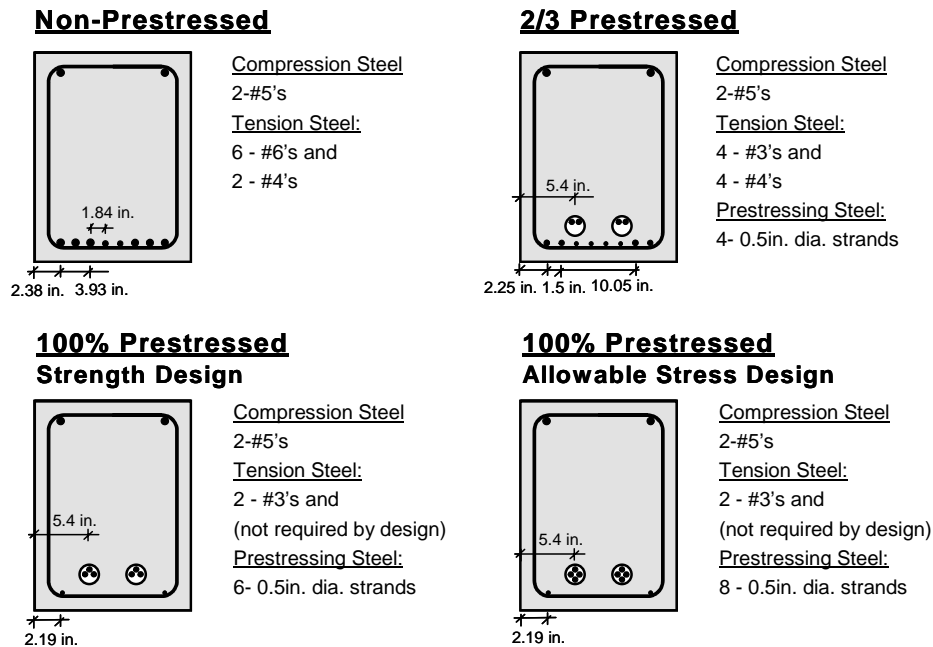


Figure 2.4 Section Reinforcement Details<sup>2</sup>

Shear reinforcement was proportioned for the shear force corresponding to the development of the nominal flexural capacity of the sections.

Anchorage zone design and reinforcement was provided following Breen et al. recommendations.<sup>15</sup> Spirals used in the anchorage zone were based on the guidelines provided by the hardware supplier. Details are included in Reference 2.

**Table 2.1 Summary of Section Details<sup>12</sup>**

Section	Prestressing Strands	Effective Prestress (after losses)	Mild Steel Bars (tension)	Nominal Capacity
Non-PS	None	n/a	6 #6 and 2 #4	4685 k
2/3 PS	4 – 0.5 in.	0.6 $f_{pu}$	4 #4 and 4 #3	4750 k
100%U PS	6 – 0.5 in.	0.6 $f_{pu}$	2 #3	4685 k
100%S PS	8 – 0.5 in.	0.55 $f_{pu}$	2 #3	5935 k

The post-tensioning system was draped with slope changes at third points. This profile was required to control stresses in the 100%S PS specimens and to ensure electrical contact among strands, since contact may influence corrosion behavior.

Type E anchorage system from VSL Corporation was used in all post-tensioned beams. 100%S PS Section used the Type E-4 with four strand capacity per tendon. 100%U PS and 2/3 PS used Type E-3 anchorage system with three strand capacity per tendon. Anchorage and grout tube details are shown in the Appendix A drawings.

#### 2.1.2.4 Analysis of Section Behavior

Each section was analyzed to determine its moment curvature behavior and applied moment versus crack width behavior. Surface crack widths were predicted using recommendations by Armstrong et al.<sup>1</sup> with the Gergely-Lutz expression. Details of these calculations are included in Reference 2. Figure 2.5 and Figure 2.6 show the computed moment-curvature and moment-crack width curves for the control Class C concrete. Full details on Section Behavior are included in Reference 2, including long-term behavior.

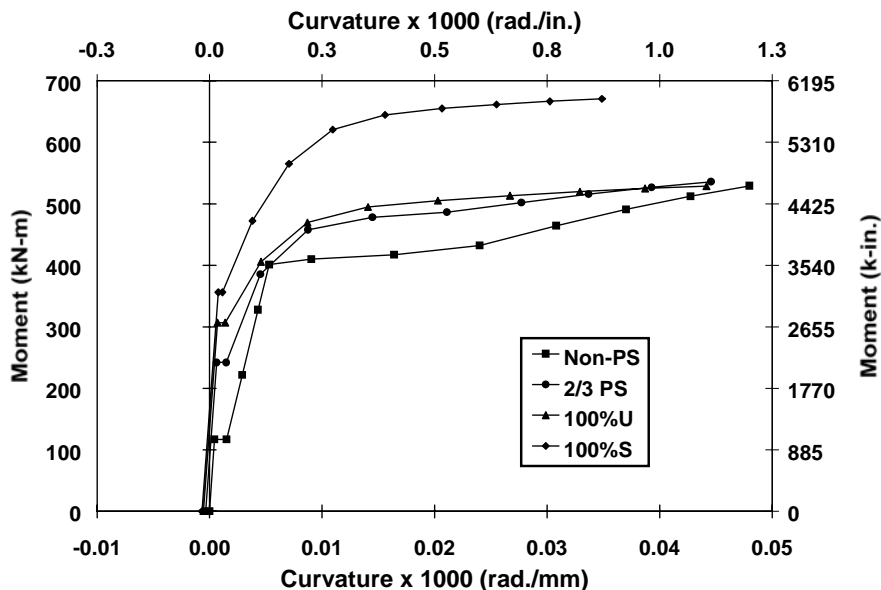


**Figure 2.5 Moment Curvature Behavior for All Sections with Class C Concrete<sup>2</sup>**

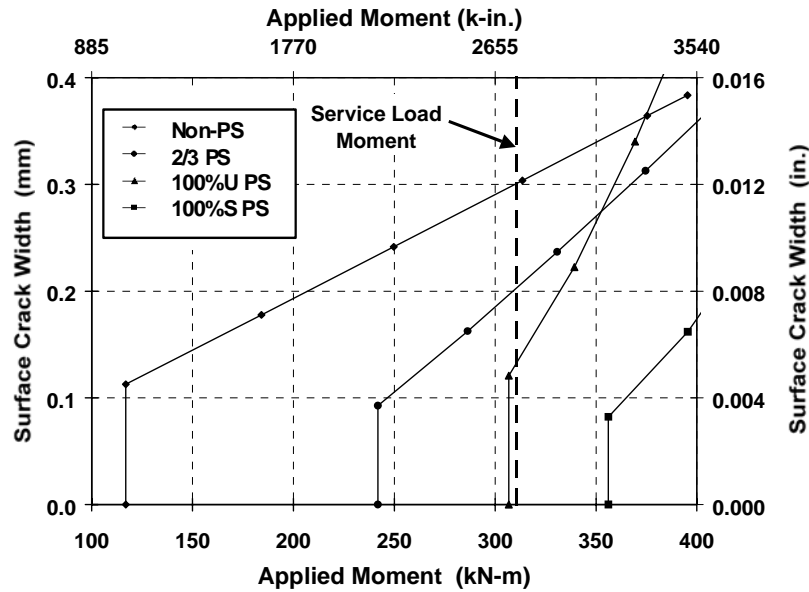


**Figure 2.6 Applied Moment- Estimated Crack Width Behavior for All Sections with Class C Concrete<sup>2</sup>**

A long-term prestress loss (creep, shrinkage, relaxation) of 4.7% was calculated for the 100%S PS section. Prestress force losses of 5% and 4.3% were calculated for the 100%U PS and 2/3 PS sections, respectively, after four years of sustained loading, since these sections were cracked prior to and during sustained loading.

## 2.2 VARIABLES

Beam Specimens were implemented in two phases, around a year apart. Phase I specimens included the following variables: level of prestress and crack width, one specimen with high performance grout, and the evaluation of duct splices. Phase II specimens include different concrete types, prestressing strand coatings and post-tensioning hardware protection, in addition to duct splice evaluation.

### 2.2.1 Control Variables

Typical TxDOT practice was considered to define the values of the variables for the control or reference specimens, as described in Table 2.2.

### 2.2.2 Phase I Variables

#### 2.2.2.1 Levels of Prestressing, Loading and Cracking

Cracking was investigated using the three sections that would be expected to crack under service loads (Non-PS, 2/3 PS and 100% U). Crack widths for investigation were selected based on a survey of relevant literature and the moment-crack width behavior computed for each section. Full description of crack width selection is presented in Reference 2. The selected crack widths and the corresponding loading and applicable sections are shown in Table 2.3. Some deviation would be expected from the planned crack widths due to the uncertain nature of cracking.

**Table 2.2 Control Variables (Adapted from Reference 2)**

<b>Variable</b>	<b>Description</b>
Concrete	Based on TxDOT Specification Item 421 TxDOT Class C concrete for bridge substructures Maximum w/c ratio = 0.533 (actual w/c will be closer to 0.45 based on slump requirements) Type I cement Slump = 4 in. Maximum coarse aggregate size = ¾ in. Retarder, Rheocrete 300 R Entrained air admixture 2 in. clear cover to main steel
Cement Grout	Based on TxDOT Specification Item 426.3.4a w/c ratio = 0.44 Type I cement Expanding admixture, Intraplast – N
PT Duct	Rigid galvanized steel duct
Anchorage Protection	Based on TxDOT guidelines Type V State epoxy bonding compound Nonshrink grout patch (Euclid NS grout)

**Table 2.3 Planned Crack Widths, Prestress Amounts and Loading<sup>2</sup>**

<b>Loading Case</b>	<b>Crack Widths</b>	<b>Applicable Sections</b>	<b>Loading</b>
1.) Constant Service Load	uncracked	100%S PS	service load
	0.1 mm (0.004 in.)	100%U PS	service load
	0.2 mm (0.008 in.)	2/3 PS	service load
	0.3 mm (0.012 in.)	Non-PS	service load
2.) Very Small Crack	0.05 mm (0.002 in.)	2/3 PS & 100%U PS	as needed and hold
3.) Unloaded	Uncracked	Non-PS & 100%U PS	None
4.) Overload & Return to Service	as measured	Non-PS, 2/3 PS & 100%U PS	up to 1.33 x service load, then return to service load

### 2.2.2.2 Duct Splices for Galvanized Steel Duct

Two duct splices were studied: standard industry splice (IS) and heat shrink splice (HS). The first consisted of a 1 ft length of oversized duct with the ends draped with duct tape. The second consisted of an 8 in. length of heat shrink tubing (original diameter of the tubing was 4 in.). Splice damages were also studied consisting of poor or incomplete duct taping on IS splices, and a 1 in. cut made in the HS tubing in the middle section. Figure 2.7 shows both duct splices used.

The following comparisons were studied:

- 1) Industry standard versus heat shrink
- 2) Industry standard versus unspliced
- 3) Effect of damage for industry standard and heat shrink splices.

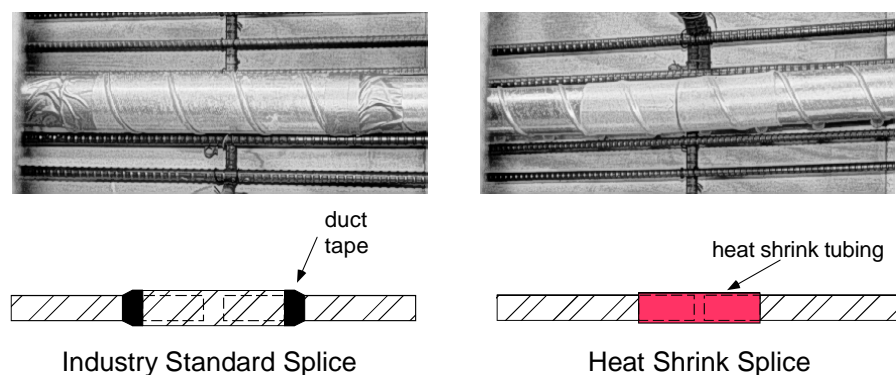


Figure 2.7 Duct Splices<sup>2</sup>

### 2.2.2.3 High Performance Fly Ash Grout

Fly ash grout was used in one beam specimen, with the following characteristics:  $w/c = 0.35$ , 30% cement replacement by weigh with Fly Ash, superplasticizer (4 milliliters per kilogram of cementitious material for fluidity).

#### 2.2.3 Phase II Variables

##### 2.2.3.1 Concrete Type

Two different concrete mixes were selected for comparison: TxDOT Class C Concrete with 25% Fly Ash and High Performance Concrete.

Fly Ash was used due to its increasing use in concrete. For this experimental program, fly ash Class F was used due to availability from local ready-mix suppliers. For the fly ash mix, the water cement ratio was 0.44 with 25% cement replacement by weight with fly ash, and no other significant changes to the standard Class C Concrete mix.

The high performance concrete mix selected had improved strength ( $f'c = 10000$  psi) and durability. The mix contained 25% cement replacement by fly ash ( $w/c = 0.29$ ) with superplasticizer added on site to reach a slump of about 8 inches. Full details of the mix designs are included in Reference 3.

##### 2.2.3.2 Prestressing strand types

Two types of prestressing strands, besides the normal uncoated strands, were chosen for comparison: epoxy-coated and galvanized. The strands were 0.5 in. diameter, 270 ksi, stress relieved.

The effect of damages to the epoxy coating was also studied. Figure 2.8 shows the location of intentional damage in one of the tendons. Damages consisted of 1/4" x 1/4" squares of epoxy removed at five selected locations. Damage locations were selected to coincide with likely crack locations and bends in the parabolic duct profile. In these areas, durability may be affected by chlorides penetrating the small gaps that may occur between the overlapping metal. One strand in the damaged tendon was repaired with an epoxy patch repair kit and the other strand was left damaged.

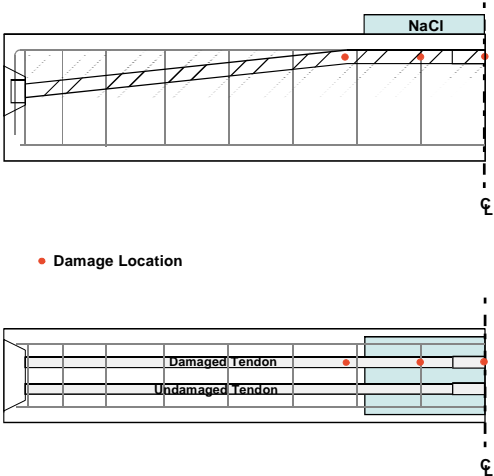


**Figure 2.8 Locations of Intentional Damage to Epoxy-Coated Strand<sup>3</sup>**

**2.2.3.3 Duct Type and End Anchorage Protection**

Polyethylene plastic ducts were used to compare with galvanized steel ducts. The VSLAB+™ system shown in Figure 2.9 was used, with an oval duct due to size limitations, to accommodate two strands. The system also allowed investigation of the end anchorage protection, since it provides an encapsulated system. The system is basically air and water tight.

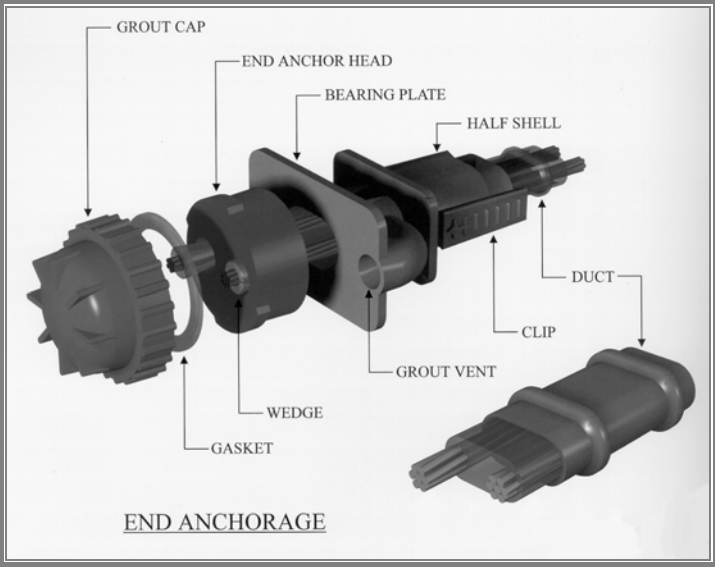


**Figure 2.9 VSLAB+™ System<sup>3</sup>**

The original intention was to evaluate an electrically isolated system, but such a system was not commercially available at the time of casting. Most specimens used galvanized steel ducts which were the industry standard at the time of casting the specimens. Poor behavior of galvanized steel ducts found subsequently led the investigators to wish that more plastic duct specimens had been utilized.

### 2.2.3.4 High Performance Antibleed Grout and Poor Grouting Procedures

Under this project, antibleed grouts were studied by Schokker<sup>3</sup> and one mix was chosen for investigation in Phase II beams. The grout had a w/c ratio of 0.33 with 2% cement weight of antibleed admixture. The duct profile used in the beams had only a small vertical rise, so bleed would not be a significant problem. The antibleed grout was chosen to compare its corrosion protection properties with the fly ash grout and TxDOT standard grout.

Poor grouting procedures were also investigated. One specimen was chosen, injecting grout with the standard method in one duct and using poor grouting procedures in the other duct (see Section 2.6).

## 2.3 SPECIMEN TYPES

Twenty seven specimens were constructed in two phases. Phase I included sixteen specimens and Phase II had eleven specimens. Table 2.4 shows the specimen types and variables on each phase. Figures 2.10 and 2.11 show the description and labeling of all beam specimens, showing the location of the duct splices.

**Table 2.4 Beam Specimen Types and Variables<sup>2</sup>**

	Main Variable	Section Type			
		Non-PS	2/3 PS	100% U	100% S
Phase I	Unloaded	1.1		3.1	
	Very Small Crack		2.1	3.2	
	Constant Service Load	1.2	2.2	3.3	4.1
	Constant Service Load (duplicate)	1.3	2.3	3.4	4.2
	Overload and Return to Service	1.4	2.4	3.5	
	High Performance Fly Ash Grout		2.11		
Phase II	Standard Concrete with 25 % Fly Ash	1.5	2.5	3.6	
	High Performance Fly Ash Concrete	1.6	2.6	3.7	
	Epoxy Coated Strands		2.7		
	Galvanized Strands		2.8		
	Poor Grouting Procedures		2.9		
	High Performance Anti-Bleed Grout		2.10		
	Encapsulated System w/ Plastic Duct		2.12		

## 2.4 MATERIALS

Construction Materials for Phase I specimens are shown in Table 2.5. Phase II specimens used the same materials as in Phase I with the additions described previously in Section 2.2.3.

Beam specimen concrete and reaction beam was sampled for strength testing using test cylinders. All cylinder strengths exceeded the minimum requirements for TxDOT Class C Concrete for Bridge Structures.



Grouts were samples according to PTI Specifications (1997). See details in Reference 2.

### Non-Prestressed Beams

Beam 1.1: Unloaded



Beam 1.2: Service Load (cracked)



Beam 1.3: Service Load (cracked)

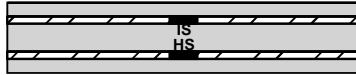


Beam 1.4: Overload & Return to Service

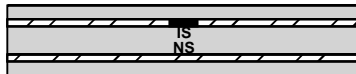


### 2/3 Prestressed Beams

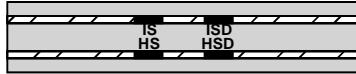
Beam 2.1: Very Small Crack



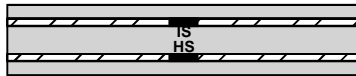
Beam 2.2: Service Load (cracked)



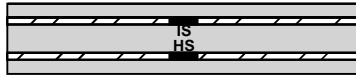
Beam 2.3: Service Load (cracked)



Beam 2.4: Overload & Return to Service

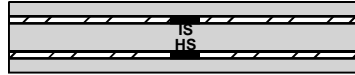


Beam 2.11: Service (Fly Ash Grout)

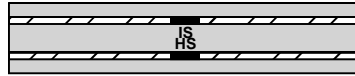


### 100%U Prestressed Beams

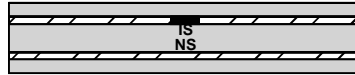
Beam 3.1: Unloaded



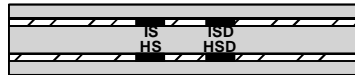
Beam 3.2: Very Small Crack



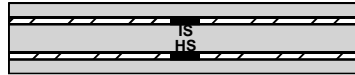
Beam 3.3: Service Load (cracked)



Beam 3.4: Service Load (cracked)

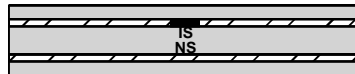


Beam 3.5: Overload & Return to Service

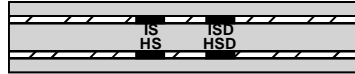


### 100%S Prestressed Beams

Beam 4.1: Service Load (uncracked)



Beam 4.2: Service Load (uncracked)



#### **SPLICE DESCRIPTIONS:**

IS - Industry Standard  
 HS - Heat Shrink  
 NS - No Splice  
 ISD - Industry Standard w/ Damage  
 HSD - Heat Shrink w/ Damage

Figure 2.10 Phase I Beam Specimens<sup>2</sup>

### Non-Prestressed Beams

Beam 1.5: Fly Ash Concrete

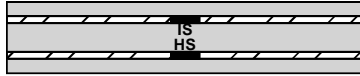


Beam 1.6: High Performance Concrete

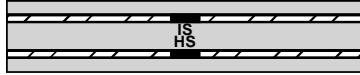


### 100%U Prestressed Beams

Beam 3.6: Fly Ash Concrete



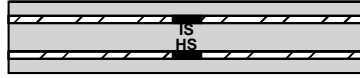
Beam 3.7: High Performance Concrete



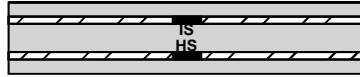
**Splice Descriptions:**  
IS - Industry Standard  
HS - Heat Shrink

### 2/3 Prestressed Beams

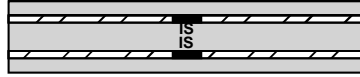
Beam 2.5: Fly Ash Concrete



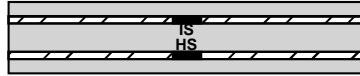
Beam 2.6: High Performance Concrete



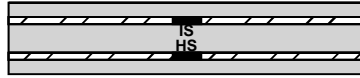
Beam 2.7: Epoxy Coated Strand



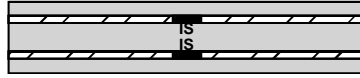
Beam 2.8: Galvanized Strand



Beam 2.9: Poor Grouting Procedures



Beam 2.10: Anti-Bleed Grout



Beam 2.12: Enc. System / Plastic Duct

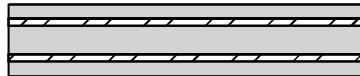


Figure 2.11 Phase II Beam Specimens<sup>3</sup>

## 2.5 EXPERIMENTAL SET-UP

The experimental set-up used is shown in Figure 2.12. The applied loading consisted on two 50-kip loads. The exposure conditions consisted of a ponded region in the middle four feet of the beam specimens, to apply a wet-dry cycle with a 3.5% NaCl solution. The salt concentration was based on ASTM G109<sup>16</sup> recommendations. Specimens were oriented tension side up and paired with a reinforced concrete reaction beam. The ponded region was covered during exposure testing to avoid contamination.

Loading was applied through a system of post-tensioning bars and railroad springs (5% maximum force loss during first year).

**Table 2.5 Construction Material Details: Phase I Beam Specimens <sup>2</sup>**

Item	Description
<b>Texas DOT Class C Concrete for Bridge Substructures</b>	<ul style="list-style-type: none"> <li>• w/c = 0.53 maximum allowable</li> <li>• w/c = 0.45 actual based on required slump</li> <li>• f'c = 25 MPa (3600 psi) minimum allowable</li> <li>• batch proportions: (per 0.764 m<sup>3</sup> (1 yd<sup>3</sup>)) <ul style="list-style-type: none"> <li>Coarse Aggregate (19 mm)(0.75 in.) 851 kg 1877 lbs</li> <li>Fine Aggregate 538 kg 1186 lbs</li> <li>Type I/II Cement 256 kg 564 lbs</li> <li>Water 115 kg 254 lbs</li> <li>Set retarder 710 ml 24 oz</li> <li>Entrained Air Admixture 118 ml 4 oz</li> </ul> </li> <li>• cylinder strengths: <ul style="list-style-type: none"> <li>7-day 30.0 MPa 4345 psi</li> <li>(average) 28-day 36.7 MPa 5320 psi</li> <li>56-day 37.9 MPa 5490 psi</li> </ul> </li> </ul>
<b>Reaction Beam Concrete</b>	<ul style="list-style-type: none"> <li>• w/c = 0.40</li> <li>• f'c = 42 MPa (6000 psi) design strength</li> <li>• batch proportions: (per 0.764 m<sup>3</sup> (1 yd<sup>3</sup>)) <ul style="list-style-type: none"> <li>Coarse Aggregate (19 mm)(0.75 in.) 848 kg 1869 lbs</li> <li>Fine Aggregate 615 kg 1355 lbs</li> <li>Type I/II Cement 234 kg 517 lbs</li> <li>Water 95 kg 210 lbs</li> <li>Set retarder 603 ml 20.4 oz</li> </ul> </li> <li>• cylinder strengths: <ul style="list-style-type: none"> <li>3-day 28.7 MPa 4160 psi</li> <li>(average) 28-day 36.7 MPa 5320 psi</li> </ul> </li> </ul>
<b>Texas DOT Grout for Post-Tensioning</b>	<ul style="list-style-type: none"> <li>• w/c = 0.44</li> <li>• batch proportions: (per 0.028 m<sup>3</sup> (1 ft<sup>3</sup>)) <ul style="list-style-type: none"> <li>Type I Cement 37.4 kg 82.4 lbs</li> <li>Water 16.4 kg 36.2 lbs</li> <li>Expanding Admixture (Intraplast-N) 0.37 kg 0.82 lbs</li> </ul> </li> <li>• cube strengths: <ul style="list-style-type: none"> <li>7-day 22.2 MPa 3215 psi</li> <li>(average) 28-day 28.8 MPa 4170 psi</li> </ul> </li> </ul>
<b>High Performance Fly Ash Grout for Post-Tensioning</b>	<ul style="list-style-type: none"> <li>• w/c = 0.35</li> <li>• batch proportions: (per 0.028 m<sup>3</sup> (1 ft<sup>3</sup>)) <ul style="list-style-type: none"> <li>Type I Cement 28.9 kg 63.8 lbs</li> <li>Class C Fly Ash 12.4 kg 27.4 lbs</li> <li>Water 14.5 kg 31.9 lbs</li> <li>Superplasticizer 165 ml 5.6 oz</li> </ul> </li> <li>• cube strengths: <ul style="list-style-type: none"> <li>7-day 38.4 MPa 5560 psi</li> <li>(average) 28-day 43.5 MPa 6310 psi</li> </ul> </li> </ul>
<b>Prestressing Strand</b>	<ul style="list-style-type: none"> <li>• 12.7 mm (0.5 in.) diameter seven wire strand</li> <li>• Grade 270 (1860 MPa, 270 ksi), low relaxation</li> <li>• Supplier: Shinko Wire, Inc.</li> </ul>
<b>Mild Steel Reinforcement</b>	<ul style="list-style-type: none"> <li>• ASTM A615, Grade 60 (400 MPa, 60 ksi)</li> </ul>

**Table 2.5 (Continued) – Construction Material Details: Phase I Beam Specimens<sup>2</sup>**

Item	Description
<b>Steel Duct</b>	<ul style="list-style-type: none"> <li>• Corrugated, semi-rigid, galvanized steel duct</li> <li>• 54 mm (2-1/8 in.) outside diameter</li> <li>• Supplier: VSL Corporation, Inc.</li> </ul>
<b>PT Anchorage Hardware</b>	<ul style="list-style-type: none"> <li>• VSL Type E anchorage system</li> <li>• Supplier: VSL Corporation</li> </ul>
<b>Epoxy Bonding Agent</b>	<ul style="list-style-type: none"> <li>• Epoxy Adhesive Type V – General Epoxy Adhesive</li> <li>• Supplier: Industrial Coating Specialties Corp.</li> </ul>
<b>Non-Shrink Grout for Anchorage Protection</b>	<ul style="list-style-type: none"> <li>• Pre-bagged non-shrink grout mix</li> <li>• Trade Name: Euclid NS-Grout</li> </ul>

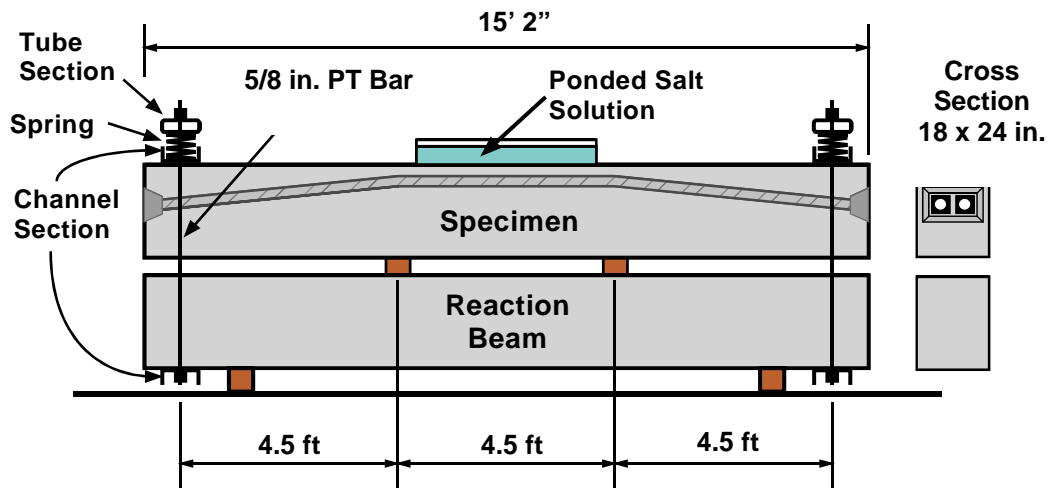


**Figure 2.12 Test Setup<sup>2</sup>**

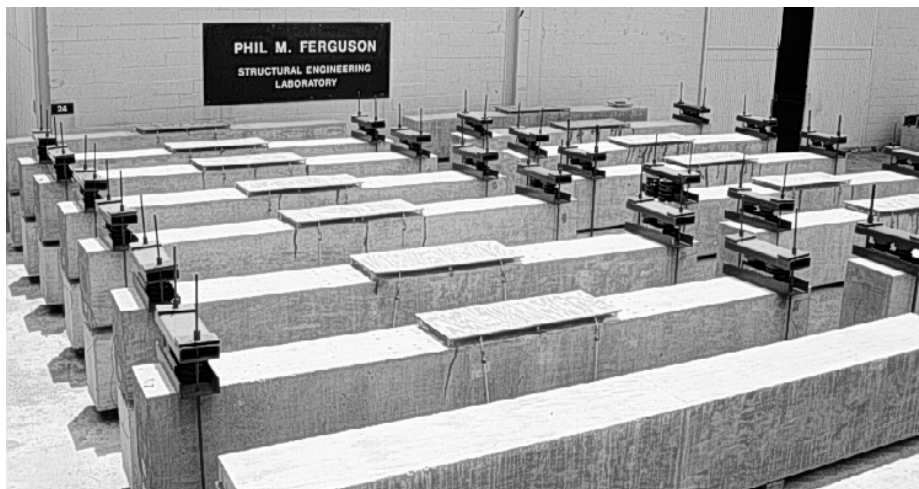


**Figure 2.13 Beam Test Setup at North End of Ferguson Laboratory<sup>2</sup>**

## 2.6 SPECIMEN FABRICATION

All specimens were constructed at the Ferguson Structural Engineering Laboratory. Full description of the construction process is included in References 2 and 3. Figure 2.14 shows details of the construction process.

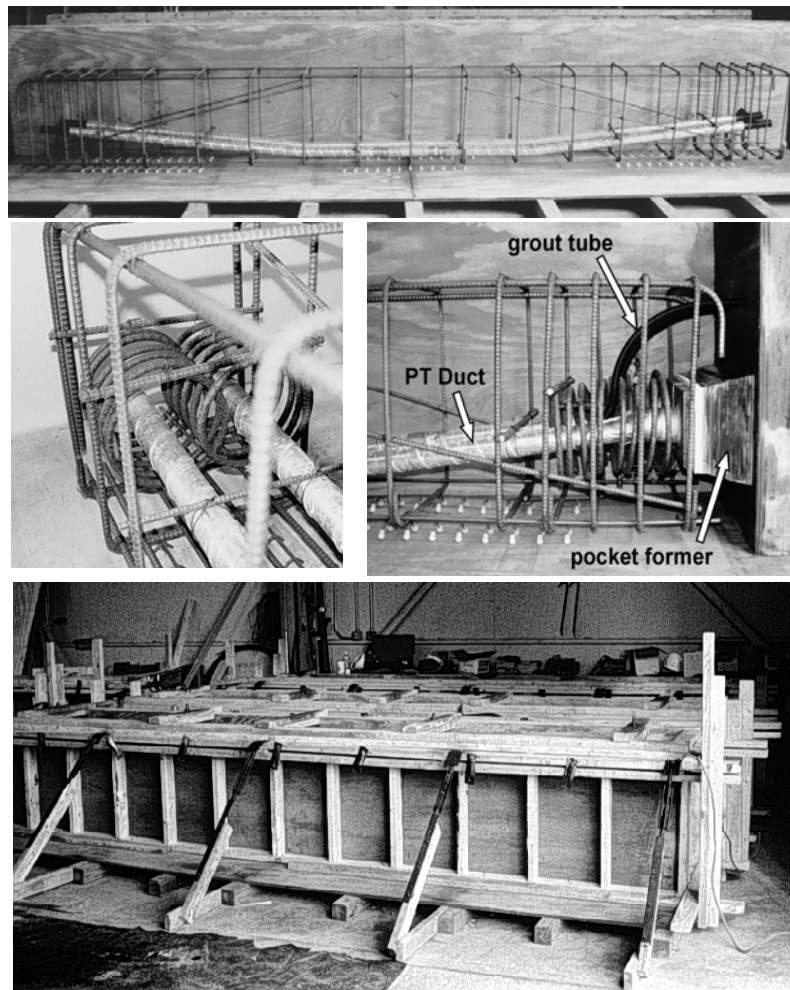


**Figure 2.14 Reinforcing Cage, End Detail for PT Beam, and Formwork<sup>2,3</sup>**

Post-tensioning losses due to elastic shortening, friction and anchorage seating were considered in the design of each section type. Post-tensioning was applied in stages as shown in Figure 2.15. Several pull off tests were performed to determine necessary power seating forces to limit seating losses to tolerable levels.

Special wedges were used with the epoxy-coated strands. These wedges were larger than standard wedges and proper anchor heads were fabricated to accommodate the wedges.

Grouting was performed following Post-Tensioning Institute recommendations. Vents were provided toward the end of the intermediate rise in the duct. Beam 2.9 had one tendon poorly grouted to compare against good practice procedures. As explain in Reference 3, for this tendon, the pump was turned off twice during pumping to allow possible pockets of air in the line. The pump was left off for approximately 10 minutes at one point during grouting to allow the grout already pumped into the tendon to reach a different consistency than that of the grout in the pumping chamber that was continuously agitated. The far end grout tube was closed at the first appearance of grout instead of letting the grout flow to reach a continuous stream.

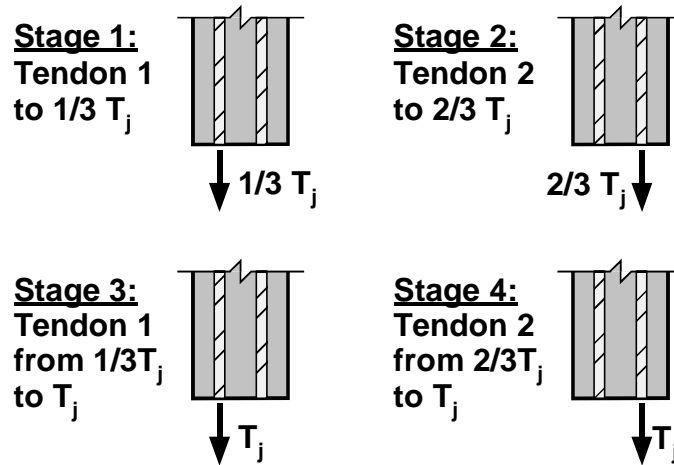


Figure 2.15 Staged Post-Tensioning Sequence <sup>2</sup>

Anchorage were protected by filling the anchorage pockets with a nonshrink grout.

## 2.7 SPECIMEN LOADING

The specimens were loaded using two 120-kip hydraulic rams, one at each end of the beam. Figure 2.16 shows the loading hardware. The force in the post-tensioning bars was locked in by tightening the nuts. Load was maintained during exposure testing with the use of two railroad springs at each end. Loading was readjusted periodically to overcome losses. Detailed description of specimen load history is included in Reference 2.

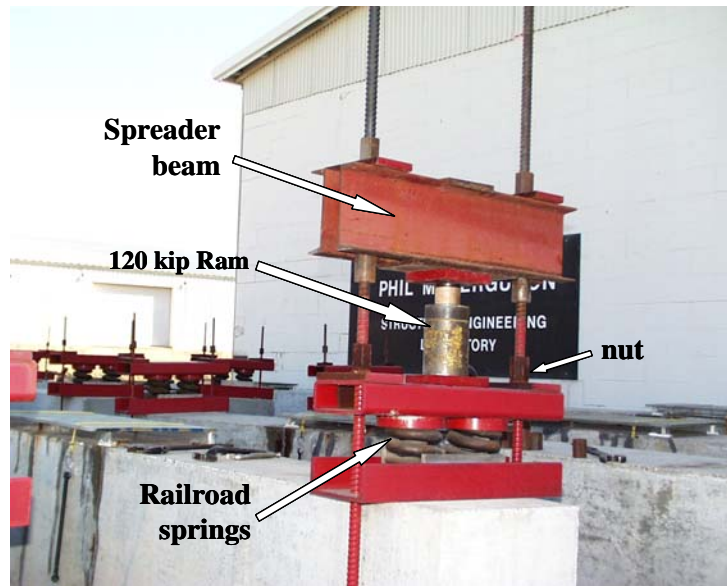
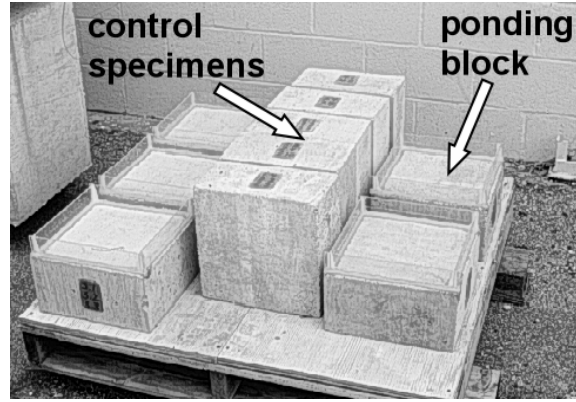


Figure 2.16 Beam Loading System

## 2.8 BLOCK SPECIMENS

Concrete blocks were fabricated and cast simultaneously as the beam specimens, to monitor chloride penetration on beams during exposure testing. The use of these blocks avoids drilling in the test area of the actual beams to extract the powder samples for chloride analysis. Concrete block dimensions were

12 x 12 x 6 in., and were based on the AASHTO T 259-80 recommendations<sup>17</sup> for evaluating chloride ion permeability of concrete. Two blocks were cast during each pour, and were termed control block and ponded block. Each ponded block was fitted with a plexiglass ponded region that was filled with a 3.5% NaCl solution following the same exposure schedule as for the beam specimens. The control blocks were used to indicate the base level of chlorides in the concrete. Concrete blocks are shown in Figure 2.17.



**Figure 2.17 Concrete Blocks for Beam Chloride Analysis<sup>2</sup>**

## **2.9 BEAM DRIPPER SYSTEM**

Three specimens were selected to evaluate the effect of saltwater dripping in the anchorage area, at the top of the nonshrink grout: Specimen 2.7 (epoxy-coated strand), Specimen 2.9 (poorly grouted) and Specimen 2.12 (encapsulated system / plastic duct). The trickle saltwater system is shown in Figure 2.18.



**Figure 2.18 Beam End Dripper System<sup>3</sup>**





## CHAPTER 3: MEASUREMENTS DURING EXPOSURE TESTING

In an attempt to monitor the corrosion activity of the specimens during exposure testing, multiple non-destructive methods were used. All these methods have advantages and limitations that became more evident after full autopsies had been performed. Non-destructive methods used in this series included: visual inspection, crack width measurements, half-cell potential readings, corrosion rate measurements and chloride penetration measurements.

### 3.1 VISUAL INSPECTION

During exposure testing, specimens were examined for any signs of distress, including changes in cracking, rust stains, and spalling.

### 3.2 CRACK WIDTH MEASUREMENTS

Surface cracks were measured using a crack microscope and a crack comparator, where each crack crossed each one of the five reference lines drawn on the beam top (tension) side, as indicated in Figure 3.1.

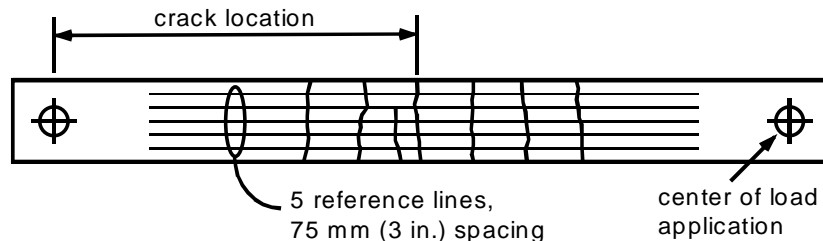


Figure 3.1 Crack Width Measurement Locations<sup>2</sup>

Cracks were measured after loading the specimens, at the beginning of exposure testing; and, at the end of testing for the selected specimens, immediately prior to full autopsies.

### 3.3 HALF-CELL READINGS

Half-cell potential measurements can provide two types of information:

- Probability of corrosion at a given location.
- Time for corrosion initiation.

Half-cell (HC) potentials were measured against a Saturated Calomel Electrode (SCE) at the end of the wet cycle. Therefore, throughout this document, HC potentials are reported as millivolts versus SCE. Other common reference electrodes and the potential of these electrodes versus the Standard Hydrogen Electrode (SHE) are shown in Table 3.1. A detailed description of the theory behind Half-Cell measurements is included in Reference 18. Also, References 2 and 3 include a description of half-cell potential theory pertaining to this research program.

Half-Cell potential measurements require the use of a reference electrode, voltmeter and electrical connection to the reinforcement. Ground clamps were used to attach a wire to the prestressing tendons before capping the anchorages. In addition, two ground wires were attached to the reinforcement cage, where electrical continuity was found on the reinforcing cage, ducts and prestressing ducts.

HC potential measurements were taken every four weeks, and were based on ASTM C876<sup>19</sup> guidelines. A grid was defined in the top of the specimens to serve as a guide for the readings. The grid spacing is

6 inches along the length of the beam. Figure 3.2 shows the example for non-prestressed beams and reading locations for other specimens.

**Table 3.1 Common Reference Electrode Potentials versus SHE<sup>18</sup>**

Reference Electrode	Half-Cell Reaction	Potential (V vs. SHE)
Copper-Copper Sulfate (CSE)	$\text{CuSO}_4 + 2e^- = \text{Cu} + \text{SO}_4^{2-}$	+0.318
Saturated Calomel Electrode (SCE)	$\text{Hg}_2\text{Cl}_2 = 2e^- = 2\text{Hg} + 2\text{Cl}^-$	+0.241
Standard Hydrogen Electrode (SHE)	$2\text{H} + 2e^- = \text{H}_2$	+0.000

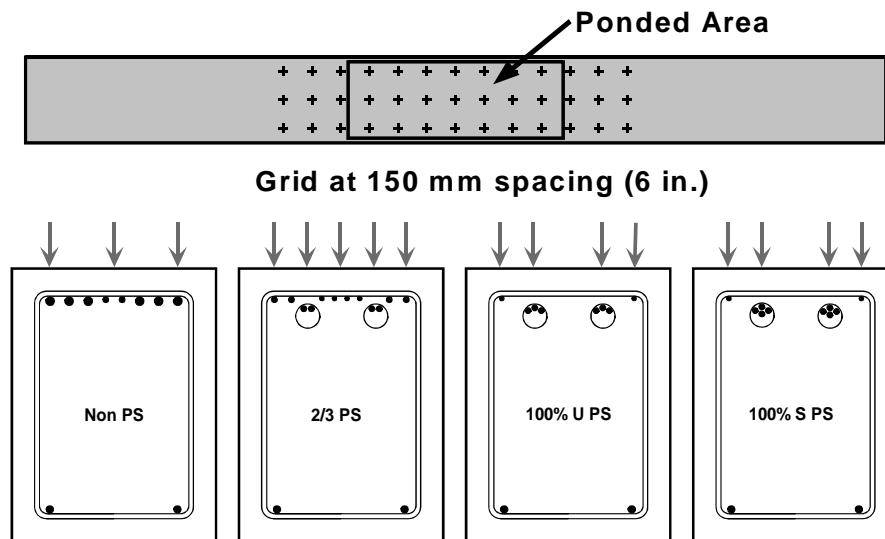


**Figure 3.2 Grid for Half-Cell Potential Readings Non-Prestressed Beams and Half-Cell Reading Locations for other beams<sup>2</sup>**

Table 3.2 shows the numerical significance of HC Potential readings. These values are reported for uncoated reinforcing steel and therefore they may not necessarily be appropriate for post-tensioned concrete. When galvanized steel ducts are used, half-cell potentials may reflect the potential of the zinc on the galvanized steel duct, which could lead to erroneous conclusions.

**Table 3.2 Interpretation of Half-Cell Potentials for Uncoated Reinforcing Steel, Based on ASTM C876-91<sup>2</sup>**

Measured Potential (vs SCE)	Probability of Corrosion
more positive than -130 mV	less than 10% probability of corrosion
Between -130 mV and -280 mV	corrosion activity uncertain
more negative than -280 mV	greater than 90% probability of corrosion

During the first months of exposure testing, HC readings were taken before the saltwater solution was removed from the ponded area. It was later found that more accurate readings were obtained when taking the readings immediately after removal of the solution. Outside the ponded area, a wetting solution was used according to ASTM standards.

### 3.4 CORROSION RATE READINGS

Full description of Corrosion Rate theory is included in Reference 2. The following description is an extract from that reference.

Polarization resistance is a useful technique for measuring instantaneous corrosion rates under laboratory and field conditions. Polarization measurements are rapid, highly sensitive, nondestructive and can be performed repeatedly. The theory states that within a small range of overvoltage (+/- 10 to 15 mV from the free corrosion potential), there is a linear relationship between applied current and electrode potential. The slope of the curve of  $\Delta E$  versus  $\Delta I_{\text{applied}}$  at the origin is defined as the polarization resistance,  $R_p$ . The polarization resistance is inversely proportional to corrosion current, which in turn is directly proportional to corrosion rate. The computed corrosion rate can be compared to established guidelines to relate corrosion rate to corrosion damage. This method for corrosion rate measurements is often referred to as linear polarization or the polarization resistance method.<sup>2</sup>

The instantaneous corrosion current is related to the polarization resistance by the Stern-Geary equation shown below.<sup>20, 21</sup>

$$i_{\text{corr}} = \frac{\beta_a \beta_c}{2.3(\beta_a + \beta_c)} \times \frac{1}{R_p} \quad \text{Eq. 1}$$

where

- $i_{\text{corr}}$  = corrosion current, mA
- $\beta_a$  = anodic Tafel constant, mV
- $\beta_c$  = cathodic Tafel constant, mV
- $R_p$  = polarization resistance, Ohms

The rate of corrosion in terms of corrosion current density,  $i$ , can be calculated by dividing the corrosion current,  $i_{\text{corr}}$ , by the area of polarized steel,  $A_p$ .

$$i = \frac{i_{\text{corr}}}{A_p} \quad \text{Eq. 2}$$

where

- $i_{\text{corr}}$  = corrosion current, mA
- $A_p$  = area of polarized steel,  $\text{cm}^2$
- $i$  = corrosion current density,  $\text{mA}/\text{cm}^2$

The computed corrosion rate, in terms of corrosion current density, can be compared to the established guidelines to relate corrosion rate to corrosion damage.

The polarization resistance,  $R_p$ , can be measured using several different techniques.<sup>21, 22</sup> The two most common methods used for reinforced concrete are the three electrode procedure, and electrochemical impedance spectroscopy (sometimes referred to as AC impedance). Each method has advantages and disadvantages.<sup>22</sup> The three electrode method is most common due to its simplicity and low equipment cost.

The basic components of the equipment for the three electrode method are shown in Figure 3.3. The working electrode is the steel reinforcement for which the corrosion rate is to be measured. The counter electrode is used to apply the polarizing current to the steel. The reference electrode measures the free corrosion potential of the working electrode and the change in potential of the working electrode due to the applied current from the counter electrode. The process of measuring the polarization resistance begins with measuring the free corrosion potential or open-circuit potential of the tested area of steel reinforcement (working electrode). The working electrode is then polarized in uniform increments from the free corrosion potential and the associated current is measured. The polarization resistance is taken as the slope of the curve when  $\Delta E$  versus  $\Delta I_{\text{applied}}$  is plotted. This relationship is normally linear for a range of up to  $\pm 10$  mV from the free corrosion potential.<sup>20</sup> When corrosion activity is low, small changes in applied current will produce a large change in potential and the polarization resistance will be large. When corrosion activity is high, large changes in applied current are needed to produce the desired potential increment, resulting in a low polarization resistance.

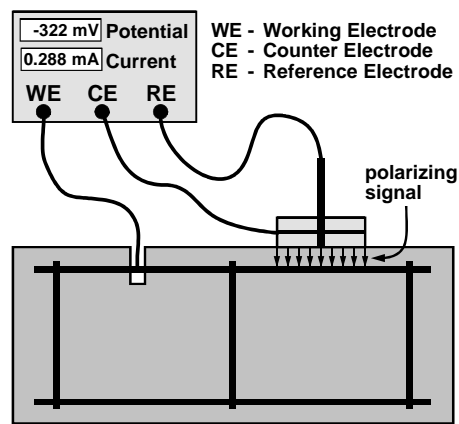


**Figure 3.3 Polarization Resistance Apparatus (Schematic)<sup>2</sup>**

Errors in corrosion rate measurements based on polarization resistance include: ohmic electrolyte resistance, uncertain polarized area, uncertain Tafel constants, use in prestressed concrete, erratic or very small polarization resistance. A detailed description of each source of error is included in Reference 2.

At the beginning of this experimental program there was no published work on using polarization resistance to monitor corrosion rates in pretensioned or post-tensioned concrete. Some of the factors listed above may have a significant influence on the usefulness of the technique in prestressed concrete. In spite of these potential limitations, it was decided to use polarization resistance as an evaluation method in this testing program since qualitative information and comparisons may still be possible. Relative corrosion rate measurements can provide an indication of relative corrosion rates between specimens with different variables. For example, the relative effectiveness of different corrosion protection measures may be evaluated by comparing corrosion rates with those from “control” specimens. Also, regular measurements may indicate the onset of corrosion through increases in corrosion rate.

This program used two different types of equipment to take corrosion rate measurements: the CORRTTEST PR-Monitor Model IN-4500 and the 3LP Equipment. Both types of equipment use the three-electrode technique. Two corrosion rate measurements were taken on each beam, one at midspan and one at a 1 ft. (305 mm) offset from midspan. The polarization resistance technique requires a direct electrical connection to the steel for which the corrosion rate is being measured. This connection was provided by the ground wires attached to the mild steel reinforcement and prestressing tendons during construction. Corrosion rate measurements require the concrete to be initially dry. A wetting solution is used to moisten the concrete surface immediately prior to testing.

The PR-Monitor device uses a portable computer to control the corrosion rate measurement process. The PR-Monitor compensates for the concrete resistance and has a guard electrode to confine the polarization signal. The default polarization scan uses six steps of 5 mV, starting at -15 mV from the free corrosion potential and ending at +15 mV. The starting and ending potentials and voltage increment may be adjusted by the user in situations where the solution resistance is large in comparison to the polarization resistance. The increased potential range for the polarization scan can improve the accuracy of the measured polarization resistance when the solution resistance is high. At the end of the polarization scan, the concrete resistance or solution resistance is measured using AC impedance. A high frequency, low voltage AC signal is used to isolate the solution resistance. The computer performs a linear regression analysis on the polarization scan data and computes the total resistance,  $R_{tot}$ , as the slope of  $\Delta E$  versus  $\Delta I_{applied}$ . The solution resistance,  $R_s$ , is subtracted from the total resistance to obtain the polarization resistance,  $R_p$  as shown below.

$$R_p = R_{tot} - R_s \quad \text{Eq. 3}$$

The corrosion current is calculated assuming a proportionality constant, B, of 26 mV, a typical value for actively corroding steel reinforcement in concrete.<sup>23</sup>

$$i_{corr} = \frac{B}{R_p} \quad \text{Eq. 4}$$

where,

$$B = \frac{\beta_a \beta_c}{2.3(\beta_a + \beta_c)} \quad \text{Eq. 5}$$

When all measurements and calculations are complete, the computer displays the free corrosion potential, polarization resistance, concrete resistance and corrosion rate in mils per year. This information and the polarization scan data are also written to an output file. The corrosion rate can be converted to current density by dividing the corrosion rate in mils per year by 0.4568.<sup>24</sup> The corrosion current density can also be calculated using the measured polarization resistance and assumed polarized area (see Equations 1 and 2). The corrosion severity is assigned based on the ranges listed in Table 3.3.

**Table 3.3 PR Monitor Corrosion Severity Based on Current Density<sup>24</sup>**

Corrosion Current Density ( $\mu\text{A}/\text{cm}^2$ )	Corrosion Severity
Less than 0.1	Passive
Between 0.1 and 0.5	Low
Between 0.5 and 1.0	Moderate
Greater than 1.0	High

The 3LP Equipment was developed by Kenneth C. Clear, Inc., USA. A photograph of the equipment and setup is shown in Figure 3.4. The 3LP device is manually operated, and polarization scan data are recorded by hand. The counter electrode is rectangular and current confinement is not provided. The equipment measures the half-cell potential of the reinforcement (working electrode) and the applied polarization current. The polarization scan uses three steps of 4 mV, starting at the free corrosion potential and ending at +12 mV. The concrete resistance is not measured by the 3LP device. The linear regression analysis on the polarization scan data must be performed using a hand calculator or computer to determine the total resistance,  $R_{tot}$ , as the slope of  $\Delta E$  versus  $\Delta I_{applied}$ . No correction is made for the concrete resistance, and the polarization resistance,  $R_p$ , is simply taken as equal to the total resistance.

The manufacturer recommends a proportionality constant, B, of 40.76 mV for calculating corrosion current. The manufacturer also provides guidance for relating corrosion current densities to expected corrosion damage. The SHRP Procedure Manual for Condition Evaluation of Bridges<sup>25</sup> indicates a proportionality constant, B, of 26 mV can be used with the 3LP device. The interpretation guidelines listed in Table 3.3 are appropriate for the 3LP device if B = 26 mV is used.<sup>25</sup>



Figure 3.4 3LP Equipment and Setup<sup>6</sup>

### 3.5 CHLORIDE PENETRATION MEASUREMENTS

By regularly monitoring the penetration of chlorides into the concrete, it is possible to determine when chloride concentrations at the level of the steel reinforcement exceed the threshold for corrosion activity. Although this is not an absolute measurement of corrosion activity, it can be used in conjunction with other data to estimate whether corrosion initiation had occurred.<sup>2</sup>

Chloride penetration is normally measured by collecting and testing samples from the concrete at varied depths. The most common method for obtaining samples is to use a rotary hammer (hammer drill). Holes are drilled in the concrete to the desired depth and the powder is collected for analysis. Samples were analyzed for acid-soluble chloride content using a specific ion probe (CL Test System by James Instruments).<sup>2</sup> Chloride sample and analysis procedure were based on AASHTO T260-94.<sup>26</sup>

Two samples were taken periodically from each concrete block at three depths: 0.5 in., 1 in., and 2 in. (bar level). The two powder samples per block were combined to give a representative sample at each depth. Several acid-soluble chloride tests were run and the results were averaged. Drill holes were filled with epoxy.<sup>3</sup>

At the end of testing, concrete samples for chloride content analysis were taken from beams scheduled for partial and full autopsy. Samples were taken at four locations from the beam transverse centerline: 2 in., 18 in., 26 in., and 32 in.; and, at three depths: 0.5 in., 1 in., and 2 in. In partial autopsy beams, 1.3 and 3.3 as described later, samples were not taken at the 2 in. depth so bars would not be damaged. For 100%U PS and 100%S PS beams, two samples were taken at each distance from the beam transverse centerline, since less reinforcement congestion allowed for drilling at these locations. Samples were combined, analyzed and results were averaged. Figures 3.5 and 3.6 shows the concrete sample locations.

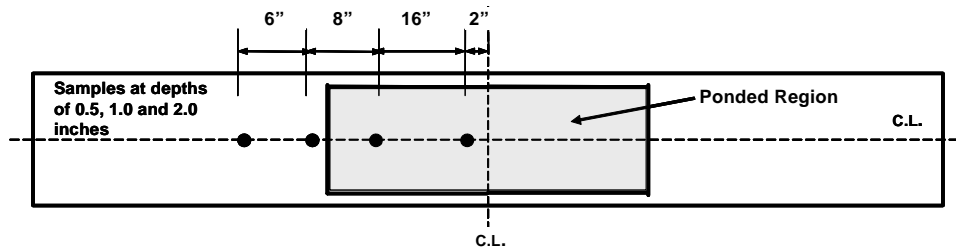
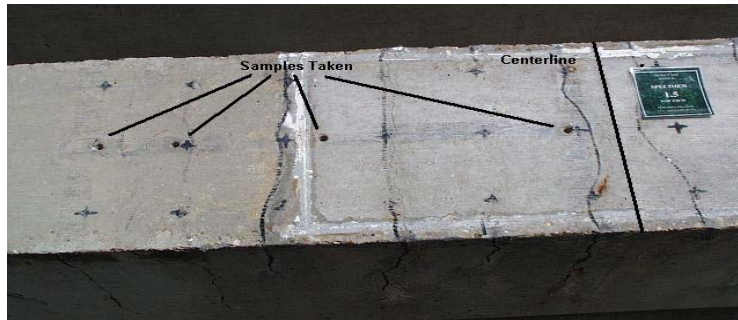


**Figure 3.5 Non-PS and 2/3 PS Beam Concrete Sample Locations (Adapted from Reference 6)**

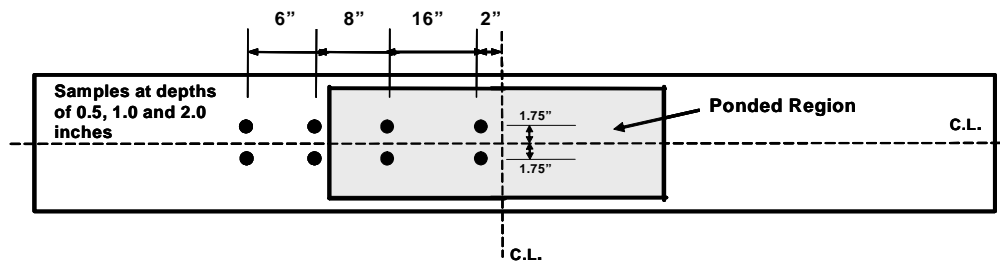
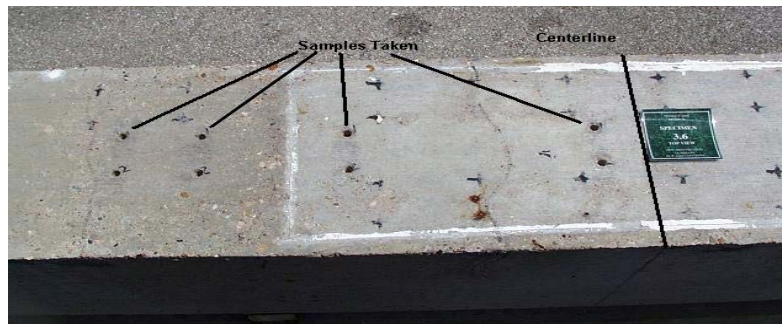


**Figure 3.6 100%U PS (and 100%S PS) Beam Concrete Sample Locations (Adapted from Reference 6)**

The above sample locations allow for investigation of the following aspects:

- Vertical penetration of chlorides through concrete
- Horizontal propagation of chlorides through concrete

- Chloride content in ponded region versus non-ponded region
- Effect of surface cracking on chloride penetration.

### **3.6 LIMITED AUTOPSY**

In order to correlate the half-cell potential readings with actual reinforcement condition, a limited autopsy was performed after 15 months of exposure testing by Schokker,<sup>3</sup> in Phase I beams 1.3, 3.3 and 3.4. Detailed description of limited autopsy procedure and findings are described in Reference 3.



## CHAPTER 4: EXPOSURE TEST RESULTS

Non-destructive testing to monitor corrosion activity in the specimens included: crack width measurements, half-cell potential readings, corrosion rate measurements, and chloride penetration and chloride content analysis. Results obtained during the exposure testing period are described herein.

### 4.1 CRACK WIDTH MEASUREMENTS

Crack widths were measured at two dates: during initial loading and, at the end of testing for the selected partial and full autopsy beams. Measurements were taken using a microscope during initial loading and a crack comparator immediately before autopsy.

#### 4.1.1 Crack Widths during Initial Loading

Crack patterns on the tension and side faces of all Phase I beams are shown in Figure 4.1. Load and reaction points are indicated in the figure. Only cracked specimens at service loading are shown. The measured crack data showed the following trends:<sup>2</sup>

- The number of cracks and extent of cracking was drastically reduced as the level of prestress increased.
- The extent of cracking along the beam was well predicted by the cracking moment for the three beam types. See Reference 2 for a detailed description of crack prediction and theory.
- Cracks commonly occurred at stirrup locations.
- The maximum surface crack widths were reduced as the level of prestress increased.

A comparison of the expected crack width versus moment curve for each of the three cracked section types is shown in Figure 4.2.

Figure 4.3 shows the measured maximum crack widths versus moment for each section type. The plots corresponding to the specimens with TxDOT standard concrete and control variables show excellent agreement with the estimated crack width values calculated prior to loading, using the Gergely-Lutz method with modifications for post-tensioned sections.<sup>1</sup> Plots of specimens with high performance concrete, high performance grout and epoxy-coated strand slightly deviated from the estimated crack width plots.<sup>3</sup>

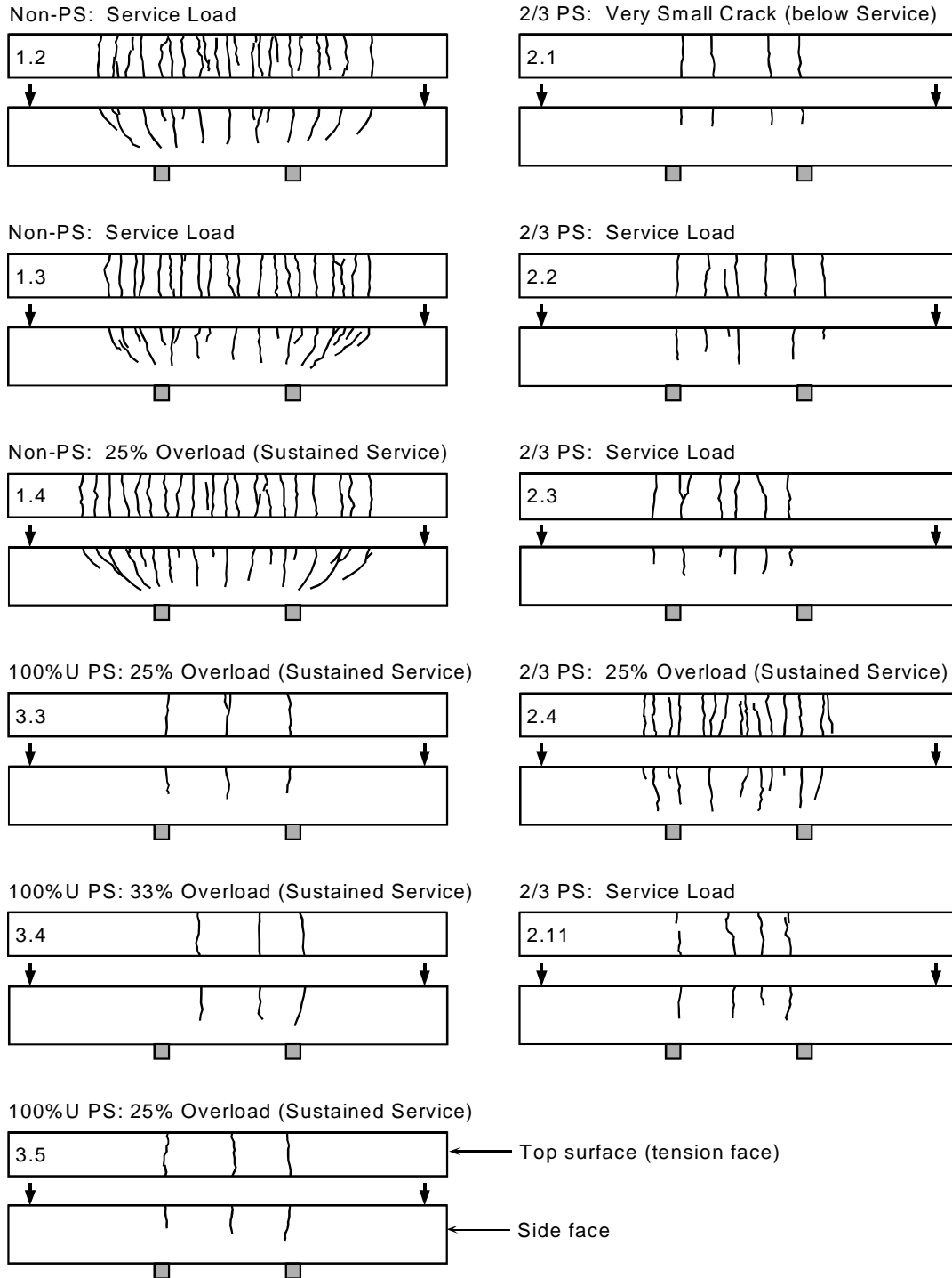


Figure 4.1 Phase I Beam Specimens Crack Patterns<sup>2</sup>

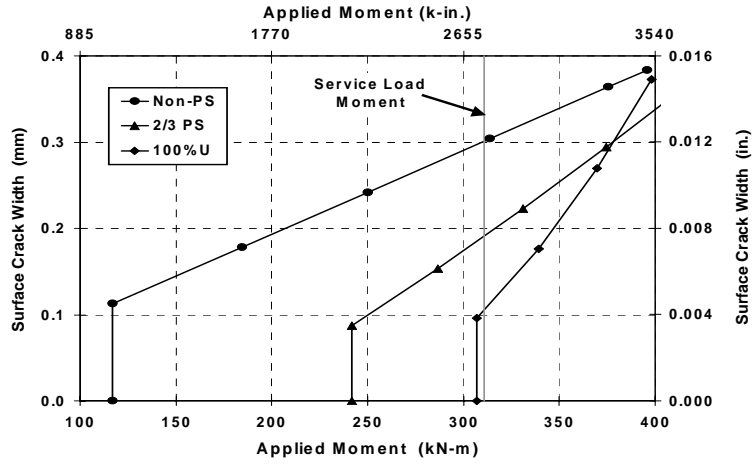


Figure 4.2 Calculated Cracking Behavior<sup>3</sup>

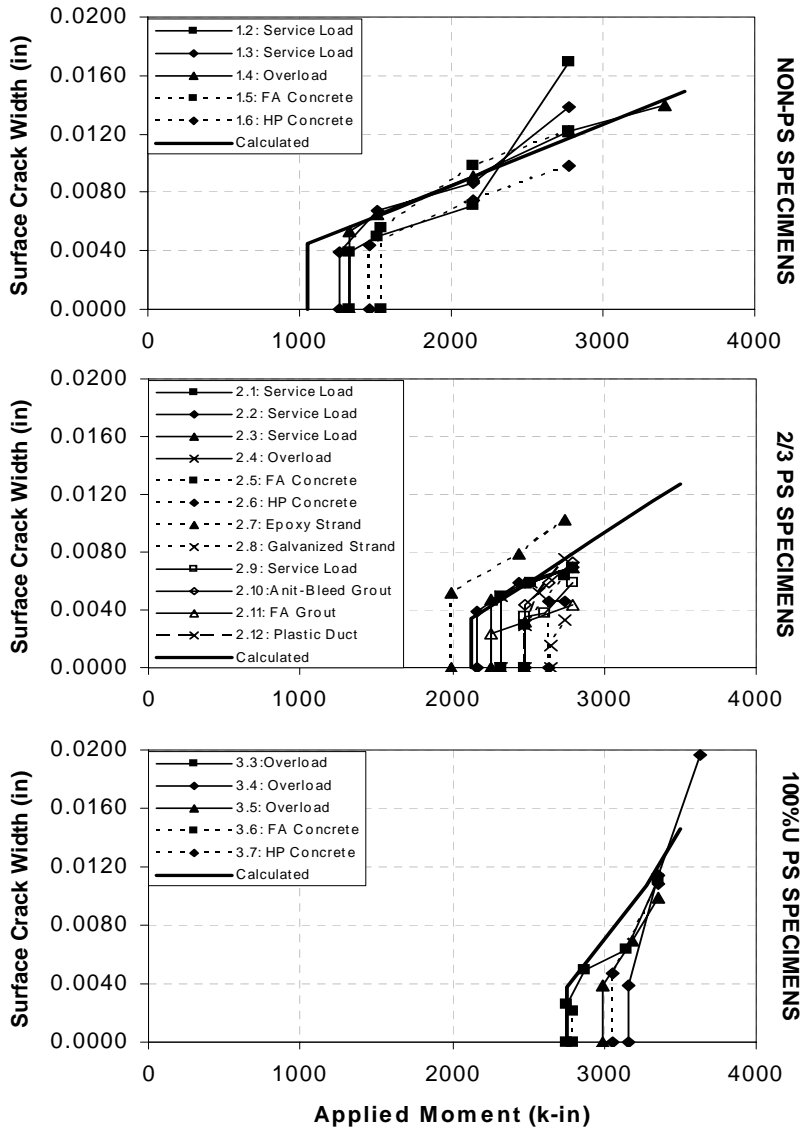


Figure 4.3 Measured Maximum Crack Widths<sup>3</sup>

#### 4.1.2 Crack Widths at the End of Testing for Autopsy Beams

Transverse and longitudinal crack width measurements were taken from all autopsy beams immediately prior to concrete demolition and reinforcement removal. Crack width measurements allowed:

- Determination of possible correlations between surface crack patterns and widths with any localized corrosion found during forensic examination
- Association of new surface cracking with corrosion products build-up.

Figures 4.4 to 4.6 show examples of each beam type from Phase II with final crack patterns and maximum and minimum crack width measurements at each crack location. Figures for all specimens are included in Appendix B. Similar figures from the initial crack width measurements can be found in Reference 2.

It is observed that crack data did not exist for Specimen 3.2 and 4.2, since they remained uncracked under service load levels.

When comparing Figure 4.4 with Figure 4.3 for Specimen 1.5, an increase in crack width can be seen from initial to final testing. The maximum crack width for this specimen grew from 0.012 in. to 0.020 in. Similar comparisons can be made for Specimens 2.5 and 3.7 from Figures 4.3, 4.5 and 4.6. The crack width for Specimen 2.5 grew from 0.007 in. to 0.020 in. (about three times larger), while for Specimen 3.7 the maximum crack width grew from 0.010 in. to 0.016 in. Loading was kept constant during exposure period. Therefore, it is concluded that additional crack opening was due to a combination of long-term concrete deformations and corrosion of active reinforcement and ducts.

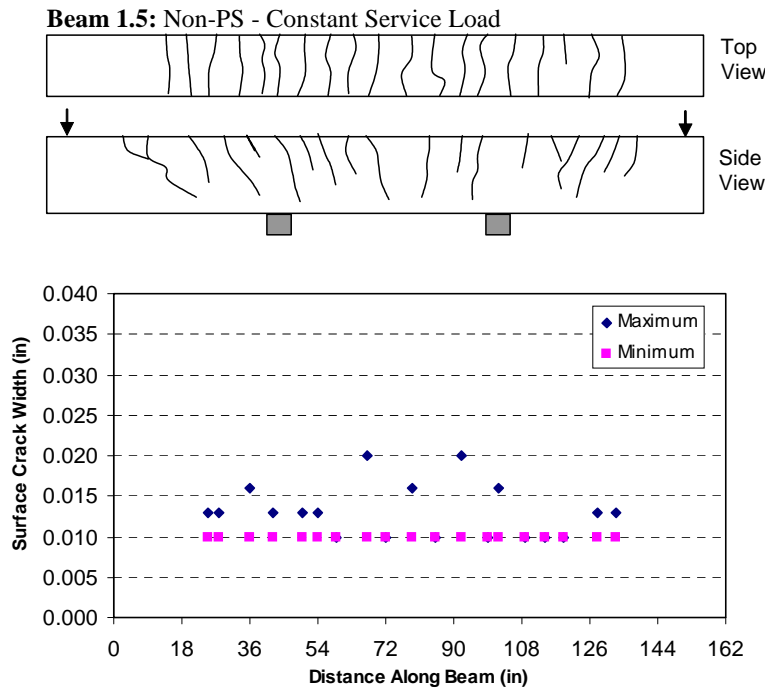


**Figure 4.4 Non-PS Section – Crack Patterns and Measurements<sup>7</sup>**

Maximum measured crack widths and the average of the maximum crack widths from each crack for Phase I specimens are shown in Figure 4.7. From this figure, no difference is observed between the Non-PS and 2/3 PS beams, but shows a small decrease in the 100% PS Beams. The average maximum

crack widths of the Phase I beams are almost identical, with Specimen 2.3 showing a slightly larger average maximum crack width. A slight trend of decreasing maximum crack width with increasing levels of prestress is observed.

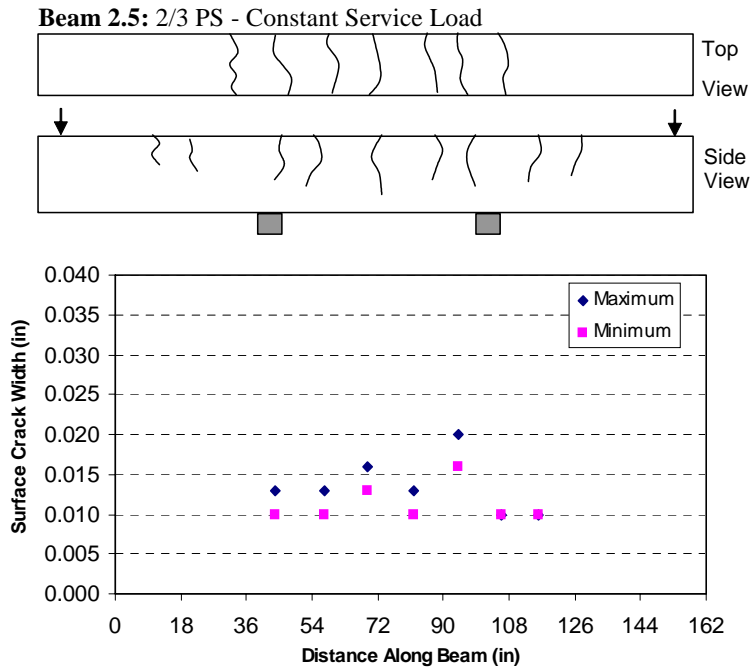


**Figure 4.5 2/3 PS Section – Crack Patterns and Measurements<sup>7</sup>**

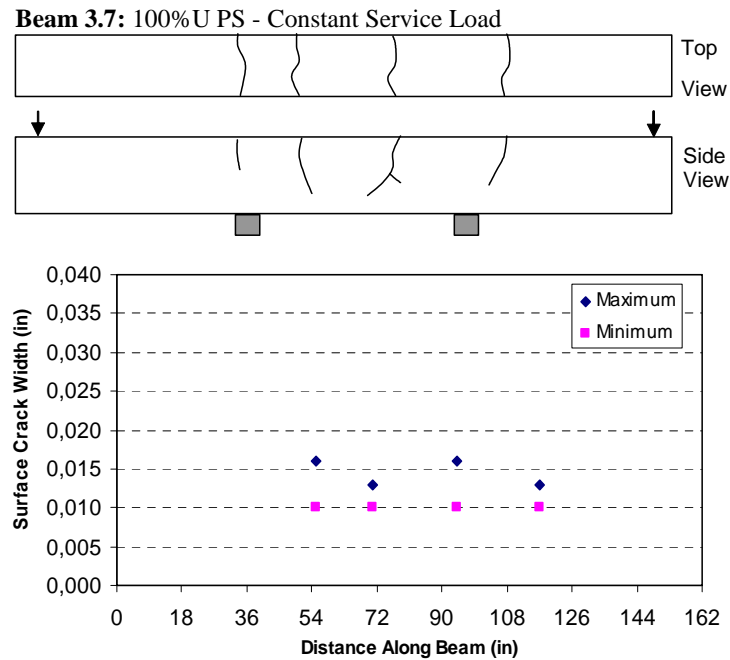


**Figure 4.6 100%U PS Section – Crack Patterns and Measurements<sup>7</sup>**

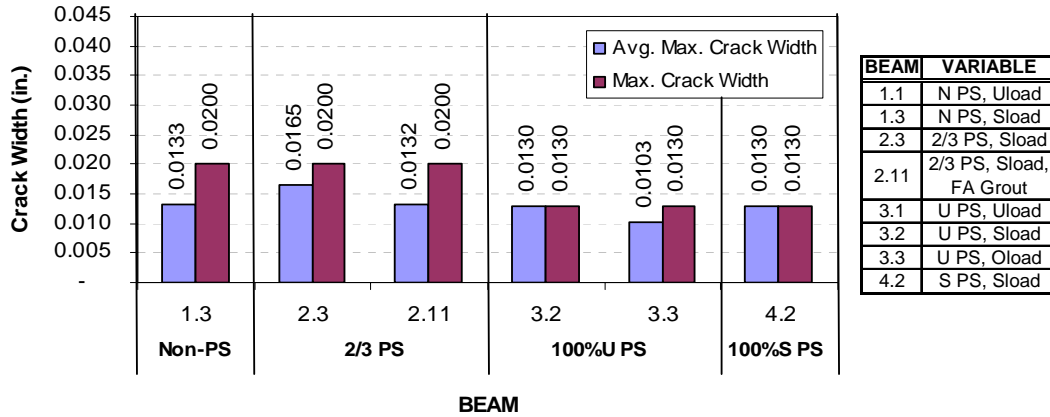


Figure 4.7 Crack Widths – Phase I Beams<sup>6</sup>

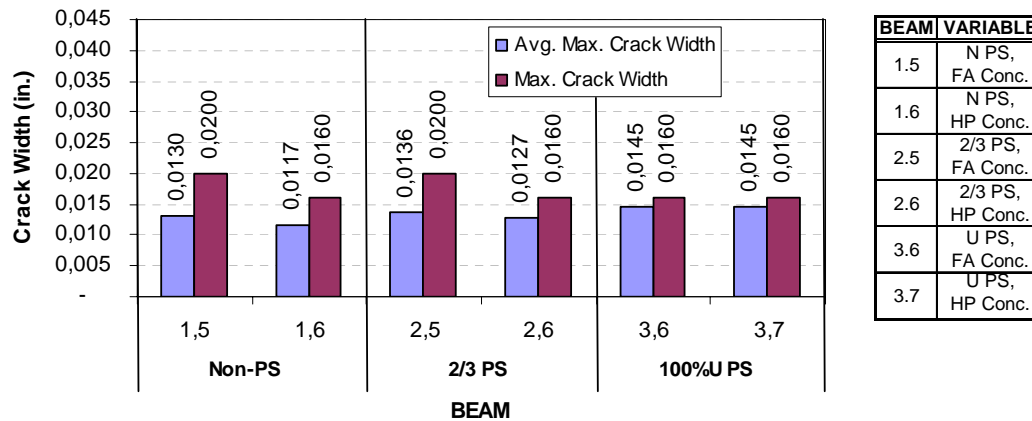


Figure 4.8 Crack Widths – Phase II Beams<sup>6</sup>

Figure 4.8 shows the maximum measured crack width and the average of the maximum crack width from each crack for Phase II beams. No distinct trends are observed between the maximum crack widths and prestress levels, and between maximum crack widths and concrete type. However, the average maximum crack widths seem to show an increase with increasing prestress levels, even when differences may be considered very small.

Wide longitudinal or splitting type cracks were found at the end of testing in Specimens 1.3, 2.3 and 2.11. Section 6.2 includes a discussion on the importance of these cracks and their relation with corrosion found after forensic examination.

#### 4.2 HALF-CELL POTENTIAL READINGS

Half-Cell potential readings were taken once every four weeks at the end of each wet cycle, as explain in Section 3.3. The graphs presented in this section include readings from the beginning of the exposure testing period until the exposure testing ceased for the specimens chosen for forensic examination, corresponding to 1594 days for Phase I beams and 1235 days for Phase II beams. Due to these significantly different exposure durations, no attempt was made to compare data from both phases. Therefore, data from each phase will always be presented separately.

Potential plots correspond to the highest value for a specimen on a given reading date. Average half-cell potentials and greatest negative potentials followed the same trend and therefore, only greatest negative potentials are shown. ASTM guidelines, as indicated in Table 3.2, are shown on the figures as a reference.

A seven-month gap of half-cell plots can be observed on each graph. This gap represents a period in which readings were not taken due to changeover in personnel.

A negligible number of half-cell readings were found to not follow the trend of the rest of the plot. These outliers were clearly identified. Due to their significant deviation from the trend, it was decided to replace the reading with an interpolation between the two adjacent readings. These outliers are considered to be due to human error or to the unreliability of the equipment. Over the course of exposure testing, complications commonly arose with the wiring system needed to take the readings. Although measures were taken to correct these problems, there was always some uncertainty of the accuracy of the readings. A description of the eleven data points considered as outliers in Phase I and the five data points in Phase II is included in Appendix E.

It is important to emphasize that half-cell potentials are only an indicator of corrosion activity, and a correlation with corrosion rate cannot be made. The ASTM C876 guidelines only indicate the probability of corrosion. Many factors can influence measured half-cell potentials, including concrete cover thickness, concrete resistivity, concrete moisture content, different metals and availability of oxygen. In some cases, these factors can lead to very negative half-cell potentials with little or no corrosion activity. For this reason it is important to consider the variation of half-cell potential measurements over an extended period of time in addition to the magnitude of the readings.<sup>2</sup>

The onset of corrosion can be determined based on the following:

- A sudden and significant change (more negative) in half-cell potentials, or
- Half-cell potential measurements more negative than -280 mV vs SCE.

When it is concluded that there is a high probability that corrosion activity is occurring within the member, it is difficult to determine which element (stirrups, rebars, ducts or prestressing strands) is corroding, since they are all electrically connected. This uncertainty can be resolved during forensic examination.

#### ***4.2.1 Phase I Beam Specimens***

Phase I beams started exposure testing in December 1997, and ended in May 2002 for the autopsy specimens, after 1594 days of testing. Figure 4.9 shows a plot of Phase I autopsy beams. At the end of testing, all specimens, except Specimen 3.1 (100%S PS, Unloaded), show high probability of corrosion activity, above 90%. Figures 4.10 through Figure 4.14 show the autopsy specimens separated according to the main variables. Half-cell potential plots for all specimens in Phase I can be found in Appendix C.

Figure 4.10 shows half-cell readings for the Non-PS beams in Phase I. The only variables on these specimens are the loading and cracking. The plot shows a decrease in the corrosion activity when the beam is unloaded and uncracked. The onset of corrosion shows also a significant difference, as would be expected, with an earlier possible initiation date for the loaded and cracked specimen. When analyzing this data, it has to be recognized that it is impractical to assume any structural member to be completely unloaded. Nevertheless, the negative effect of cracking is an important conclusion.

Figure 4.11 shows half-cell readings for mixed reinforcement beams in Phase I. Both specimens are identical except for the grout type. Based on this plot, it does not appear that the grout type has any effect on corrosion protection. However, care must be exercised when analyzing these results since readings could be reflecting the potential of the mild steel reinforcement and not the post-tensioning strands. If this is the case, it is reasonable to find both specimens with very similar potentials. The results will be confirmed after forensic examination.

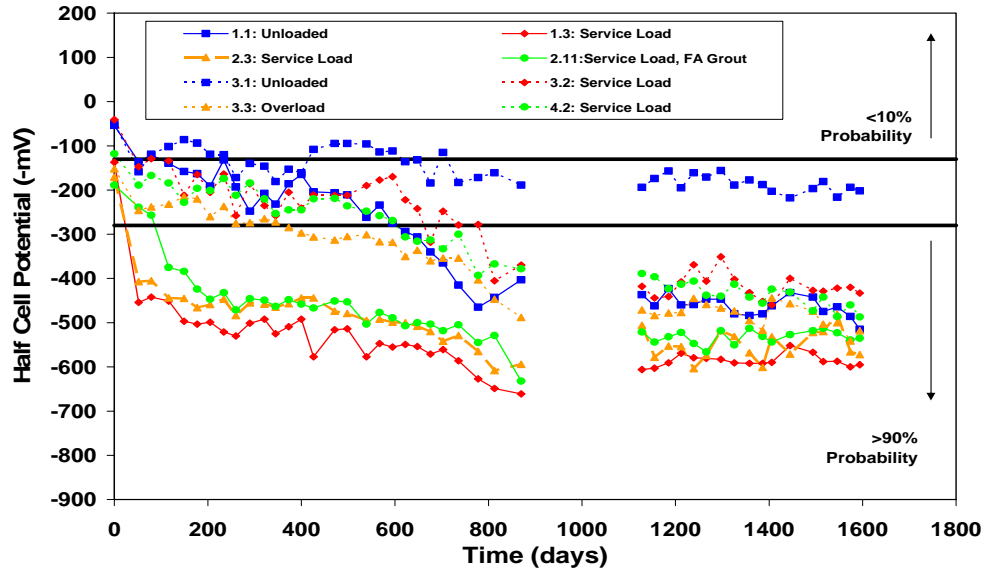


Figure 4.9 Half-Cell Potential Readings for Phase I Autopsy Beams<sup>7</sup>

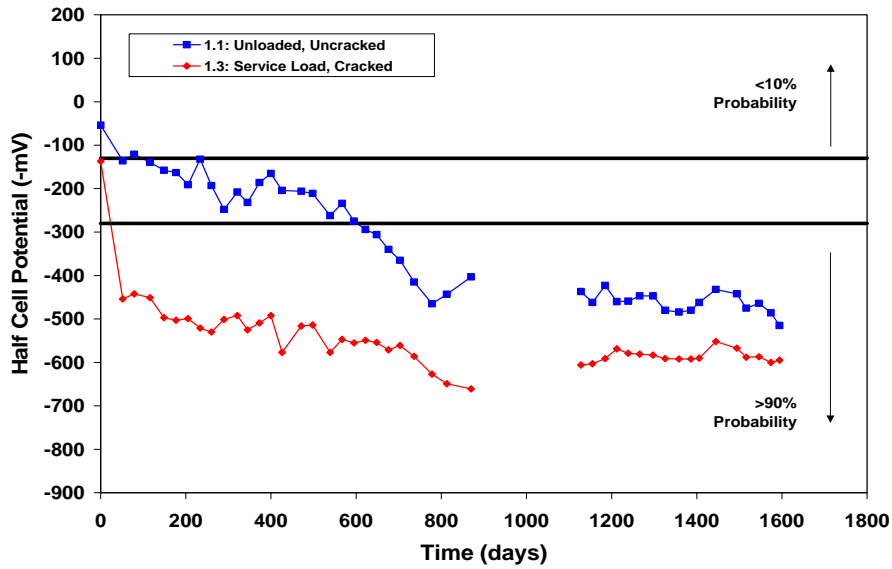
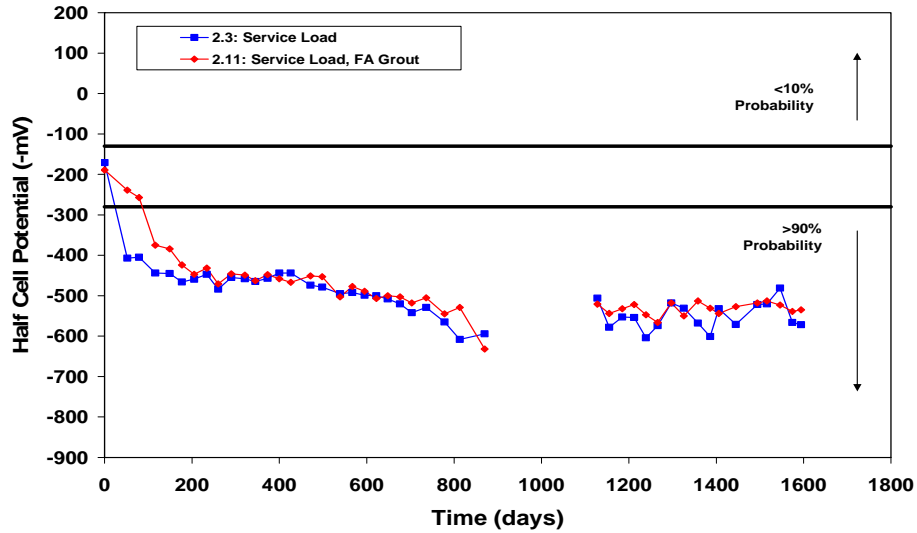


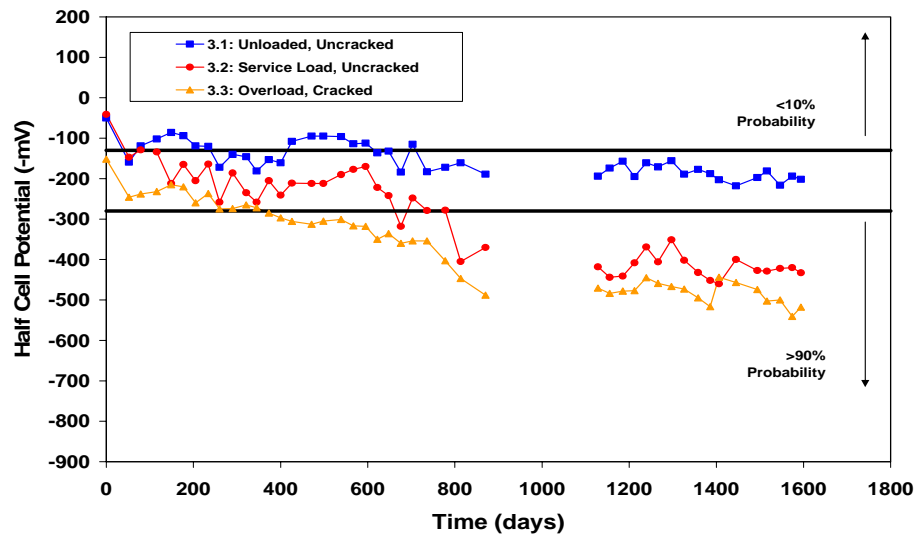
Figure 4.10 Half-Cell Potential Readings for Non-PS Specimens in Phase I Autopsy Beams<sup>7</sup>





**Figure 4.11 Half-Cell Potential Readings for 2/3 PS Specimens in Phase I Autopsy Beams<sup>7</sup>**

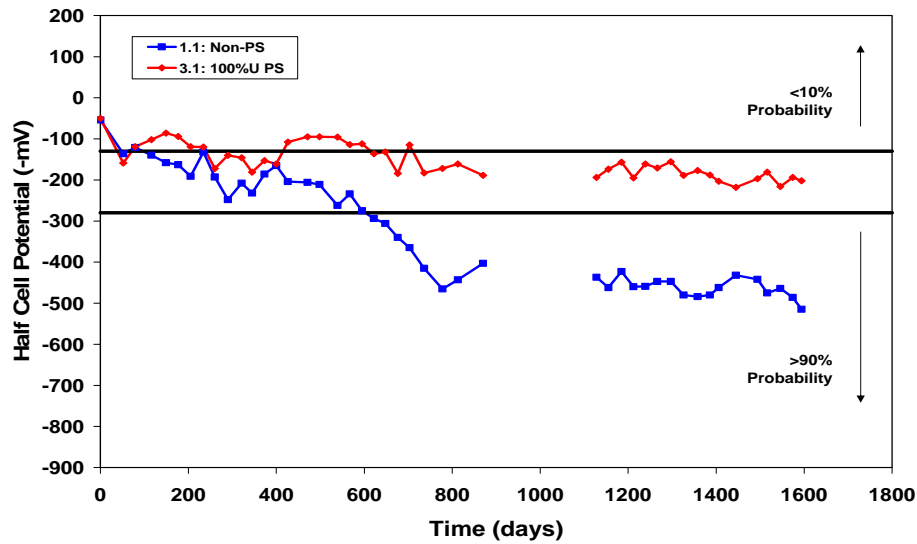
Figure 4.12 shows half-cell readings for the 100%U PS beams in Phase I. Variables include applied load and cracking. There is a distinct trend showing a decrease in the performance of the specimens with increasing loading. The unloaded specimen had half-cell readings in the uncertain range, between 10% and 90% probability of corrosion, while loaded specimens exceeded the 90% probability line. Again, an increase in corrosion protection is observed when the specimen is uncracked through both time to initiation of corrosion and final potential readings. It should be noted that while Specimen 3.2 was uncracked at the beginning of testing, a fine crack at the end of testing was found on the specimen surface. The effect of this crack will be clearly determined after forensic examination.



**Figure 4.12 Half-Cell Potential Readings for 100%U PS Specimens in Phase I Autopsy Beams<sup>7</sup>**

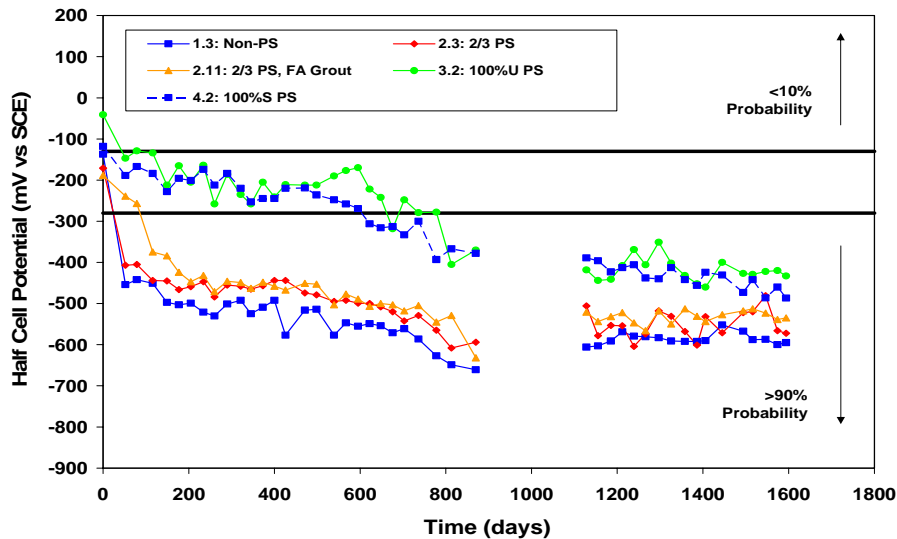
Figure 4.13 shows half-cell readings for unloaded specimens in Phase I. The only variable is the level of prestress. A distinct trend is shown with higher probability of corrosion in the non-prestressed specimen with respect to the 100%U PS beam. The non-prestressed beam shows potentials above the 90% probability of corrosion line, while the 100%U PS specimen is in the uncertain range, between the 10% and the 90%

probabilities. Both specimens were uncracked during exposure testing. Therefore, the results could suggest the importance of concrete permeability and the effect of increased compressive stresses in post-tensioned specimens, since the only possible form of chloride ingress was through the concrete.



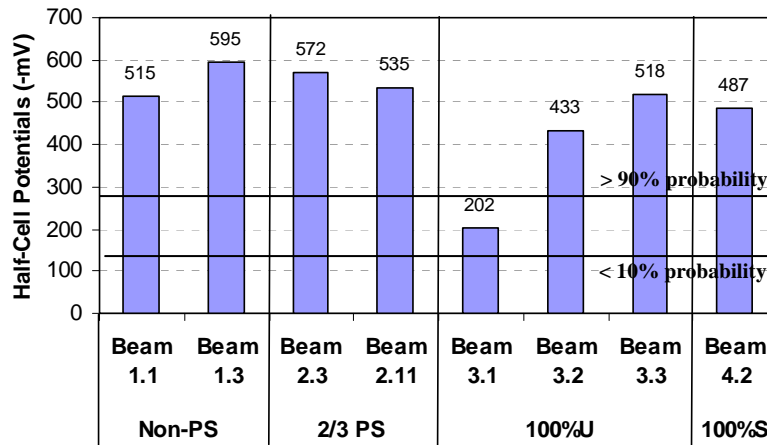
**Figure 4.13 Half-Cell Potential Readings for Unloaded Specimens in Phase I Autopsy Beams<sup>7</sup>**

Figure 4.14 shows half-cell potentials for beams subjected to service load in Phase I. The only variable is the level of prestress. As in the previous case, performance increases as the level of prestress increases. Mixed reinforced beams show similar performance as Non-PS beams, with a distinct difference with respect to 100% PS beams. Comparison among 100%U PS and 100%S PS shows a slightly better performance of the 100%S PS. However, the difference is very small to draw definite conclusions.



**Figure 4.14 Half-Cell Potential Readings for Service Load Specimens in Phase I Autopsy Beams<sup>7</sup>**

Figure 4.15 shows the greatest negative half-cell potentials for all Phase I autopsy beams at the final reading date, corresponding to 1594 days of exposure. All specimens except Specimen 3.1 (100%U PS, Unloaded) show very negative potential readings, exceeding the value of -280 mV representing the 90% probability of corrosion. Non-prestressed and mixed reinforced (2/3 PS) beams show slightly greater negative potentials at the end of testing than 100% PS beams. Again, prestressing in the unloaded and uncracked Specimen 3.1 seems to play the major role in delaying chloride penetration and corrosion activity, when compared to Specimen 1.1.



**Figure 4.15 Greatest Negative Half-Cell Potential Reading at 1594 Days (End of Testing) for Phase I Autopsy Beams**

Table 4.1 shows the time to initiation of corrosion activity for each Phase I autopsy beam. The onset of corrosion activity is defined as the date when a reading more negative than -280 mV is recorded, indicating a probability of corrosion greater than 90%.

**Table 4.1 Time to Initiation of Corrosion for Phase I Autopsy Beams**

Specimen	Description	Time to Corrosion (days)
1.1	Non-PS, Unloaded	622
1.3	Non-PS, Service Load	52
2.3	2/3 PS, Service Load	52
2.11	2/3 PS, Service Load, Fly Ash Grout	116
3.1	100% U PS, Unloaded	Never crosses threshold
3.2	100%U PS, Service Load	676
3.3	100% U PS Overload	373
4.1	100%S PS, Service Load	622

Figure 4.16 shows the half-cell potential contour maps for all Phase I specimens after 1594 days of exposure testing. Contour maps for the same beam specimens after 498 days are shown in Appendix D.

After half-cell potential readings had been analyzed from the Phase I specimen plots the following main conclusions are drawn:

- Probability of corrosion increases with increasing loading

- Probability of corrosion increases with increasing cracking
- Probability of corrosion decreases with increasing levels of prestress
- Performance of mixed reinforced (2/3 PS) specimens resemble more that of Non-Prestressed specimens, as opposed to 100% PS specimens
- No distinct difference is observed between the performance of 100%U PS and 100%S PS specimen.

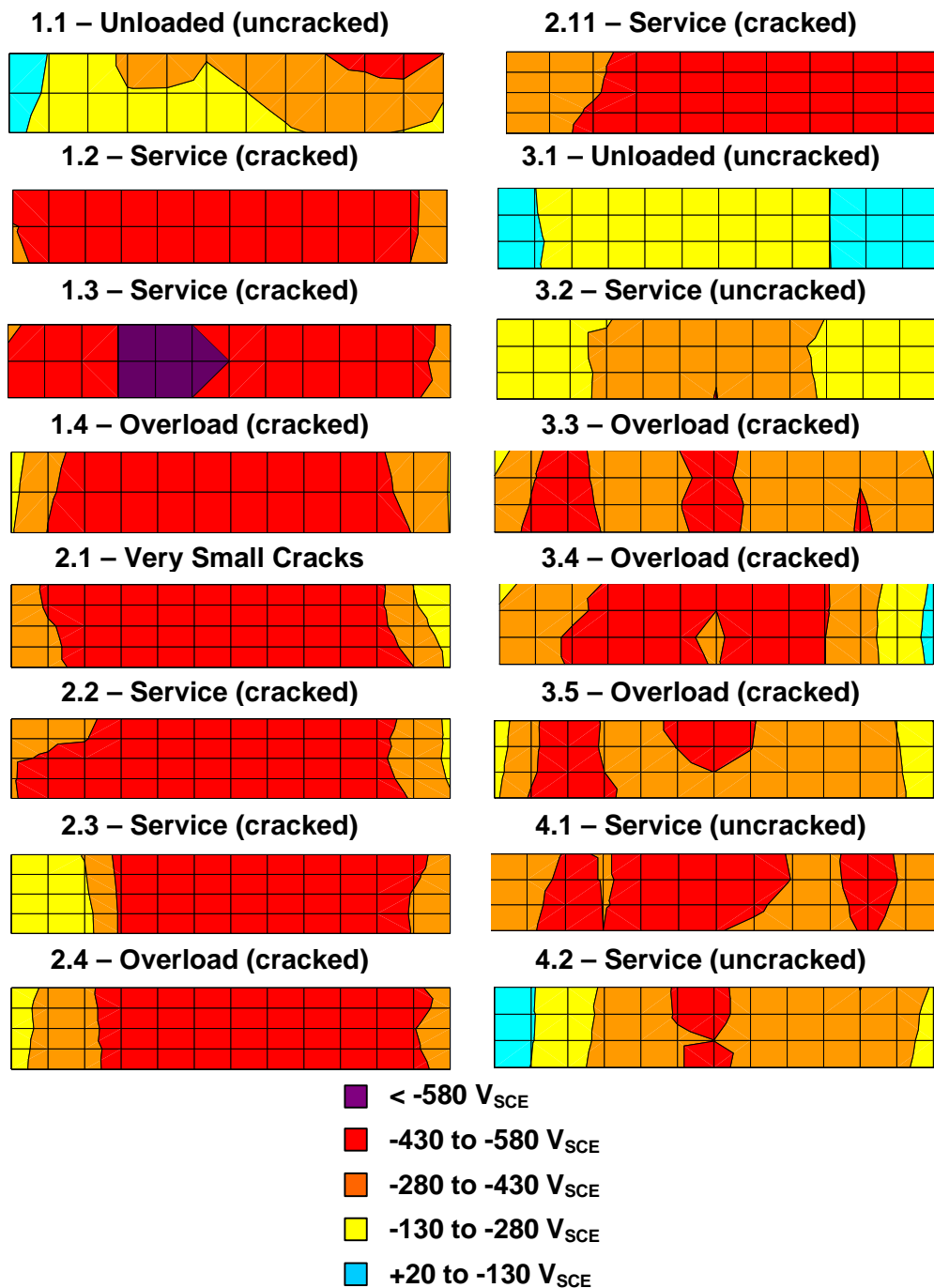


Figure 4.16 Half-Cell Potential Contour Maps at 1594 Days for All Phase I Beams

### 4.2.2 Phase II Beam Specimens

Phase II beams started exposure testing in December 1998, and ended in May 2002 for the autopsy specimens, after 1235 days of testing. Figure 4.17 shows a plot of Phase II autopsy beams. At the end of testing, all specimens, show high probability of corrosion activity, above 90%.

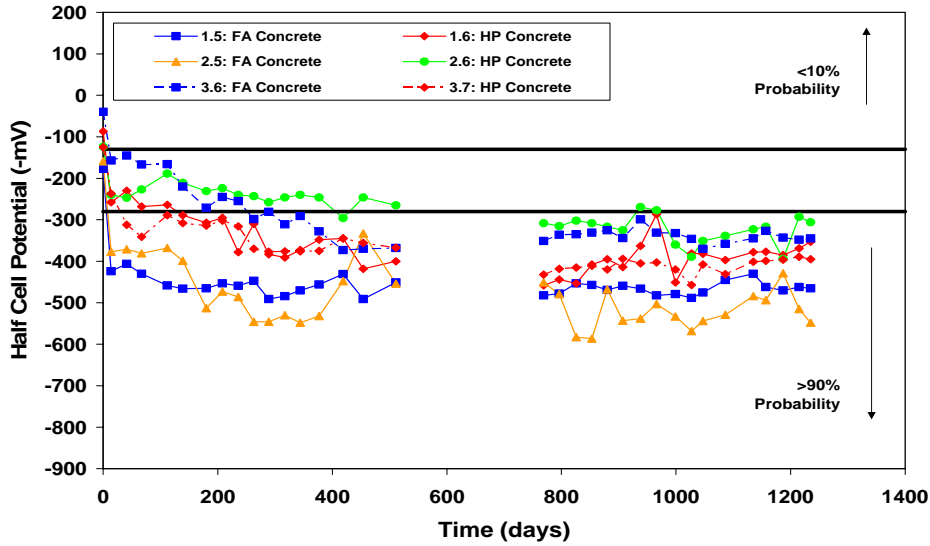


Figure 4.17 Half-Cell Potential Readings for Phase II Autopsy Beams<sup>7</sup>

Figures 4.18 through Figure 4.22 show the autopsy specimens separated according to the main variables. Half-cell potential plots for all specimens in Phase II are included in Appendix C.

Figure 4.18 shows half-cell readings for the Non-PS beams in Phase II. The only variable being compared for these specimens is the concrete type. According to the time to initiation of corrosion and the potential readings throughout the exposure testing period, it appears that high performance concrete performed better than the fly ash concrete. However, both appear to merge to the same potential range.

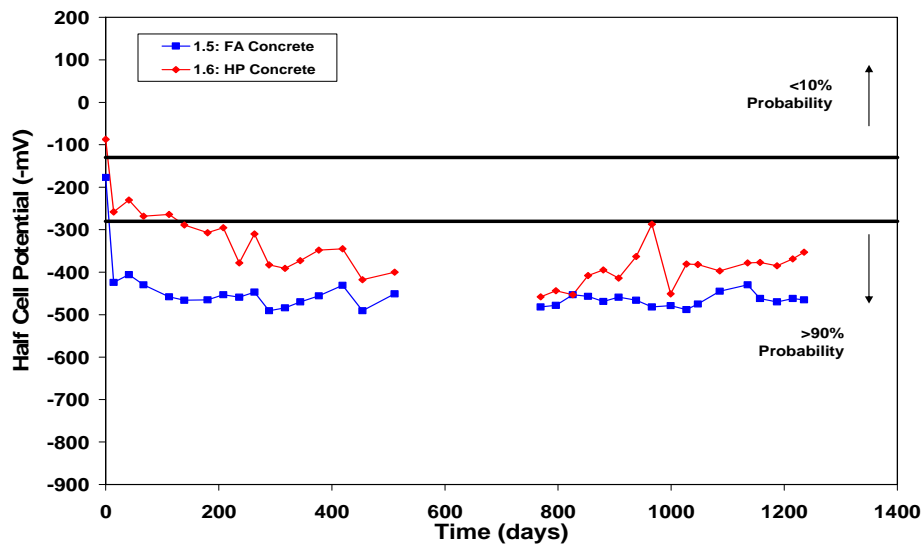
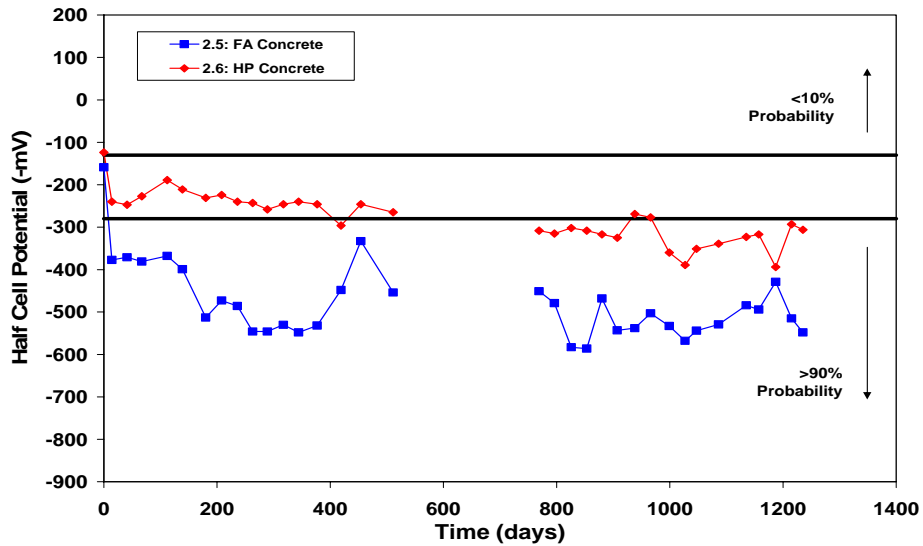


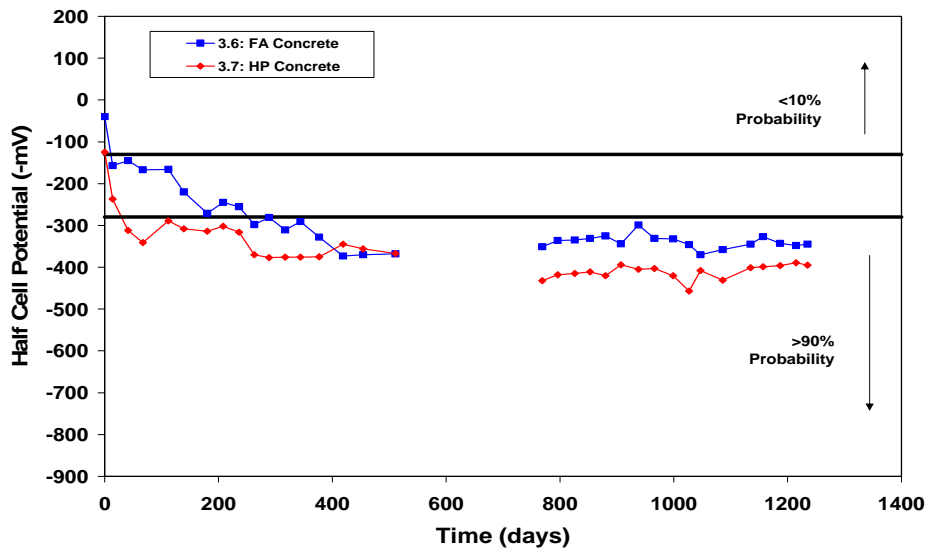
Figure 4.18 Half-Cell Potential Readings for Non-PS Specimens in Phase II Autopsy Beams<sup>7</sup>

Figure 4.19 shows half-cell readings for the mixed reinforced beams (2/3 PS) in Phase II. As in the previous case, all the variables are the same, with the exception of concrete type. Based on the time to initiation of corrosion and potential readings, the high performance concrete performed better than the fly ash concrete. These results show the positive effect of less permeable concrete, even when these specimens were cracked at service load levels.



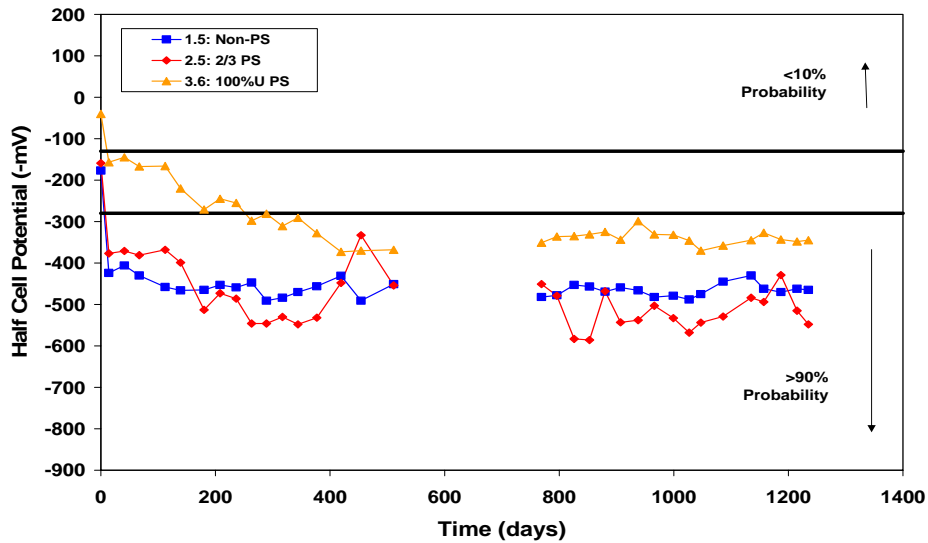
**Figure 4.19 Half-Cell Potential Readings for 2/3 PS Specimens in Phase II Autopsy Beams<sup>7</sup>**

Figure 4.20 shows half-cell readings for the 100%U PS beams in Phase II. The only variable being compared among these specimens is concrete type. The plot shows that the fly ash performed slightly better than high performance concrete, in contrast to the previous plots. However, the half-cell potential difference between both curves is very small, and appears to be merging to the same potential range.



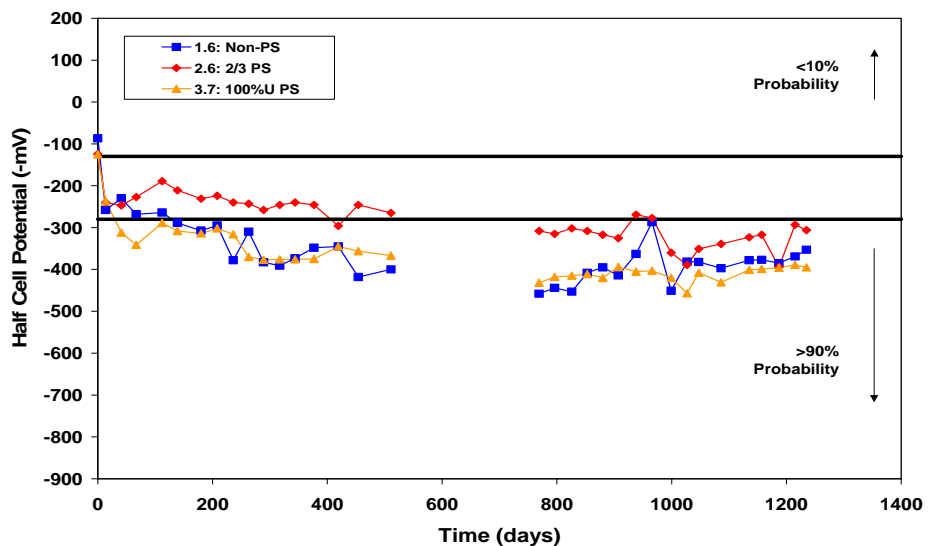
**Figure 4.20 Half-Cell Potential Readings for 100%U PS Specimens in Phase II Autopsy Beams<sup>7</sup>**

Figure 4.21 shows half-cell potential readings of the fly ash concrete beams in Phase II. The three specimens differ only on the level of prestress. As observed from the plot, based on the time to initiation of corrosion and the half-cell potential values, the fully prestressed (100%U PS) beam performed better than the Non-PS and 2/3 PS beams. Both the simple reinforced and the mixed reinforced concrete specimens show the same corrosion initiation time, but the potential of the mixed reinforced beam becomes slightly more negative over the exposure period.



**Figure 4.21 Half-Cell Potential Readings for Fly Ash Concrete Specimens in Phase II Autopsy Beams<sup>7</sup>**

Figure 4.22 shows half-cell potentials for the high performance concrete beams in Phase II. The only difference among the specimens is the level of prestress. As can be observed, it appears that the 2/3 PS beam performed better than both the 100%U PS and the Non-PS beams that performed very similar throughout the testing period. However, the final potentials are very similar for all three specimens.



**Figure 4.22 Half-Cell Potential Readings for High Performance Concrete Specimens in Phase II Autopsy Beams<sup>7</sup>**

When comparing Figures 4.21 and 4.22, it is observed that high performance concrete specimens performed slightly better than fly ash specimens. Both specimens have cement replacement by fly ash, but the high performance concrete, had a lower water-cement ratio.

Figure 4.23 shows the greatest negative half-cell potentials for all Phase II autopsy beams at the final reading date, corresponding to 1235 days of exposure.

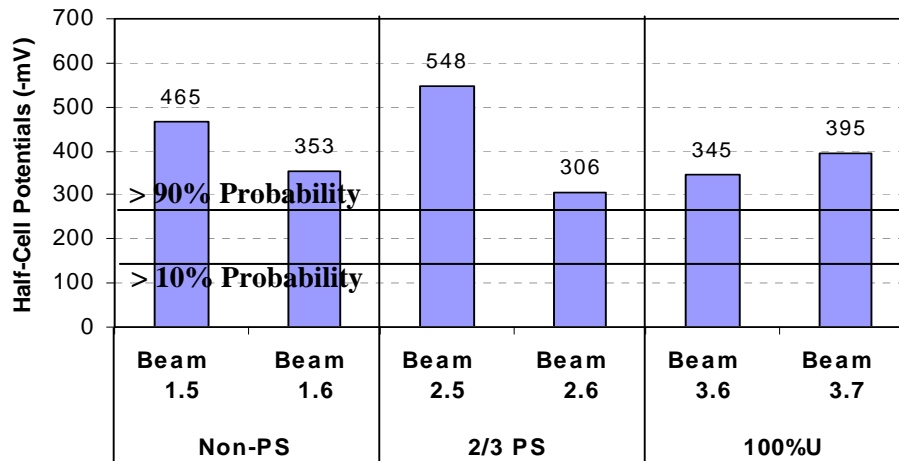


**Figure 4.23 Greatest Negative Half-Cell Potential Reading at 1235 Days (End of Testing) for Phase II Autopsy Beams**

All specimens show very negative potentials and there is not a clear distinction among the Non-PS, 2/3 PS and 100%U PS specimens. Specimen 2.5 (mixed reinforced, fly ash concrete) show a slightly higher potential at the final date than the other specimens, but all were above the level of 90% probability of corrosion.

Table 4.2 shows the time to initiation of corrosion activity for each Phase II autopsy beam. The onset of corrosion activity is defined as the date when a reading more negative than -280 mV is recorded, indicating a probability of corrosion greater than 90%.

**Table 4.2 Time to Initiation of Corrosion for Phase II Autopsy Beams**

Specimen	Description	Time to Corrosion (days)
1.5	Non-PS, Fly Ash Concrete, Service Load	15
1.6	Non-PS, High Performance (HP) Concrete, Service Load	139
2.5	2/3 PS, Service Load, Fly Ash Concrete	14
2.6	2/3 PS, HP Concrete, Service Load	419
3.6	100% U PS, Unloaded, Fly Ash Concrete	263
3.7	100%U PS, HP Concrete, Service Load	41

Figure 4.24 shows the half-cell potential contours maps for all Phase II specimens after 1235 days of exposure testing. Contour maps at 139 days of testing are shown in Reference 12.



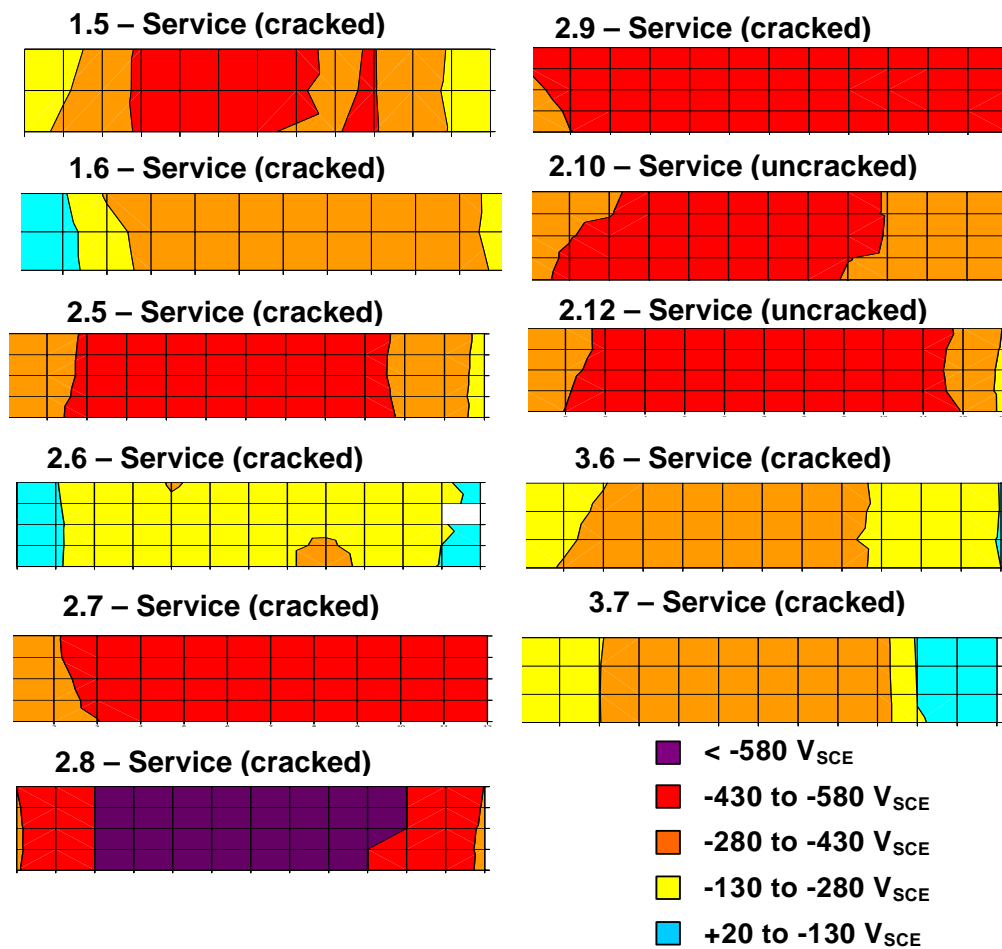


**Figure 4.24 Half-Cell Potential Contour Maps at 1235 Days for All Phase II Beams**

After half-cell potential readings had been analyzed from the Phase II specimen plots the following main conclusions were drawn:

- Performance of mixed reinforced (2/3 PS) specimen is closer to that of a non-prestressed specimen than to a fully prestressed specimen.
- High Performance concrete, appears to perform slightly better than Class C concrete with cement replacement by Fly Ash. However, the difference is not significant.
- Phase II series lacked a control specimen with Class C concrete without fly ash. Therefore, the effect of fly ash concrete and high performance concrete could not be directly evaluated against common practice.

### 4.3 CORROSION RATE MEASUREMENTS

The procedure and theory for the corrosion rate measurements is explained in Section 3.4. Four measurements were taking up to the forensic examination date. Two types of equipment were used: PR Monitor and 3LP. Phase I specimen measurements were taken at seven, twelve, fifteen and forty-seven months of exposure. Phase II specimen measurements were taken at 37 months of exposure. Difficulties with the measurement equipment did not permit taking of readings immediately prior to autopsy. The following discussion of corrosion rate results was reported in Reference 6.

### 4.3.1 Phase I Beam Measurements

Corrosion rate measurements of all the Phase I beams were performed after seven months of exposure testing using the PR Monitor equipment. Readings were taken midway (one week) through the dry portion of the exposure cycle. Corrosion rate measurements were performed after twelve months of exposure testing using the 3LP equipment. Readings were taken on day five of the two-week dry portion of the exposure cycle. The next measurements were performed after fifteen months of exposure testing using both the PR Monitor and 3LP equipment. Readings were taken sixteen days after the start of the dry portion of the exposure cycle (the dry period was extended beyond the normal two weeks because work was being performed on the beams). The final successful corrosion rate measurements of the Phase I beams were performed after 47 months of exposure testing using the 3LP equipment.

As recommended in the SHRP Procedure Manual for Condition Evaluation of Bridges,<sup>25</sup> a proportionality constant, B, of 26 mV was used in the calculation of the corrosion current when the 3LP equipment was used. This assumption was made so the interpretation guidelines in Table 3.3 (shown on each graph) could be used to rank the corrosion severity according to the measurements.

Corrosion rate readings, in terms of corrosion current density, for the Phase I autopsy beams are shown in Figures 4.25 and 4.26, and are listed in Table 4.3. Graphs of the corrosion rate readings of all the Phase I beams can be found in Appendix F.

Figure 4.25 is a graph of the maximum corrosion rate readings taken of the Phase I autopsy beams using the PR Monitor equipment. The graph shows a consistent trend that the corrosion rate decreased over time. This does not make practical sense. Therefore, further investigation of the corrosion rate readings will be made after the forensic examination to determine the reliability of the use of the PR Monitor equipment as a means of assessing corrosion rate. Through comparison of the three 100%U PS beams, both sets of readings show that the corrosion rate increases as the applied load, which corresponds to crack width increases.

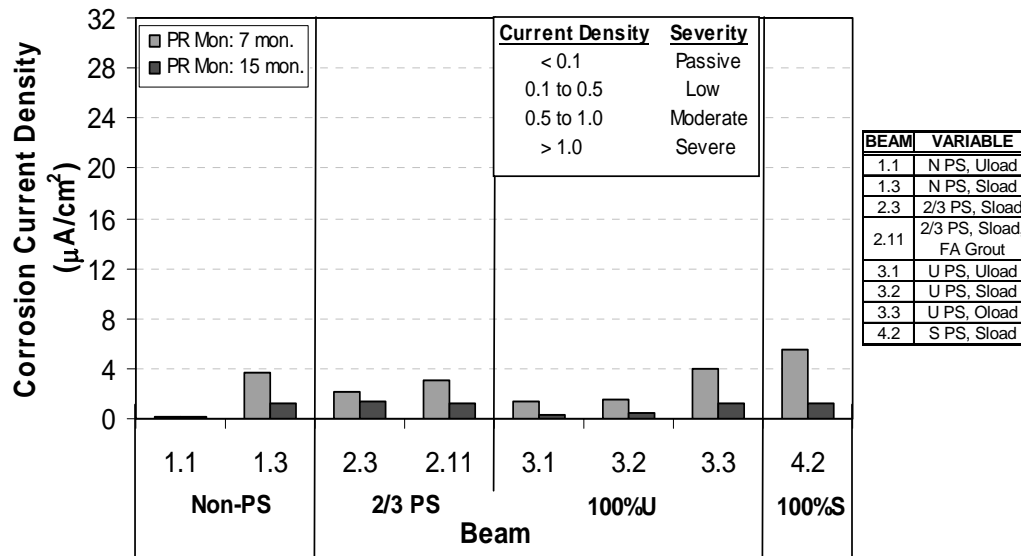


Figure 4.25 Maximum Corrosion Rate Readings Using PR Monitor for Phase I Autopsy Beams<sup>6</sup>

Figure 4.26 is a graph of all the maximum corrosion rate readings taken of the Phase I autopsy beams using the 3LP equipment. The graph shows a consistent trend that the corrosion rate increased over time, with the exception of Specimen 3.1. Again, comparison of the 100%U PS sections show increasing corrosion rates with increasing applied load. There is a significant increase from Specimen 3.2 (uncracked) to Specimen 3.3 (cracked).

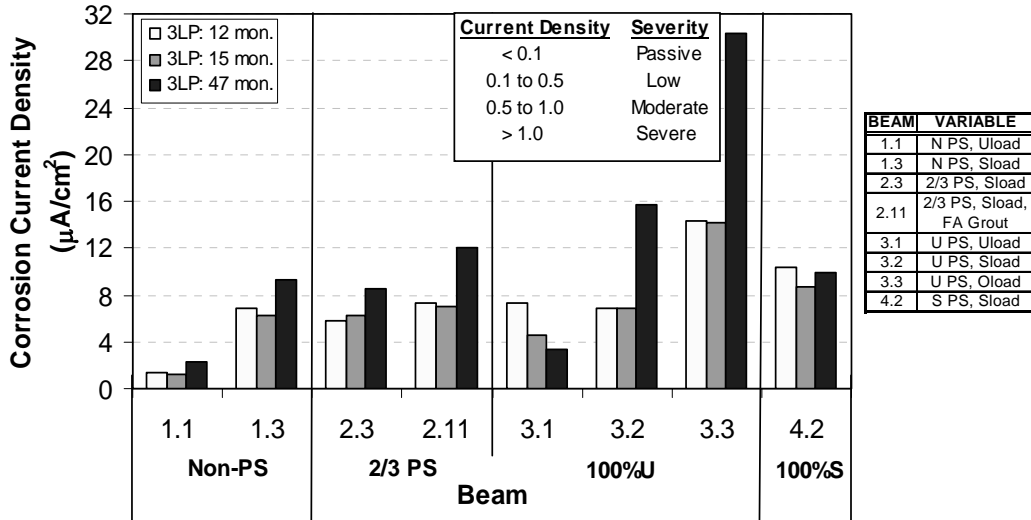


Figure 4.26 Maximum Corrosion Rate Readings Using 3LP for Phase I Autopsy Beams<sup>6</sup>

The corrosion severities determined in Table 4.3 are based on the last corrosion rate readings taken with the PR Monitor equipment. All readings taken with the 3LP equipment are extremely high, showing severe corrosion for all measurements. This indicates that, although they can be used to make relative comparisons and identify trends, readings using the 3LP are not reliable for determining actual corrosion rates and severities. For this reason, the corrosion severities assigned were based on the most recent reading taken with the PR Monitor.

Table 4.3 Phase I Autopsy Beam Corrosion Current Density Measurements<sup>6</sup>

Beam & Location	7 months	12 months	15 months		47 months	Corrosion Severity at 15 Months
	PR Monitor µA/cm <sup>2</sup>	3LP µA/cm <sup>2</sup>	PR Monitor µA/cm <sup>2</sup>	3LP µA/cm <sup>2</sup>	3LP µA/cm <sup>2</sup>	
1.1: Offset	0.18	1.31	0.19	1.15	2.32	Low
Midspan	0.20	1.09	0.12	0.76	1.21	Low
1.3: Offset	3.70	6.83	1.29	6.29	9.27	Severe
Midspan	1.07	4.64	1.06	3.50	8.03	Severe
2.3: Offset	2.17	5.85	1.43	4.79	8.02	Severe
Midspan	1.53	4.93	0.47	6.32	8.52	Low
2.11: Offset	1.90	7.39	1.16	7.08	11.28	Severe
Midspan	3.09	6.61	1.26	6.70	12.07	Severe
3.1: Offset	1.29	7.06	0.31	4.62	3.03	Low
Midspan	1.34	7.37	0.14	4.44	3.30	Low
3.2: Offset	1.42	6.33	0.42	6.83	15.74	Low
Midspan	1.49	6.84	0.31	5.43	7.46	Low
3.3: Offset	0.99	7.50	0.45	6.56	5.62	Low
Midspan	3.92	14.27	1.21	14.14	30.32	Severe
4.2: Offset	4.95	10.31	1.21	8.75	9.43	Severe
Midspan	5.58	9.47	1.06	7.16	9.86	Severe

### 4.3.1.1 Differences Between 3LP and PR Monitor Corrosion Rates

The PR Monitor and 3LP equipment both use the three electrode technique for measuring polarization resistance. However, several differences exist between the two pieces of equipment. The 3LP equipment represents the first generation of polarization resistance equipment for measuring corrosion rates of steel in concrete. The PR Monitor reflects several advancements, including the use of a guard ring electrode to confine the polarizing signal of the counter electrode, and measurement of the concrete resistance to compensate for solution resistance. The possible effects of these differences are discussed in West.<sup>2</sup>

Figure 4.27 is a graph of maximum corrosion rate readings taken after 15 months of exposure. The purpose of this graph is to compare the two types of equipment used for taking the readings over the duration of this experimental program. The 3LP corrosion rates measured after fifteen months of testing are significantly higher than the PR Monitor corrosion rates. Other research and field experience with various devices for corrosion rate measurement have consistently shown that the 3LP equipment indicates higher corrosion rates than other devices.<sup>2</sup> Although there is a large difference in the readings from the two types of equipment, the trends in corrosion activity are similar. This suggests that the large discrepancy in magnitude is likely due to inherent differences between the two devices. Although the magnitude measured by the 3LP equipment may not be reliable, it appears to be a good method for determining corrosion trends of individual specimens and comparing these trends among multiple specimens.

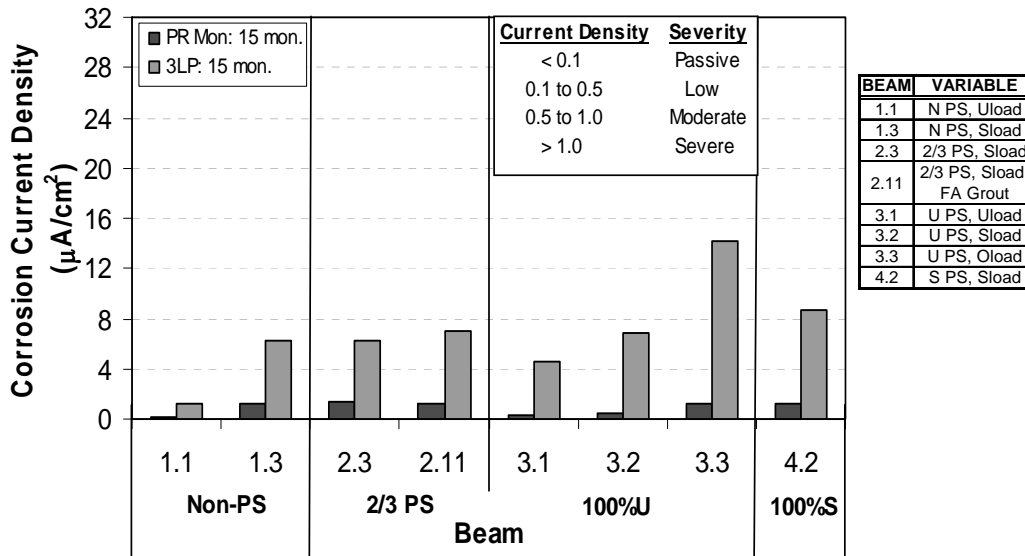
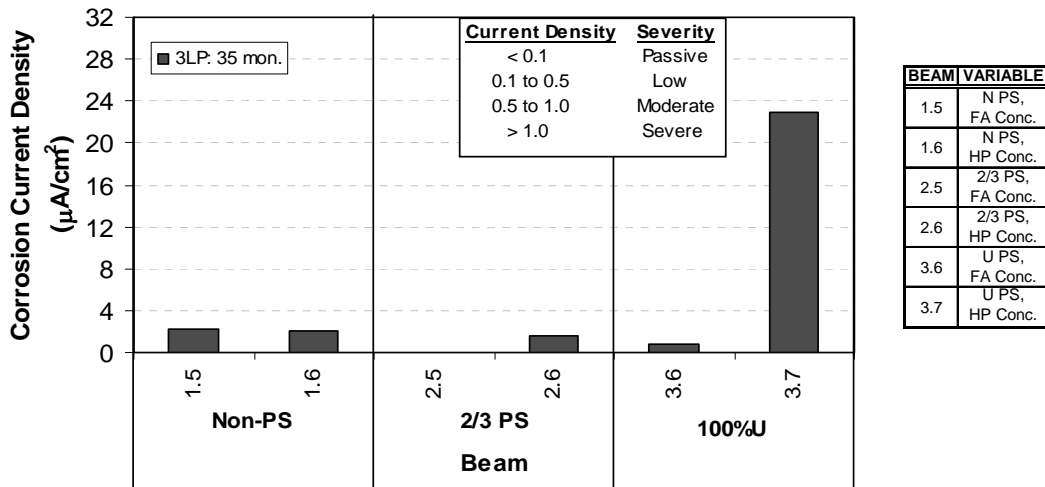


Figure 4.27 Comparison of Corrosion Rate Measurement Equipment<sup>6</sup>

### 4.3.2 Phase II Beam Measurements

Only one successful set of corrosion rate readings was obtained for the Phase II beams. They were performed after 35 months of exposure testing using the 3LP equipment. As with the measurements of the Phase I beams, a proportionality constant, B, of 26 mV was used in the corrosion current calculations. Corrosion rate readings, in terms of corrosion current density, for the Phase II autopsy beams are plotted in Figure 4.28 and listed in Table 4.4. A graph of the corrosion rate readings for all Phase II beams can be found in Appendix F.

Figure 4.28 shows higher corrosion rates in the 100%U PS than the 2/3 PS beams for both concrete types. Specimen 3.7 is significantly higher than all the other readings. The reason for this will be determined after the forensic examination. The readings do not show a consistently better concrete type. Since only one set of measurements was obtained, comparisons among readings over time or between equipment cannot be made for the Phase II specimens.



**Figure 4.28 Corrosion Rate Readings Using 3LP for Phase II Autopsy Beams<sup>6</sup>**

Because corrosion severities were only assigned according to readings taken with the PR Monitor, and no readings of the Phase II beams were taken using this equipment, corrosion severities could not be assigned to the Phase II beams in Table 4.4.

**Table 4.4 Phase II Autopsy Beam Corrosion Current Density Measurements<sup>6</sup>**

Beam & Location		35 months 3LP µA/cm <sup>2</sup>
1.5:	Offset	2.17
	Midspan	2.01
1.6:	Offset	1.86
	Midspan	2.05
2.5:	Offset	0.06
	Midspan	0.07
2.6:	Offset	1.45
	Midspan	1.55
3.6:	Offset	no reading
	Midspan	0.78
3.7:	Offset	9.66
	Midspan	22.90

#### 4.4 CHLORIDE CONTENT ANALYSIS

Acid Soluble Chloride Analysis was performed as described in Section 3.5. Samples were taken at the following dates:

- From Phase I Concrete Blocks: Seven, fourteen, forty-one and fifty-four months of exposure testing.
- From Phase II Concrete Blocks: Twenty-nine and forty-two months of exposure testing.

- From Autopsy Beam Specimens: Immediately prior to forensic examination.

Chloride Threshold value is indicated in the figures at 0.033%. This value, intended as a guide only, is based on the widely accepted chloride threshold value of 0.2% of the weight of cement.<sup>27</sup>

#### 4.4.1 Phase I Concrete Block Specimens

All Phase I specimens were constructed with Standard TxDOT Class C Concrete. However, concrete mixtures varied a little, which was the purpose of casting and testing the different block specimens. Figure 4.29 shows the acid soluble chloride content at different depths from the Phase I Pondered Block Specimens, representing only autopsy beams. The same results are presented in Table 4.5. Each block may have also represented non-autopsy beams, since various specimens were casted from the same batch of concrete. Appendix G includes the acid soluble chloride content graphs for all concrete blocks.

In addition to pondered blocks, control blocks were also constructed and analyzed for chloride content. Concrete blocks were maintained without saltwater ponding. As expected, control blocks showed negligible chloride content at all depths.

From the chloride content graphs for Phase I concrete pondered blocks it is concluded that:

- Chloride content decreases with depth.
- All the chloride contents at the bar level are below the threshold for corrosion, except for Specimen 1.1 and 1.3 after 54 months.
- Although all specimens were made of TxDOT Class C Concrete (same concrete mix), concrete in Beam 4.2 consistently shows the highest permeability, and that used in Beams 2.3 and 2.11 consistently shows the lowest permeability.

**Table 4.5 Phase I Pondered Block Chloride Penetration Measurements<sup>6</sup>**

Beams Represented	Depth (inches)	Acid Soluble Chloride Content (% by weight of concrete)			
		7 months	14 months	41 months	54 months
1.1, 1.3	0.5	0.0000	0.0152	0.0774	0.1399
	1.0	0.0000	0.0000	0.0300	0.0982
	2.0	0.0000	0.0000	0.0112	0.0490
2.3, 2.11	0.5	0.0000	0.0086	0.0029	0.0862
	1.0	0.0000	0.0000	0.0027	0.0068
	2.0	0.0000	0.0000	0.0035	0.0031
3.1, 3.2, 3.3	0.5	0.0004	0.0013	0.1586	0.1303
	1.0	0.0000	0.0000	0.0417	0.0501
	2.0	0.0000	0.0000	0.0125	0.0039
4.2	0.5	0.0004	0.0440	0.1904	0.2149
	1.0	0.0001	0.0000	0.0994	0.1162
	2.0	0.0000	0.0000	0.0250	0.0048

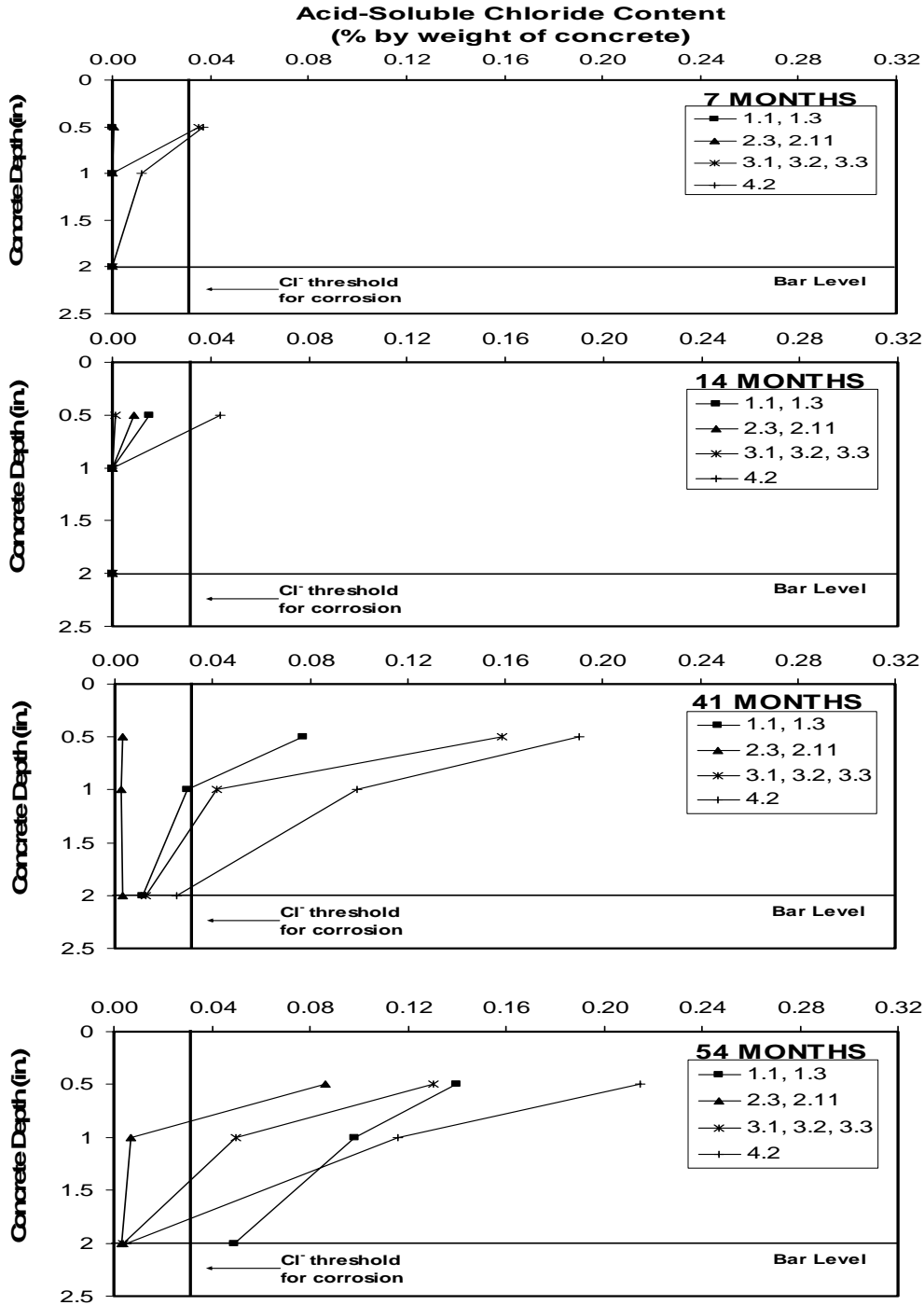


Figure 4.29 Acid-Soluble Chloride Content for Phase I Ponded Block Specimens<sup>6</sup>

#### 4.4.2 Phase II Concrete Block Specimens

Figure 4.30 shows the acid soluble chloride content for Phase II Ponded Block Specimens representing autopsy beams. The same information is presented in Table 4.6. For these series, concrete type is the main variable. Again, as in the previous case, control blocks show negligible chloride content at all depths. Plots of the chloride content results for all the blocks can be found in Appendix G.

From these results it is found that:

- Acid-soluble chloride content progressively increases over time and decreases with depth, as expected.
- All chloride contents at one-inch and two-inch (bar level) depths are well below the threshold for corrosion and show little variation between the concrete types.
- Results at 0.5 inches after 29 and 42 months of exposure confirm that the high performance concrete was less permeable.

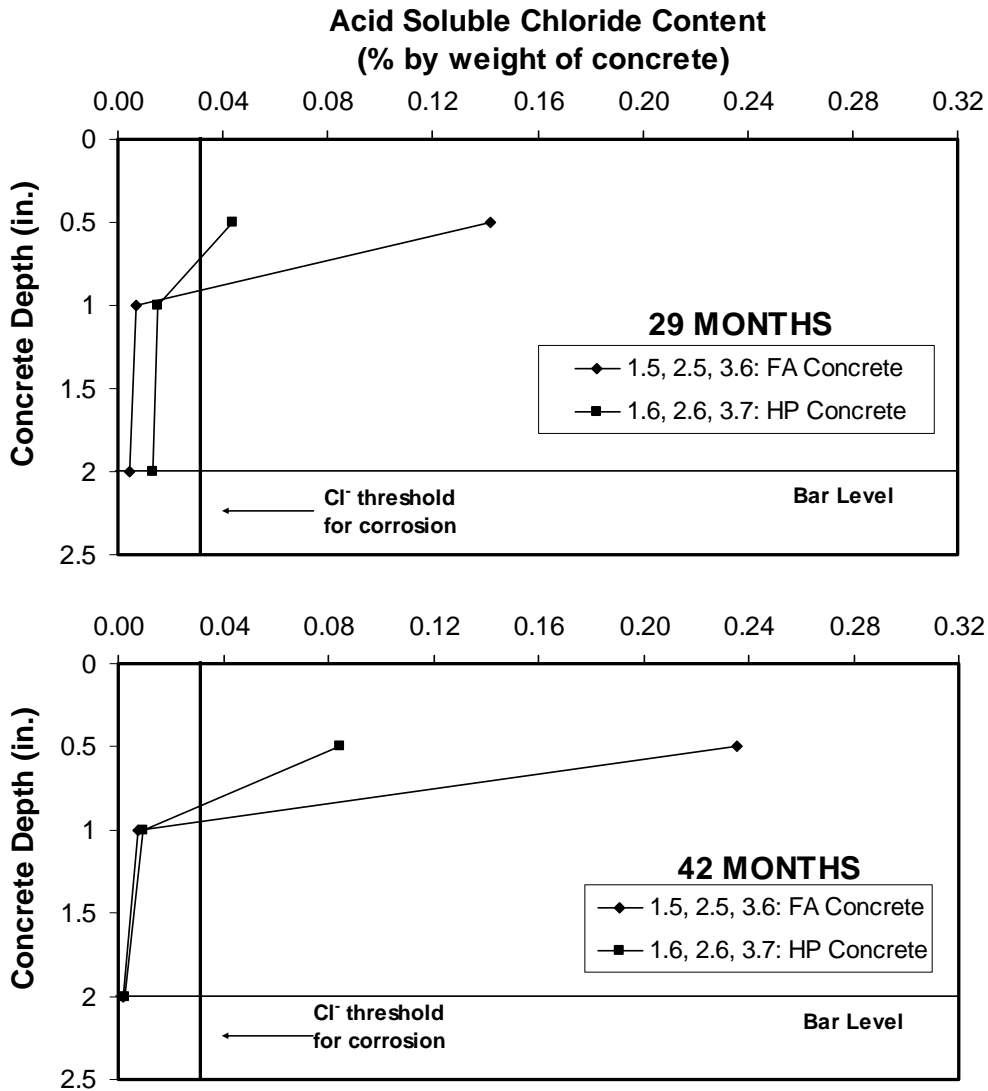


Figure 4.30 Acid-Soluble Chloride Content for Phase II Poned Block Specimens<sup>6</sup>



**Table 4.6 Phase II Ponded Block Chloride Penetration Measurements<sup>6</sup>**

Beams Represented	Depths (inches)	Acid-Soluble Chloride Content (% by weight of concrete)	
		29 months	42 months
1.5, 2.5, 3.6	0.5	0.1422	0.2359
	1.0	0.0072	0.0078
	2.0	0.0046	0.0017
1.6, 2.6, 3.7	0.5	0.0439	0.0846
	1.0	0.0151	0.0097
	2.0	0.0133	0.0025

#### 4.4.3 Phase I Autopsy Beam Specimens

As described in Section 4.4.1, all Phase I beams were made of Standard TxDOT Class C Concrete. Figure 4.31 shows the beam and block chloride content plots at 1594 days (end of testing for autopsy beams), in the ponded region. Block chloride content is shown again for comparison. As shown on this graph, higher chloride content was found on the beams, in comparison to their corresponding blocks. The reason for this difference could be the result of cracking, which would allow ease of chloride ingress. This is clear in Specimen 1.3, since both concrete samples were taken at crack locations. The three-inch offset samples for Specimens 2.11 and 4.2 were also taken at crack locations, which would explain their high values at the bar level since the values from their blocks is essentially zero.

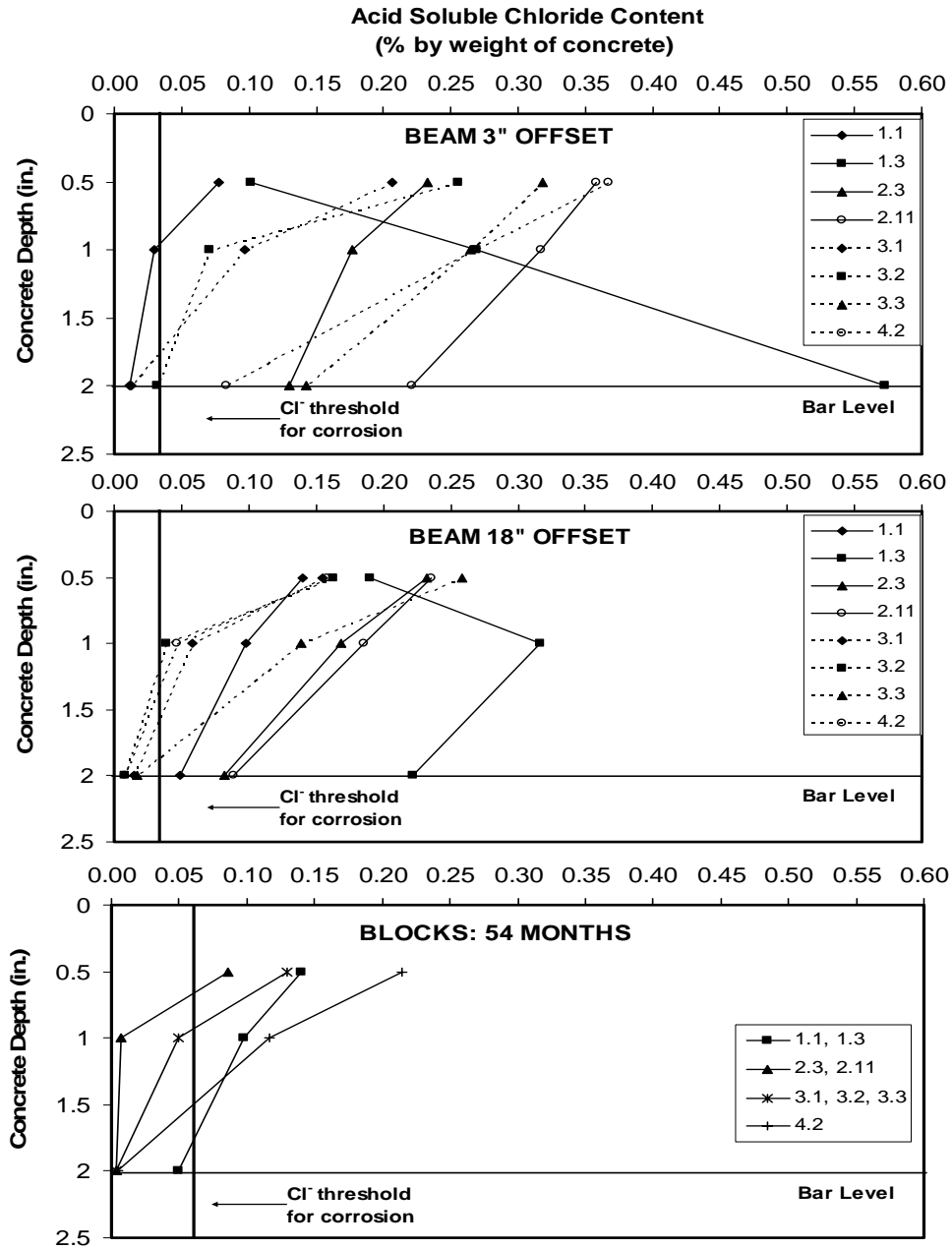
Figure 4.32 shows similar data for those samples taken outside the ponded region on the beams (at 27-inch and 32-inch offset). From this graph it is observed that most measurements at the bar level at both locations are at or below the threshold, with the exception of Specimen 1.3 whose 32-inch sample was taken at a crack location. Generally, chloride levels at the one-inch depth of the Non-PS and 2/3 PS beams are significantly higher at the 27-inch offset (immediately outside the ponded region) in comparison with those from the 32-inch offset. This is not observed in the 100% PS beam, which suggests that the horizontal propagation of chlorides decreases with increasing levels of prestress.

Table 4.7 shows the results in a tabular form, for all Phase I autopsy beam acid-soluble chloride contents.

Figure 4.33 shows the chloride content results at the bar and top-of-duct level (at the two-inch depth from the concrete surface), after 1594 days of exposure.

The following results are found:

- Chloride content in the ponded region is consistently higher at the bar level than outside the ponded region.
- Unloaded and uncracked specimens (1.3 and 3.1) show very low chloride contents at all locations.
- Measurements taken at crack locations give significantly larger chloride content values, as in the case of Specimens 1.3 and 2.3 at the three-inch offset.
- An increase in the level of prestress results in lower chloride contents due to fewer cracks and higher compressive stresses in the concrete.
- Minimal difference is observed in the performance of the 100%S and 100%U PS beams. The larger value from the 100%U PS beam at the three-inch offset location is due to the small crack at the sample locations.



**Figure 4.31 Beam and Block Chloride Penetration at 1594 Days  
for Phase I – Ponded Region on Beams<sup>6</sup>**

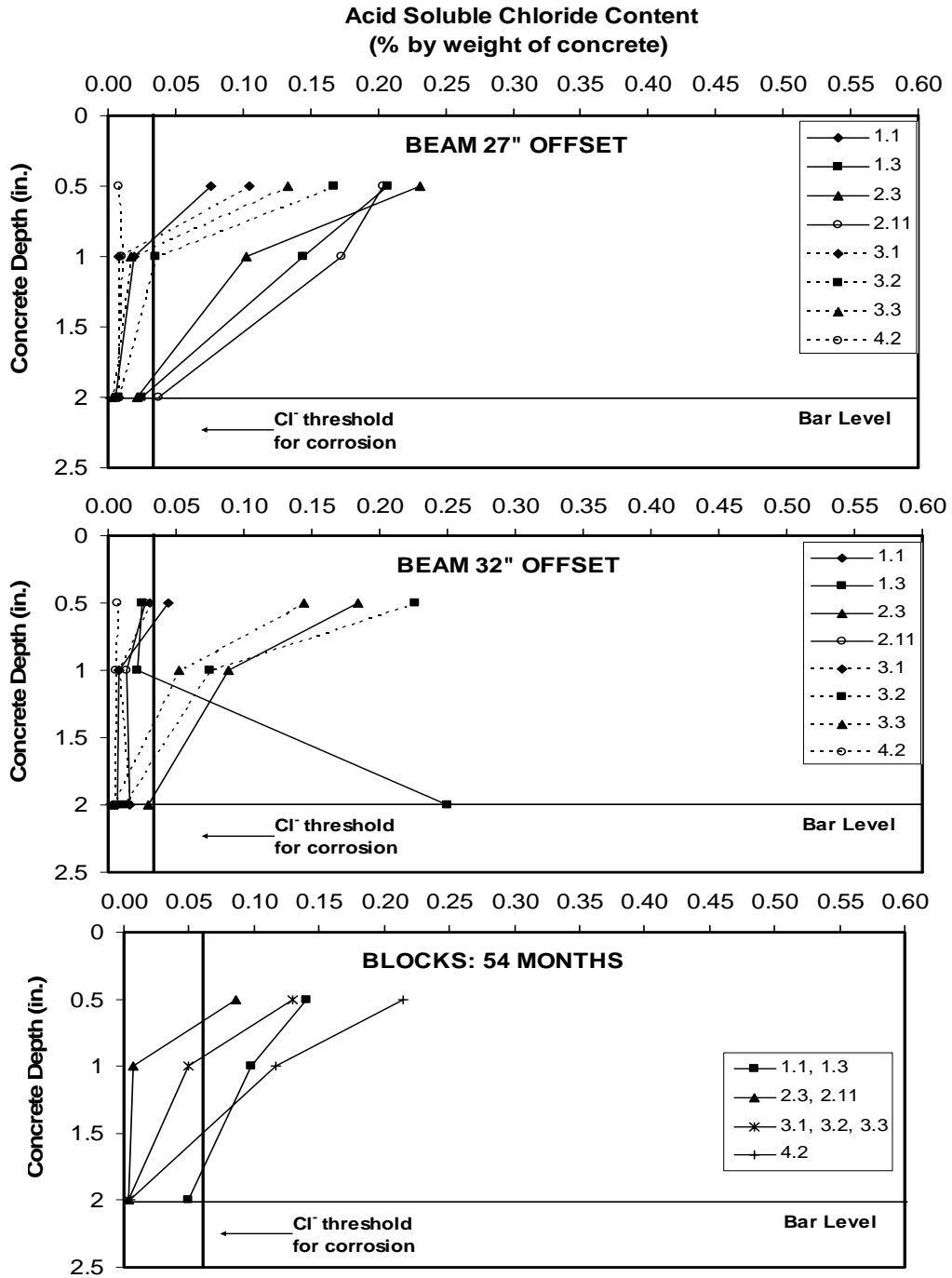


**Figure 4.32 Beam and Block Chloride Penetration at 1594 Days for Phase I – Unponded Region on Beams<sup>6</sup>**

**Table 4.7 Phase I Autopsy Beam Chloride Penetration Measurements<sup>6</sup>**

Beam	Depth (inches)	Chloride Content (% by weight of concrete)			
		3" Offset	18" Offset	27" Offset	32" Offset
1.1	0.5	0.0774	0.1399	0.0757	0.0448
	1.0	0.0300	0.0982	0.0199	0.0080
	2.0	0.112	0.0490	0.0058	0.0064
1.3	0.5	0.1020	0.1901	0.2070	0.0250
	1.0	0.2695	0.3169	0.1447	0.0219
	2.0	0.5729	0.2216	0.0250	0.2496
2.3	0.5	0.2326	0.2326	0.2306	0.1836
	1.0	0.1765	0.1689	0.1025	0.0883
	2.0	0.1299	0.0820	0.0214	0.0296
2.11	0.5	0.3583	0.2352	0.2038	0.0277
	1.0	0.3173	0.1852	0.1735	0.0138
	2.0	0.2213	0.0890	0.0373	0.0157
3.1	0.5	0.2064	0.1547	0.1047	0.0307
	1.0	0.0965	0.0583	0.0082	0.0079
	2.0	0.0120	0.0150	0.0076	0.0154
3.2	0.5	0.2557	0.1626	0.1676	0.2258
	1.0	0.0712	0.0384	0.0355	0.0746
	2.0	0.0317	0.0079	0.0084	0.0116
3.3	0.5	0.3182	0.2581	0.1330	0.1445
	1.0	0.2641	0.1389	0.0171	0.0520
	2.0	0.1424	0.0169	0.0030	0.0031
4.2	0.5	0.3675	0.1583	0.0082	0.0064
	1.0	0.2668	0.0464	0.0097	0.0054
	2.0	0.0837	0.0084	0.0064	0.0050

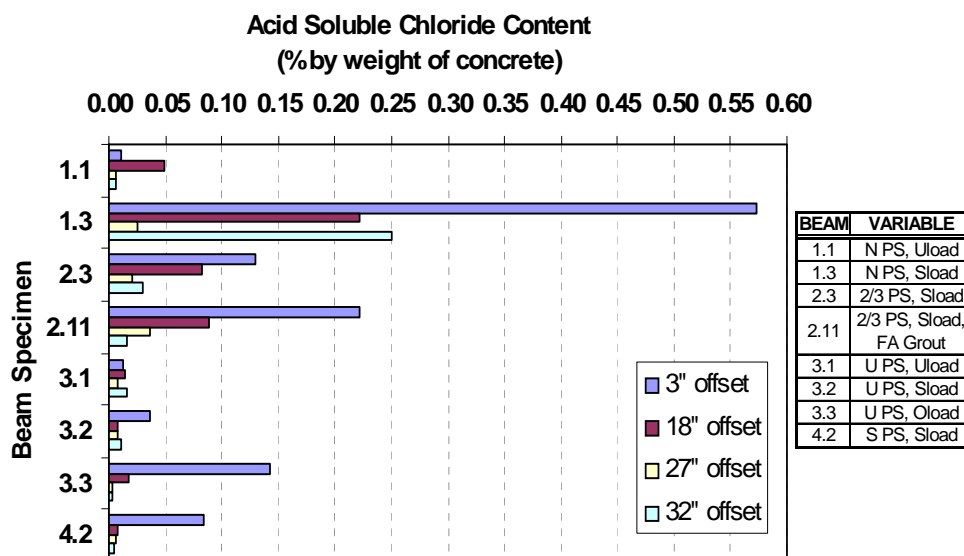


**Figure 4.33 Acid-Soluble Chloride Content at Bar and Top-of-Duct Level for Phase I Beams<sup>6</sup>**

#### ***4.4.4 Phase II Autopsy Beam Specimens***

Concrete type is the only variable of interest when comparing Phase II autopsy beams, since all were loaded at the service load level. Figure 4.34 shows the beam and block chloride content plots at 1235 days (end of testing for autopsy beams), in the ponded region. Block chloride content is shown again for comparison. As can be observed, high performance concrete specimens consistently shows as the superior concrete type in both the beam and block specimens at 0.5 inch and one-inch depth. All samples from inside the ponded region at the bar level show negligible chloride contents, implying that both types of concrete are effective in limiting chloride penetration for this time period.

Figure 4.35 shows similar data for those samples taken outside the ponded region on the beams (at 27-inch and 32-inch offset). From this graph it is observed that most measurements taken outside the ponded region of the Phase II specimens show negligible chloride contents. The only notable measurements were found in the fly ash concrete specimens, supporting the above conclusion that high performance concrete appears to be superior.

When comparing concrete block results with beam results, it is observed that inside the ponded region, chloride contents from the blocks are unconservative for beams 1.5 (Non-PS, Fly Ash Concrete) and 2.5 (2/3 PS, Fly Ash Concrete), at the one-inch depth, but very approximate at all depths for beams 1.6 (Non-PS, High Performance HP Concrete), 2.6 (2/3 PS, HP Concrete) and 3.7 (100%U PS, HP Concrete). In general, actual chloride contents at the two-inch depth were slightly higher than those measured from the concrete blocks.

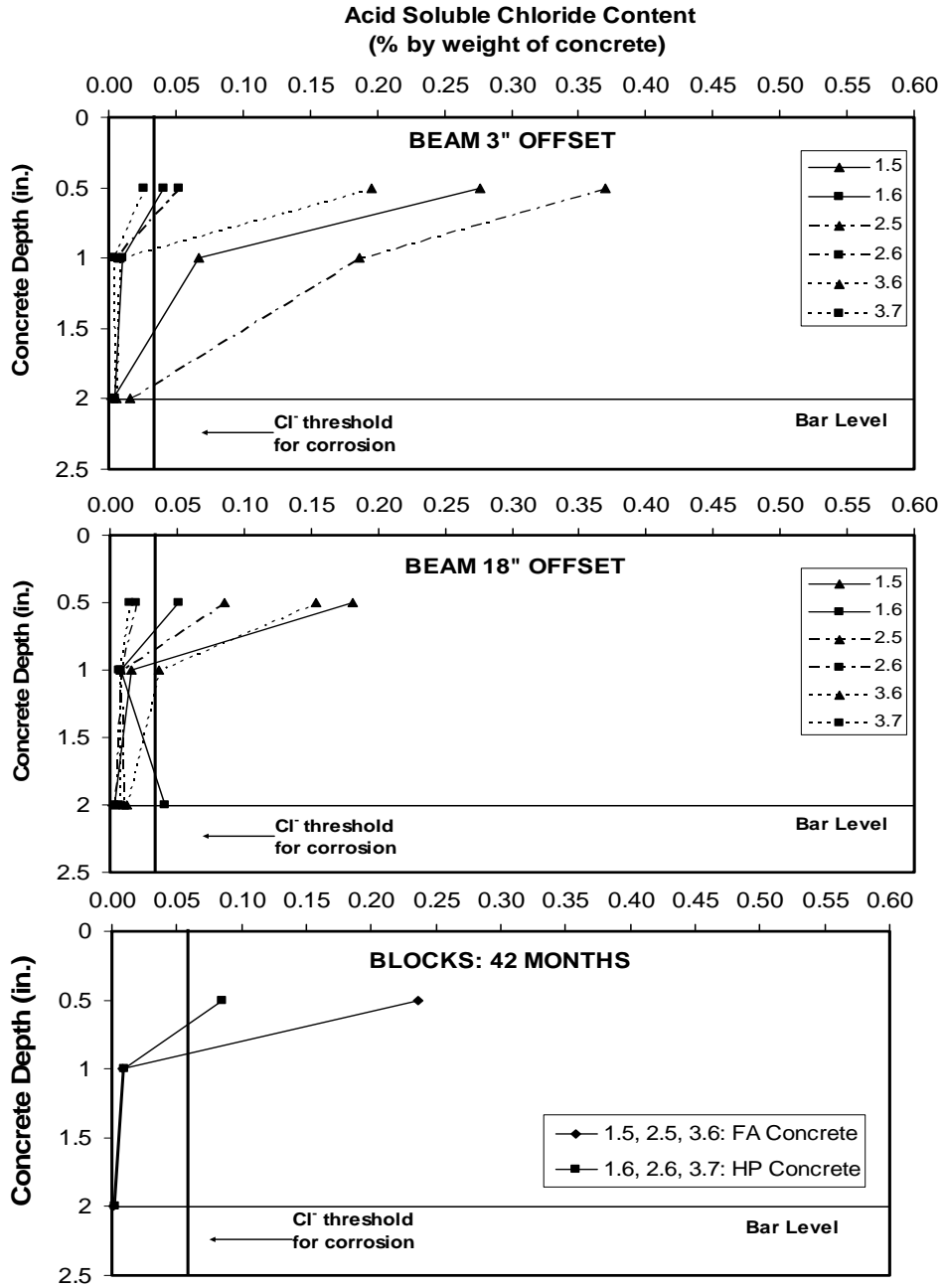


**Figure 4.34 Beam and Block Chloride Penetration at 1235 Days for Phase II – Ponded Region on Beams<sup>4,5</sup>**

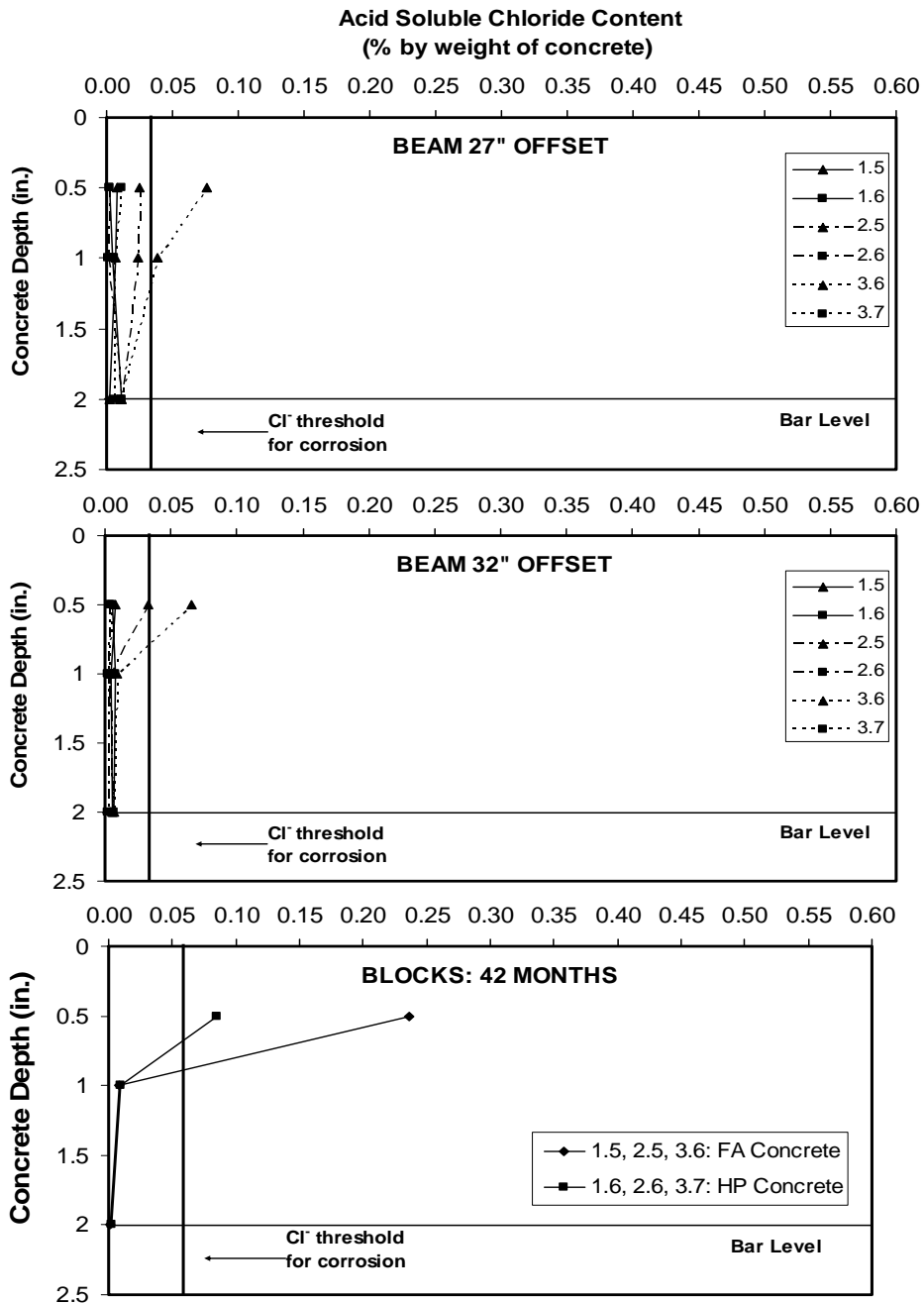


Figure 4.35 Beam and Block Chloride Penetration at 1235 Days for Phase II – Unponded Region on Beams<sup>6</sup>

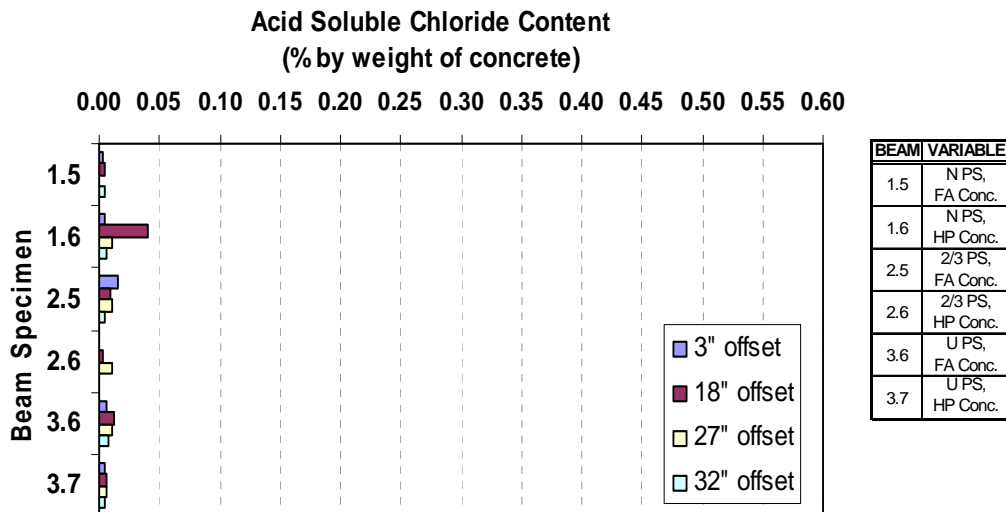
Table 4.8 shows the results from Figures 4.34 and 4.35 in a tabular form, for all Phase II autopsy beam acid-soluble chloride contents.

Figure 4.36 shows the chloride content results at the bar and top-of-duct level (at the two-inch depth from the concrete surface), after 1235 days of exposure.

**Table 4.8 Phase II Autopsy Beam Chloride Penetration Measurements<sup>6</sup>**

Beam	Depth (inches)	Chloride Content (% by weight of concrete)			
		3" Offset	18" Offset	27" Offset	32" Offset
1.5	0.5	0.2770	0.1810	0.0076	0.0077
	1.0	0.0674	0.0163	0.0067	0.0043
	2.0	0.0034	0.0039	0.0021	0.0052
1.6	0.5	0.0410	0.0515	0.0019	0.0057
	1.0	0.0108	0.0082	0.0048	0.0076
	2.0	0.0046	0.0409	0.0111	0.0066
2.5	0.5	0.3700	0.0854	0.0250	0.0333
	1.0	0.1868	0.0077	0.0236	0.0039
	2.0	0.0156	0.0099	0.0109	0.0051
2.6	0.5	0.0525	0.0196	0.0018	0.0029
	1.0	0.0030	0.0076	0.0015	0.0019
	2.0	no reading	0.0033	0.0114	0.0021
3.6	0.5	0.1959	0.1540	0.0766	0.0652
	1.0	0.0081	0.0366	0.0381	0.0089
	2.0	0.0058	0.0120	0.0103	0.0070
3.7	0.5	0.0263	0.0144	0.0116	0.0045
	1.0	0.0035	0.0066	0.0057	0.0040
	2.0	0.0040	0.0064	0.0056	0.0051

As observed from Figure 4.36, it is confirmed that acid-soluble chloride contents at the bar and top-of-duct level of the Phase II beams are very low, with respect to the chloride threshold value of 0.033%, meaning that the use of fly ash concrete and high performance concrete are effective in minimizing the penetration of chlorides through the concrete matrix.



**Figure 4.36 Acid-Soluble Chloride Content at Bar and Top-of-Duct Level for Phase II Beams<sup>6</sup>**



## CHAPTER 5: FORENSIC EXAMINATION

After four and a half years of exposure testing for Phase I Beam Specimens and three and a half years for Phase II Beam Specimens, a detailed visual inspection of the exterior condition was performed on all 27 specimens, and exposure testing data were thoroughly analyzed. Based on this evaluation, it was decided to perform a forensic examination that included full and partial autopsies of approximately half of the beams. The forensic examination was performed according to the program objectives, which relate to the evaluation of the effect of post-tensioning on durability, and the evaluation of the relative performance of a large number of corrosion protection variables including prestress level and crack width, duct splices, grout type, concrete type, strand type, duct type, and end anchorage protection.

Specific forensic examination objectives were as follows:

1. To obtain visual evaluation of the overall exterior condition of beam specimens.
2. To determine chloride ion penetration through the concrete.
3. To obtain visual evaluation of corrosion damage on duct, duct splice, strand and mild steel reinforcement.
4. To determine chloride ion content in the grout.
5. To determine the most effective variables in corrosion protection.

### 5.1 AUTOPSY PROCEDURE

#### 5.1.1 Specimen Selection for Forensic Examination

Originally, all beam specimens were scheduled for full autopsy in May 2002. This date marked four and a half or three and a half years of exposure testing for Phase I and Phase II beams, respectively. However, results from the final segmental joint macrocell durability tests,<sup>7</sup> suggested that for a modest extension of the exposure testing program, it would be possible to obtain increased benefit from the full-size durability specimens. Half of the duplicated macrocell specimens were autopsied after four and a half years of very aggressive exposure. The remaining duplicates were autopsied after eight years of exposure. When the results from the longer exposure period were compared with the preliminary conclusions reported after four years of exposure testing, it was found that a number of significant changes had occurred. For example, while no corrosion had been found after four and a half years in epoxy jointed specimens, after eight years there was some corrosion (away from the joint) in epoxy jointed specimens and there was corrosion at one epoxy joint that was found to be incompletely filled with epoxy. More importantly, after eight years there was extremely large destruction of galvanized duct and clear indication of the superiority of the plastic duct, an aspect that was not so evident after the first autopsy. If all exposure testing had been halted after four and a half years in the macrocell series, a great deal of important information would have been missed.

For the above reason, it was decided to select approximately half of the beam specimens for autopsy in May 2002. Twelve out of the total of twenty-seven specimens in Phase I and Phase II were selected for full autopsy, while two specimens were selected for partial autopsy. The remaining specimens were left under continuous exposure testing for future autopsy. Tables 5.1 and 5.2, and Figure 5.1 show the specimens selected for examination and the corresponding test variables. The autopsy specimen selection was made based on visual inspection, measurements taken during exposure testing and the necessity for comparison of the test variables.

Specimens 1.1 and 3.1 were selected for partial autopsy, since they would be needed for both the present and future autopsies because they were the only uncracked and unloaded specimens. Thus, they served as control specimens for comparison. Since these beams were not loaded or cracked, a portion of the specimen could be removed while the remainder was returned to the exposure testing. The partial autopsy consisted of exposing and removing half of the mild steel/duct/strand section that was completely removed for each fully autopsied beam, leaving the other half for continued exposure testing.

**Table 5.1 Phase I Beams Selected for Forensic Examination<sup>7</sup>**

Specimen	Prestress Level	Cracking (mm)	Applied Load	Concrete Type	Splice Type	Damage to Duct	Grout type	Strand	PT Anchorage
1.1	Non-PS	Uncracked	Unloaded	(1)	--	--	--	--	--
1.3	Non-PS	0.3	Constant Service	(1)	--	--	--	--	--
2.3	2/3 PS	0.2	Constant Service	(1)	(2)	(3)	(4)	(7)	(8)
2.11	2/3 PS	0.2	Constant Service	(1)	(2)	None	Fly Ash (5)	(7)	(8)
3.1	100% U PS	Uncracked	Unloaded	(1)	(2)	None	(4)	(7)	(9)
3.2	100% U PS	Uncracked	Constant Service	(1)	(2)	None	(4)	(7)	(9)
3.3	100% U PS	Cracked	124% - Return to Service	(1)	(6)	None	(4)	(7)	(9)
4.2	100% S PS	Uncracked	Constant Service	(1)	(2)	(3)	(4)	(7)	(10)




- (1) TxDOT Class C (0.45 w/c, cement Type I, retarder, air entrainment agent)
- (2) Industry Standard (IS) and Heat Shrink (HS)
- (3) IS with damage and HS with damage
- (4) TxDOT Class C (0.44 w/c, cement Type I, expanding admixture)
- (5) 0.33 w/c, 30% Fly Ash replacement.
- (6) Industry Standard (IS)
- (7) 7-wire 0.5 in. low relaxation (270 ksi) strand
- (8) VSL Type E5-3 (with third strand opening unused)
- (9) VSL Type E5-3
- (10) VSL Type E5-4

**Table 5.2 Phase II Beams Selected for Forensic Examination<sup>7</sup>**

Specimen	Prestress Level	Cracking (mm)	Applied Load	Concrete Type	Splice Type	Damage to Duct	Grout type	Strand	PT Anchorage
1.5	Non-PS	0.3	Constant Service	(11)	--	--	--	--	--
1.6	Non-PS	0.3	Constant Service	(12)	--	--	--	--	--
2.5	2/3 PS	0.2	Constant Service	(11)	(13)	None	(14)	(15)	(16)
2.6	2/3 PS	0.2	Constant Service	(12)	(13)	None	(14)	(15)	(16)
3.6	100% U PS	0.1	Constant Service	(11)	(13)	None	(14)	(15)	(17)
3.7	100% U PS	0.1	Constant Service	(12)	(13)	None	(14)	(15)	(17)

- (11) TxDOT Class C with Fly Ash (0.44 w/c, with 25% Class F Fly Ash)
- (12) High Performance (0.29 w/c, 25% Fly Ash, superplasticizer)
- (13) Industry Standard Splice (IS) and Heat Shrink Splice (HS)
- (14) TxDOT Class C (0.44 w/c, cement Type I, expanding admixture)
- (15) 7-wire 0.5 in. low relaxation (270 ksi) strand
- (16) VSL Type E5-3 (with third strand opening unused)
- (17) VSL Type E5-3

Main Variable		Section Type			
		Non-PS	2/3 PS	100%U	100%S
Phase I	Unloaded	1.1		3.1	
	Very Small Crack		2.1	3.2	
	Constant Service Load	1.2	2.2	3.3	4.1
	Constant Service Load (duplicate)	1.3	2.3	3.4	4.2
	Overload and Return to Service	1.4	2.4	3.5	
	High Performance Fly Ash Grout		2.11		
Phase II	Standard Concrete with 25% Fly Ash	1.5	2.5	3.6	
	High Performance Fly Ash Concrete	1.6	2.6	3.7	
	Epoxy Coated Strands		2.7		
	Galvanized Strands		2.8		
	Poor Grouting Procedures		2.9		
	High Performance Anti-Bleed Grout		2.10		
	Encapsulated System w/ Plastic Duct		2.12		

 Full autopsy    
 Partial Autopsy    
 Continue Testing

**Figure 5.1 Selected Beams for Forensic Examination<sup>7</sup>**

### 5.1.2 Specimen Condition at End of Testing

The appearance of the specimens can indicate corrosion activity. The exterior surface of each beam specimen was examined for signs of additional cracking, rust staining and concrete spalling.

### 5.1.3 Crack Measurements

One of the main objectives of the forensic examination was to determine the influence of cracking on specimen performance and reinforcement corrosion (onset of corrosion and propagation) due to chloride and moisture ingress. Crack widths were measured at the beginning of exposure (after post-tensioning and first loading) and at the end of exposure. The crack width measurement procedure and the results are described in Section 3.2 and Section 4.1, respectively.

### 5.1.4 Concrete Powder Samples for Chloride Analysis

Concrete Powder Samples were collected from concrete block and beam specimens to assess the chloride penetration. Powder samples were tested for their acid soluble chloride content. The procedure for obtaining the samples is explained in Section 3.5 and the results of the chloride analysis are given in Section 4.4.

### 5.1.5 Saw Cuts and Concrete Removal

#### 5.1.5.1 Full Autopsies

Analysis of duct, strand and mild steel was limited to a total length of 72 inches (42 inches from centerline to one side and 30 inches to the other side). Figure 5.2 shows a diagram of the section removed for investigation. The section included the entire 48-inch ponded region, and extended six inches outside the ponded region on one side and 18 inches on the other side. It was decided that this section would sufficiently provide the following information:

1. Reinforcement corrosion performance from the area in the ponded region

2. Possible horizontal penetration of chlorides through the concrete from the area immediately outside of the ponded region
3. A section of reinforcement not exposed to a corrosive environment for comparison

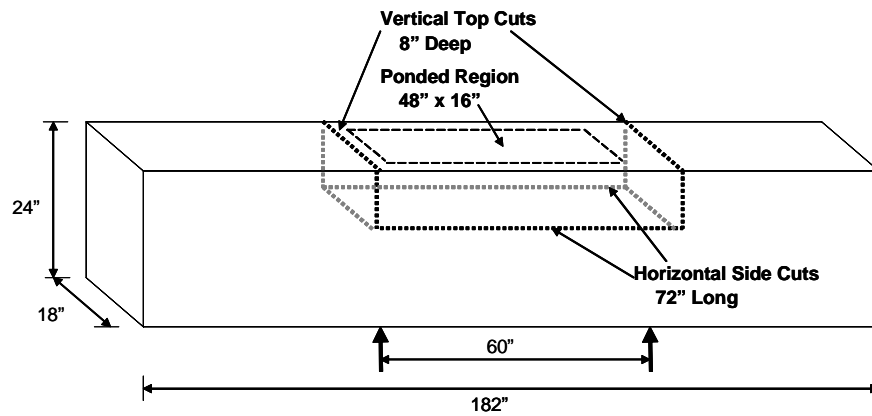


**Figure 5.2 Beam Section Removed for Investigation<sup>6</sup>**

The concrete saw with a 27-inch circular blade shown in Figure 5.3 was used to make all the cuts in the specimens. Two eight-inch deep vertical cuts were made on the top of the beam, and a horizontal cut was made on each side of the beam, below the duct line. These cuts separated the portion of the beam to be analyzed from the rest of the specimen, allowing the area of interest to be removed with a forklift.

Jack hammers and chipping hammers were used to carefully remove all existing concrete around post-tensioning ducts and mild steel reinforcement, as illustrated in Figure 5.4.



**Figure 5.3 Concrete Saw used in Autopsy<sup>6</sup>**



**Figure 5.4 Concrete Removal to Expose Duct and Mild Steel<sup>7</sup>**

### **5.1.5.2 Partial Autopsies**

The partial autopsy procedure consisted of exposing and removing half of the mild steel/duct/strand concrete section that was used for each fully autopsied beam, leaving the other half for continued exposure testing. Figure 5.5 shows one partial autopsied beam after the first half analysis portion has been removed. The beam had the cut section epoxied to seal the surface and was returned to exposure testing.

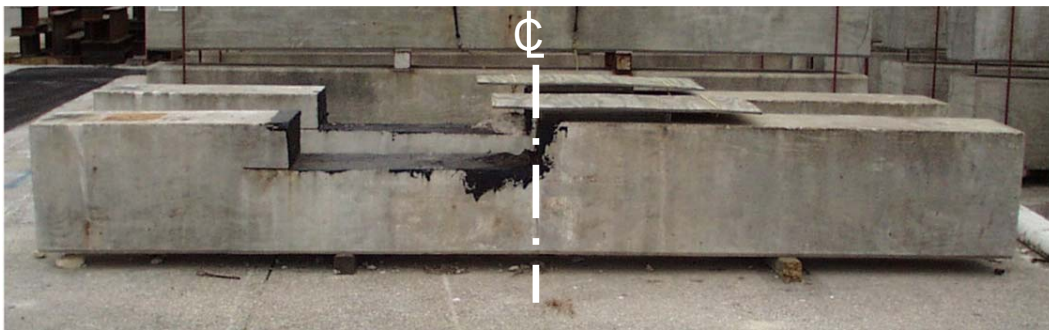


**Figure 5.5 Partial Autopsied Beam<sup>7</sup>**

### **5.1.6 Exposure and Removal of Ducts**

Metal duct was exposed after removing all concrete. The duct and strand were then removed from the concrete as one unit. Immediately after exposing the duct, the surface was examined for rust staining and color, salt collection and damage.

### **5.1.7 Splice Condition Examination**

Splices (Heat-Shrink or Industry Standard) were examined after removing the duct/strand piece. Splices were thoroughly inspected for corrosion, salt deposits, zinc corrosion products and rust staining.

### **5.1.8 Duct Opening and Grout Condition Examination**

After external splice examination, splices were cut open in half longitudinally, and the duct was also cut open by making two longitudinal cuts along the sides of the duct/strand using a small air grinder. The grout was examined for bleed water voids, incomplete duct filling and excessive porosity. Grout was also examined for cracking and any indication of moisture and chloride ingress. Since grout is injected after the stressing of post-tensioning steel, hardened grout is susceptible to service cracking due to deflections and vibrations.

### **5.1.9 Grout Samples for Chloride Analysis**

Grout Samples were collected from every duct at six-inch intervals over the entire length of 72 in. The grout pieces were crushed between two steel plates and ground into powder using a mortar and pestle. Powder samples were analyzed for acid-soluble chlorides using a specific ion probe (CL Test System by James Instrument).

### **5.1.10 Grout Removal and Strand Exposure**

After the desired grout samples were removed, the remainder of the grout was carefully removed, exposing the strand for examination. The extent and severity of corrosion on both the strand and duct was rated according to the corrosion rating scheme described in Section 5.2.

### **5.1.11 Mild Steel Exposure and Removal**

The mild steel bars and stirrups were removed after ducts had been removed, using the jackhammers and chipping hammers. Analysis of longitudinal steel was limited to 72 in. corresponding to the same analysis length used for the post-tensioning ducts and strands. Stirrups were analyzed only in the top portion and two 3 in. legs at each side, as shown in Figure 5.7.



**Figure 5.6 Mild Steel Reinforcement Cage**

## **5.2 EVALUATION AND CORROSION RATING SYSTEM USED DURING FORENSIC EXAMINATION**

After all steel elements were exposed and removed, they were thoroughly examined and rated. The rating system selected for evaluation was the same used for the Macrocell Corrosion Tests in TxDOT Project 0-1405. The procedure was created by West et al.<sup>28,29</sup> in a universal form with the intention of applying

the same rating system to various situations. For the beam corrosion tests, the length (72 inches) of longitudinal mild steel, duct and strand was subdivided into 36 two-inch intervals. At each interval, the steel was examined and a rating was assigned to describe the corrosion severity within that interval. By assigning a corrosion severity at 36 locations, both the extent and severity of corrosion are determined.

As described in West et al.<sup>28</sup> the rating system is essentially the same for prestressing strand, mild steel reinforcement and galvanized duct, with some modifications to reflect unique corrosion aspects of each type of steel. In general, the evaluation system doubles the severity rating for each category of increasing corrosion damage.

### 5.2.1 Mild Steel Reinforcement

The longitudinal mild steel was examined at 36 two-inch intervals, as indicated in Figure 5.7. Corrosion ratings were assigned to indicate for each interval or segment, the corrosion severity on both the top and bottom bar surfaces. The same procedure was applied to the stirrups, except the interval division varied slightly. As with the longitudinal bars, the top portion of stirrups was divided into 7 two-inch intervals. Due to the dimensions of the section removed from each beam for forensic examination, there were 2 three-inch sections (legs) from the sides of the stirrup to be analyzed. (see Figure 5.7) Each three-inch leg was considered one interval, for a total of nine intervals per stirrup. One rating was assigned to the inside and outside surfaces of each leg.

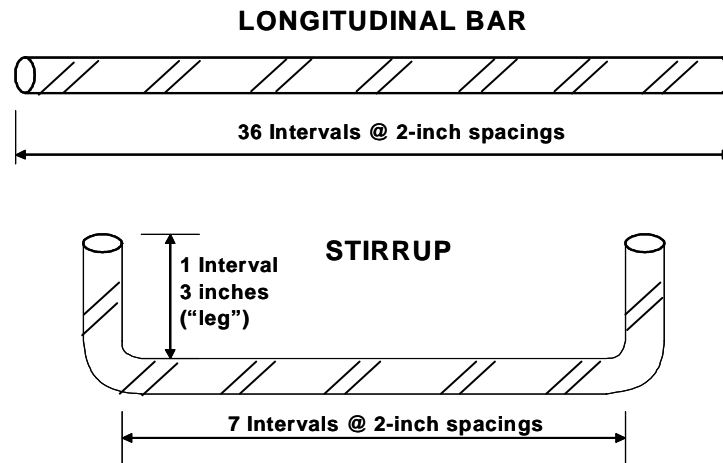


Figure 5.7 Intervals for Corrosion Rating on Mild Steel

The total bar corrosion rating was calculated as follows:

$$R_{Bar} = \sum_{i=1}^{36} (R_{Top\ i} + R_{Bot\ i}) \quad \text{Eq. 6}$$

$$\text{Total Bar Corrosion Rating} = \sum_{n=1}^m R_{Bar\ n} \quad \text{Eq. 7}$$

where,

$R_{Top\ i}$  = corrosion rating on top bar surface, interval  $i$

$R_{Bot\ i}$  = corrosion rating on bottom bar surface, interval  $i$

$R_{Bar\ n}$  = total bar corrosion rating, bar  $n$

$i$  = interval, 1 to 36

- n = bar number, 1 to m  
m = total number of bars on each specimen (2 or 8)

The corrosion rating system is described in Table 5.3. Each beam design had a different number of mild steel bars (m), depending on the post-tensioning level. The Non-PS beams had 6#6 and 2#4 bars as the tensile steel reinforcement (m=8). The mixed reinforced beams (2/3 PS) had 4#3 and 4#4 bars (m=8). The 100% PS specimens, designed either with the strength design method or the allowable stress design method, had 2#3 mild steel bars (m=2). These bars were not required by design, but were included for construction purposes. The variation in number of longitudinal bars is accounted for in the analysis of the data.

The stirrups were also rated using Table 5.3. However, a different equation was used to calculate the total stirrup rating. As with the longitudinal mild steel, the ratings for the top and bottom bar surface of each interval were summed to give a total corrosion rating for the stirrup.

The total stirrup rating was calculated as follows:

$$R_{Stirrup} = \sum_{i=1}^9 (R_{Top\ i} + R_{Bot\ i}) \quad Eq.8$$

$$Total\ Stirrup\ Corrosion\ Rating = \sum_{n=1}^6 R_{Stirrup\ n} \quad Eq. 9$$

- where,
- R<sub>Top i</sub> = corrosion rating on top bar surface, interval i
  - R<sub>Bot i</sub> = corrosion rating on bottom bar surface, interval i
  - R<sub>Stirrup n</sub> = total stirrup corrosion rating, stirrup i
  - i = interval, 1 to 9
  - n = stirrup number, 1 to 6

**Table 5.3 Evaluation and Rating System for Corrosion Found on Mild Steel Bars<sup>28</sup>**

Code	Meaning	Description	Rating
NC	No Corrosion	No evidence of corrosion	0
D	Discoloration	No evidence of corrosion, but some discoloration from original color	1
L	Light	Surface corrosion on less than one half of the interval, no pitting. Surface corrosion can be removed using cleaning pad.	2
M	Moderate	Surface corrosion on more than one half of the interval, no pitting. <b>and/or</b> Corrosion can not be completely removed using cleaning pad.	4
P	Pitting	Pits visible to unaided eye.	8
AR	Area Reduction	Measurable reduction in bar cross-sectional area due to corrosion	R <sup>2</sup>

R = Estimated cross-sectional area reduction in percent



### 5.2.2 Galvanized Steel Duct/Duct Splice

The galvanized steel duct was examined at 36 two-inch intervals, and the duct splices at 6 two-inch intervals as indicated in Figure 5.8. At each location, a corrosion rating was assigned to indicate the severity of corrosion on the inside and outside surfaces of the top and bottom of each duct.

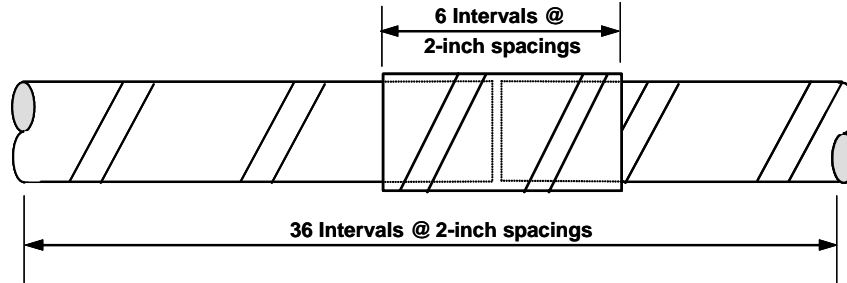


**Figure 5.8 Intervals for Corrosion Ratings on Galvanized Steel Duct/Splice<sup>7</sup>**

The corrosion rating system for the galvanized steel ducts and duct splices is described in Table 5.4. The total duct corrosion rating was calculated as follows:

$$\text{Duct Corrosion Rating} = \sum_{i=1}^{36} R_{\text{TopOuter},i} + R_{\text{BotOuter},i} + R_{\text{TopInner},i} + R_{\text{BotInner},i} \quad \text{Eq. 10}$$

where,

- $R_{\text{TopOuter},i}$  = top outer surface corrosion rating, interval  $i$
- $R_{\text{BotOuter},i}$  = bottom outer surface corrosion rating, interval  $i$
- $R_{\text{TopInner},i}$  = top inner surface corrosion rating, interval  $i$
- $R_{\text{BotInner},i}$  = bottom inner surface corrosion rating, interval  $i$
- $i$  = interval, 1 to 36

**Table 5.4 Evaluation and Rating System for Corrosion Found on Galvanized Steel Duct /Duct Splice<sup>28</sup>**

Code	Meaning	Description	Rating
NC	No Corrosion	No evidence of corrosion	0
D	Discoloration	No evidence of corrosion, but some discoloration from original color	1
L	Light	Surface corrosion on less than one half of the interval, no pitting.	2
M	Moderate	Surface corrosion on more than one half of the interval, no pitting.	4
S	Severe	Corrosion completely covers the interval. <b>and/or</b> Presence of pitting.	8
H	Hole Through Duct	Hole corroded through duct. Used in conjunction with ratings D, L, M and S.	$32 + A_h$

$$A_h = \text{Area of hole(s) in mm}^2$$

### 5.2.3 Prestressing Strand

The strands were examined at 36 two-inch intervals, like the longitudinal mild steel bars. Corrosion ratings were assigned to indicate the severity of corrosion on the outer six wires of the strand and on the center wire (after de-stranding) at each interval. This was done to address the possibility of different corrosion activity on the strand exterior and interstices between wires. The corrosion rating system for prestressing strands is described in Table 5.5. The total strand corrosion rating was calculated as follows:

$$\text{Strand Corrosion Rating} = \sum_{i=1}^{36} R_{Outer,i} \times n_i + R_{Center,i} \quad \text{Eq. 11}$$

where,

- $R_{outer,i}$  = corrosion rating on outer wires, interval  $i$
- $n_i$  = number of corroded outer wires, interval  $i$
- $R_{center,i}$  = corrosion rating on center wire, interval  $i$
- $i$  = interval, 1 to 36

**Table 5.5 Evaluation and Rating System for Corrosion Found on Prestressing Strand**<sup>28</sup>

Code	Meaning	Description	Rating
NC	No Corrosion	No evidence of corrosion.	0
D	Discoloration	No evidence of corrosion, but some discoloration from original color.	1
L	Light	Surface corrosion on less than one half of the interval, no pitting. Surface corrosion can be removed using cleaning pad.	2
M	Moderate	Surface corrosion on more than one half of the interval, no pitting. <b>and/or</b> Corrosion can not be completely removed using cleaning pad.	4
P1	Mild Pitting	Broad shallow pits with a maximum pit depth not greater than 0.02 in.	8
P2	Moderate Pitting	Pitting where the maximum pit depth ranged between 0.02 and 0.04 in.	16
P3	Severe Pitting	Pitting where the maximum pit depth is greater than 0.04 in.	32

As reported by West et al.<sup>28</sup> the corrosion rating for prestressing strand was adapted from Poston<sup>30</sup> and Hamilton.<sup>9</sup> The use of a cleaning pad to assess corrosion severity was proposed by Sanson<sup>31</sup> for classifying the degree of rusting on prestressing strand for new construction. The recommended cleaning pad is a 3M Scotch Brite Cleaning Pad. The pad is held by hand and rubbed longitudinally along the strand axis with a pressure similar to that used when cleaning pots and pans. The classification of pitting severity was based on tensile tests performed on corroded prestressing strand. The tests were used to assign a reduced tensile capacity of 97% GUTS to pitting damage at the level of P1. Moderate pitting (P2) was assigned a capacity of 90% GUTS, and severe pitting (P3) 77% GUTS. In general, the presence of any pitting visible to the unaided eye is deemed cause for rejection in new construction.

### 5.2.4 Duct Splices

All Industry Standard and Heat-Shrink duct splices were thoroughly inspected for corrosion, salt deposits, zinc corrosion products, rust staining and damage. Additionally, all Industry Standard duct splices were galvanized steel and were rated using the procedure in Section 5.2.2.

### 5.2.5 Grout

Since grout is injected after the stressing of post-tensioning steel, hardened grout is vulnerable to service cracking due to deflections and vibrations.

## 5.3 FORENSIC EXAMINATION RESULTS FOR PHASE I BEAMS

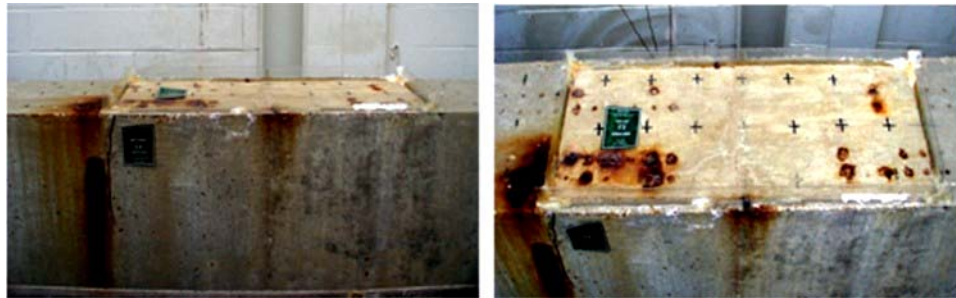
Forensic examination for all autopsy specimens and the written description for each one was performed by Kotys<sup>6</sup> and Salas<sup>7</sup> jointly. For more detail refer to References 6 and 7.

### 5.3.1 Beam Specimen 1.1 - Non-PS, Unloaded

At the end of exposure testing, rust stains were visible in the North side of the specimen, as shown in Figure 5.9. On the South side, only two small rust spots were visible. In most cases, corrosion stains were attributed to corrosion of the bolster strips used to support the reinforcement during construction. This was evident due to the concrete spalling around the “feet” of many of the strips. The bolster strips were plastic tipped, but still corroded very early during testing, as reported by West.<sup>2</sup> The spots of rust were aligned and at regular intervals.

#### Corrosion Rating:

Specimen	Generalized Rating	Localized Rating
Stirrups	101	295
Long. mild steel	1	8
Duct	NA	NA
Strand	NA	NA



*Lateral (North) view*

*Top view (from North side)*

**Figure 5.9 Specimen 1.1 – Condition Prior to Autopsy<sup>6,7</sup>**

A 0.03 in. maximum width crack extended from the Northeast corner of the ponded region down the side of the beam a distance of 11 inches. Hairline cracks were visible in the Northeast corner of the ponded region between the corroded bolster tips.

This specimen was partially autopsied as explained in Section 5.1.1, exposing and removing the mild steel bars only in a 42 inch length, west of the beam centerline. The analysis length extended half of the ponded region (24 inches) and an additional foot and a half (18 inches) outside the ponded region.

After removing all mild steel bars in the autopsy region, severe corrosion was found in three out of eight longitudinal bars. The corrosion was very localized, at approximately 14 inches from the beam centerline. These localized corrosion areas coincided with the rust stains found previously on the top of the specimen in the Northeast corner of the ponded region. In Figure 5.10, the measurement tape

indicates the localized corrosion at 28 inches from the left end of the mild steel bar. This location corresponds to 14 inches from the beam centerline.

Stirrups were placed at 12-inch spacings in all specimens. Therefore, four stirrups were included in the partial autopsy region. After a detailed visual inspection, severe localized corrosion was found in the stirrup located 14 inches from the beam centerline. (The actual location of the center stirrup was two inches from the beam centerline.) The most severe corrosion was found in the north top corner of the stirrup, as shown in Figure 5.10. The stirrups located at 26 and 38 inches from the beam centerline had moderate to light corrosion in the top section, with no section loss. These stirrups were located outside the ponded region. The center stirrup, located 2 inches from the beam centerline, had only minor discoloration and light corrosion in localized areas.

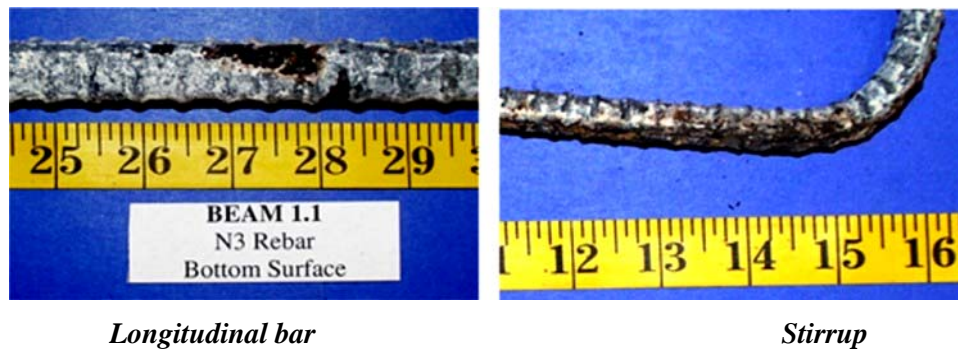


**Figure 5.10 Specimen 1.1 – Mild Steel Bar and Stirrup<sup>6,7</sup>**

Figure 5.11 shows the longitudinal bar and stirrup corrosion rating graphs. Corrosion rating values for the east side of the beam were extrapolated from the west side, due to the partial autopsy procedure. This was done to compare results of the partial autopsy beams with those of the full autopsy beams. By doing so, it was assumed that the bars and stirrups to the east side of the beam centerline performed similarly to those west of the centerline.

**5.3.2 Beam specimen 1.3 - Non-PS, Constant Service Load**

Specimen condition after testing included nine transverse cracks in the constant moment region (seven in the ponded region), with a maximum transverse crack width of 0.020 inches. Longitudinal cracks were also visible at 4.5 inches from the sides of the beam, with a maximum crack width of 0.050 in. Heavy rust stains and salt deposits were visible in the top of the cracks in localized areas, as shown in Figure 5.12.

Very severe corrosion, pitting and section loss were observed for all longitudinal bars, corresponding with crack locations.

All the stirrups were also severely corroded, with large pits and section loss. Crack locations coincided with the stirrup locations. Therefore, the stirrups were severely damaged, especially under the ponded region. Figure 5.13 shows examples of the typical longitudinal bar and stirrup corrosion in Specimen 1.3. Figure 5.14 shows the crack pattern in the top of the specimen after exposure and the rebar and stirrup corrosion ratings across the analyzed section.

Specimen	Corrosion Rating:	
	Generalized Rating	Localized Rating
Stirrups	1231	770
Long. mild steel	91	261
Duct	NA	NA
Strand	NA	NA

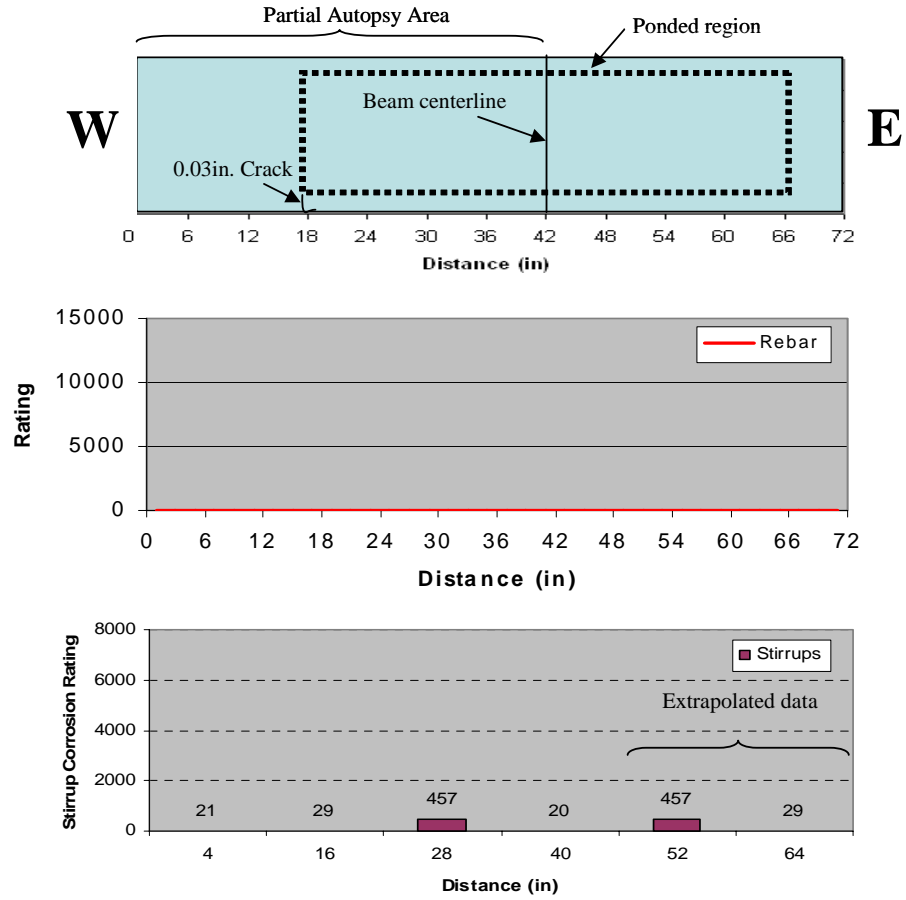


Figure 5.11 Specimen 1.1 – Crack Pattern and Specimen Corrosion Rating Graphs<sup>6,7</sup>



*Lateral (South) view*



*Top view (from South side)*

Figure 5.12 Specimen 1.3 – Condition Prior to Autopsy<sup>6,7</sup>



*Longitudinal Steel*

*Stirrup*

**Figure 5.13 Specimen 1.3 – Mild Steel Bar and Stirrup<sup>6,7</sup>**

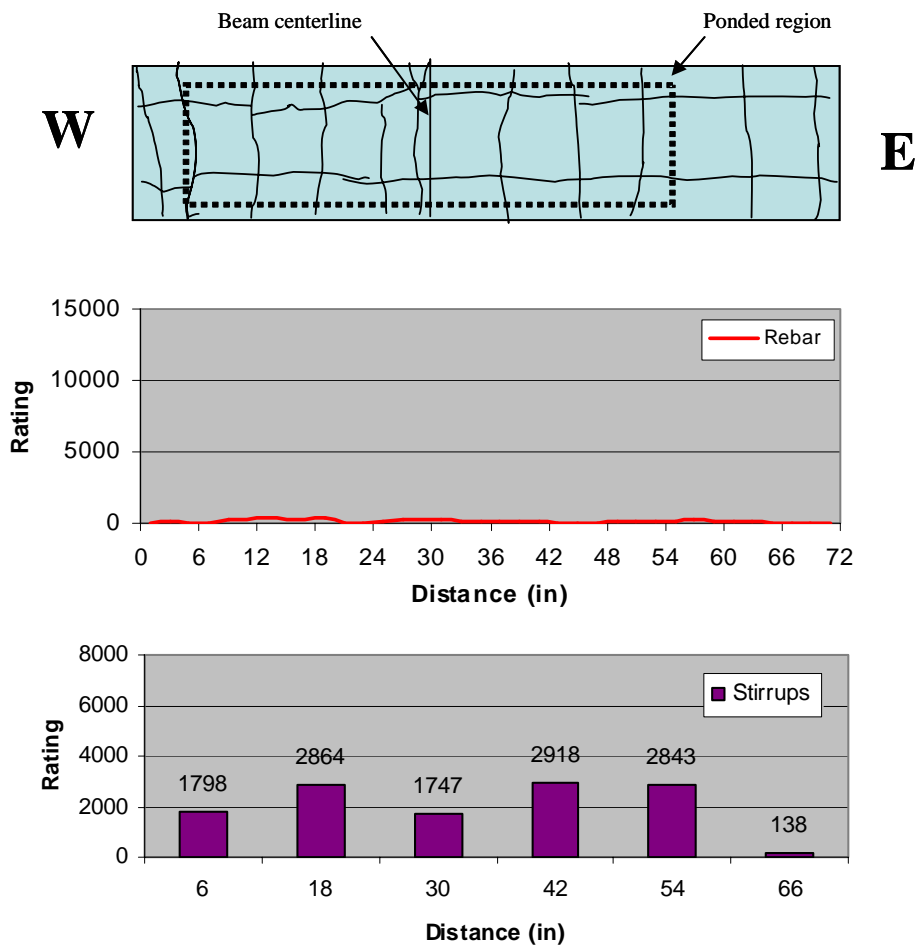


**Figure 5.14 Specimen 1.3 – Crack Pattern and Specimen Corrosion Rating Graphs<sup>6,7</sup>**

### 5.3.3 Beam Specimen 2.3 – 2/3 PS, Service Load

Three main transverse cracks, with a maximum crack width of 0.02 inches, and two longitudinal cracks, with a maximum crack width of 0.05 inches, were found at the end of exposure. These cracks were located on the top of the specimen in the ponded region. Salt deposits and large rust stains were visible on the sides of the beam, as shown in Figure 5.15.

Very severe pitting and section loss was found on the mild steel bars in the northeast corner of the ponded region (see Figure 5.17). The corrosion was located 24 inches from the beam centerline, which corresponded with the border of the ponded region. The stirrups were also severely corroded, as seen in Figure 5.16. It was found that severely corroded stirrups coincided with crack locations (see Figure 5.18).

Extremely severe corrosion and area loss, corresponding to crack locations, was found in both post-tensioning ducts. (See Figure 5.17 and graphs in Figure 5.18) Corrosion was aggravated at locations where large grout voids existed, as shown in Figure 5.16. A large accumulation of corrosion products from the ducts was found attached to the grout.

**Corrosion Rating:**

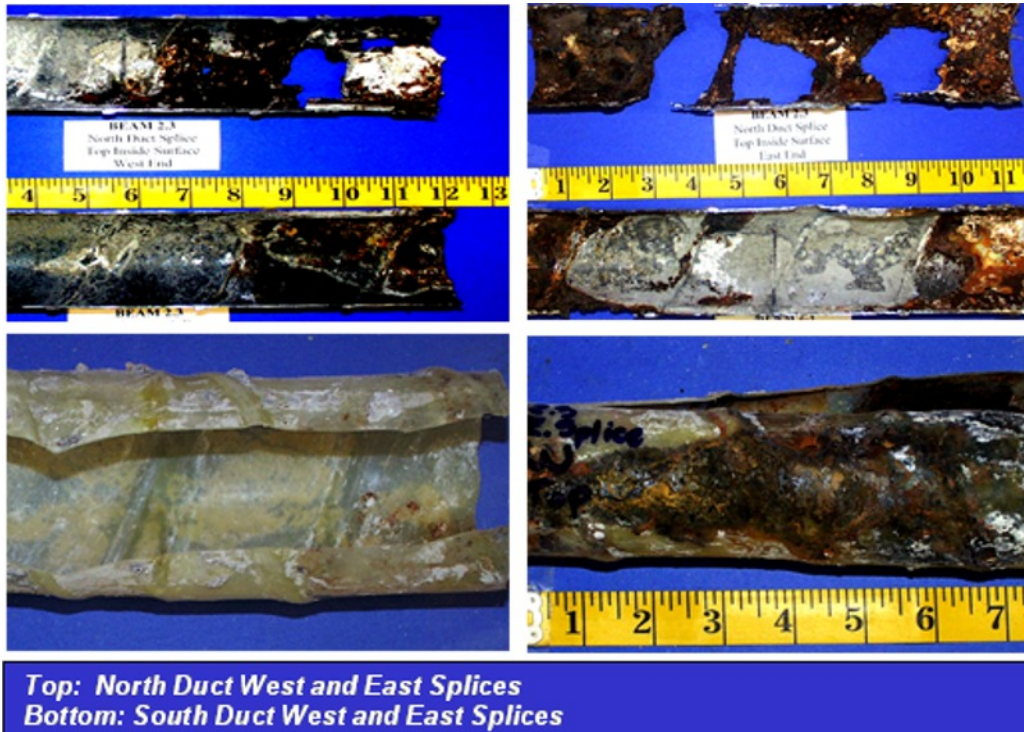
Specimen	Generalized Rating	Localized Rating
Stirrups	1359	2236
Long. mild steel	467	6241
North Duct	4299	2107
South Duct	5069	6248
North Strands	96	20
South Strands	122	56



*Lateral (South) View*

*Top View (from South Side)*

**Figure 5.15 Specimen 2.3 – Condition Prior to Autopsy<sup>6,7</sup>**



**Top: North Duct West and East Splices  
Bottom: South Duct West and East Splices**

**Figure 5.16 Specimen 2.3 – Duct Splices<sup>6,7</sup>**

Moderate localized corrosion and pitting in a few wires was found on the south strands. The north strands show only moderate to light uniform corrosion. As with the mild steel bars, stirrups and ducts, localized corrosion in the strands corresponded to crack locations in the ponded region.

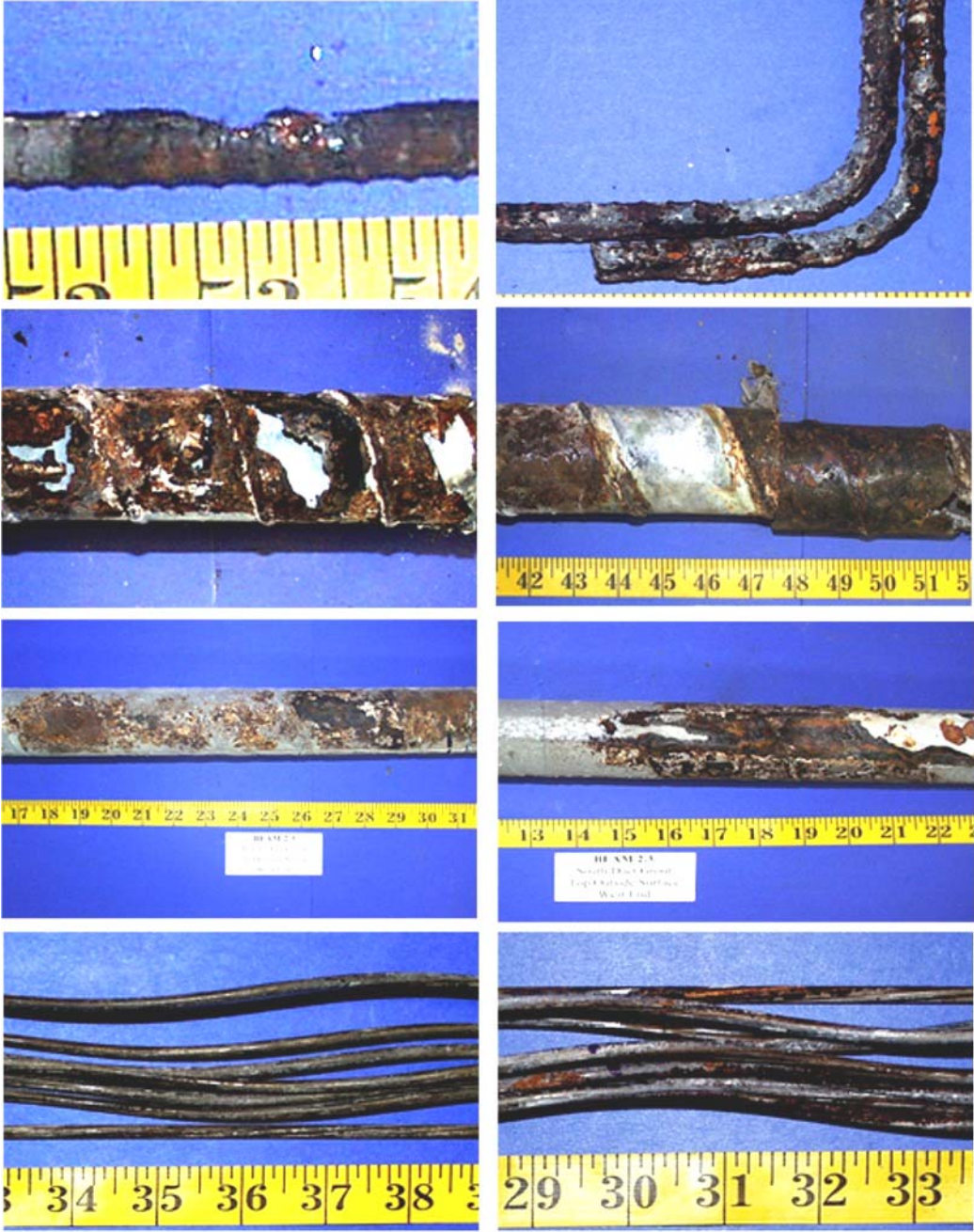
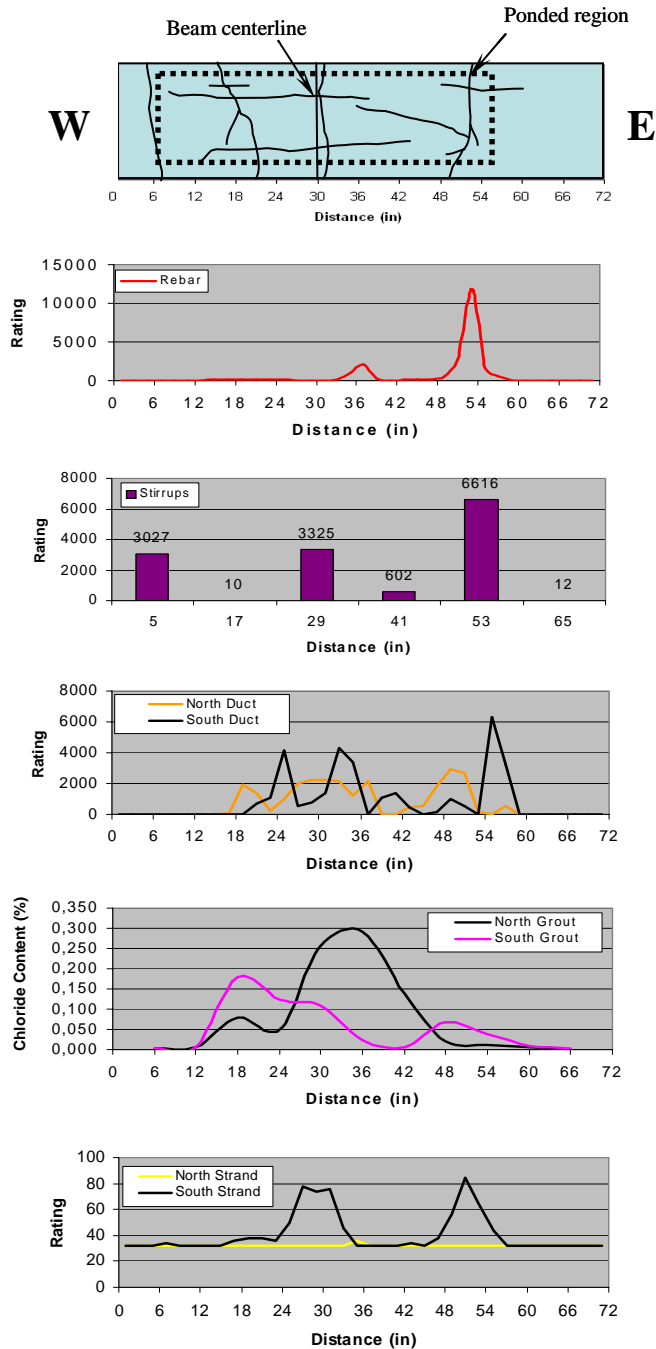


Figure 5.17 Specimen 2.3 – Reinforcing Elements<sup>6,7</sup>

The acid soluble chloride content in the grout reached a maximum value of 0.3% by weight of grout inside the south duct, and 0.18% inside the north duct. These values are much higher than the critical chloride threshold value of 0.033% by weight of grout (corresponding to 0.2% by weight of cement).



Chloride samples were taken at 6-inch intervals within the forensic analysis length and chloride content plots were obtained, as observed in Figure 5.18.



**Figure 5.18 Specimen 2.3 – Crack Pattern and Specimen Corrosion Rating Graphs<sup>6,7</sup>**

Beam specimen 2.3 had four duct splices. The north duct had two industry standard splices, and the south duct had two heat-shrink splices. Figure 5.16 shows the condition of the duct splices at the end of exposure testing. Severe area loss and extremely severe corrosion were found on the oversized piece of both industry standard splices in the north duct. As shown in the photographs, moisture was able to enter the sides of the splice at the duct tape locations. This accelerated the corrosion by allowing corrosive

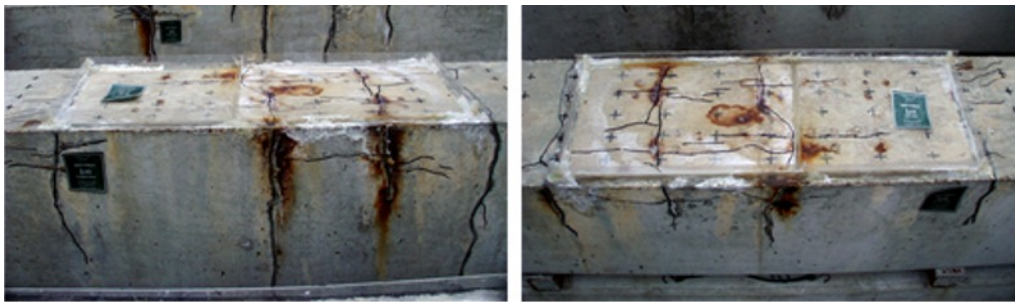
attack from the inside of the splice as well as the outside. Voids in the grout at the splice locations also aggravated the corrosion in the galvanized steel pieces. The west duct splice on the north duct had been intentionally damaged during construction. The role the damage played with respect to the splice corrosion protection is not clear due to the effect of the other contributing factors, such as splice locations, crack locations, moisture ingress and chloride contents. The heat-shrink splices in the south duct also performed poorly. As can be seen from Figure 5.16, the east heat-shrink splice trapped moisture from the grout bleed water and accelerated the galvanized duct deterioration. The west side splice was intentionally damaged during construction, with a small cut (less than 1 inch) in the center. The generalized duct corrosion under the splice and the uniform rust stains on the inside of the heat-shrink splice indicate that the damage was not the main cause of duct corrosion. Nevertheless, the damage is considered as one of the duct deterioration contributing factors.

#### 5.3.4 Beam Specimen 2.11 – 2/3 PS, Service Load, Fly Ash Grout

As shown in Figure 5.19, four main transverse cracks and several small longitudinal cracks were visible on the top of Specimen 2.11 in the constant moment region at the end of exposure. A maximum transverse crack width of 0.03 inches was found in the southwest area of the ponded region. The maximum longitudinal crack width was also 0.030 in. Heavy rust stains were visible on the top of the specimen in localized areas extending out of the cracks, as shown in Figure 5.19. The additional rust stains corresponded to the location of the “legs” of the bolster strips, used to support the reinforcement.

Specimen	Corrosion Rating:	
	Generalized Rating	Localized Rating
Stirrups	1923	2978
Long. mild steel	476	7757
North Duct	1504	2440
South Duct	1413	1673
North Strands	97	20
South Strands	92	26

A full autopsy of Specimen 2.11 was performed, providing a total length of 72 inches of the longitudinal bars, ducts, grout and strands and six stirrups to be analyzed. Thirty inches of the analysis length extended to the west of the centerline of the beam and the remaining 42 inches extended to the east.



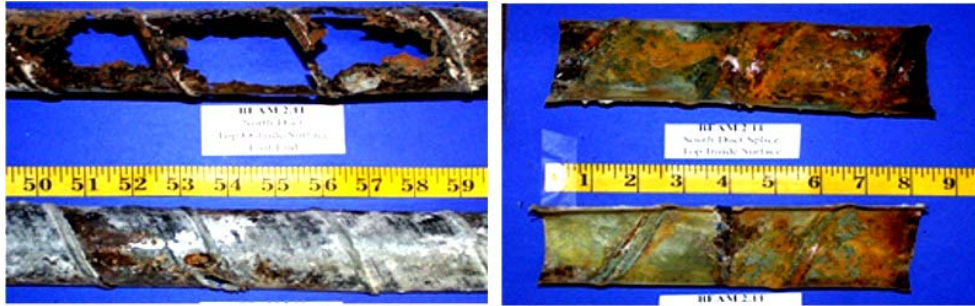
*Lateral (North) View*

*Top View (from South Side)*

**Figure 5.19 Specimen 2.11 – Condition Prior to Autopsy<sup>6,7</sup>**

Very severe section loss and pitting was observed in all longitudinal mild steel bars corresponding to all crack locations (see Figure 5.21). The most severe corrosion was found at the beam centerline crack. Similar results were found on the stirrups, where the beam centerline stirrup had extensive corrosion and section loss.

Figure 5.21 shows the severe corrosion and area loss found in the south duct. Extensive duct deterioration was mostly located to the west of the centerline. Zinc and steel corrosion products covered the remaining areas on the top of the duct. The bottom of the duct was found to be in better condition, with some areas of zinc and steel corrosion products. Corrosion on the north duct was less severe than on the south duct. It was also found to have a few areas of severe localized corrosion, section loss, and build up of zinc and steel corrosion products. The corrosion on the north duct was significant at the centerline of the beam, under the industry standard splice.



*North Duct Splice*

*South Duct Splice*

**Figure 5.20 Specimen 2.11 – Duct Splices**

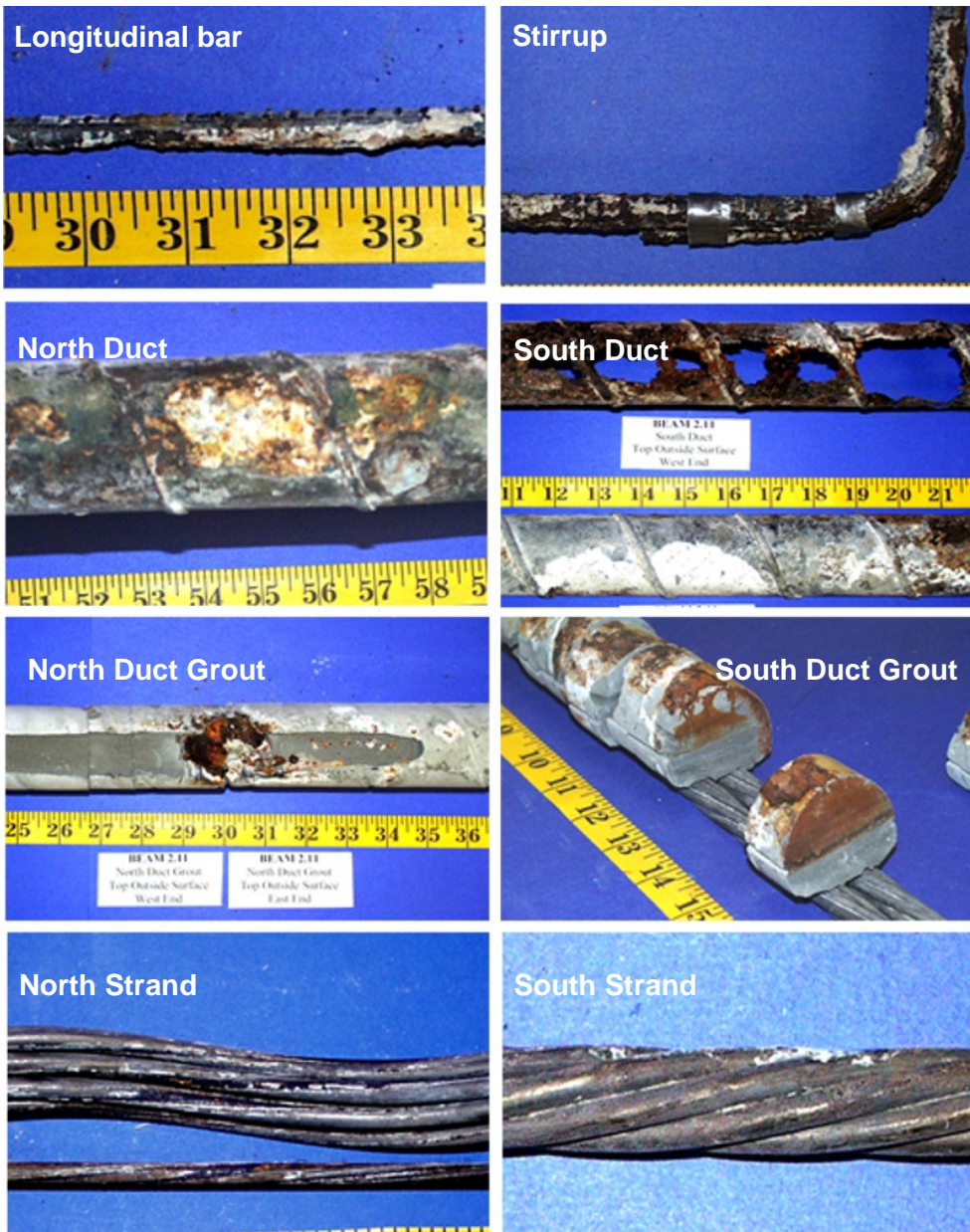


**Figure 5.21 Specimen 2.11 – Reinforcing Elements<sup>6,7</sup>**

The south duct grout had several transverse cracks, with a maximum crack width of 0.060 inches. This crack coincided with the location of the heavy duct corrosion and area loss. Duct corrosion stains were found inside the grout cracks, where moisture had traveled down from the grout surface (see Figure 5.21). The north duct grout had one large void due to bleed water that was 22 inches in length and 0.013 inches deep. Corrosion products were found attached to the grout in the void. This location corresponded with the splice location at the centerline of the beam. Three transverse cracks, with a maximum crack width of 0.010 inches, were found on the east side of the grout. The cracks coincided with the area where severe duct corrosion and duct area loss were found. The acid soluble chloride content in the grout reached a maximum value of 0.31% by weight of grout inside the north duct, and 0.033% inside the south duct. The content in the north duct was from the sample taken at the centerline of the beam, under the industry standard splice. It was much higher than the critical chloride threshold value of 0.033% by weight of grout. Chloride samples were taken at 6-inch intervals within the forensic analysis length and chloride content plots were obtained, as observed in Figure 5.22.

Light to moderate corrosion was found on the outer wires of the strands in both ducts, with the center wires presenting a slight increase in corrosion severity.

Specimen 2.11 had two duct splices. The north duct had an industry standard splice, and the south duct had a heat-shrink splice. Both splices were located at the centerline of the beam. Figure 5.20 shows the condition of the duct splices at the end of exposure testing. The top of the north duct splice was found to be severely deteriorated. The heat-shrink splice showed severe signs of rust staining from the duct corrosion.

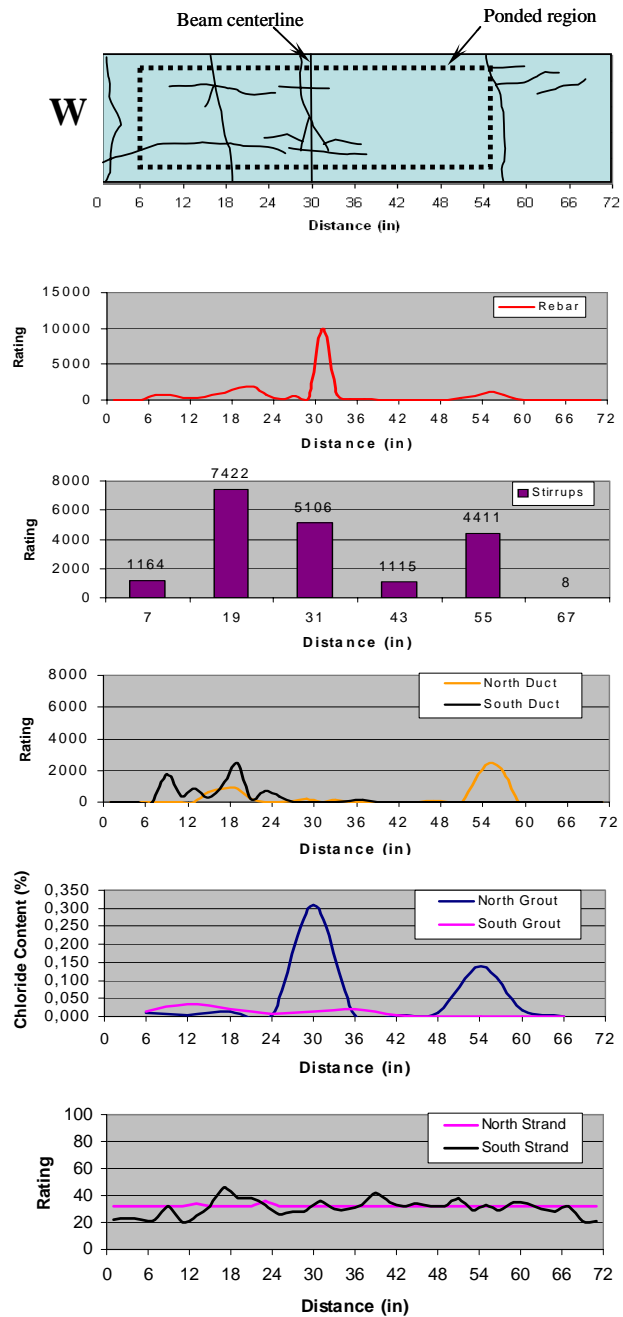


Figure 5.22 Specimen 2.11 – Crack Pattern and Specimen Corrosion Rating Graphs<sup>6,7</sup>

### 5.3.5 Beam Specimen 3.1 – 100%U PS, Unloaded

As seen in Figure 5.23, a visual inspection of Specimen 3.1 at the end of exposure found that it remained uncracked. Any rust staining on Specimen 3.1 was due to the bolster strips.

This specimen was partially autopsied, as explained in Section 5.2.2. The analysis length included half of the ponded region (24 inches) and an additional foot and a half (18 inches) outside the ponded region. Forty-two inches of the mild steel bars, ducts, grout and strands west of the centerline were exposed and removed. The section autopsied only included three stirrups for analysis.

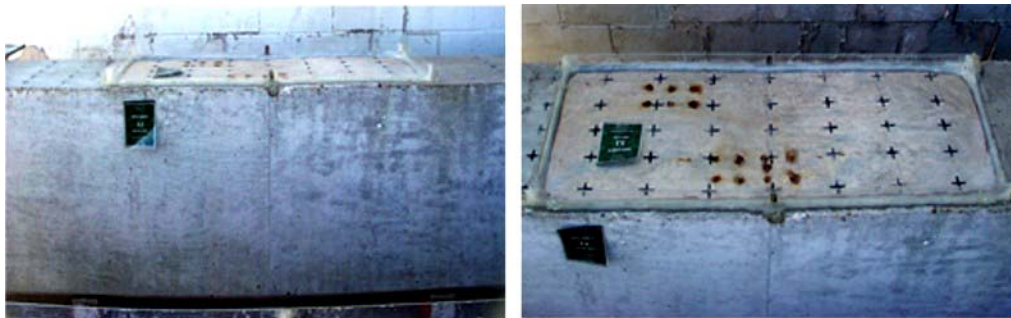
As shown in Figure 5.25, there was no corrosion found on either of the mild steel bars in Specimen 3.1.

Light uniform corrosion was found on the three stirrups included in the partial autopsy. The centerline stirrup was intended to be included in the partial autopsy, but its actual location was outside of the section removed. This is why there is no analysis or rating for the centerline stirrup.

There were no signs of corrosion on either of the ducts.

The grout in the north and south ducts showed multiple small voids over the entire length. Neither of the duct grouts had significantly large voids. The acid soluble chloride content in the north duct grout was negligible. The chloride content in the south duct grout was also negligible, except for the single measurement of 0.021% by weight of grout. The sample yielding this value was taken 36 inches to the west of the centerline. It was determined that this value was due to an error in the equipment and considered an outlier. Chloride samples were taken at 6-inch intervals within the forensic analysis length and chloride content plots were obtained, as shown in Figure 5.26.

Specimen	Corrosion Rating:	
	Generalized Rating	Localized Rating
Stirrups	15	4
Long. mild steel	0	0
North Duct	0	0
South Duct	0	0
North Strands	119	20
South Strands	96	22



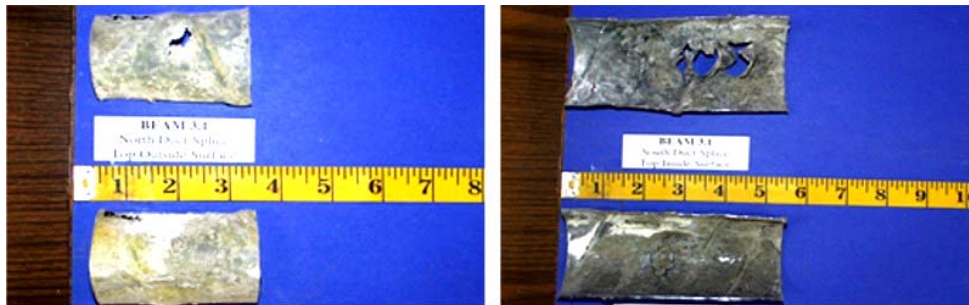
*Lateral (North) View*      *Top View (from North Side)*

**Figure 5.23 Specimen 3.1 – Condition Prior to Autopsy<sup>6,7</sup>**

Moderate uniform corrosion was found on the strands in the north duct, and light uniform corrosion was found on those located in the south duct. (See Figure 5.25)

Specimen 3.1 had two duct splices. The south duct had an industry standard splice and the north duct had a heat-shrink splice. Both splices were located at the centerline of the beam. Therefore, only half of each splice was included in the section autopsied. Figure 5.24 shows the condition of the duct splices at the end of exposure testing. No signs of corrosion were found on either splice.

Figure 5.26 shows the chloride content and corrosion rating graphs for each reinforcing element. Corrosion rating values for the east side of the beam were extrapolated from the west side, due to the partial autopsy procedure. This was done to compare results of the partial autopsy beam with those of the full autopsy beams. By doing so, it was assumed that the reinforcing elements to the east side of the beam centerline performed similarly to those west of the centerline.



*North Duct Splice*

*South Duct Splice*

**Figure 5.24 Specimen 3.1 – Duct Splices**

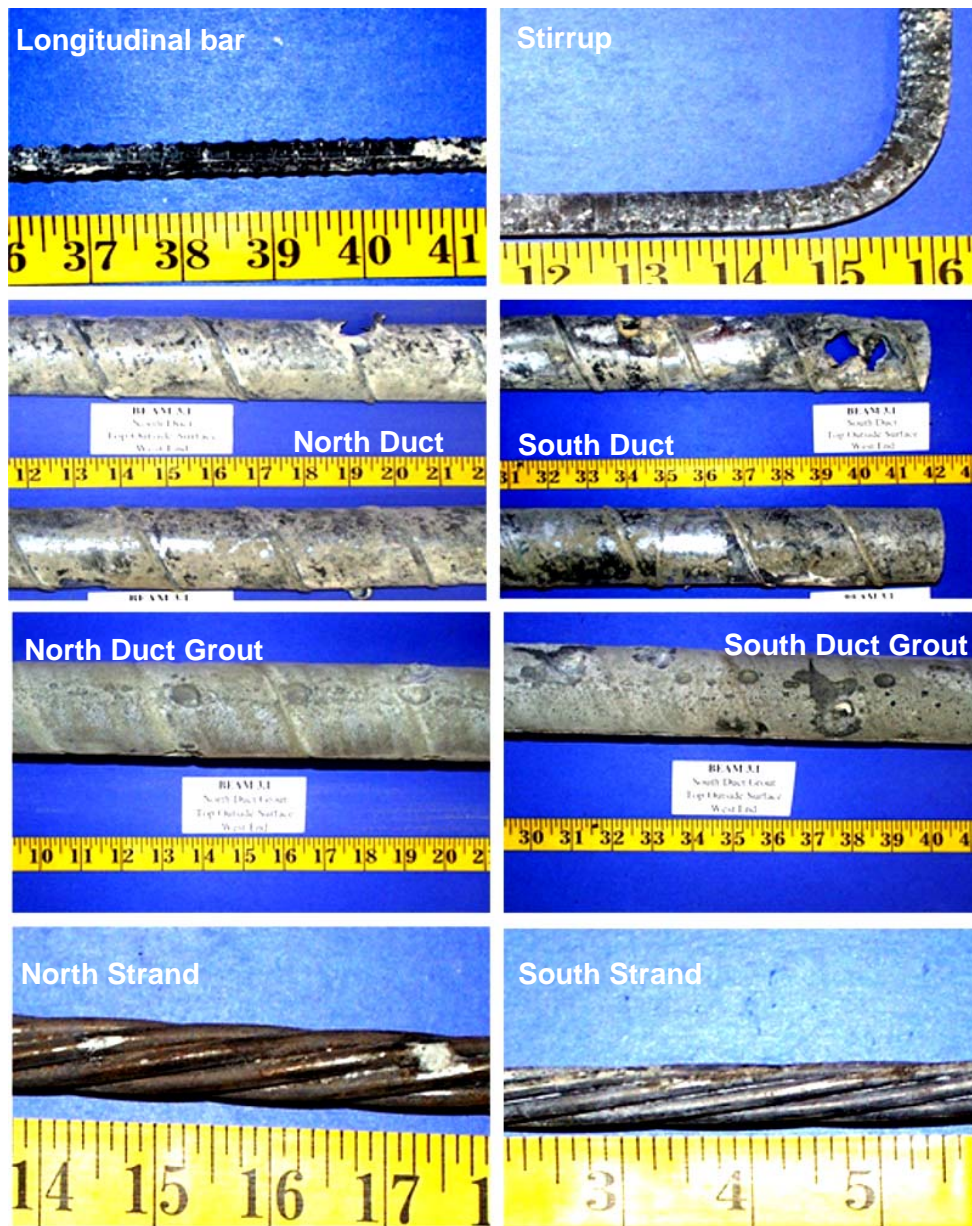


**Figure 5.25 Specimen 3.1 – Reinforcing Elements<sup>6,7</sup>**

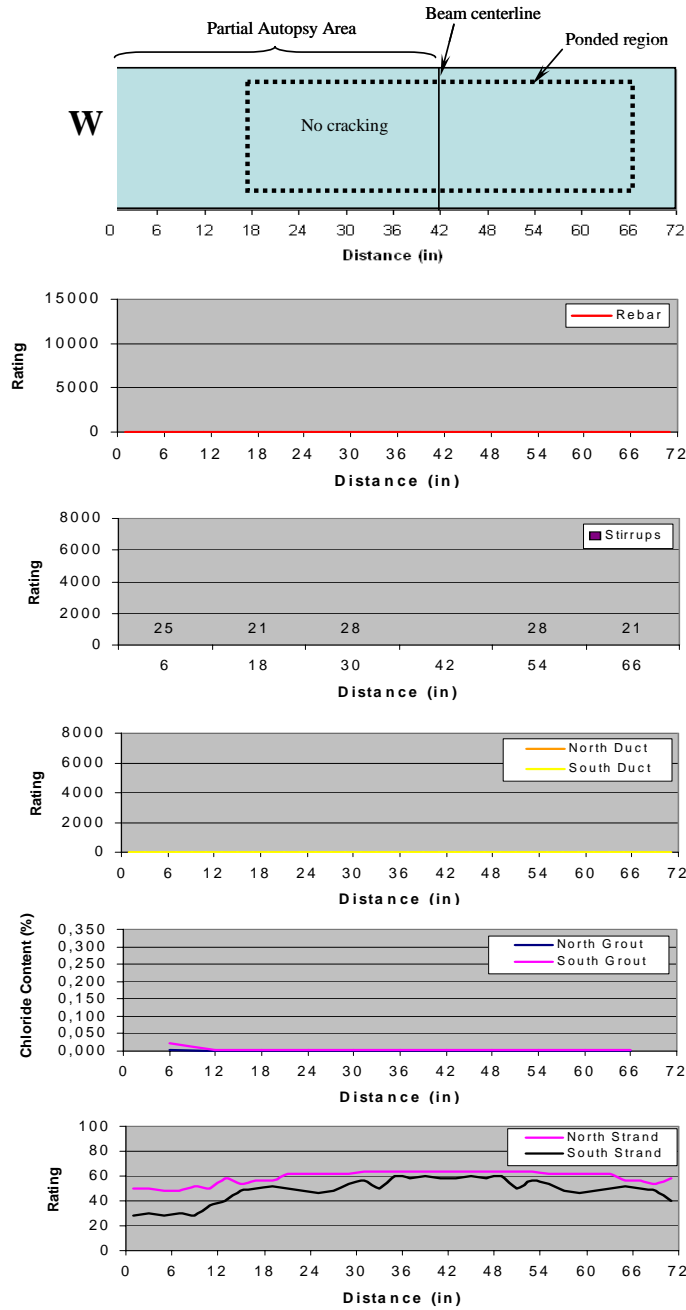


**Figure 5.26 Specimen 3.1 – Crack Pattern and Specimen Corrosion Rating Graphs<sup>6,7</sup>**

**5.3.6 Beam Specimen 3.2 – 100%U PS, Service Load**

A visual inspection found that Specimen 3.2 had one transverse crack (See Figure 5.27) across the top of the beam at the end of exposure even though this specimen was designed to remain uncracked. The crack had a maximum width of 0.01 inches and was located 12 inches to the west of the centerline of the beam. This location was directly above a stirrup. As seen in Figure 5.27, any rust staining was due to the bolster strips.

A full autopsy of Specimen 3.2 was performed, providing a total length of 72 inches of the longitudinal bars, ducts, grout and strands and six stirrups to be analyzed (see Figure 5.30). Forty-two inches of the analysis length extended to the west of the centerline of the beam and the remaining 30 inches extended to the east.

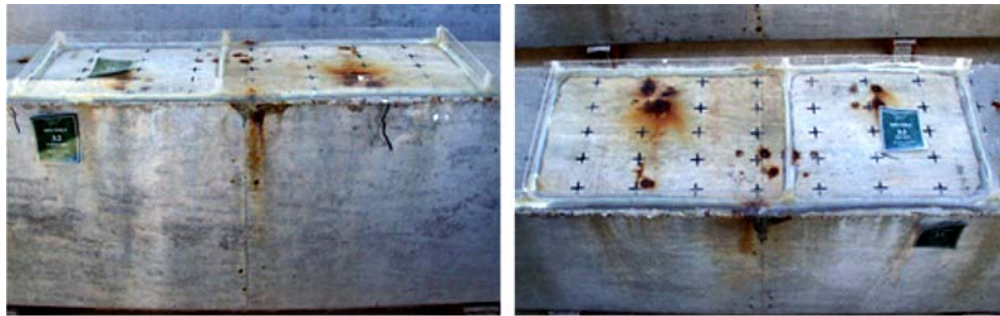
The only corrosion found on the mild steel bars was a small localized area of light corrosion. It was located 10 inches to the east of the centerline.

Two localized areas of severe corrosion and area loss were found on the stirrups. These areas were found on the stirrups located 13 and 25 inches to the west of the centerline. The stirrup 13 inches to the west corresponds to the crack described above. The remaining stirrups showed light uniform corrosion.

The only corrosion found on the north duct was located under the heat-shrink splice at the centerline of the beam. It showed two very light spots of corrosion. The south duct showed no signs of corrosion (see Figure 5.30).

**Corrosion Rating:**

Specimen	Generalized Rating	Localized Rating
Stirrups	95	462
Long. mild steel	1	4
North Duct	1	2
South Duct	0	2
North Strands	168	28
South Strands	168	28



*Lateral (North) View*

*Top View (from South Side)*

**Figure 5.27 Specimen 3.2 – Condition Prior to Autopsy<sup>6,7</sup>**

The grout in the north duct showed multiple small voids over the entire length. The south duct grout had three large voids. A 14-inch long void was located at the centerline, as shown in Figure 5.30. Two six-inch long voids were found 24 inches to the east and to the west of the centerline. Figure 5.28 was included to illustrate the good grouting quality of both ducts in Specimen 3.2. The acid soluble chloride content in the north and south duct grout was negligible. Chloride samples were taken at 6-inch intervals within the forensic analysis length and chloride content plots were obtained, as shown in Figure 5.31.

Light uniform corrosion was found on all of the strands located in the north and south ducts.



**Figure 5.28 Specimen 3.2 – Grouted Duct<sup>6,7</sup>**

Specimen 3.2 had two duct splices. The south duct had an industry standard splice and the north duct had a heat-shrink splice. Both splices were located at the centerline of the beam. Figure 5.29 shows the condition of the duct splices at the end of exposure. Both splices showed no signs of corrosion, with only a minor salt stain on the industry standard splice.





*North Duct Splice*

*South Duct Splice*

**Figure 5.29 Specimen 3.2 – Duct Splices<sup>6,7</sup>**



**Figure 5.30 Specimen 3.2 – Reinforcing Elements<sup>6,7</sup>**

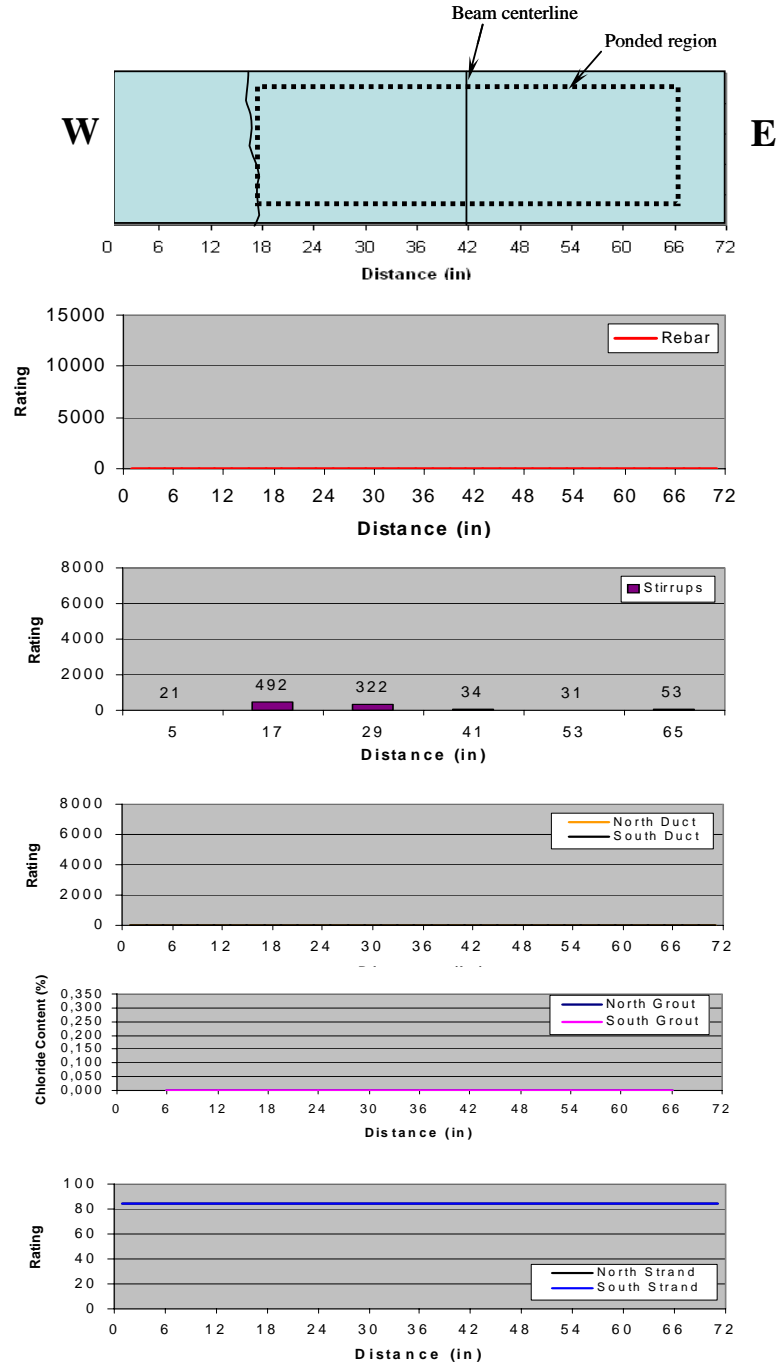


Figure 5.31 Specimen 3.2 – Crack Pattern and Specimen Corrosion Rating Graphs<sup>6,7</sup>

### 5.3.7 Beam Specimen 3.3 – 100%U PS, Overload

As shown in Figure 5.32, Specimen 3.3 had three transverse cracks across the top of the beam at the end of exposure. The largest crack had a maximum width of 0.013 inches and was located at the centerline of the beam. This location was directly above a stirrup. The other two cracks had a maximum width of 0.01 inches. They were located 24 inches to the east and west of the centerline. Both of these cracks also coincided with stirrup locations. As seen in Figure 5.32, there was minor rust staining around the cracks on the sides of the beam. A majority of the rust spots on the top were from the bolster strips.

A full autopsy of Specimen 3.3 was performed, providing a total length of 72 inches of the longitudinal bars, ducts, grout, and strands and six stirrups to be analyzed. Forty-two inches of the analysis length extended to the west of the centerline of the beam and the remaining 30 inches extended to the east (see Figure 5.32).

Two areas with severe corrosion with area loss were found on one of the mild steel bars. They coincided with the stirrups located at the centerline and 24 inches to the west.

Severe uniform corrosion and section loss was found on the three stirrups located under the cracks described above. The remaining stirrups showed light uniform corrosion.

Specimen	Corrosion Rating:	
	Generalized Rating	Localized Rating
Stirrups	423	867
Long. mild steel	36	294
North Duct	429	924
South Duct	220	685
North Strands	161	64
South Strands	118	32

Severe corrosion and area loss corresponding to the three crack locations was found on the north duct. The south duct also showed signs of severe corrosion and area loss at the centerline, and moderate corrosion under the other two cracks (see Figure 5.34). The remainder of the ducts showed no signs of corrosion.



*Lateral (North) View*

*Top View (from North Side)*

**Figure 5.32 Specimen 3.3 – Condition Prior to Autopsy<sup>6,7</sup>**

The grout in the north duct had two voids located at the centerline and 24 inches to the east. Corrosion products from the duct were found coinciding with the three crack locations. Two voids were also present in the south duct grout. They were located 30 inches to the west and 14 inches to the east of the centerline. Neither of these voids coincided with any duct corrosion or crack locations. Corrosion products from the south duct were found coinciding with three crack locations. The acid soluble chloride content in the grout reached a maximum value of 0.0423% by weight of grout inside the north duct at the centerline. The maximum chloride content in the south duct grout was 0.0457% by weight of grout. This sample was located 24 inches to the east of the centerline, which is the same location as one of the cracks and severe duct corrosion. These values are higher than the critical chloride threshold value of 0.033% by weight of grout. Chloride samples were taken at 6-inch intervals within the forensic analysis length and chloride content plots were obtained, as shown in Figure 5.35.

Moderate to severe uniform corrosion was found on all three prestressing strands in the north duct. As shown in Figure 5.34, severe localized corrosion was found 24 inches to the west of the centerline, which again coincides with a crack location. Moderate to severe uniform corrosion was also found on all three prestressing strands in the south duct.

Specimen 3.3 had one duct splice. It was an industry standard splice located on the north duct at the centerline. Figure 5.33 shows the condition of the duct splice at the end of exposure testing. The top of the north duct splice was found to be severely corroded with significant section loss.



Figure 5.33 Specimen 3.3 – North Duct Splice<sup>6,7</sup>



Figure 5.34 Specimen 3.3 – Reinforcing Elements<sup>6,7</sup>

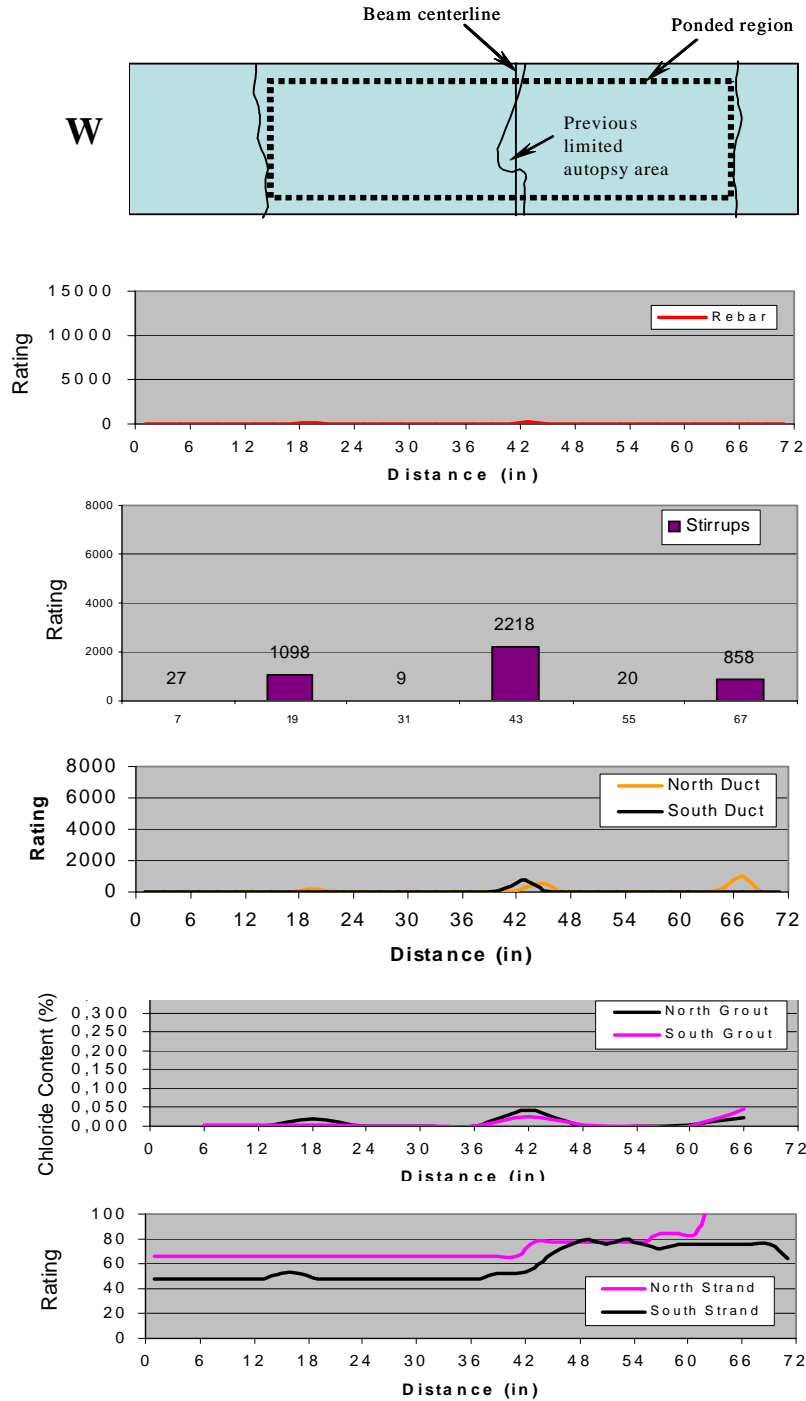


Figure 5.35 Specimen 3.3 – Crack Pattern and Specimen Corrosion Rating Graphs<sup>6,7</sup>

### 5.3.8 Beam Specimen 4.2 – 100%S PS, Service Load

As shown in Figure 5.36, a visual inspection found that Specimen 4.2 had two transverse cracks across the top of the beam at the end of exposure. This specimen was designed to remain uncracked. The first crack had a maximum width of 0.013 inches and was located one inch to the west of the centerline of the beam. This location was directly above a stirrup. The second crack had a maximum width of 0.01 inches.

It was located 22 inches to the east of the centerline, also above a stirrup. As seen in Figure 5.36, there was no rust staining around the cracks. Any rust spots were again from the bolster strips.

A full autopsy of Specimen 4.2 was performed, providing a total length of 72 inches of the longitudinal bars, ducts, grout and strands and six stirrups to be analyzed. Thirty inches of the analysis length extended to the west of the centerline of the beam and the remaining 42 inches extended to the east (see Figure 5.39).

Signs of corrosion were only found on one of the mild steel bars. It was severe localized corrosion with minor section loss at the centerline (see Figure 5.38).

Severe localized corrosion and section loss were found on the two stirrups located under the cracks described before. The remaining stirrups showed light uniform corrosion with a few areas of moderate localized corrosion.

Specimen	Corrosion Rating:	
	Generalized Rating	Localized Rating
Stirrups	189	236
Long. mild steel	15	169
North Duct	7	8
South Duct	4	4
North Strands	96	22
South Strands	96	16



*Lateral (South) View*      *Top View (from East Side)*  
**Figure 5.36 Specimen 4.2 – Condition Prior to Autopsy<sup>6,7</sup>**

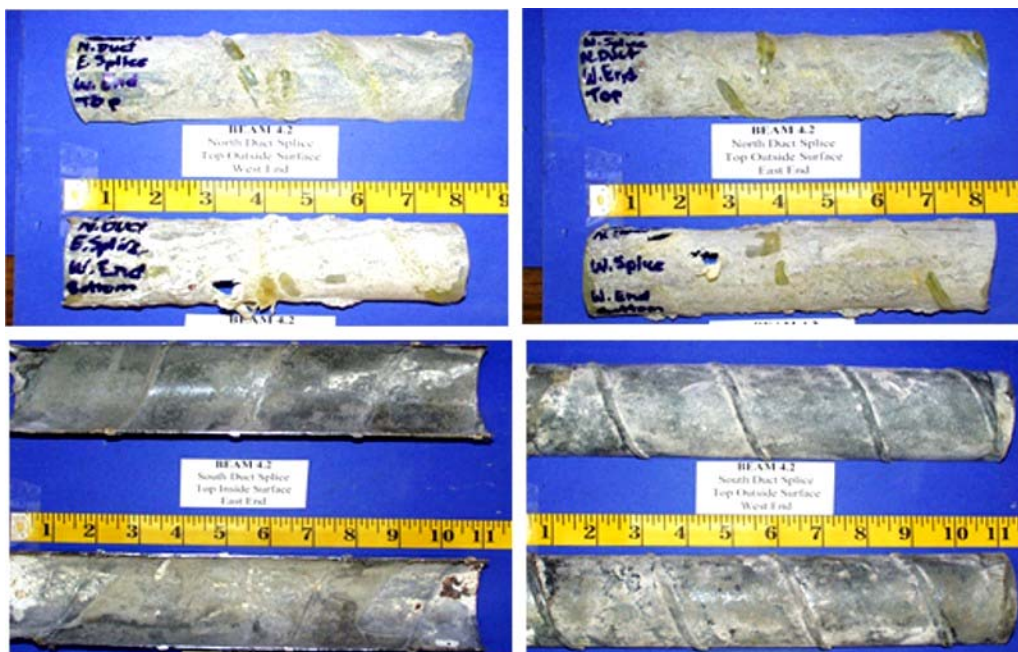


**Figure 5.37 Specimen 4.2 – Duct Splices<sup>6,7</sup>**

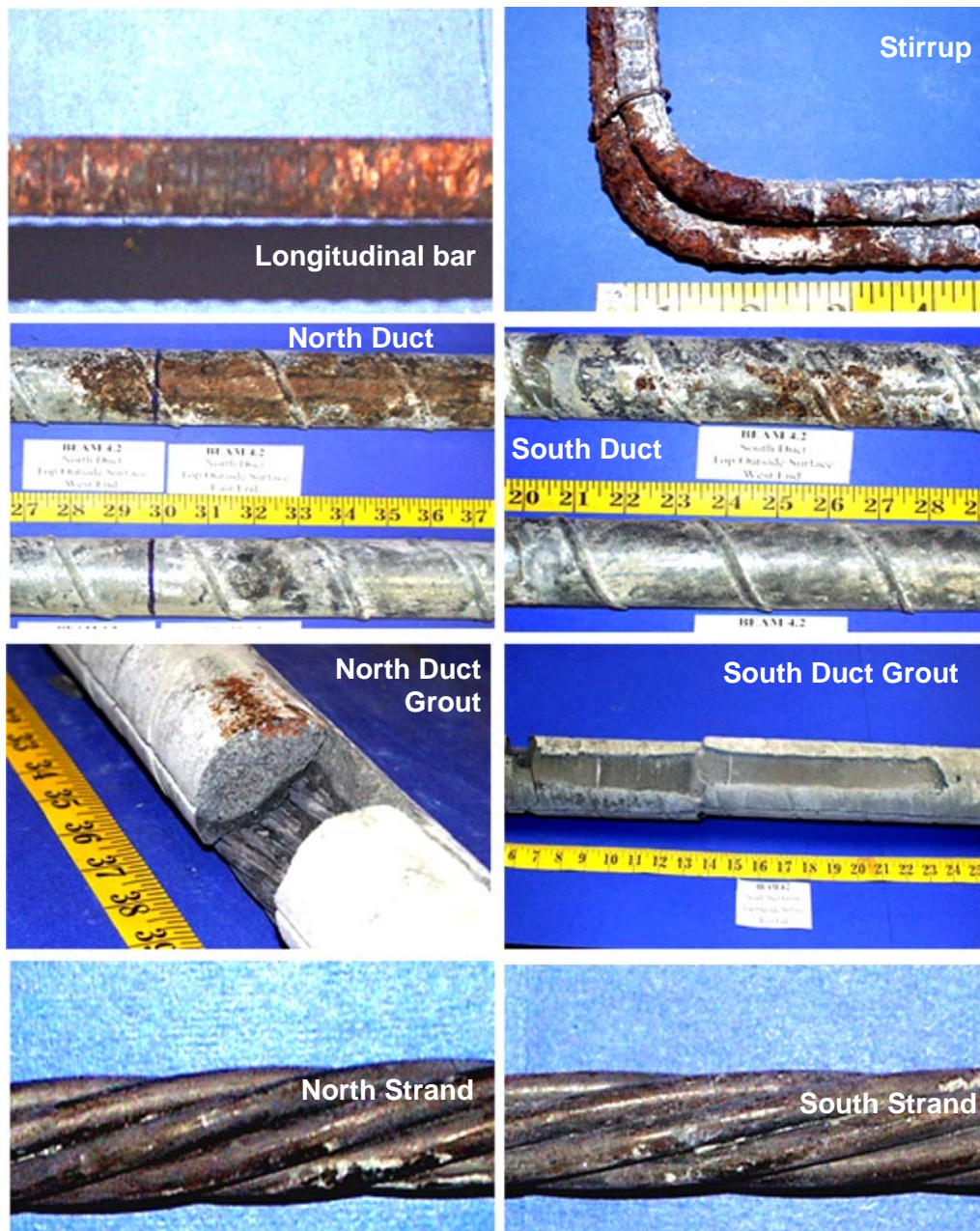


**Figure 5.38 Specimen 4.2 – Reinforcing Elements<sup>6,7</sup>**

Severe corrosion corresponding to the maximum crack location at the centerline was found on the north duct. The south duct showed signs of light to moderate corrosion corresponding with the two cracks on the specimen. The remainder of the ducts showed no signs of corrosion (see Figure 5.38).

The grout in the north duct had a large void approximately 12 inches long. It was located under the smaller crack to the east of the centerline. Corrosion stains from the duct were found a few inches to the east of the centerline. As seen in Figure 5.38, a large crack in the grout was also present at this location, showing rust stains on the face of the crack. Two large voids were present in the south duct grout. One began six inches to the west of the centerline, extending 18 inches. (See Figure 5.38) The second void was 14 inches in length and began 20 inches to the east. The acid soluble chloride content in the grout reached a maximum value of 0.0023% by weight of grout inside the north and south ducts. This value is much lower than the critical

chloride threshold value of 0.033%. Chloride samples were taken at 6-inch intervals within the forensic analysis length and chloride content plots were obtained, as shown in Figure 5.39.

Light uniform corrosion was found on all of the strands located in the north and south ducts.

Specimen 4.2 had four duct splices. The south duct had two industry standard splices, one beginning 12 inches to the east of the centerline and the other 12 inches to the west. The north duct had two heat-shrink splices at the same locations. Figure 5.37 shows the condition of the duct splices at the end of exposure testing. The only corrosion found on the industry standard splices was very light and located on the end of the splice. Both heat-shrink splices showed no signs of rust staining.

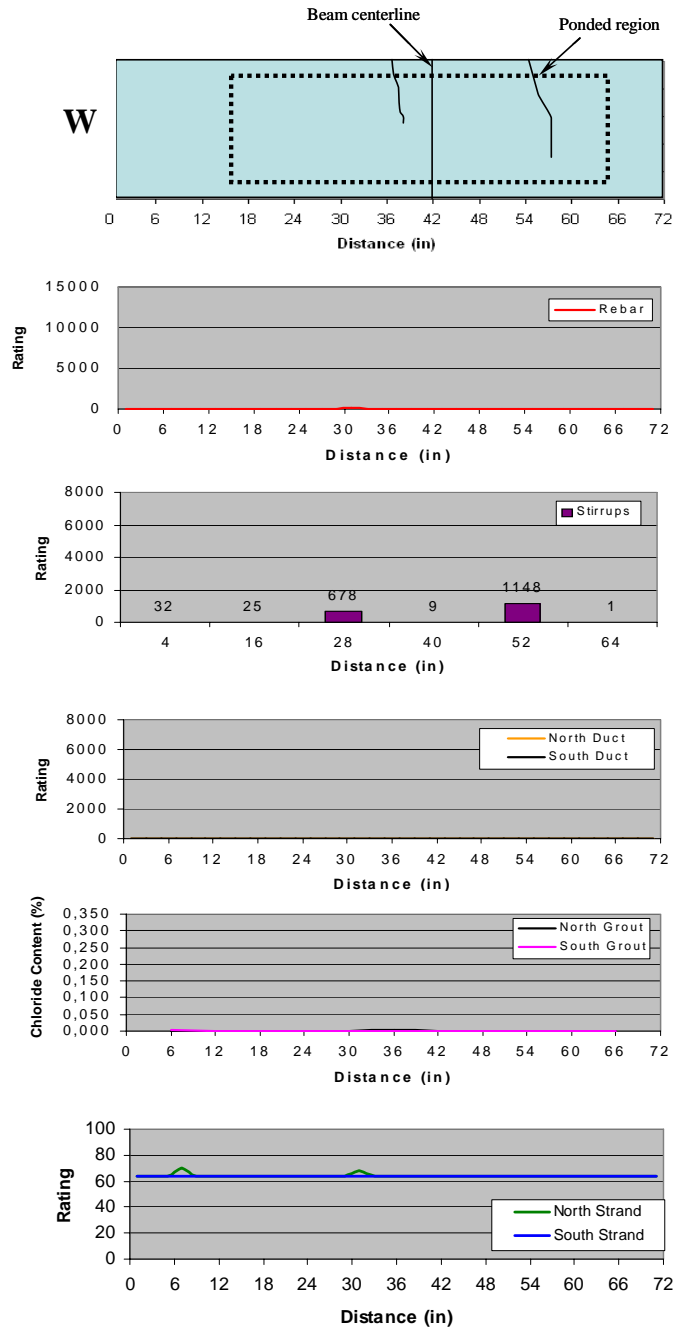


Figure 5.39 Specimen 4.2 – Crack Pattern and Specimen Corrosion Rating Graphs<sup>6,7</sup>



## 5.4 FORENSIC EXAMINATION RESULTS FOR PHASE II BEAMS

### 5.4.1 Beam Specimen 1.5 – Non-PS, Fly Ash Concrete

At the end of exposure, Specimen 1.5 had a large number of cracks on the top face and both sides (see Figure 5.40). A majority of the cracks were confined to the constant maximum moment region. There was a large amount of rust staining, corresponding to the cracks, on both sides of the specimen. Rust stains did not surround the cracks located outside the ponded region. Specimen 1.5 had a maximum crack width of 0.02 inches located 14 inches to the west and 11 inches to the east of the centerline.



*Lateral (North) View*

*Top View (from South Side)*

**Figure 5.40 Specimen 1.5 – Condition Prior to Autopsy<sup>6,7</sup>**

A full autopsy of Specimen 1.5 was performed, providing a total length of 72 inches of the longitudinal bars and six stirrups to be analyzed. Forty-two inches of the analysis length extended to the west of the centerline of the beam and the remaining 30 inches extended to the east.

After removing all mild steel bars in the autopsy region, very mild corrosion was found on the eight longitudinal bars, with only a few locations showing moderate to severe corrosion. Five of the eight bars showed localized corrosion (see Figure 5.41) 14 inches to the west of the beam centerline.

This location coincides with one of the maximum crack width locations.

#### Corrosion Rating:

Specimen	Generalized Rating	Localized Rating
Stirrups	224	296
Long. mild steel	6	8
North Duct	NA	NA
South Duct	NA	NA
North Strands	NA	NA
South Strands	NA	NA



*Longitudinal Bar*

*Stirrup*

**Figure 5.41 Specimen 1.5 – Mild Steel Bar and Stirrup<sup>6,7</sup>**

The actual location of the centerline stirrup was offset one inch to the east of the centerline of the beam. After a detailed visual inspection, pitting and severe corrosion was found on the top portion of four out of the six stirrups. The two remaining stirrups also showed moderate to severe corrosion. All of the severely corroded stirrups were located inside the ponded region, with the exception of one, which was only one

inch outside the ponded region. Figure 5.41 shows the longitudinal bar and stirrup corrosion rating graphs across the analysis length.

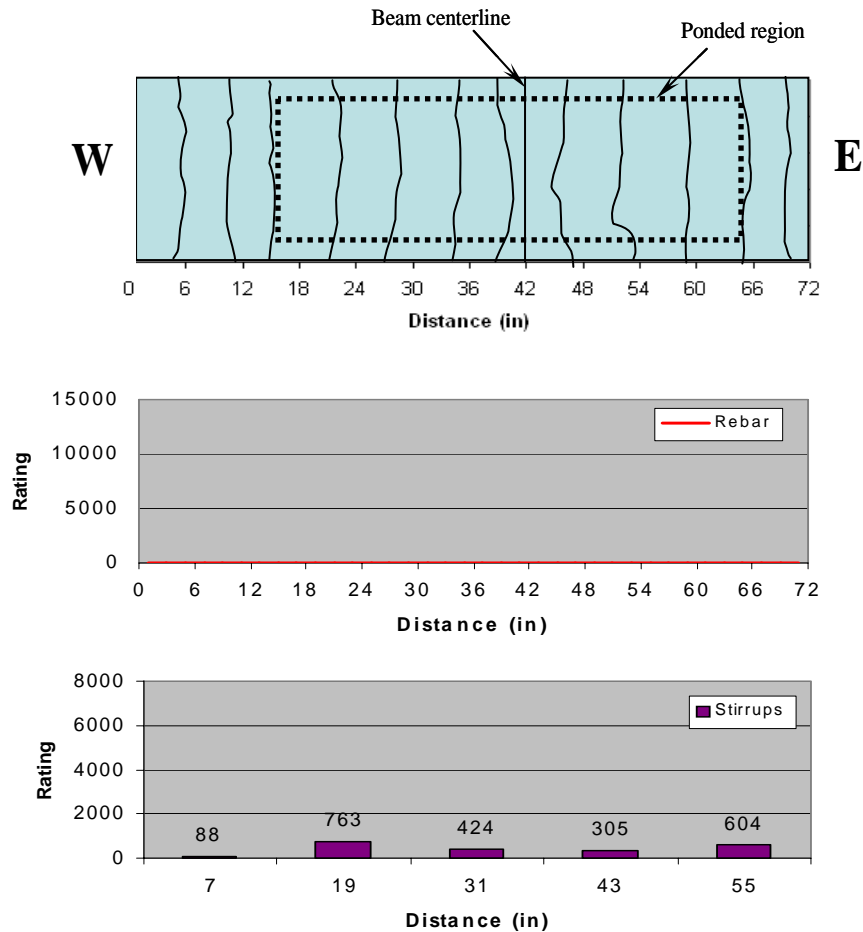


Figure 5.42 Specimen 1.5 – Crack Pattern and Specimen Corrosion Rating Graphs<sup>6,7</sup>

#### 5.4.2 Beam Specimen 1.6 – Non-PS, High Performance Concrete

Specimen 1.6 had a large number of cracks on the top face and both sides at the end of exposure. (See Figure 5.43) A majority of the cracks were confined to the constant maximum moment region. There was minimal rust staining around a few of the cracks. Figure 5.43 shows moisture surrounding the cracks, indicating that the chlorides are traveling through the cracks. Specimen 1.6 had a maximum crack width of 0.016 inches on the crack located 13 inches to the west of the centerline.

A full autopsy of Specimen 1.6 was performed, providing a total length of 72 inches of the longitudinal bars, ducts, grout and strands and six stirrups to be analyzed. Forty-two inches of the analysis length extended to the west of the centerline of the beam and the remaining 30 inches extended to the east.

After removing all mild steel bars in the autopsy region, spots of moderate to severe corrosion were found on all eight longitudinal bars. (See Figure 5.44) The most severe corrosion was found on all the bars in

Specimen	Corrosion Rating:	
	Generalized Rating	Localized Rating
Stirrups	92	361
Long. mild steel	7	15
North Duct	NA	NA
South Duct	NA	NA
North Strands	NA	NA
South Strands	NA	NA

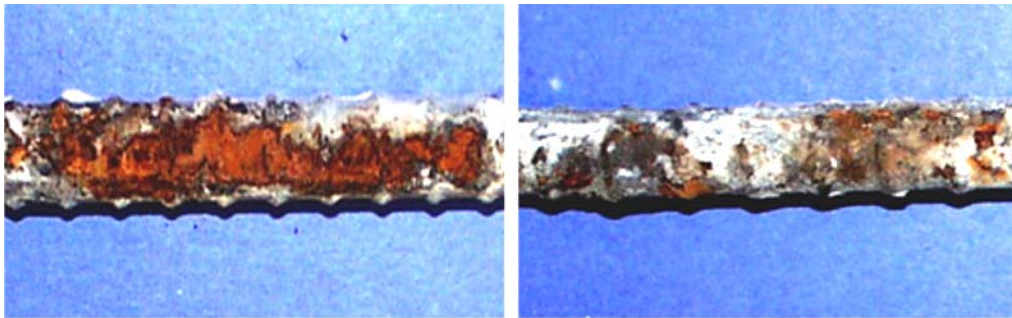
the same location as the maximum crack width. Other spots of corrosion on the bars were consistently located in the same areas, all of which coincided with crack locations.



*Lateral (North) view*

*Top view (from North side)*

**Figure 5.43 Specimen 1.6 – Condition Prior to Autopsy<sup>6,7</sup>**



*Longitudinal Bar*

*Stirrup*

**Figure 5.44 Specimen 1.6 – Mild Steel Bar and Stirrup<sup>6,7</sup>**

The actual location of the centerline stirrup was offset one inch to the west of the centerline of the beam. After a detailed visual inspection, severe pitting and section loss were found on the top portion of the stirrup located 23 inches to the east of the centerline. Cracks were located two inches to each side of the stirrup. Pitting was also found on the stirrup located 25 inches to the west of the centerline, which was one inch from a crack. These two stirrups were included in the ponded region. The remaining stirrup showed light corrosion. Figure 5.45 shows a plot of the longitudinal bar and stirrup corrosion ratings across the analysis length.

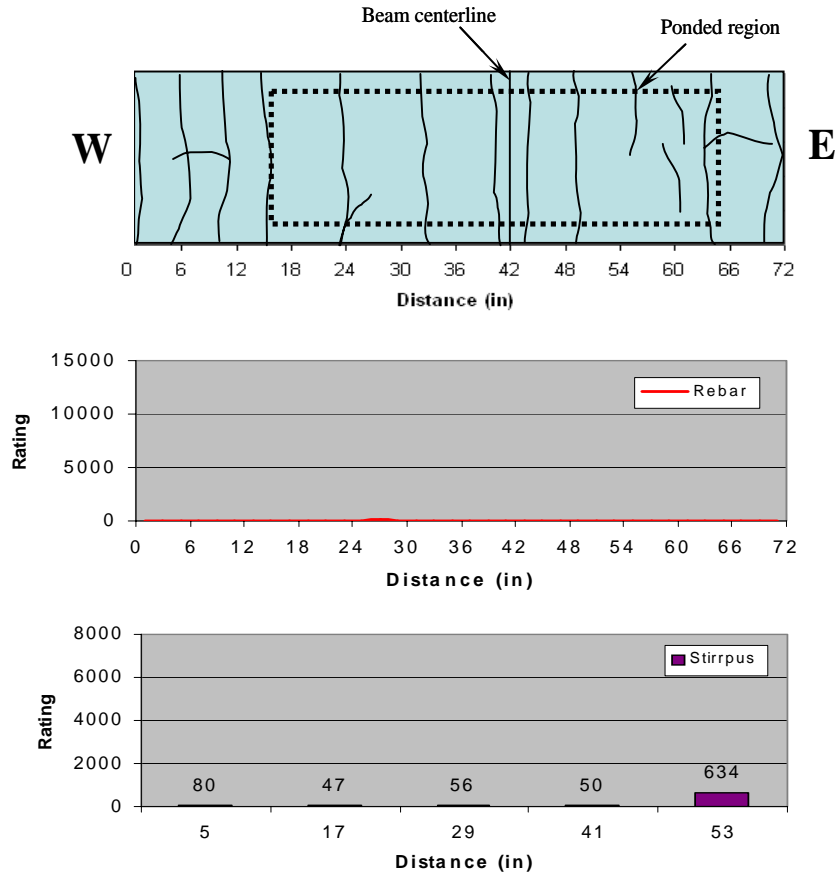


Figure 5.45 Specimen 1.6 – Crack Pattern and Specimen Corrosion Rating Graphs<sup>6,7</sup>

### 5.4.3 Beam Specimen 2.5 – 2/3 PS, Fly Ash Concrete

As seen in Figure 5.46, Specimen 2.5 had five major transverse cracks at the end of exposure. Each of these cracks coincided with the stirrup locations. (See graphs in Figure 5.49) The maximum crack widths were 0.016 and 0.013 inches, located 13 inches to the east and 12 inches to the west of the beam centerline, respectively. Rust staining on the concrete was minimal for this specimen.

A full autopsy of Specimen 2.5 was performed, providing a total length of 72 inches of the longitudinal bars, duct, grout and strands, and six stirrups for analysis. (See Figure 5.48) Forty-two inches of the analysis length extended to the west of the centerline of the beam and the remaining 30 inches extended to the east.

Any corrosion found on the mild steel bars was moderate to severe and very localized. No bars had any section loss. Seven of the eight bars had localized corrosion that corresponded to the maximum crack width. Four of the eight bars experienced moderate corrosion that corresponded to the second maximum crack width of 0.013 inches. No corrosion was found anywhere on any of the bars, except in these two previously described locations.

After a thorough visual inspection, severe uniform corrosion, pitting and section loss were found covering the stirrups located under the largest crack and at the centerline of the beam. The stirrup coinciding with

Specimen	Corrosion Rating:	
	Generalized Rating	Localized Rating
Stirrups	356	866
Long. mild steel	4	20
North Duct	21	8
South Duct	309	1776
North Strands	168	32
South Strands	168	28

the second largest crack was completely covered with uniform corrosion and pitting. The stirrup 20 inches to the east of the centerline did not show signs of uniform corrosion, but did have one large area of severe corrosion and section loss. This stirrup was also located beneath a crack. The remaining two stirrups showed few signs of corrosion.

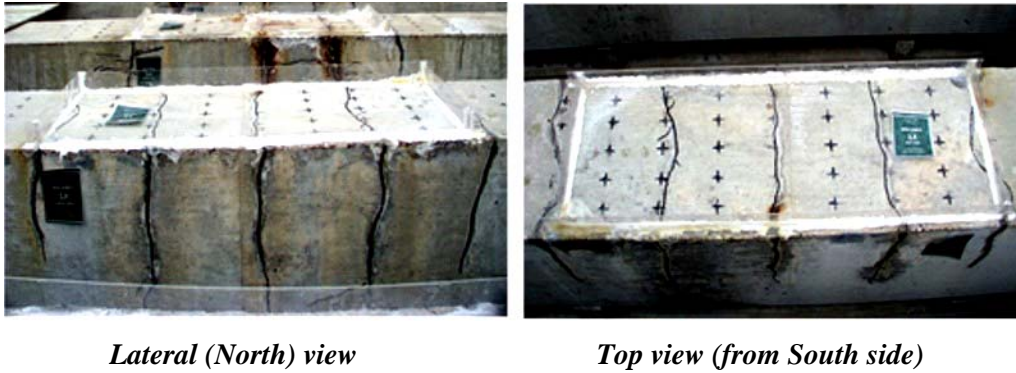


**Figure 5.46 Specimen 2.5 – Condition Prior to Autopsy<sup>6,7</sup>**

Extremely severe corrosion and area loss, corresponding to the second maximum crack location, were found on the south duct. (See Figure 5.48 and graphs in Figure 5.49) Both ducts showed signs of light corrosion at the centerline.

The grout in both ducts showed large voids in the top due to bleed water. The void did not affect the north duct; however it appears to have contributed to the consumption of the south duct. A large accumulation of corrosion products from the south duct was found attached to the grout. (See Figure 5.48) The corrosion rating of the south duct and the chloride content of the south duct are significantly higher at the second maximum crack location. The acid soluble chloride content in the grout reached a maximum value of 0.0036% by weight of grout inside the south duct, and 0.0013% by weight of grout inside the north duct. These values are much lower than the critical chloride threshold value of 0.033% by weight of grout. Chloride samples were taken at 6-inch intervals within the forensic analysis length and chloride content plots were obtained, as shown in Figure 5.49.

Light uniform corrosion was found on all of the strands located in the north and south ducts.



**Figure 5.47 Specimen 2.5 – Duct Splices<sup>6,7</sup>**

Specimen 2.5 had two duct splices. The south duct had an industry standard splice, and the north duct had a heat-shrink splice. Both splices were located at the centerline of the beam. Figure 5.47 shows the

condition of the duct splices at the end of exposure. Severe corrosion and minor section loss were found on the center half of the top of the oversized piece of the industry standard splice. The heat-shrink splice on the north duct showed signs of rust staining on one side. This is due to the lack of sufficient adhesion between the steel duct and splice, allowing moisture to be trapped under the splice.

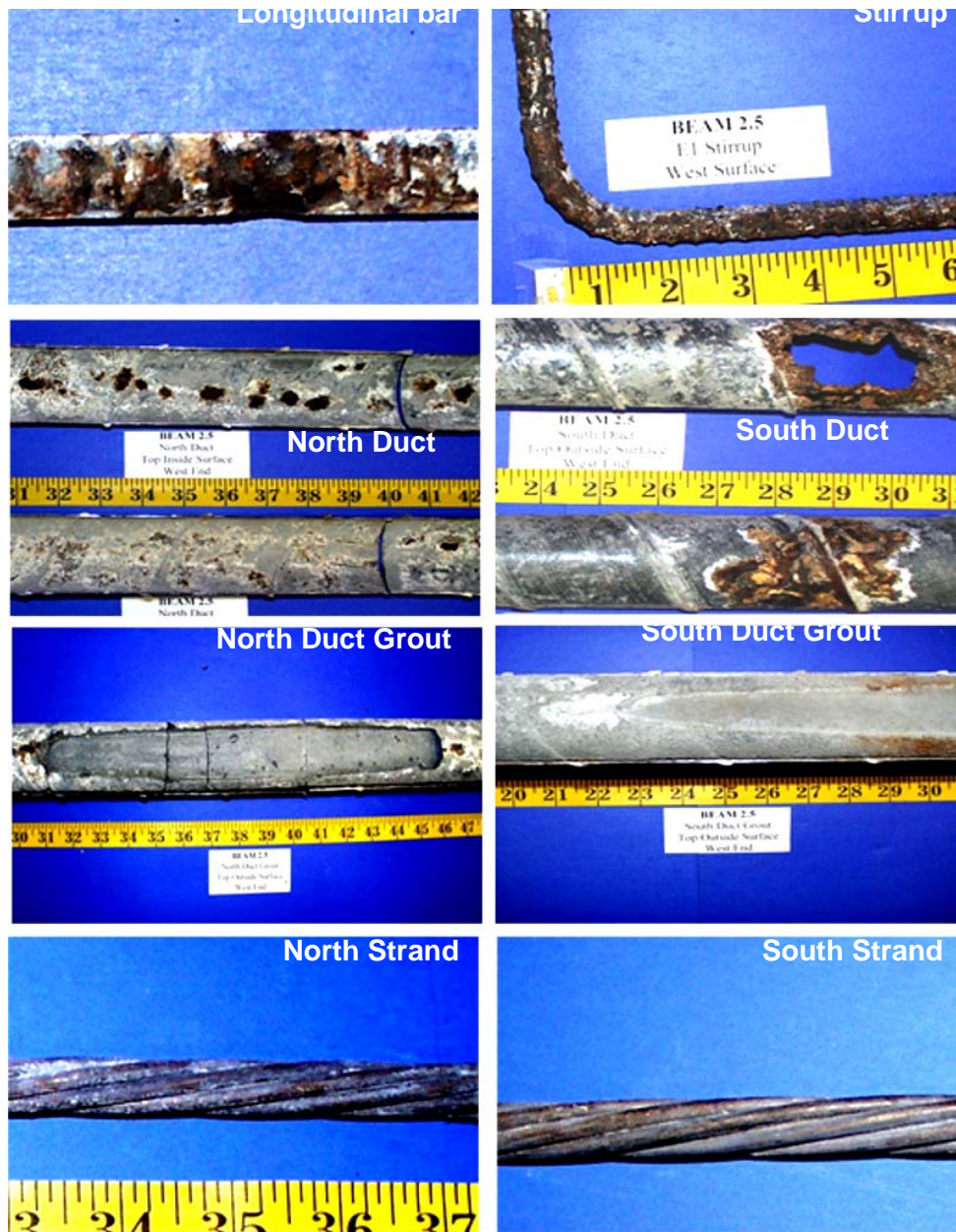
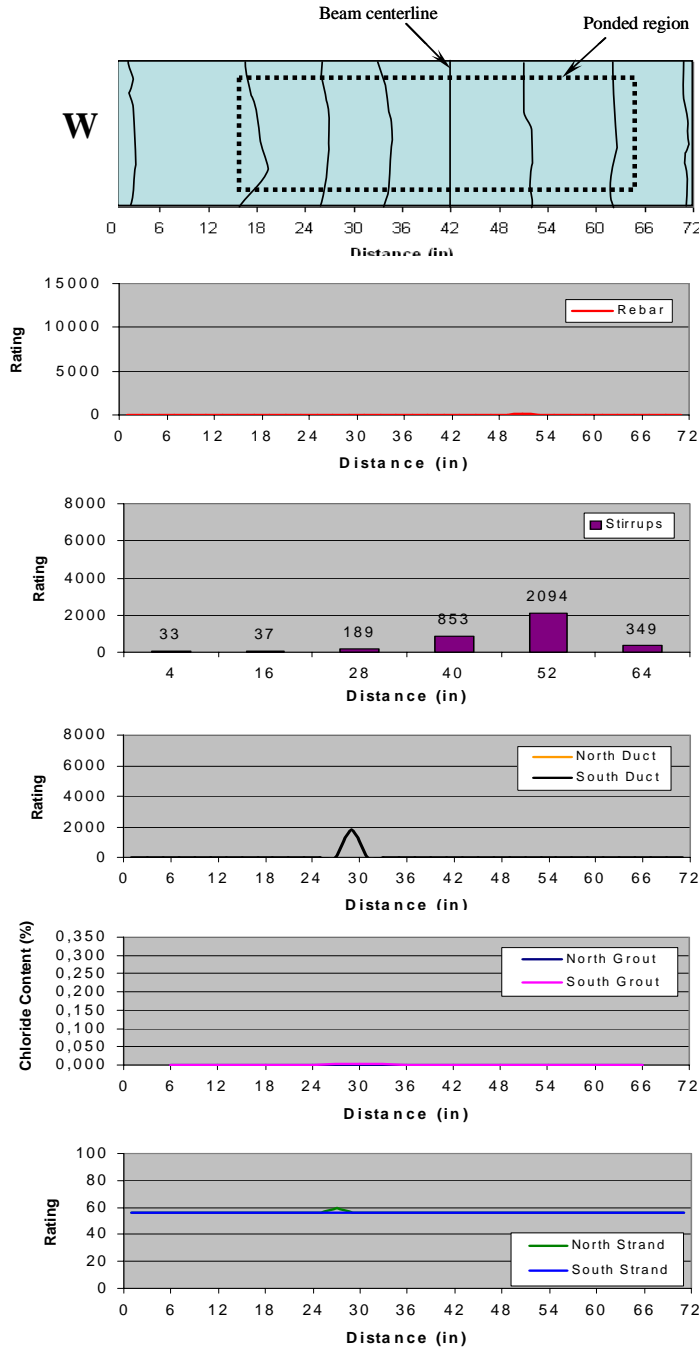


Figure 5.48 Specimen 2.5 – Reinforcing Elements<sup>6,7</sup>



**Figure 5.49 Specimen 2.5 Crack Pattern and Specimen Corrosion Rating Graphs<sup>6,7</sup>**

**5.4.4 Beam Specimen 2.6 – 2/3 PS, High Performance Concrete**

Figure 5.50 shows Specimen 2.6 as having five major cracks at the end of exposure. Each of these cracks coincided with the stirrup locations. (See graphs in Figure 5.53) The maximum crack width was 0.016 inches, located 26 inches to the east and 23 inches to the west of the beam centerline. As seen in Figure 5.50, rust staining on the concrete was present around a few of the cracks.

A full autopsy of Specimen 2.6 was performed, providing a total length of 72 inches of the longitudinal bars, duct, grout and strands, and six stirrups for analysis. Forty-two inches of the analysis length

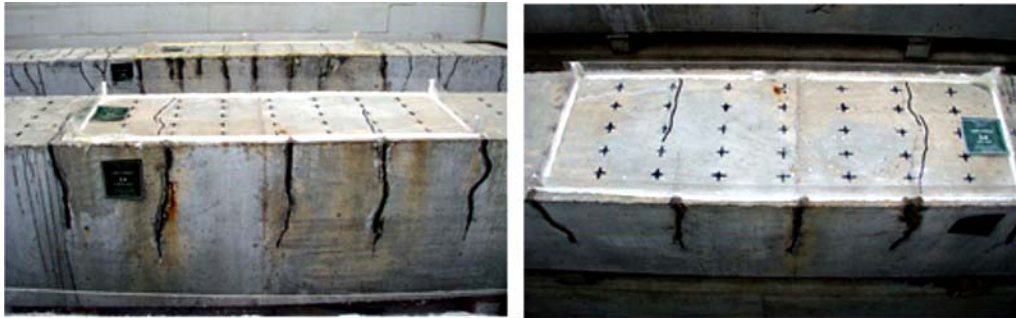
extended to the west of the centerline of the beam and the remaining 30 inches extended to the east. (See Figure 5.52)

The only corrosion found on the mild steel bars was confined to one bar. It was severe corrosion with significant section loss. This area was located 22 inches to the west of the centerline. It was found to be due to its contact with cross bars that were present for construction purposes only.

The only significant corrosion found on the stirrups was present on those located 14 and two inches to the west of the centerline. These two stirrups had minor section loss in very localized areas. The remaining stirrups showed little signs of corrosion.

**Corrosion Rating:**

Specimen	Generalized Rating	Localized Rating
Stirrups	41	88
Long. mild steel	7	190
North Duct	2	4
South Duct	10	34
North Strands	95	16
South Strands	96	16



*Lateral (North) view*

*Top view (from South side)*

**Figure 5.50 Specimen 2.6 – Condition Prior to Autopsy<sup>6,7</sup>**

Few signs of corrosion were found on both ducts in Specimen 2.6. One area of localized corrosion was found 11 inches to the east of the centerline, as shown in Figure 5.52. The only corrosion found on the south duct was at the centerline, located under the industry standard splice. This area showed severe corrosion with minor area loss.

The grout in both ducts showed large voids in the top due to bleed water. The void in the north duct extended from about 22 to 32 inches west of the centerline, as shown in Figure 5.52. This void did not appear to affect the corrosion protection of the duct. The void in the south duct grout extended from 20 inches west of the centerline to 22 inches to the east, also pictured in Figure 5.52. It is likely that this void contributed to the corrosion of the south duct at the centerline, as it trapped the bleed water under the duct. The acid soluble chloride content in the grout reached a maximum value of 0.0016% by weight of grout inside the north duct, and 0.005% inside the south duct. These values are much lower than the critical chloride threshold value of 0.033% by weight of grout. Chloride samples were taken at 6-inch intervals within the forensic analysis length and chloride content plots were obtained, as shown in Figure 5.53.

Light uniform corrosion was found on all the strands located in the north and south ducts.

Specimen 2.6 had two duct splices. The south duct had an industry standard splice, and the north duct had a heat-shrink splice. Both splices were located at the centerline of the beam. Figure 5.51 shows the condition of the duct splices at the end of exposure testing. Severe corrosion and minor section loss was found on the center two inches of the top of the oversized piece of the industry standard splice. The heat-shrink splice, pictured with the north duct, showed minor signs of rust staining on the inside only.



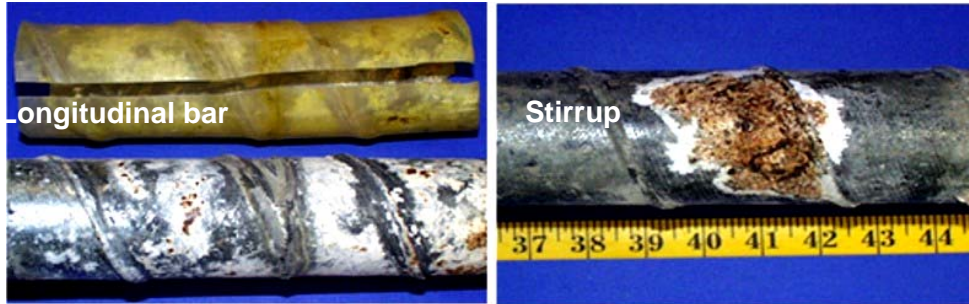


Figure 5.51 Specimen 2.6 – Duct Splices<sup>6,7</sup>

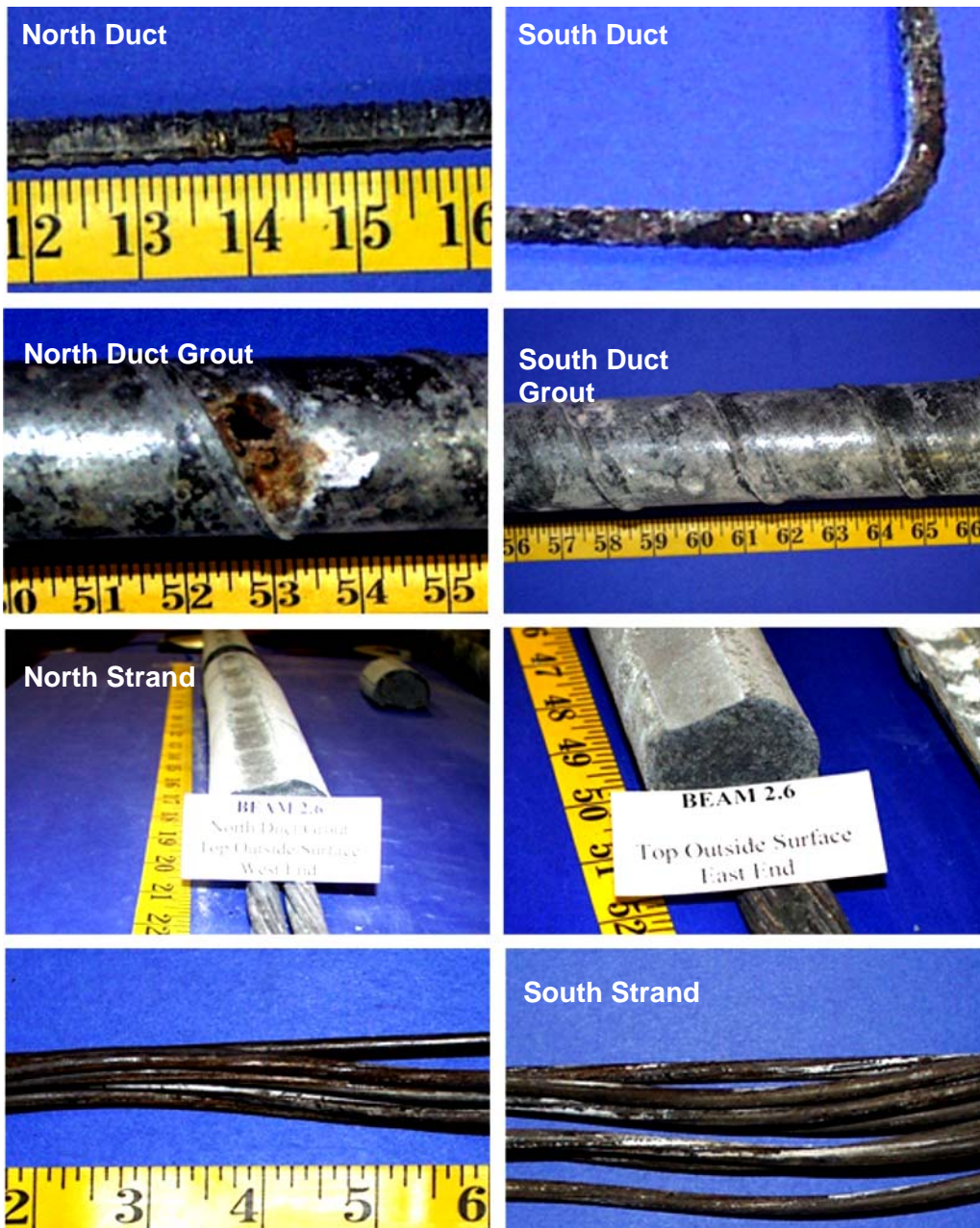


Figure 5.52 Specimen 2.6 – Reinforcing Elements<sup>6,7</sup>

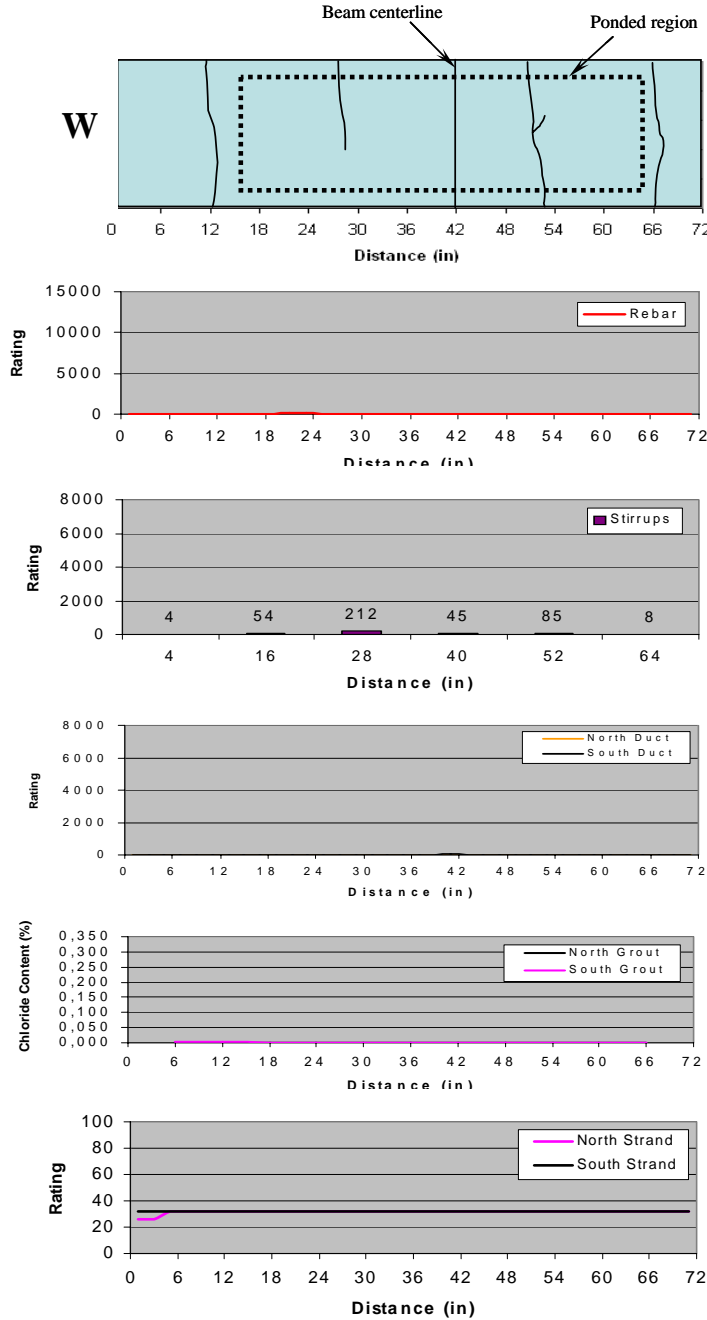


Figure 5.53 Specimen 2.6 – Crack Pattern and Specimen Corrosion Rating Graphs<sup>6,7</sup>

#### 5.4.5 Beam Specimen 3.6 – 100%U PS, Fly Ash Concrete

Specimen 3.6 had only two major transverse cracks across the top of the beam, as shown in Figure 5.54. The location of both of these cracks coincided with a stirrup. (See Figure 5.57) The maximum crack width was 0.016 inches, located 13 inches to the east. The second crack, located 11 inches to the west of the centerline, had a maximum width of 0.013 inches. As shown in Figure 5.54, rust staining around the cracks was minimal. A majority of the rust spots were again from the bolster strips.

A full autopsy of Specimen 3.6 was performed, providing a total length of 72 inches of the longitudinal bars, duct, grout and strands, and six stirrups for analysis. (See Figure 5.56) Forty-two inches of the

analysis length extended to the west of the centerline of the beam and the remaining 30 inches extended to the east.

The only corrosion found on the two mild steel bars was light to moderate, and coincided with the two cracks.

Uniform light to moderate corrosion was found on all the stirrups, except the two located directly under the cracks. These stirrups were severely corroded in many areas, with some section loss.

Corrosion in the north duct was found at the centerline and directly under the larger crack. The centerline corrosion was a result of the industry standard splice on the outside and the large void in the grout on the inside. There was minor area loss at the location, which was due to the alignment with the larger crack and the void in the grout. The only corrosion found on the south duct was moderate to severe corrosion with no area loss, located under the larger crack (see Figure 5.56).

**Corrosion Rating:**

Specimen	Generalized Rating	Localized Rating
Stirrups	78	245
Long. mild steel	4	4
North Duct	24	44
South Duct	6	8
North Strands	91	16
South Strands	96	16



*Lateral (North) view*

*Top view (from South side)*

**Figure 5.54 Specimen 3.6 – Condition Prior to Autopsy<sup>6,7</sup>**

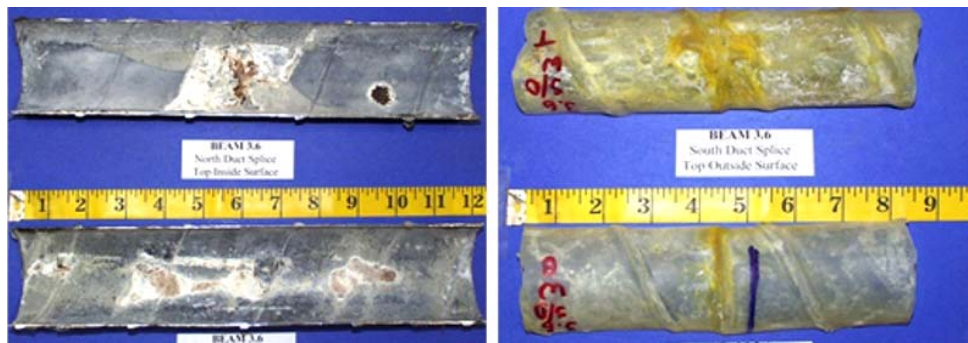


**Figure 5.55 Specimen 3.6 – Duct Splices<sup>6,7</sup>**

The grout in the north duct showed a large void in the top due to bleed water. The void extended from the centerline across the entire east side. The effect of the void in the corrosion of the duct is apparent in Figure 5.56. The corrosion on the north duct and the corrosion products on the north grout are confined to the area above the void. A few small voids were present on the south duct grout, with the most significant one located 13 inches to the east of the centerline. This location is again directly under the larger crack. The acid soluble chloride content in the north duct grout reached a maximum value of 0.0022% by weight of grout at the location under the larger crack. The grout in the south duct reached 0.0021%. These values are much lower than the critical chloride threshold value of 0.033% by weight of grout. Chloride samples

were taken at 6-inch intervals within the forensic analysis length and chloride content plots were obtained, as shown in Figure 5.57.

Light uniform corrosion was found on all the strands located in the north and south ducts.

Specimen 3.6 had two duct splices. The north duct had an industry standard splice, and the south duct had a heat-shrink splice. Both splices were located at the centerline of the beam. Figure 5.55 shows the condition of the duct splices at the end of exposure. Minor corrosion and salt staining was found on the center of the oversized piece of the industry standard splice. The heat-shrink splice showed no signs of rust staining or corrosion.



Figure 5.56 Specimen 3.6 – Reinforcing Elements<sup>6,7</sup>

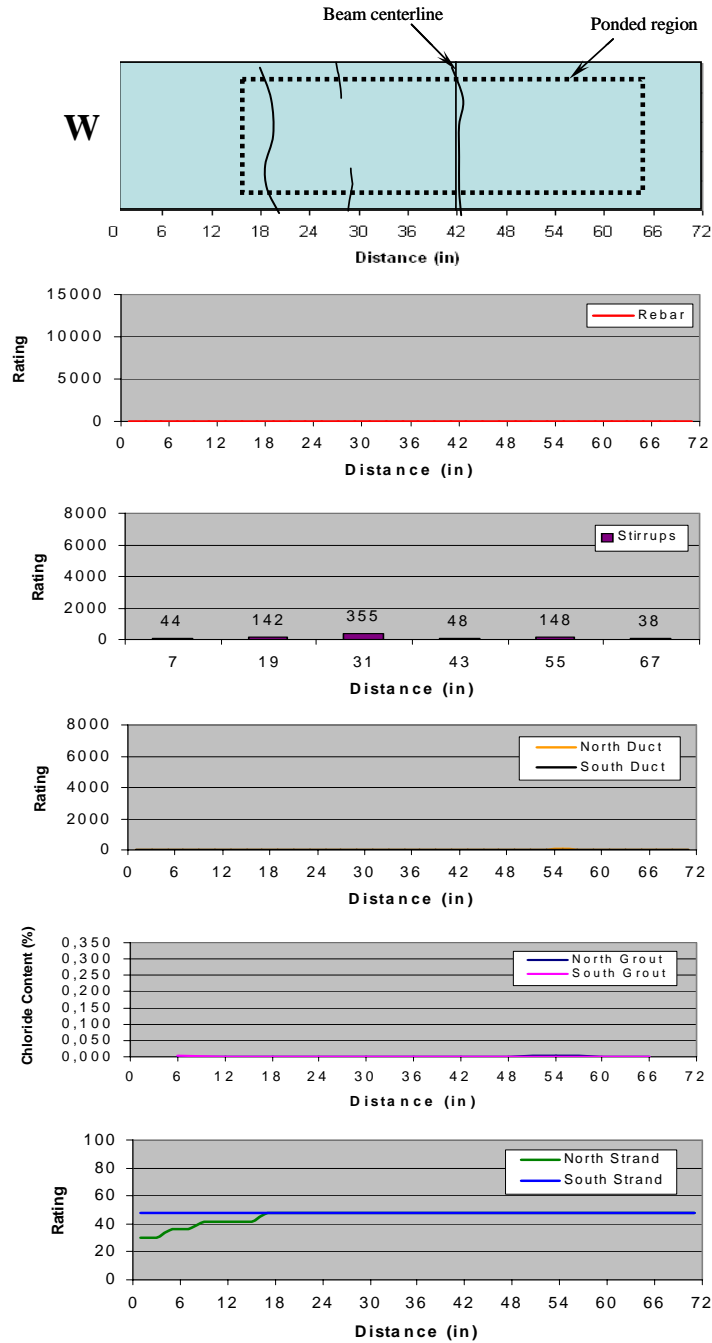


Figure 5.57 Specimen 3.6 – Crack Pattern and Specimen Corrosion Rating Graphs<sup>6,7</sup>

#### 5.4.6 Beam Specimen 3.7 – 100%U PS, High Performance Concrete

Specimen 3.7 had four major transverse cracks across the top of the beam, two of which were located outside the ponded region (see Figure 5.58). The maximum crack width was 0.04 inches, located outside the ponded region at 26 inches to the west of the centerline. The second largest crack, located 13 inches to the east of the centerline, had a maximum width of 0.016 inches. As seen in Figure 5.58, rust staining around the cracks was present on the sides of the beam.

A full autopsy of Specimen 3.7 was performed, providing a total length of 72 inches of the longitudinal bars, duct, grout and strands, and six stirrups for analysis. (See Figure 5.60) Forty-two inches of the analysis length extended to the west of the centerline of the beam and the remaining 30 inches extended to the east.

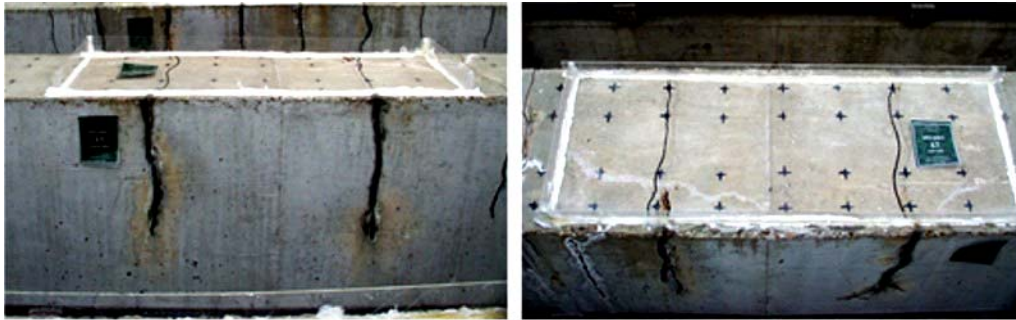
No corrosion was found on the two mild steel bars in Specimen 3.7.

Moderate to severe uniform corrosion was found on the stirrups 10 inches to the west and 14 inches to the east. Both of these stirrups were located directly under cracks. The remaining stirrups showed light uniform corrosion.

A significant amount of area loss was found on the north duct, as shown in Figure 5.60. This location was very close to a 0.013-inch crack. There was severe corrosion and minor area loss at this same location on the south duct. (See Figure 5.60) These were the only significant areas of corrosion found on the ducts in Specimen 3.7.

**Corrosion Rating:**

Specimen	Generalized Rating	Localized Rating
Stirrups	27	16
Long. mild steel	0	2
North Duct	214	1164
South Duct	12	20
North Strands	168	28
South Strands	168	28



*Lateral (North) view*

*Top view (from South side)*

**Figure 5.58 Specimen 3.7 – Condition Prior to Autopsy<sup>6,7</sup>**

The grout in the north duct showed a large void in the top due to bleed water. The void extended from 30 inches west of the centerline to six inches west. Corrosion products from the north duct at the location of area loss were found on the grout. (See Figure 5.60) A few small voids were present on the south duct grout, with the most significant one located under the location of minor area loss in the south duct. The acid soluble chloride content in the north duct grout reached a maximum value of 0.004% by weight of grout. A value of 0.0199% in the south duct was found in the region of the duct area loss. These values are much lower than the critical chloride threshold value of 0.033% by weight of grout. Chloride samples were taken at 6-inch intervals within the forensic analysis length and chloride content plots were obtained, as shown in Figure 5.61.

Light uniform corrosion was found on all the strands located in the north and south ducts.

Specimen 3.7 had two duct splices. The north duct had an industry standard splice, and the south duct had a heat-shrink splice. Both splices were located at the centerline of the beam. Figure 5.59 shows the condition of the duct splices at the end of exposure. The only corrosion found on the industry standard splice was located under the duct tape. The heat-shrink splice showed no signs of rust staining or corrosion.



Figure 5.59 Specimen 3.7 – Duct Splices<sup>6,7</sup>

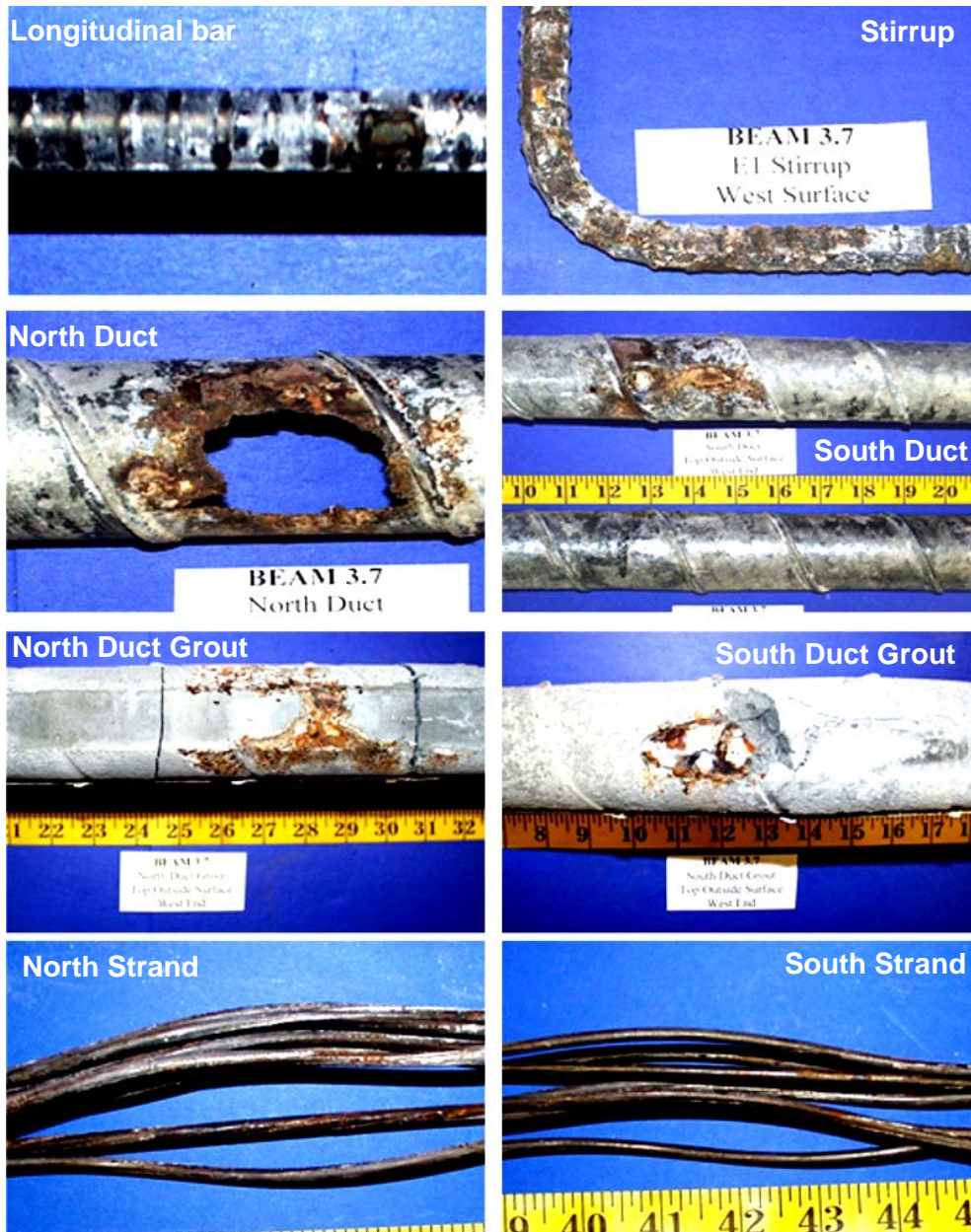


Figure 5.60 Specimen 3.7 – Reinforcing Elements<sup>6,7</sup>

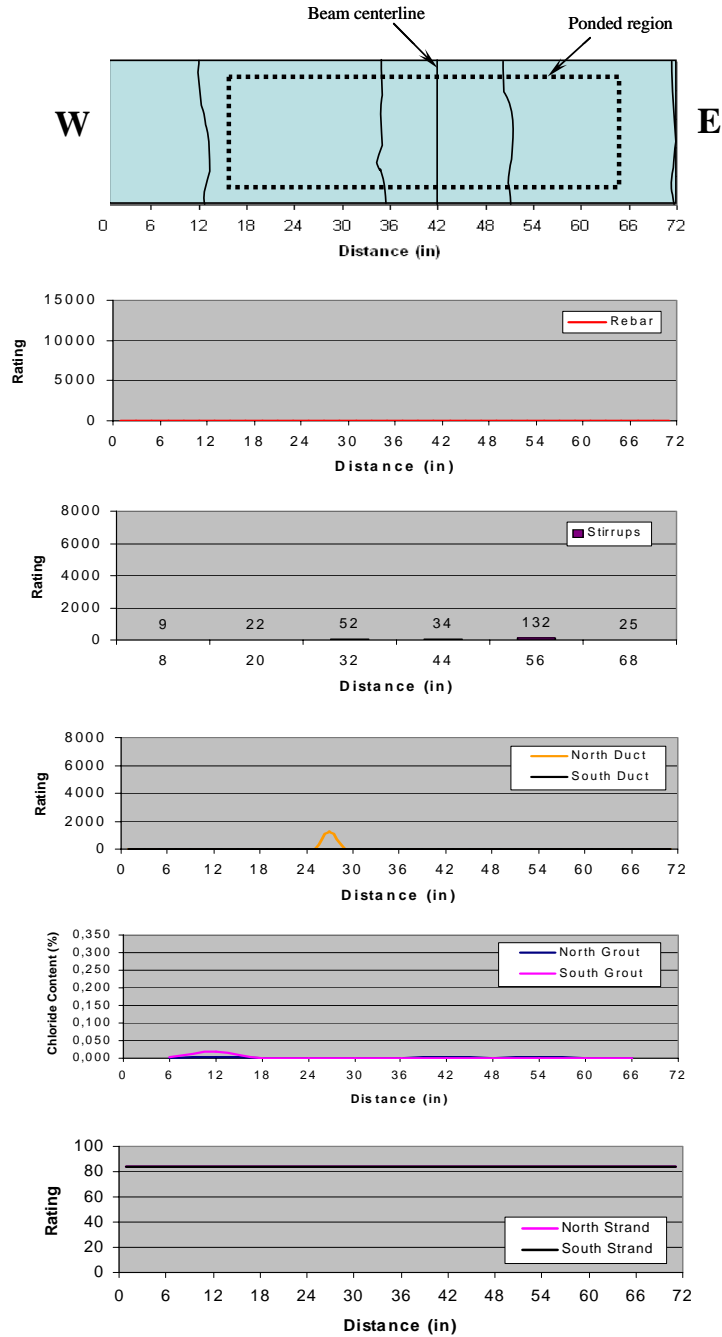


Figure 5.61 Specimen 3.7 – Crack Pattern and Specimen Corrosion Rating Graphs<sup>6,7</sup>

## 5.5 CORROSION RATING SUMMARY

The extent of corrosion is analyzed by obtaining the “generalized” corrosion rating for stirrups, mild steel reinforcement, ducts and strands for all autopsy specimens. Generalized corrosion ratings are calculated by dividing the total corrosion rating by the total length of each element. The result is a rating per unit foot of each element. For longitudinal reinforcing bars, since the number varied among specimens, the total rebar rating for each beam was divided by the total length of rebar being evaluated. The same procedure was followed for strands, where the number of strands per duct in each type of prestressed specimen also varied. In this case, the total strand rating for each duct was divided by the total length of



prestressing strand being evaluated. The total length used for stirrups was 10.5 ft, for rebar 48 ft (for Non-PS and 2/3 PS beams) and 12 ft (for 100% PS beams), for ducts 6 ft, and for strands 12 ft (for 2/3 PS beams), 18 ft (for 100%U PS beams) and 24 ft (for 100%S PS beams).

The severity of corrosion is analyzed by obtaining the “localized” corrosion rating for all elements. Localized corrosion is of great interest in this research program since this is the type of corrosion that will ultimately result in failure of the structural element, or structure. Localized corrosion rating was taken as the maximum rating recorded for any 2-inch interval for each element.

### 5.5.1 Stirrup Corrosion Ratings

Figure 5.62 shows the generalized stirrup corrosion ratings for Phase I and Phase II beams. The analysis of this figure shows that:

- Specimen performance increases as the level of prestress increases from 2/3 PS to 100% PS
- Performance of 2/3 prestress beams appears to be much more similar to that of the Non-PS beams, as opposed to that of the 100% PS beams
- Corrosion index increases as the loading, and thus transverse cracking increases
- High performance concrete specimens perform better than Class C Concrete specimens with Fly Ash
- Mixed reinforcing beams (2/3 PS) show the worst stirrup performance, even when comparing with non prestressed beams.

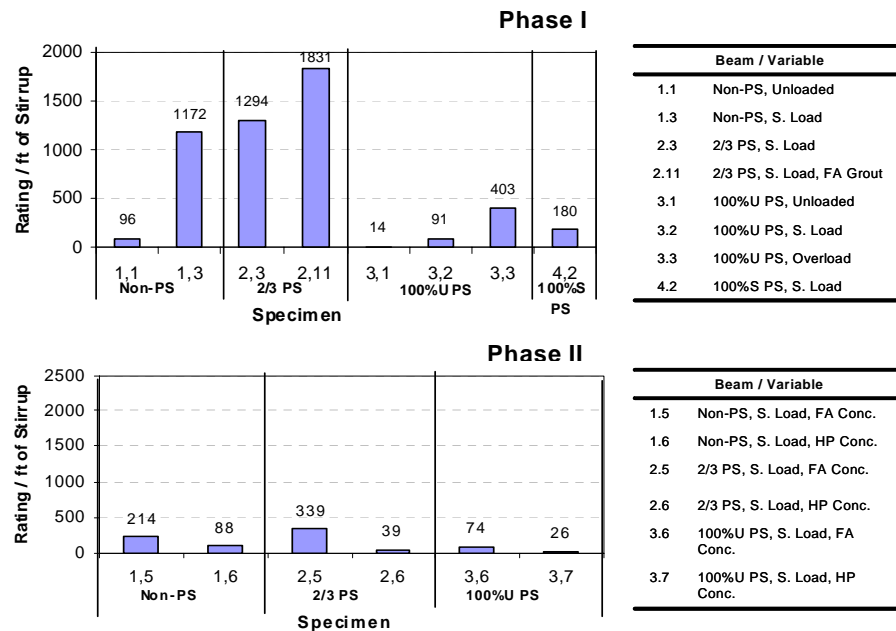
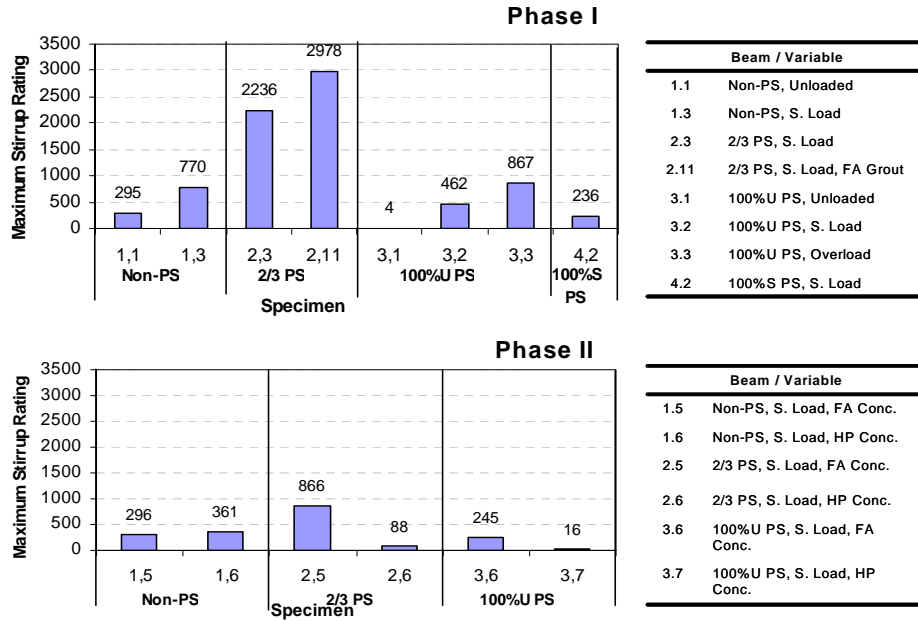


Figure 5.62 Generalized Stirrup Corrosion Ratings<sup>6,7</sup>

Figure 5.63 shows the localized stirrup corrosion ratings for all autopsy beams. Similar trends as found from the generalized corrosion ratings. The increase in corrosion rating as the crack width increases is more apparent as the localized ratings significantly increase from Specimen 1.3 to Specimens 2.3 and 2.11. Also, the corrosion rating increase from Specimen 3.1 (uncracked - unloaded) to Specimens 3.2 (service load) and 3.3 (overloaded) is significant.



**Figure 5.63 Localized Stirrup Corrosion Ratings<sup>6,7</sup>**

### 5.5.2 Rebar Corrosion Ratings

Figure 5.64 shows the generalized bar corrosion ratings for all autopsy beams. The plots show that:

- Mixed reinforced beams (2/3 PS) show extremely poor performance when compare with non prestressed and fully prestressed beams
- The negative effects of cracking clearly show when comparing non prestressed beams 1.1 (unloaded, uncracked) and 1.3 (Service load, cracked)
- All ratings for Phase II beams are very low, which is possible due to the use of fly ash concrete and high performance concrete. However, results cannot be compared against Phase I beams since there is a one year exposure testing difference.

Figure 5.65 shows the corresponding localized bar corrosion ratings. This figure shows the same trends as in Figure 5.64.

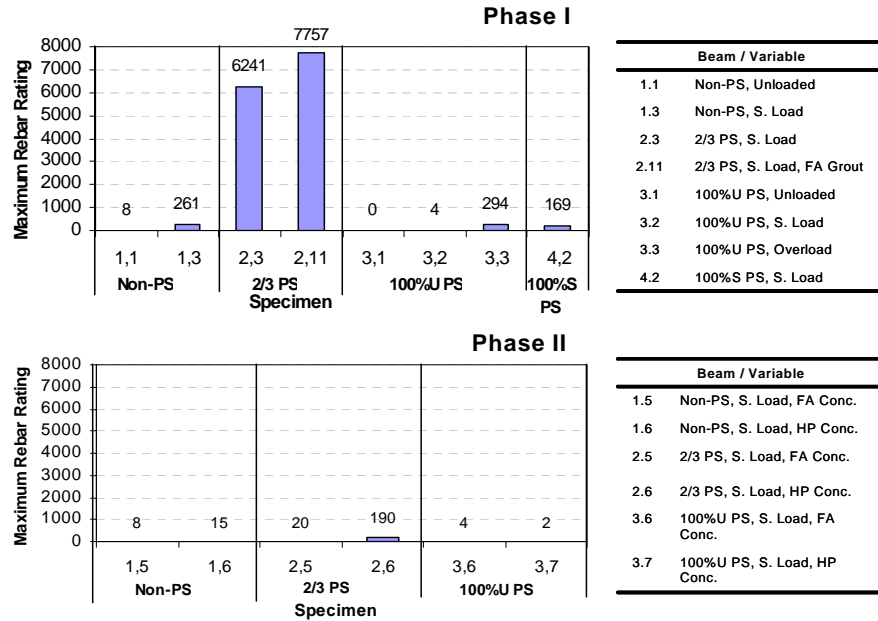


Figure 5.64 Generalized Bar Corrosion Rating <sup>6,7</sup>

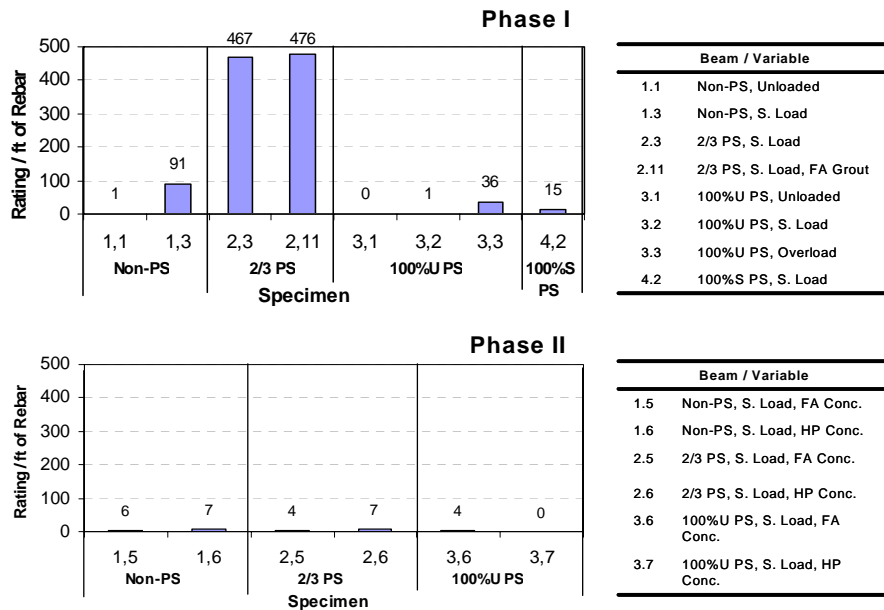


Figure 5.65 Localized Bar Corrosion Ratings <sup>6,7</sup>

### 5.5.3 Galvanized Steel Duct Ratings

Figure 5.66 shows the generalized corrosion rating for all autopsy beams. The two ducts on each specimen are clearly indicated by D1 and D2. From this figure it can be concluded that:

- Phase I beams show a significantly worse performance of the 2/3 PS beams with respect to 100% PS beams
- The negative effect of cracking is observed when comparing Specimen 3.1 (uncracked, unloaded) and Specimen 3.3 (cracked, overloaded)

- Fly Ash added to the grout seems to provide better duct corrosion protection, when comparing Specimen 2.3 (2/3 PS, service load, normal grout) to Specimen 2.11 (2/3 PS, service load, fly ash grout)
- The large rating of Specimen 3.7 in the Phase II beams does not follow the trend of an increase in corrosion resistance with an increase of prestressing
- Phase II specimens do not show a distinct trend with respect to concrete types. Fly ash – class C concrete and high performance concrete appear to be performing well and in a similar manner.

Figure 5.67 shows the corresponding localized duct corrosion ratings for all autopsy specimens. The same trends are observed as in Figure 5.66.

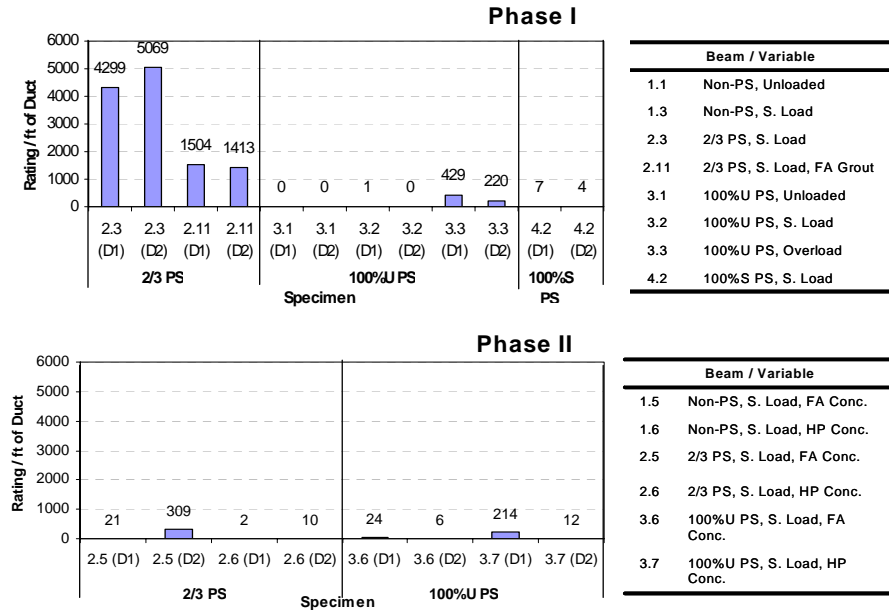


Figure 5.66 Generalized Duct Corrosion Ratings<sup>6,7</sup>

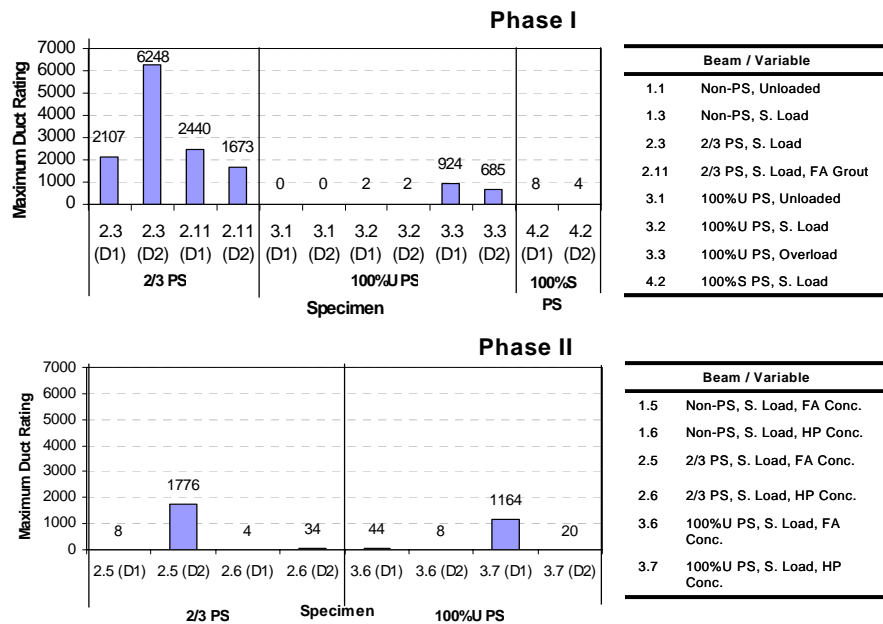
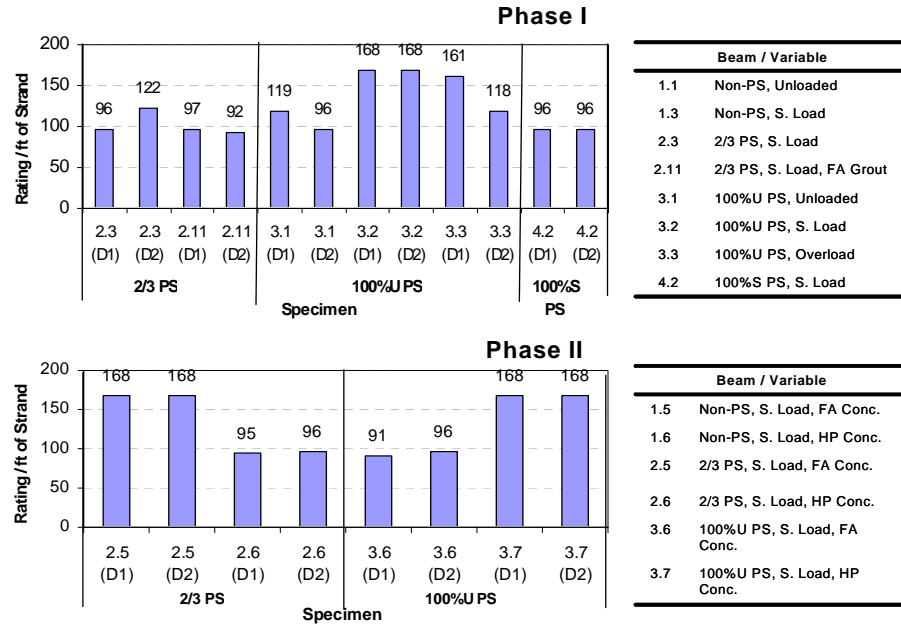


Figure 5.67 Localized Duct Corrosion Ratings<sup>6,7</sup>

### 5.5.4 Prestressing Strand Ratings

Figure 5.68 shows the generalized strand corrosion ratings for all autopsy beams. Findings from this plot include:

- All strands appear to be performing similarly
- After visual inspection only minimal variation was found on the performance of the strands. Therefore, it appears that specimens require more exposure time to indicate differences and trends
- The difference between Specimen 2.3 (normal grout) and 2.11 (fly ash grout) indicates that the addition of fly ash to the grout does not have a large effect on the corrosion protection of the strand



**Figure 5.68 Generalized Strand Corrosion Ratings<sup>6,7</sup>**

Figure 5.69 shows the localized strand corrosion ratings. Phase II beams show very similar results as those from Phase I. However, Specimens 2.3 (D1) and 3.3 (D1) show larger ratings, corresponding with crack locations.

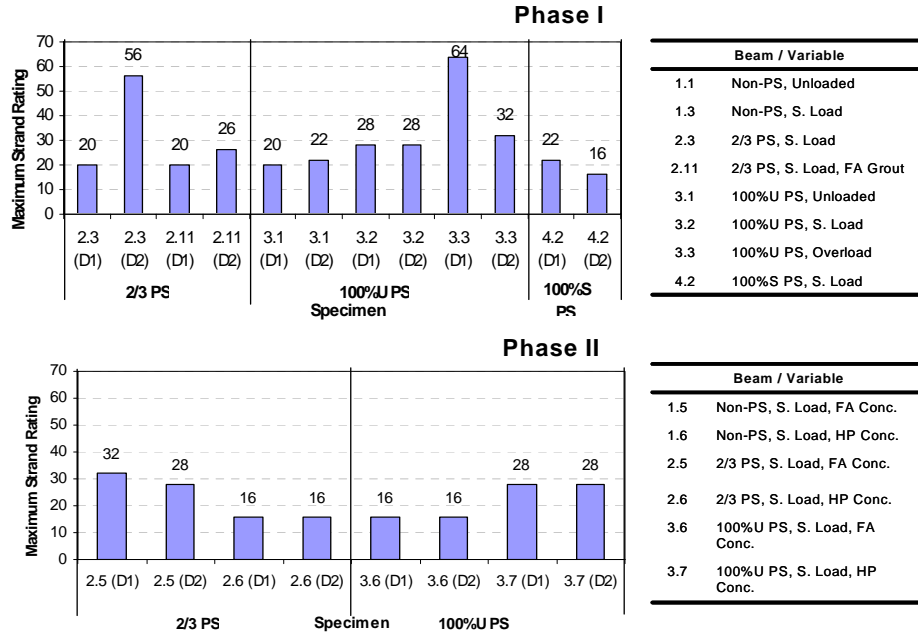


**Figure 5.69 Localized Strand Corrosion Ratings<sup>6,7</sup>**

## CHAPTER 6: ANALYSIS AND DISCUSSION OF RESULTS

After four and a half years of exposure for phase I beams and three and a half years for phase II beams, the effect of many of the variables involved in this testing program can be analyzed and compared.

### 6.1 OVERALL PERFORMANCE

The use of the large-scale beam specimen was found to be a very good method for analyzing relative specimen performance and for evaluating the adequacy of corrosion protection variables, especially when considering different loading and prestressing levels.

After four and a half years in Phase I beams distinct differences are shown in stirrup, rebar and duct corrosion ratings among the autopsy specimens. Strand corrosion was found to be somewhat similar in all specimens, and therefore, it was clear the need for additional exposure testing for the remaining specimens. Similar results were obtained from Phase II beams.

The relative performance of the specimens in this testing program was studied by looking at the corrosion ratings for stirrups, rebar, ducts and strands, ordered from highest to lowest. Figure 6.1 and Figure 6.2 show the generalized stirrup corrosion ratings for Phase I autopsy beams and phase II autopsy beams, respectively. Figure 6.3 and Figure 6.4 show the generalized rebar corrosion ratings for Phase I and Phase II, respectively. The corrosion rating system used for stirrups and rebar was the same, but the horizontal scale on the graphs is shown differently to clearly indicate the relative performance of the specimens with respect to the element under analysis.

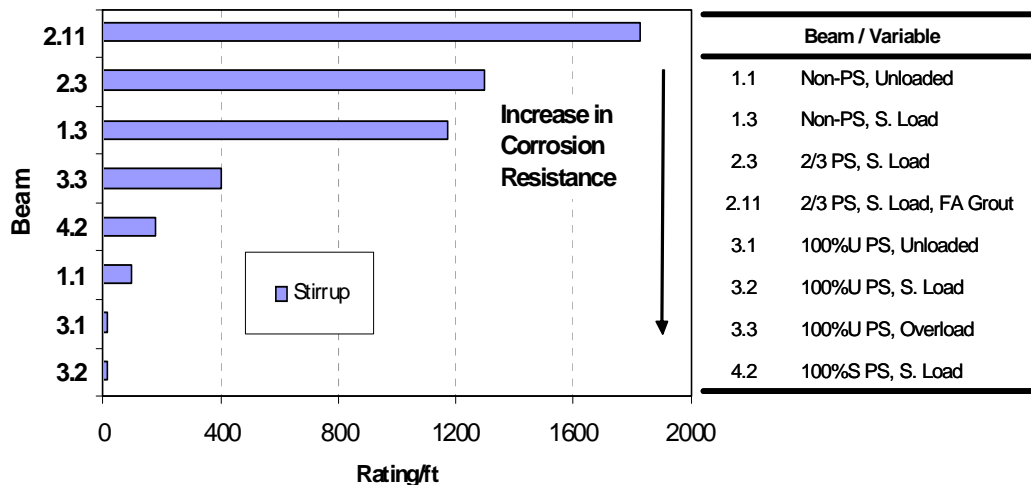


**Figure 6.1 Generalized Stirrup Corrosion Ratings for Phase I Autopsy Beams Ordered According to Performance<sup>6,7</sup>**

As observed from these graphs, phase I specimens follow basically the same order according to performance for stirrup and rebar corrosion ratings. As shown, mixed reinforced (2/3 PS) beams show the worst corrosion resistance, followed by the loaded Non-PS beam, the 100% U PS and the 100%S PS beam. Unloaded specimens show the best overall performance. These results clearly indicate the negative effect of cracking on corrosion resistance. Except for the relative good performance of Specimen 1.3 (non prestressed, loaded), the graphs show a distinct trend with lower corrosion ratings for higher levels of prestress.

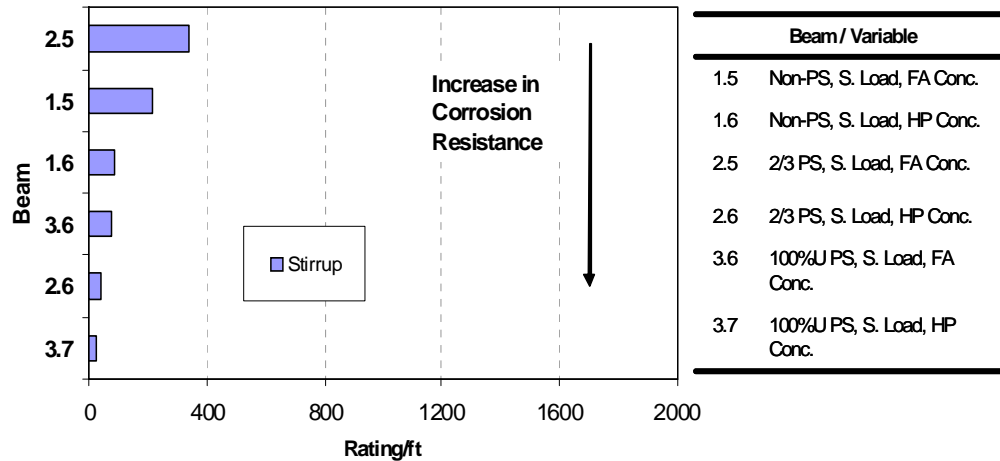


**Figure 6.2 Generalized Stirrup Corrosion Ratings for Phase II Autopsy Beams Ordered According to Performance<sup>6,7</sup>**

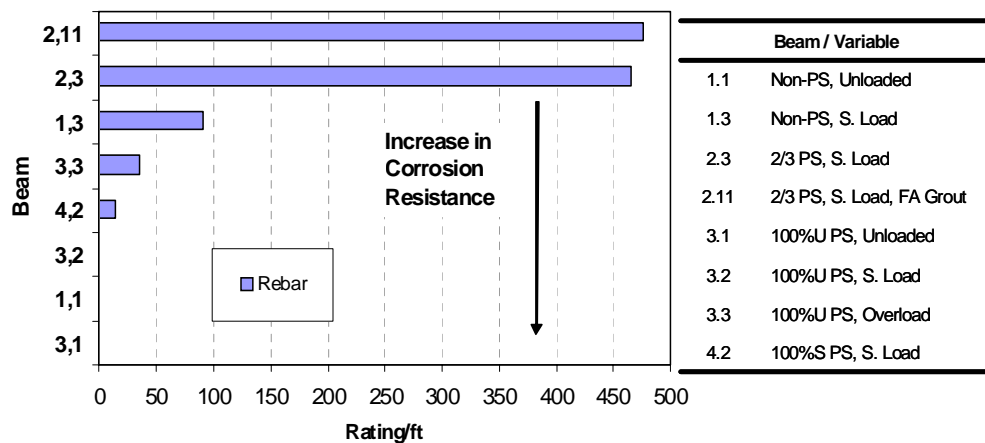


**Figure 6.3 Generalized Rebar Corrosion Ratings for Phase I Autopsy Beams Ordered According to Performance<sup>6,7</sup>**

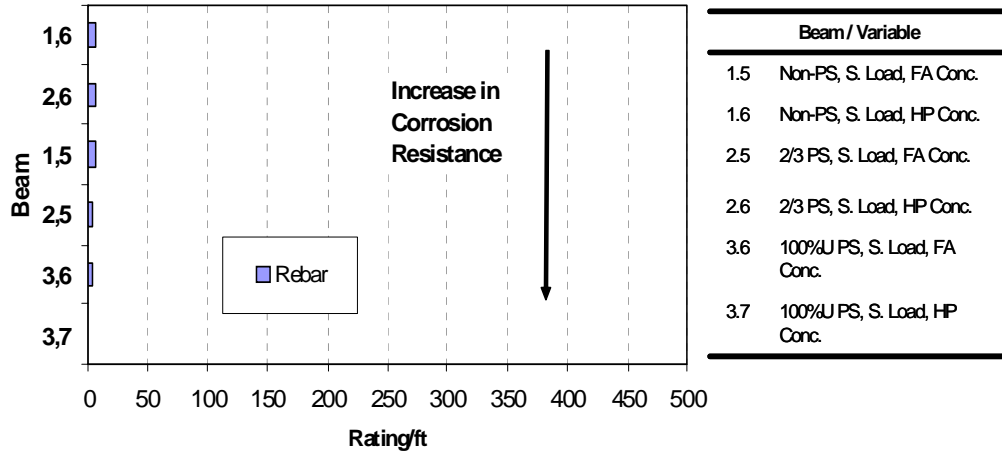
Relative performance of Phase II beams appears to show better corrosion protection in 100% PS beams with respect to mixed reinforced (2/3 PS) beams. There is not a clear distinction with respect to non-prestressed and prestressed members. Also, there is not a clear distinction among class C (with fly ash) concrete specimens and high performance concrete specimens.

The overall performance of the specimens is better compared by considering the total corrosion rating, obtained by summing the ratings for the rebar, duct and strand, as shown in Figure 6.5 and Figure 6.6.

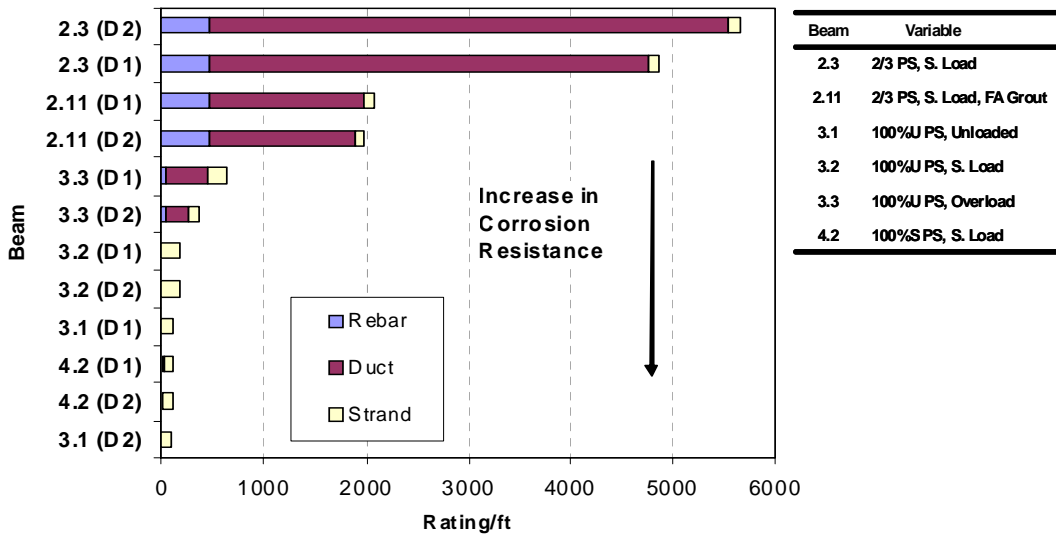
Figure 6.5 shows a clear trend with respect to the level of prestress. As the level of prestress increases, the corrosion resistance increases. In this graphs, it is observed that the strand rating is very similar for all specimens, which suggest the need for a longer period of exposure testing, in order to obtain more conclusive results with respect to strand corrosion.

Figure 6.5 also shows that galvanized duct corrosion is a major problem, even when rebar and corrosion ratings cannot be compared because they are the result of different rating systems.





**Figure 6.4 Generalized Rebar Corrosion Ratings for Phase II Autopsy Beams Ordered According to Performance<sup>6,7</sup>**



**Figure 6.5 Generalized Corrosion Ratings for Phase I Autopsy Beams Ordered According to Performance<sup>6,7</sup>**

The uncracked and unloaded Specimen 3.1 shows the overall best performance as expected. This is a clear indication of the very negative effects of cracking in the other specimens, and the positive effect of precompression force in the concrete.

Figure 6.6 does not show a clear trend with respect to concrete type and levels of prestress. By comparing Phase I and Phase II results, the need for longer periods of exposure testing appears evident and may reflect the relative better performance of specialty concretes (with fly ash) with respect to standard class C concrete specimens. Care must be exercised when making this conclusion, since Phase II autopsy beams had around 23% less exposure time than Phase I autopsy beams.

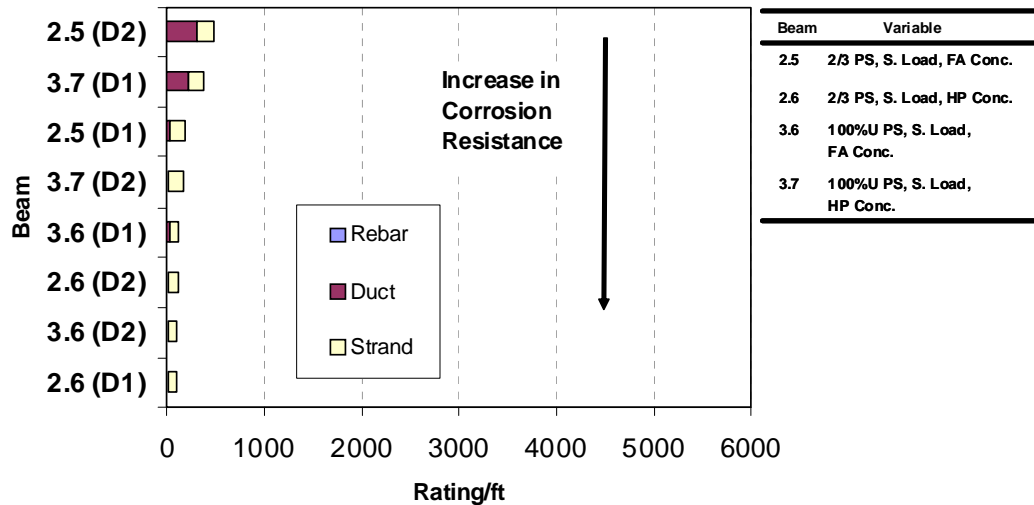


**Figure 6.6 Generalized Corrosion Ratings for Phase II Autopsy Beams Ordered According to Performance<sup>6,7</sup>**

A summary table of results is presented in Table 6.1. In this table, generalized and localized corrosion ratings from Section 5.5 are used to conclude on the relative performance of the testing variables.

**Table 6.1 Summary of Forensic Examination Corrosion Rating Results<sup>6</sup>**

Method of Comparison	Beams Compared	Variable Analyzed	Result
Gen. Stirrup	1.3, 2.3, 3.2, 4.2	Prestress	<ul style="list-style-type: none"> <li>Non and 2/3 PS much worse corrosion protection than 100%S and U PS</li> </ul>
Loc. Stirrup	1.3, 2.3, 3.2, 4.2	Prestress	<ul style="list-style-type: none"> <li>2/3 PS is much worse corrosion protection than all others, including Non-PS</li> </ul>
Gen. and Loc. Duct	2.3, 3.2, 4.2	Prestress	<ul style="list-style-type: none"> <li>2/3 PS the worst corrosion protection by a significant amount</li> </ul>
Gen. and Loc. Strand	2.3, 3.2, 4.2	Prestress	<ul style="list-style-type: none"> <li>All corrosion protections about the same, with 100%U PS a little worse</li> </ul>
Gen. Stirrup	1.5, 2.5, 3.6 1.6, 2.6, 3.7	Prestress	<ul style="list-style-type: none"> <li>100%U PS consistently best corrosion protection</li> <li>corrosion protection of Non and 2/3 PS similar, no consistent superiority</li> </ul>
Gen. and Loc. Bar	1.5, 2.5, 3.6 1.6, 2.6, 3.7	Prestress	<ul style="list-style-type: none"> <li>2/3 PS shows worst corrosion protection by a significant amount</li> </ul>
Gen. and Loc. Duct	2.5, 3.6	Prestress	<ul style="list-style-type: none"> <li>2/3 and 100%U PS corrosion protection similar, no consistent superior PS</li> </ul>
Gen. and Loc. Strand	2.5, 3.6	Prestress	<ul style="list-style-type: none"> <li>2/3 and 100%U PS corrosion protection similar, no consistent superior PS</li> </ul>
Gen. Stirrup	1.1, 1.3 3.1, 3.2, 3.3	Load/Cracking	<ul style="list-style-type: none"> <li>Much worse corrosion protection when cracking is present</li> <li>Corrosion protection decreases as loading increases</li> </ul>

**Table 6.1 (Continued) Summary of Forensic Examination Corrosion Rating Results<sup>6</sup>**

Method of Comparison	Beams Compared	Variable Analyzed	Result
Loc. Stirrup	1.1, 1.3 3.1, 3.2, 3.3	Load/Cracking	<ul style="list-style-type: none"> <li>• Much worse corrosion protection when cracking is present</li> <li>• Corrosion protection decreases as loading increases</li> </ul>
Gen. and Loc. Bar	1.1, 1.3 3.1, 3.2, 3.3	Load/Cracking	<ul style="list-style-type: none"> <li>• Cracked beams show a little worse corrosion protection</li> </ul>
Gen. and Loc. Duct	3.1, 3.2, 3.3	Load/Cracking	<ul style="list-style-type: none"> <li>• Much worse corrosion protection when cracking is present</li> </ul>
Gen. and Loc. Stirrup	1.5, 1.6 2.5, 2.6 3.6, 3.7	Concrete Type	<ul style="list-style-type: none"> <li>• HP concrete consistently better corrosion protection</li> </ul>
Gen. and Loc. Bar	1.5, 1.6 2.5, 2.6 3.6, 3.7	Concrete Type	<ul style="list-style-type: none"> <li>• All similar corrosion protection and all low ratings...both concretes provide good corrosion protection</li> </ul>
Gen. and Loc. Duct	1.5, 1.6 2.5, 2.6 3.6, 3.7	Concrete Type	<ul style="list-style-type: none"> <li>• All corrosion protections similar, no consistent superior concrete</li> </ul>
Gen. and Loc. Strand	1.5, 1.6 2.5, 2.6 3.6, 3.7	Concrete Type	<ul style="list-style-type: none"> <li>• All corrosion protections similar, no consistent superior concrete</li> </ul>
Gen. Duct	2.3, 2.11	Grout Type	<ul style="list-style-type: none"> <li>• Fly ash grout shows much better corrosion protection</li> </ul>
Gen. and Loc. Strand	2.3, 2.11	Grout Type	<ul style="list-style-type: none"> <li>• No difference in corrosion protection between grout types</li> </ul>

## 6.2 EFFECT OF CRACKING

Cracking effects were investigated using the three sections that would be expected to crack under service loads (Non-PS, 2/3 PS and 100% U). In addition, Specimen 4.2 (100%U PS) was found to be cracked at the end of the exposure period, and therefore, it is included in the comparisons.

Specimens 1.3 (Non-PS), 2.3 (2/3 PS) and 2.11 (2/3 PS) developed substantial longitudinal (splitting type) cracking during exposure. None of the other autopsied specimens evidenced longitudinal cracking. Since the longitudinal cracks were very wide and could provided additional paths for chloride penetration, they were considered in crack ratings.

### 6.2.1 Crack Density

Crack ratings for all autopsied specimens in Phase I have been plotted along with stirrup, rebar, duct and strand generalized corrosion ratings, in Figure 6.7 and Figure 6.8. In a similar manner, crack ratings for all autopsied specimens in Phase II have been plotted along with generalized corrosion ratings in Figure 6.9 and Figure 6.10. Crack ratings are defined as indicated in Equation 12.

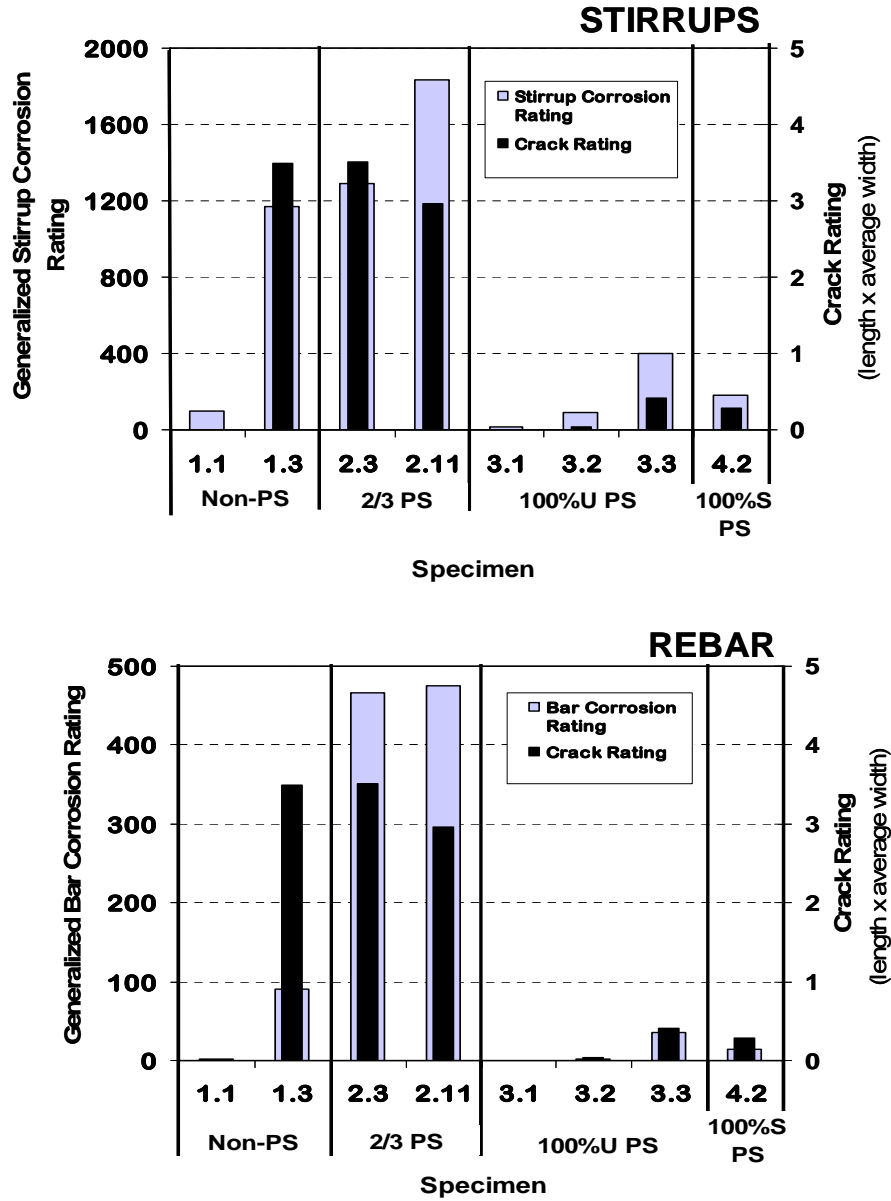


Figure 6.7 Effect of Crack Density on Stirrup and Rebar Corrosion for Phase I Autopsy Beams<sup>7</sup>

$$\text{Crack Rating for each Specimen} = \sum_{i=1}^m (\bar{w}_i \times l_i) \quad \text{Eq. 12}$$

- where,
- $\bar{w}_i$  = average crack width, for crack i
  - $l_i$  = crack length at the end of testing, for crack i
  - m = number of longitudinal and transverse cracks on the specimen top surface, in the 72-inch analysis length
  - i = crack under consideration

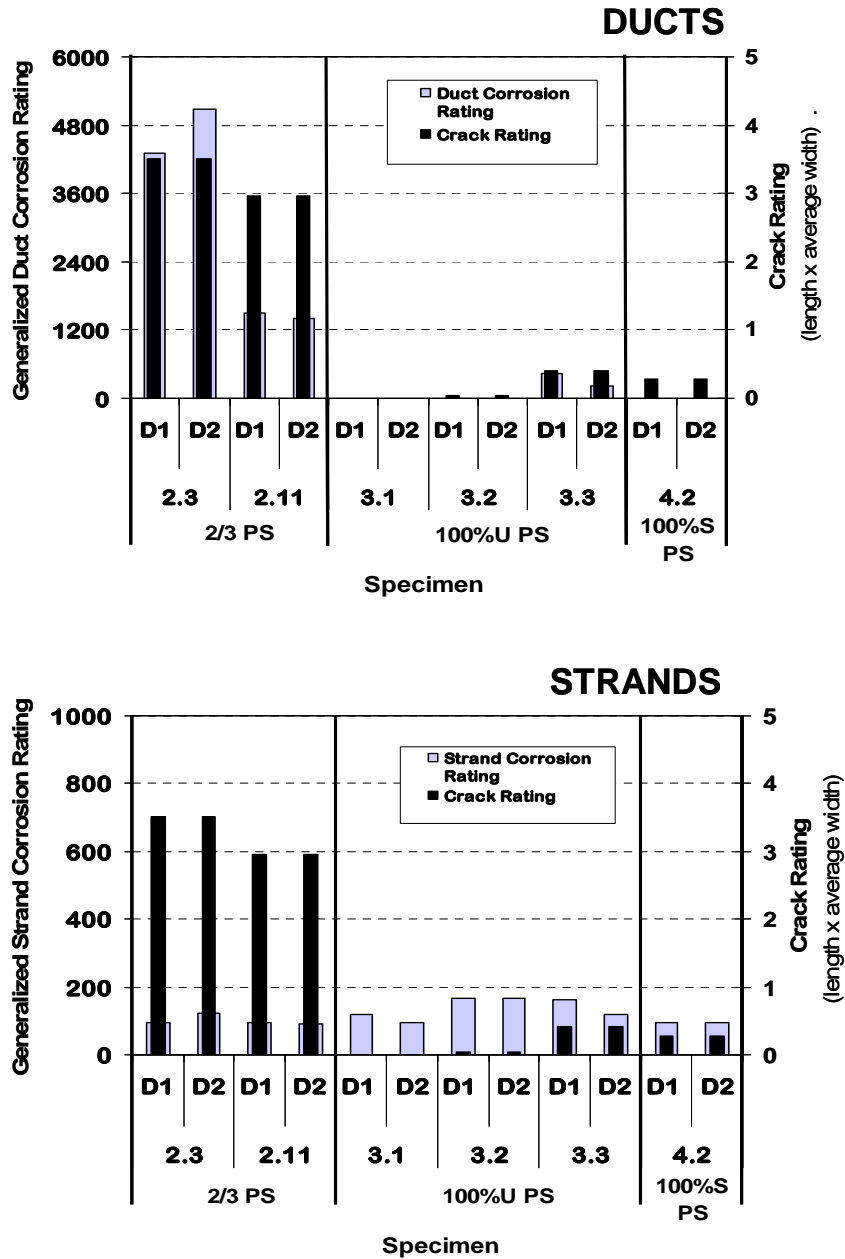


Figure 6.8 Effect of Crack Density on Duct and Strand Corrosion for Phase I Autopsy Beams<sup>7</sup>

With the purpose of clearly showing the relationship between crack and corrosion ratings Figure 6.7 through Figure 6.10 have been plotted maintaining the same crack rating scale, and selecting the adequate generalized corrosion rating scale depending on the level of corrosion found on each element. For Phase II beams, the generalized corrosion rating scale for stirrups, rebar and ducts has been changed to one fifth of that used in Phase I, since corrosion ratings in Phase II beams were much smaller. The generalized corrosion rating scale for Phase II beam strands was selected as half of that used in Phase I beams.

As observed from Figures 6.7 and 6.8, there seems to be a correlation in Phase I beams between stirrup, rebar and duct corrosion ratings and crack density (by means of a crack rating), with some deviations as in the case of rebar corrosion of Specimen 1.3 in Figure 6.7, and, duct corrosion in Specimens 2.11 and 4.2 in Figure 6.8. The proportionality is not shown for the strands, which do not show any distinct trend.

It appears that the proportionality is better shown on those elements closer to the top surface of the specimens, and therefore, those receiving the effect of moisture and chlorides in a more direct means.

For Phase II autopsy beams, Figures 6.9 and 6.10 do not show any distinct correlation. These beams constructed with high performance concrete or fly ash concrete, had three years and a half of exposure testing at the time of autopsy, as opposed to Phase I beams that had four years and a half. It is not clear from these results if the non-proportionality observed is the result of the effect of the different concrete types or the shorter exposure testing period. It is anticipated that final autopsies of the remaining specimens in the beam series will yield more conclusive results after several additional years of exposure testing.

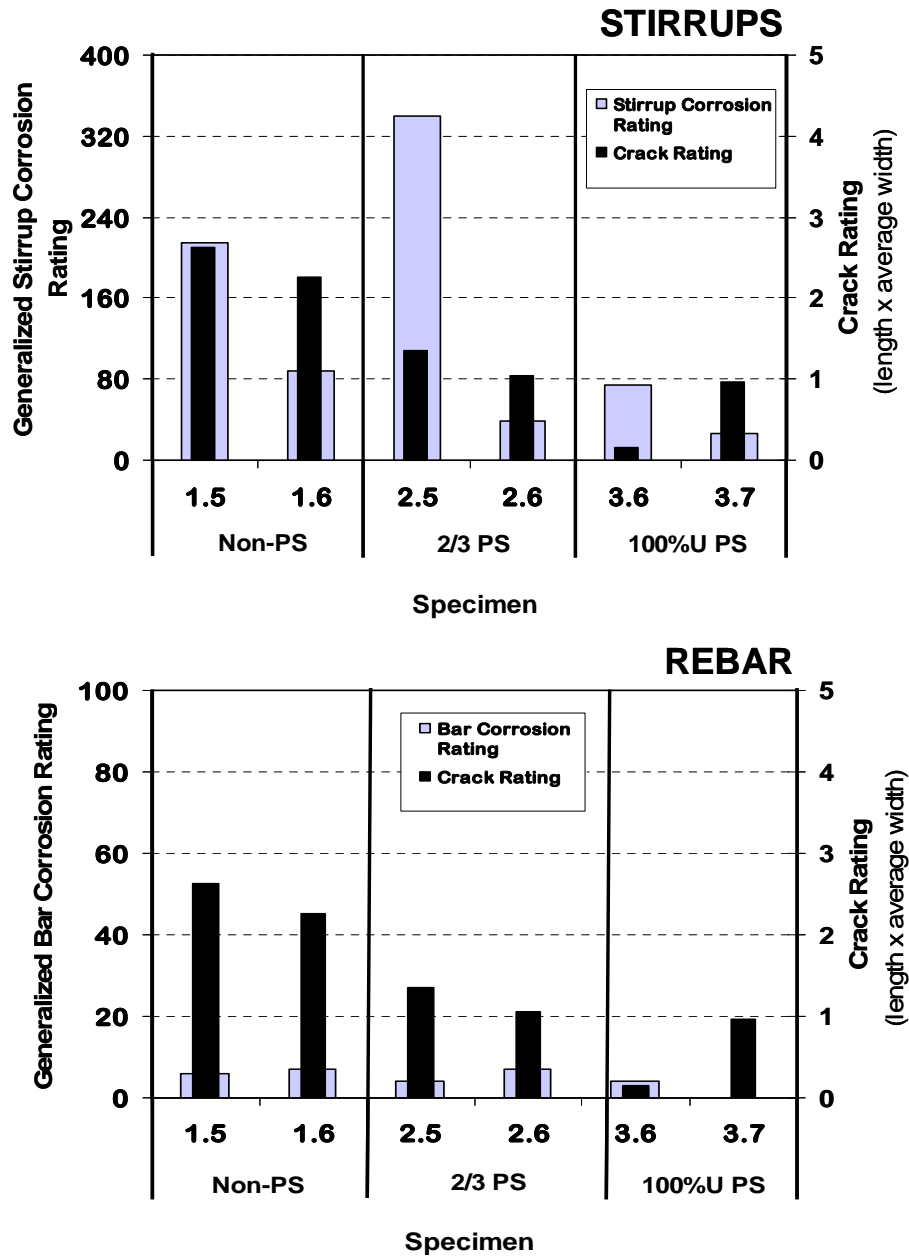


Figure 6.9 Effect of Crack Density on Stirrup and Rebar Corrosion for Phase II Autopsy Beams<sup>7</sup>

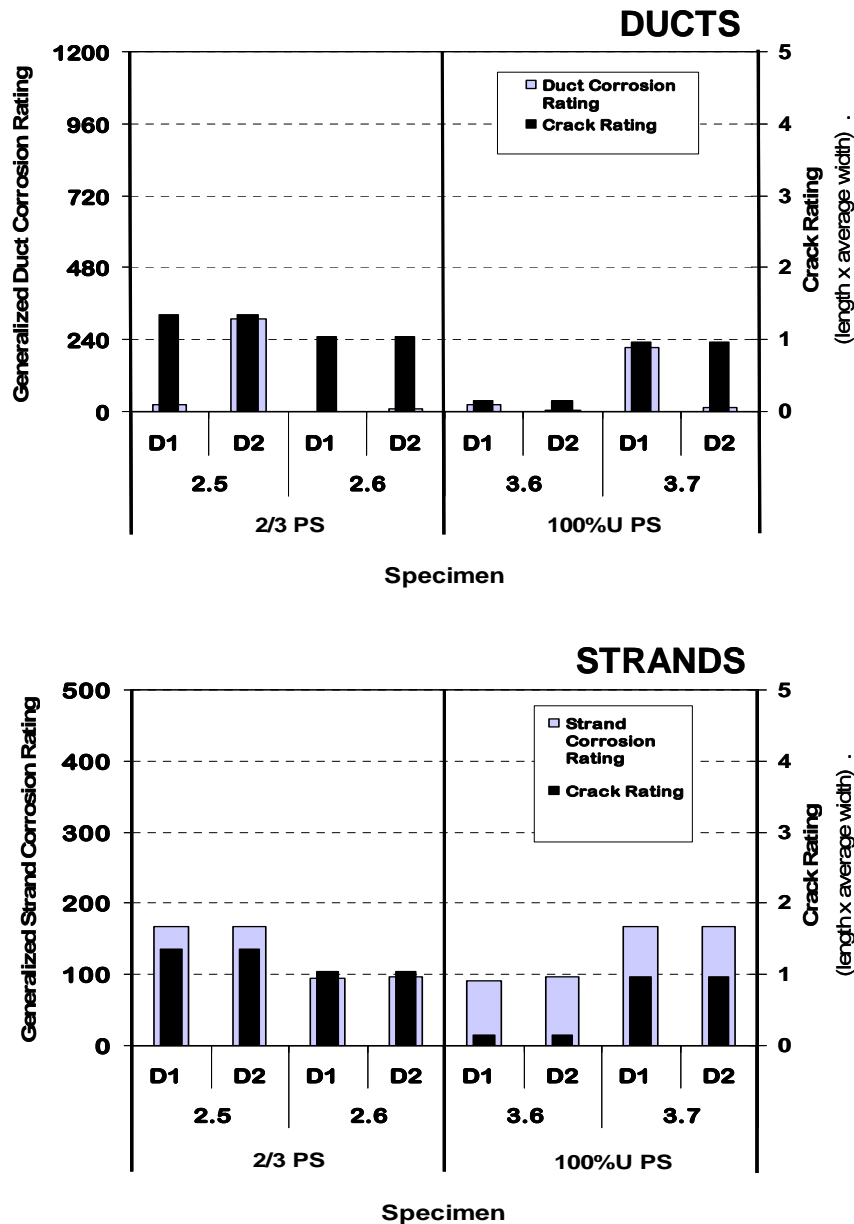


Figure 6.10 Effect of Crack Density on Duct and Strand Corrosion for Phase II Autopsy Beams<sup>7</sup>

### 6.2.2 Crack Width

In discussing crack width it is assumed that transverse cracks (formed originally prior to exposure testing) are causes and longitudinal or splitting type cracking formed after substantial exposure due to corrosion products are effects. Thus, all correlations in this section are made with transverse crack widths only.

The effect of transverse crack width on stirrup, rebar, galvanized steel duct and strand corrosion is illustrated on Figure 6.11 and Figure 6.12 for Phase I beams, and on Figure 6.13 and Figure 6.14 for Phase II beams. In these figures, the localized corrosion rating (maximum corrosion rating recorded for any 2-inch interval for each element) is plotted versus the maximum transverse crack width. The scale used for the corrosion rating (y scale) has been adjusted for every element, to clearly show any proportionality among the variables. The plots for Phase II beams use half of the corrosion rating scale in Phase I beam plots, except for the strand rating that uses half of the scale.

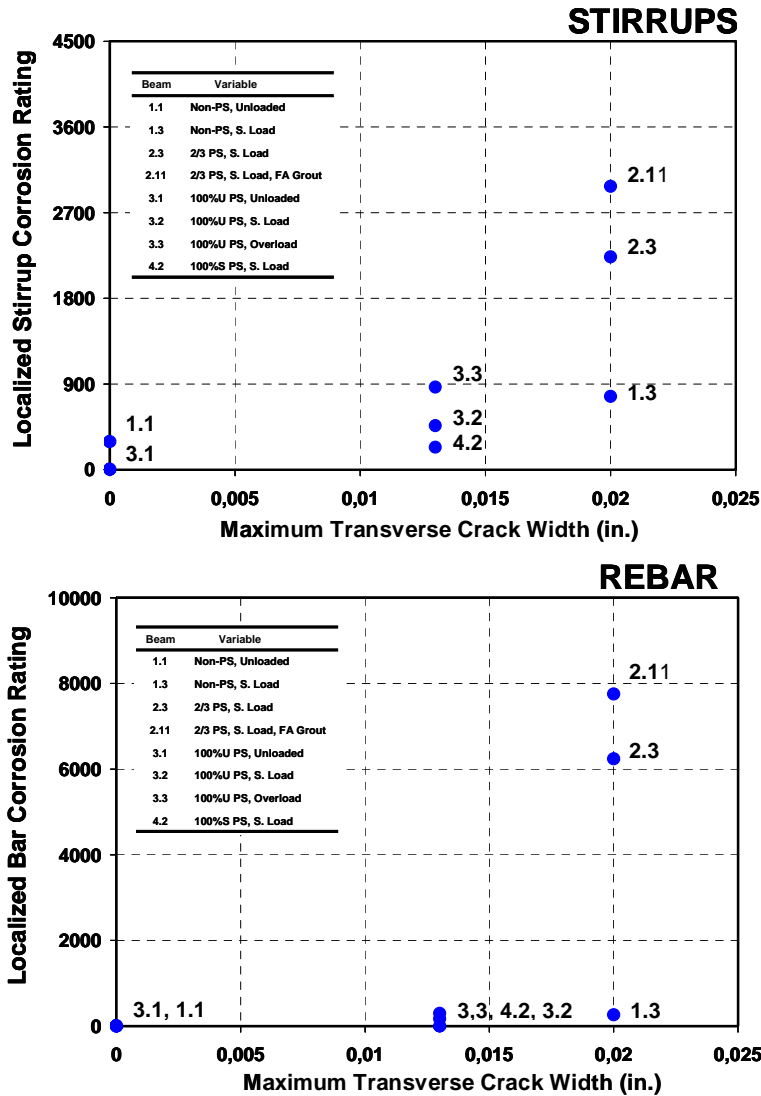


Figure 6.11 Localized Stirrup and Rebar Corrosion Rating versus Maximum Crack Width for Phase I Autopsy Specimens<sup>7</sup>

As observed from Figure 6.11 there is a distinct trend among localized corrosion rating and maximum crack width for post-tensioned specimens. Mixed reinforced (2/3 PS) beams with wider cracks show higher stirrup, rebar and duct corrosion ratings than 100% PS beams. The trend is not clearly observed for the Non-PS beams nor for the strands. However, from Section 5.5.4 it was shown that strands were all performing similarly, with only minimal variations, and therefore, it appears that specimens would require more exposure time to indicate distinct performance differences.

The performance of Specimen 1.3, as observed from Figure 6.11, shows a similar behavior to fully post-tensioned (100%U PS and 100%S PS beams). This conclusion differs from the trend observed for mixed reinforced specimens and from the expected results. The reason for this difference it is not apparent.

Figures 6.11 and 6.12 show the excellent performance of uncracked specimens (see Specimens 1.1 and 3.1).

For Phase II specimens, Figure 6.13 and Figure 6.14 show a trend with respect to stirrup, and strand corrosion, and maximum crack width for fly ash concrete post-tensioned specimens. As the level of post-



tensioning decreases, cracking and corrosion rating increase. The trend is not clearly shown for rebar corrosion and for high performance concrete specimens.

In spite of the few deviations observed from the general trends, the above results confirm the negative effect of cracking and wide crack widths on corrosion of steel and post-tensioning system reinforcement.

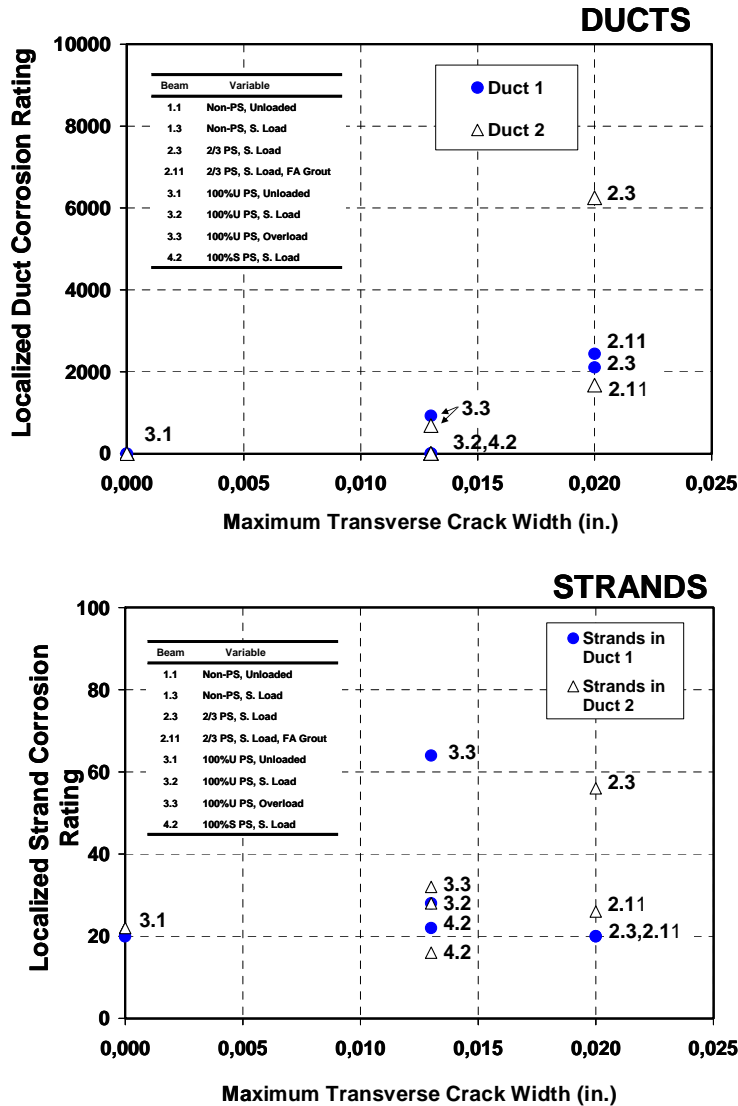


Figure 6.12 Localized Duct and Strand Corrosion Rating versus Maximum Crack Width for Phase I Autopsy Specimens<sup>7</sup>

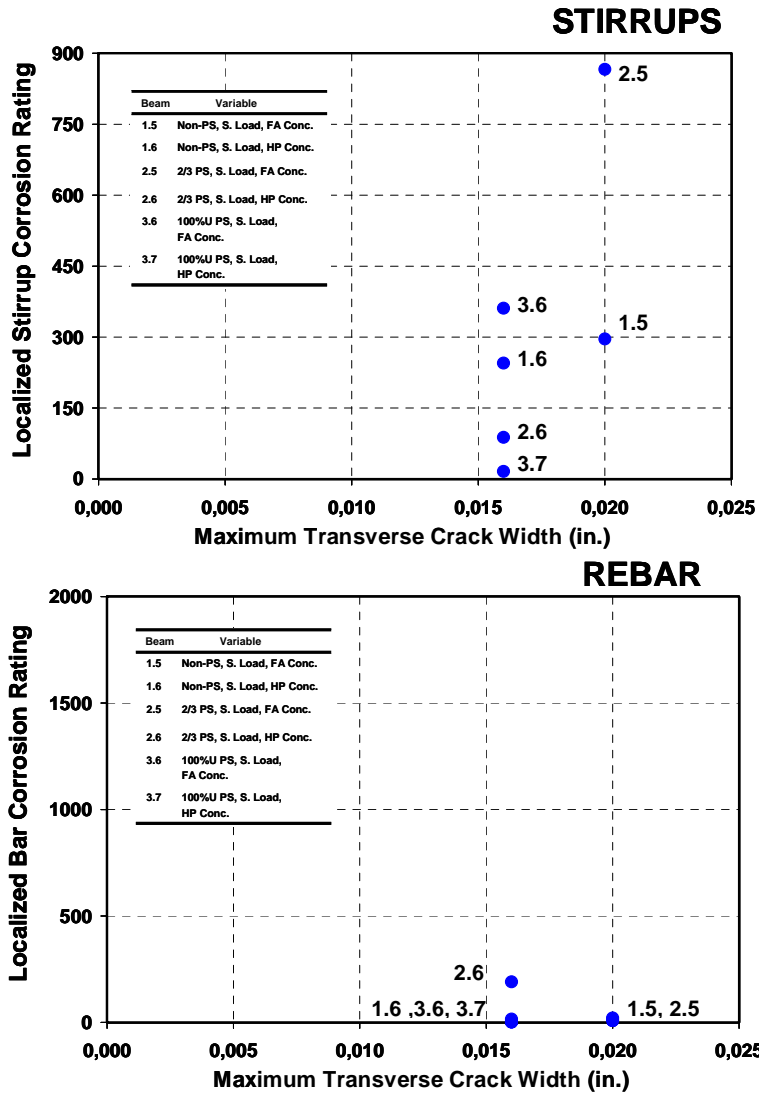


Figure 6.13 Localized Stirrup and Rebar Corrosion Rating versus Maximum Crack Width for Phase II Autopsy Specimens<sup>7</sup>

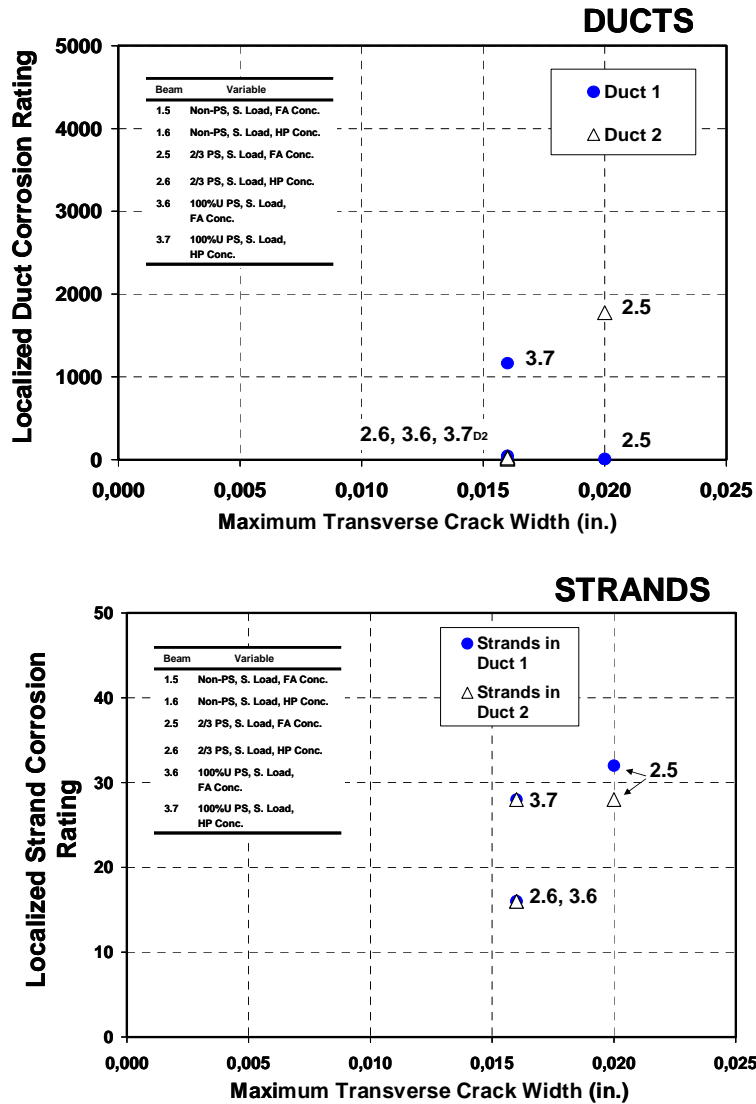


Figure 6.14 Localized Duct and Strand Corrosion Rating versus Maximum Crack Width for Phase II Autopsy Specimens<sup>7</sup>

### 6.2.3 Longitudinal Cracking

Longitudinal or splitting type cracks were found at the end of testing in Specimens 1.3, 2.3 and 2.11, corresponding with those specimens with the maximum generalized stirrup, rebar and duct (in the case of post-tensioned specimens) corrosion ratings, as shown in Figures 5.62, 5.64 and 5.66, respectively. Longitudinal cracks are the result of very severe reinforcement or duct corrosion occurring within the concrete member.

Longitudinal cracks for Specimen 1.3, 2.3 and 2.11 corresponded with the location of the mild steel reinforcement, as shown in Figures 5.14, 5.18, 5.22, referring to the reinforcement location in Figure 2.4. Longitudinal cracks in Specimens 2.3 and 2.11 were also very close and along the location of the post-tensioning galvanized ducts.

Without any other methods of externally monitoring the condition of the concrete members, longitudinal or splitting cracks by themselves appear to be a definite sign of very severe corrosion and are enough to generate concern.

### 6.2.4 Loading Levels

The effect of loading on reinforcement corrosion is clearly shown in Figures 6.1 and 6.3 when comparing Specimens 1.1 and 1.3, and Specimens 3.2 and 3.3. Also, when comparing Specimens 3.2 and 3.3 in Figure 6.5. The results are also shown in Figure 6.7 through Figure 6.14. The corrosion rating (and therefore, corrosion extent and severity) increases when loading increases. An increase in loading is associated with an increase in cracking.

### 6.2.5 Prestressing Levels

The effect of prestressing levels is shown in Figures 6.1 and 6.3 for Phase I beam Specimens: 1.3, 2.3, 3.2 and 4.2. The corrosion severity decreases with increasing prestressing levels. In particular, mixed reinforcing (2/3 PS) beams show the worst corrosion protection and perform similar to loaded Non-PS beams. An increase in prestressing level is associated with a decrease in crack density and maximum crack widths.

## 6.3 EFFECT OF CONCRETE TYPE

Concrete type effects are determined from Phase II beam specimens. Figure 6.2 shows a distinct trend for stirrup corrosion, with higher corrosion ratings for Class C concrete specimens with fly ash, in comparison to the high performance concrete specimens. The opposite trend is shown in Figure 6.4 for rebar corrosion ratings, but in this case all ratings are very close to each other, and therefore the trend is not clear. Figure 6.6 shows a better performance of Specimen 2.6 (high performance concrete) when compared to Specimen 2.5 (Class C with Fly Ash concrete). However, the opposite results are obtained when comparing Specimens 3.6 and 3.7.

It appears that concrete type will be better compared when the remaining beams are left under continuous exposure for additional testing time.

## 6.4 EFFECT OF SPLICE TYPE

Two splice types were tested: Industry Standard splice (IS) and Heat Shrink splice (HS). Figure 6.15 shows both types of splices and the corrosion and stains typically found. As observed, the industry standard splice allows moisture to enter through the sides of the splice and get trapped between the duct and the splice due to inefficiency of duct tape. This results in moisture and chlorides attacking the splice from both sides.

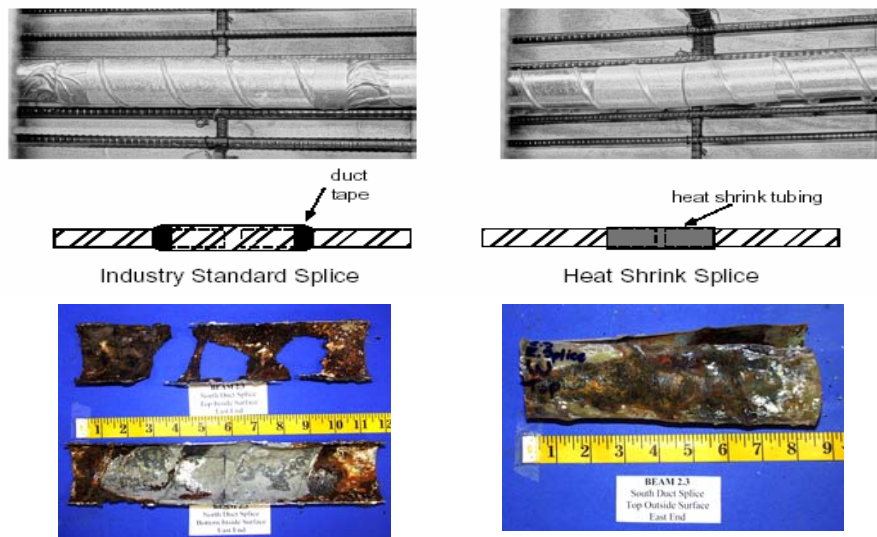


Figure 6.15 Duct Splice Performance<sup>7</sup>

The heat-shrink splice also allows moisture to enter through the sides and get trapped due to insufficient adhesion between the splice and the duct. It also traps bleed water from the grout.

Neither the IS nor the HS splice appears to be a satisfactory duct splice with respect to corrosion protection of galvanized steel ducts.

### 6.5 EFFECT OF SPLICE DAMAGE

Since the basic undamaged splices were so ineffective, the intentional damage on the duct splices does not show a direct correlation with the severity of corrosion.

### 6.6 EFFECT OF GROUT TYPE

Strand corrosion ratings for Specimens 2.3 and 2.11 are all very low and close in value and therefore, there is not a distinct trend with respect to grout type (standard Class C versus fly ash grout). The remaining specimens in this testing program are expected to yield more conclusive results with regard to the use of different types of grout, including anti-bleed grout.

### 6.7 SPECIAL AUTOPSY FINDINGS

Since grout is injected after post-tensioning of the element, it is susceptible to cracking due to deflections from loading and vibrations. Cracking in the grout may serve as direct paths for moisture and chlorides to the strands.

Figure 6.16 shows the grout condition found during forensic examination for Specimen 2.11. As shown in this figure, moisture and corrosion stains coming from the galvanized duct were present in many grout transverse slices. At the time of forensic examination, it appeared that only a short time more would have been required for the moisture to get to the strand level. Similar findings were also reported before by Hamilton.<sup>9</sup> However, this aspect in the multilayer strand corrosion protection concept has not received enough attention to date.

Bleed water voids were also found inside the ducts on a few specimens, even when they were supposed to have been grouted following correct procedures. Figure 6.17 shows the negative effects of a bleed water void. It was found that grout voids do not only affect the corrosion protection of the strands, but they also appear to be detrimental to the duct.



Figure 6.16 Effect of Grout Cracking<sup>7</sup>



Figure 6.17 Bleed Water Void and Duct Corrosion<sup>7</sup>

## 6.8 EXPOSURE TESTING MEASUREMENTS VERSUS FORENSIC EXAMINATION RESULTS

Table 6.2 shows the summary of exposure test results with respect to the main test variables. This table can be compared to Table 6.1, which shows the forensic examination results.

### 6.8.1 Half-Cell Potential Readings versus Forensic Examination Results

Half-cell potential readings have been ordered according to specimen performance in Figures 6.18 through Figure 6.21, including readings at the time to initiation of corrosion and at the end of testing for all autopsied specimens.

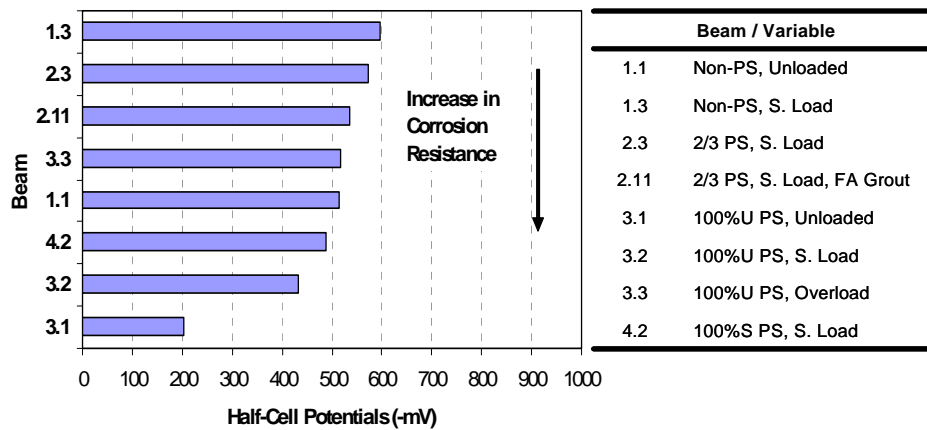


Figure 6.18 Half-Cell Potential at 1594 Days (End of Testing) for Phase I Autopsy Beams<sup>6,7</sup>

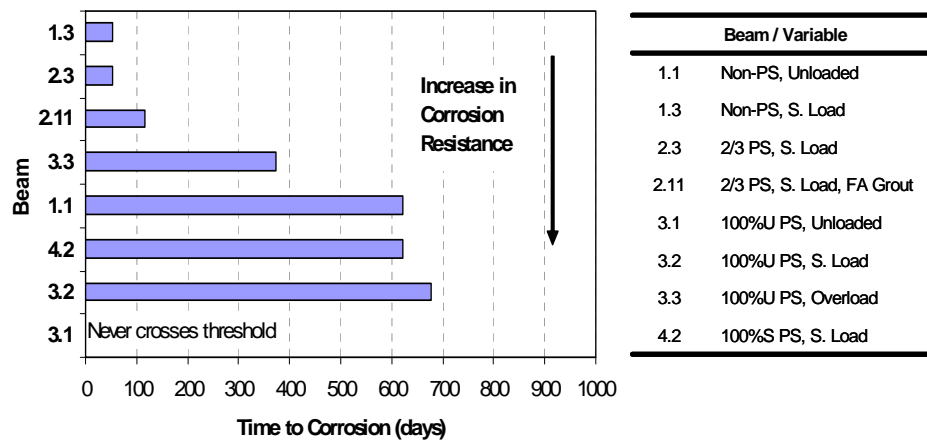


Figure 6.19 Time to Initiation of Corrosion for Phase I Autopsy Beams<sup>6,7</sup>

**Table 6.2 Summary of Exposure Test Results<sup>6</sup>**

<b>Method of Comparison</b>	<b>Beams Compared</b>	<b>Variable Analyzed</b>	<b>Result</b>
Half-Cell	1.1, 3.1	Prestress	<ul style="list-style-type: none"> <li>• 2/3 PS worse than 100%U PS</li> </ul>
Half-Cell	1.3, 2.3, 3.2, 4.2	Prestress	<ul style="list-style-type: none"> <li>• Increase in corrosion protection with increase in PS</li> <li>• 2/3 PS corrosion protection much more similar to Non-PS than 100% PS</li> <li>• No significant difference between 100%U and 100%S PS</li> </ul>
Half-Cell	1.5, 2.5, 3.6	Prestress	<ul style="list-style-type: none"> <li>• Increase in corrosion protection with increase in PS</li> <li>• 2/3 PS corrosion protection almost identical to Non-PS</li> </ul>
Half-Cell	1.6, 2.6, 3.7	Prestress	<ul style="list-style-type: none"> <li>• All levels of PS similar (due to very large crack in 100%U PS beam)</li> </ul>
Corr. Rate	1.5, 2.5, 3.6	Prestress	<ul style="list-style-type: none"> <li>• Increase in corrosion protection with increase in PS</li> </ul>
Cl <sup>-</sup> Content	All Phase I Beams	Prestress	<ul style="list-style-type: none"> <li>• Increase in horizontal chloride penetration with decrease in PS</li> <li>• Increase in corrosion protection with increase in PS</li> </ul>
Half-Cell	1.1, 1.3	Load/Cracking	<ul style="list-style-type: none"> <li>• Decrease in corrosion protection with increase in loading</li> </ul>
Half-Cell	3.1, 3.2, 3.3	Load/Cracking	<ul style="list-style-type: none"> <li>• Decrease in corrosion protection with increase in loading</li> <li>• Significant decrease in corrosion protection with cracking present</li> </ul>
Corr. Rate	3.1, 3.2, 3.3	Load/Cracking	<ul style="list-style-type: none"> <li>• Decrease in corrosion protection with increase in loading and cracking</li> </ul>
Cl <sup>-</sup> Content	1.3, 2.11, 4.2	Load/Cracking	<ul style="list-style-type: none"> <li>• Significantly higher chloride content at bar level when samples taken at crack location</li> </ul>
Half-Cell	1.5, 1.6 2.5, 2.6	Concrete Type	<ul style="list-style-type: none"> <li>• HP concrete corrosion protection better than FA</li> </ul>
Half-Cell	3.6, 3.7	Concrete Type	<ul style="list-style-type: none"> <li>• FA concrete corrosion protection better than HP (this HP beam is the one with a very large crack)</li> </ul>
Half-Cell	All Phase II Beams	Concrete Type	<ul style="list-style-type: none"> <li>• HP concrete corrosion protection better than FA</li> </ul>
Corr. Rate	1.5, 1.6 2.5, 2.6 3.6, 3.7	Concrete Type	<ul style="list-style-type: none"> <li>• No significant difference in corrosion protection of HP and FA concrete</li> </ul>
Cl <sup>-</sup> Content	Blocks	Concrete Type	<ul style="list-style-type: none"> <li>• HP concrete corrosion protection better than FA</li> </ul>
Cl <sup>-</sup> Content	1.5, 1.6 2.5, 2.6 3.6, 3.7	Concrete Type	<ul style="list-style-type: none"> <li>• HP concrete better at preventing chloride penetration</li> <li>• Both concrete types minimize chloride penetration to bar level</li> </ul>
Half-Cell	2.3, 2.11	Grout Type	<ul style="list-style-type: none"> <li>• No difference in corrosion protection between normal and FA grout</li> </ul>

Legend:

**PHASE I BEAMS:** 1.1 Non-PS, Unloaded; 1.3 Non-PS, S. Load; 2.3 2/3 PS, S. Load; 2.11 2/3 PS, S. Load; 3.1 100% U PS, Unloaded, 3.2 100% U PS, S. Load; 3.3 100% U PS, Overload; 4.2 100% S PS, S. Load  
**PHASE II BEAMS:** 1.5 Non-PS, S. Load, FA Conc.; 1.6 Non-PS, S. Load, HP Conc.; 2.5 2/3 PS, S. Load, FA Conc.; 2.6 2/3 PS, S. Load, HP Conc.; 3.6 100% U PS, S. Load, FA Conc.; 3.7 100% U PS, S. Load, HP Conc.

The half-cell potentials show an excellent inverse correlation in specimen performance between the negative potential and the time to corrosion.

Half-cell potential readings at the end of testing versus forensic examination results are directly compared in Figure 6.22 through Figure 6.25. In these figures, the same scales used in Section 6.2 for stirrup, rebar, duct and strand corrosion ratings have been maintained for consistency and clarity.

With the Phase I beams shown in Figure 6.22 and 6.23, it can be seen that there is not a clear-cut correlation between the half-cell readings and forensic examination results. The loaded Non-PS and 2/3 PS beams (1.3, 2.3, 2.11) show very fine correlation. However, the other specimens generally show quite poor correlation. Some very high negative potential readings occurred in specimens that evidenced very small amounts of actual corrosion (1.1, 3.1, 3.2).

With the Phase II beams, shown in Figures 6.24 and 6.25 there is little relationship between the half-cell potential and the corrosion rating for most specimens other than stirrups, but this is due to the actual corrosion ratings for bars, ducts and strands being very low and close in values.

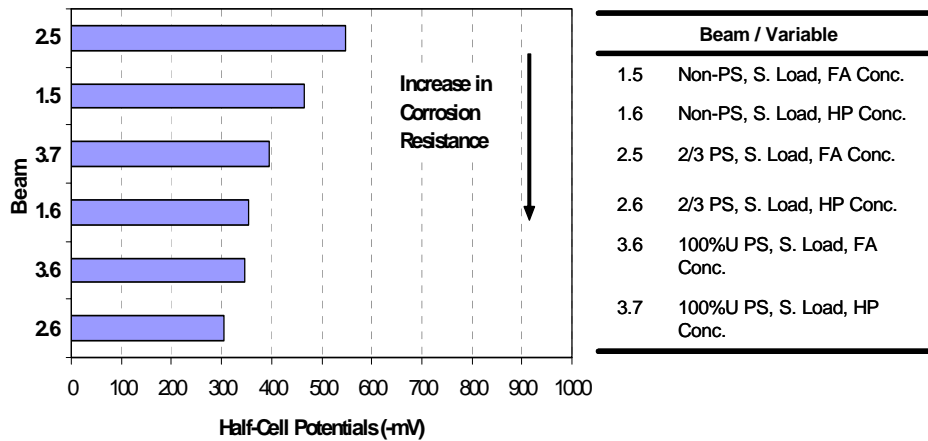


Figure 6.20 Half-Cell Potential at 1594 days (end of testing)for Phase II Autopsy Beams<sup>6,7</sup>

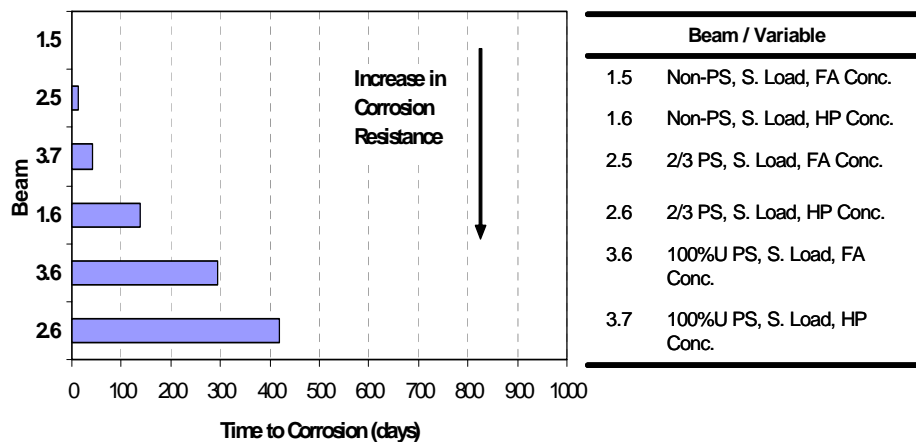


Figure 6.21 Time to Initiation of Corrosion for Phase II Autopsy Beams<sup>6,7</sup>



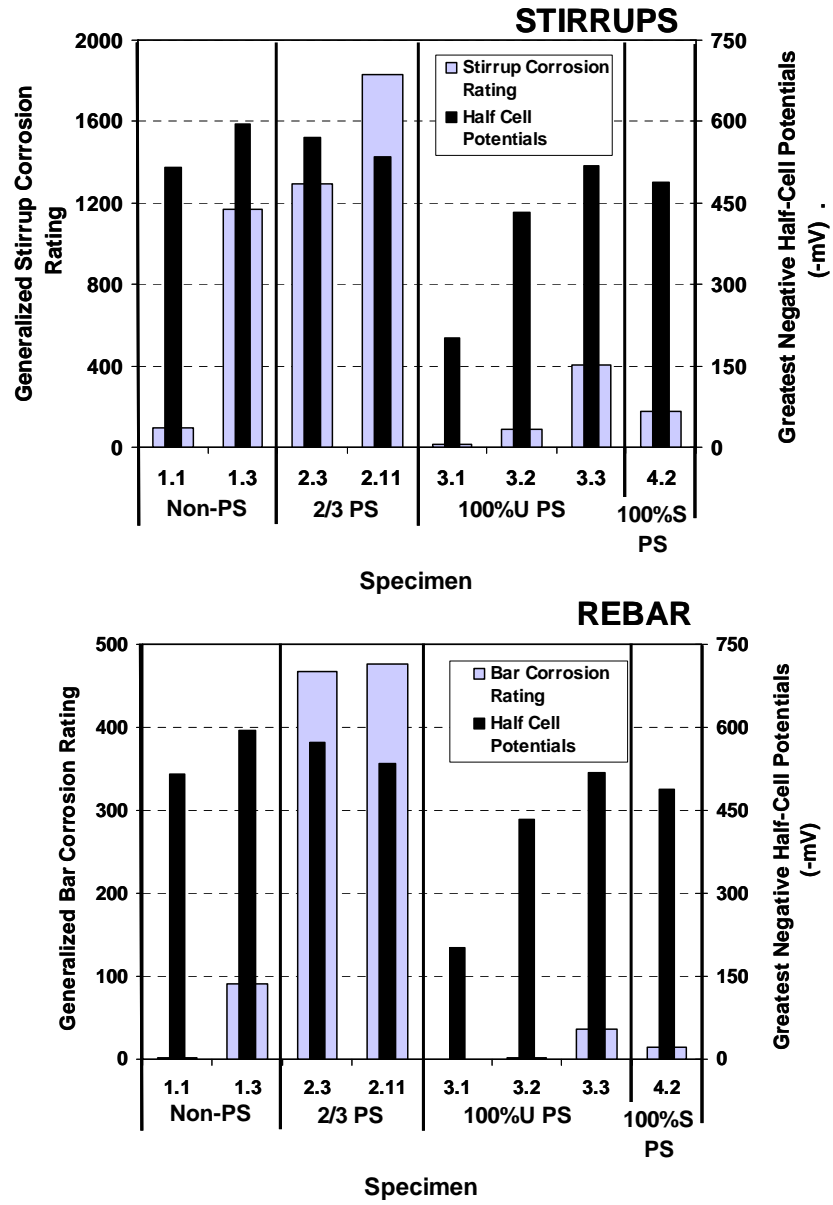


Figure 6.22 Half-Cell Readings at the End of Testing versus Stirrup and Rebar Corrosion Ratings for Phase I Autopsy Specimens<sup>7</sup>

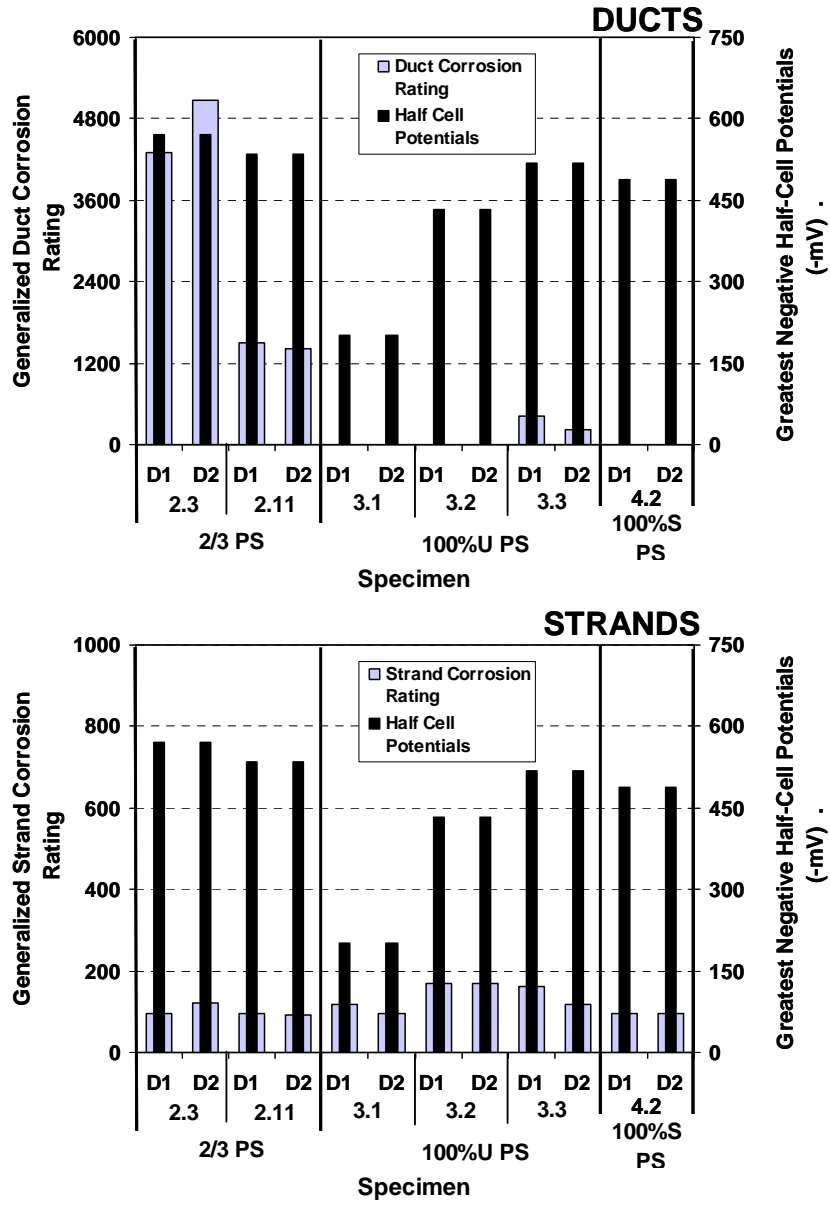


Figure 6.23 Half-Cell Readings at the End of Testing versus Duct and Strand Corrosion Ratings for Phase I Autopsy Specimens<sup>7</sup>

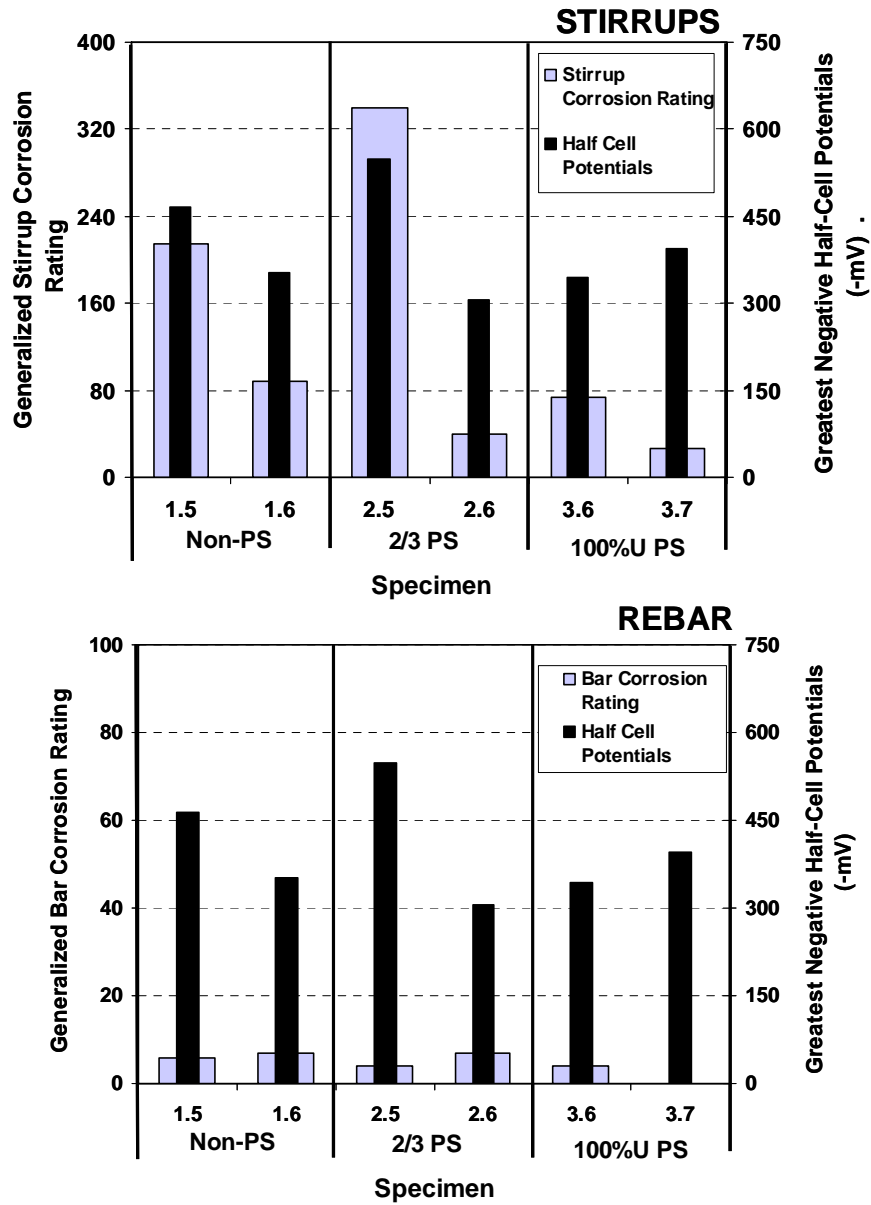
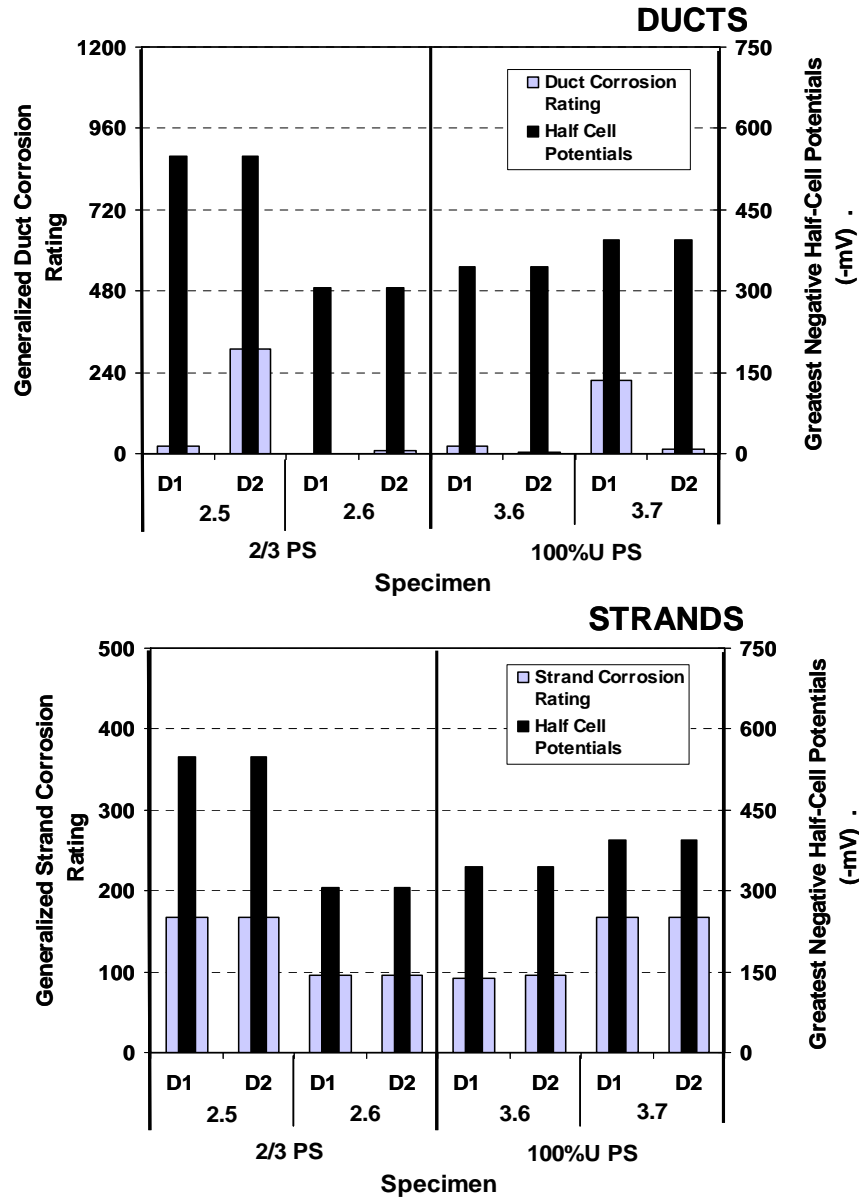


Figure 6.24 Half-Cell Readings at the End of Testing versus Stirrup and Rebar Corrosion Ratings for Phase II Autopsy Specimens<sup>7</sup>



**Figure 6.25 Half-Cell Readings at the End of Testing versus Duct and Strand Corrosion Ratings for Phase II Autopsy Specimens<sup>7</sup>**

**6.8.2 Corrosion Rate Measurements versus Forensic Examination Results**

Final corrosion rate measurements taken from Phase I and Phase II autopsy beams are shown in Figure 6.26 and Figure 6.27, respectively, ordered according to performance. As will be shown in Figures 6.28 through 6.31, these corrosion rate indicators are highly misleading. For example, the worst corrosion performance was generally Specimens 1.3, 2.3 and 2.11. These specimens are not as critical in the corrosion rate measurements as more lightly corroded specimens 3.2 and 3.3.

Corrosion rate measurements versus forensic examination results are directly compared in Figure 6.28 through Figure 6.31.

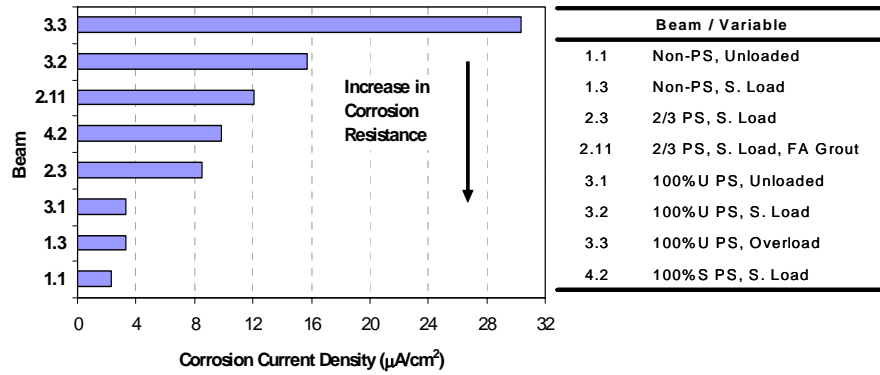


**Figure 6.26 Final Corrosion Rate Measurements Using 3LP Equipment for Phase I Autopsy Beams<sup>6,7</sup>**

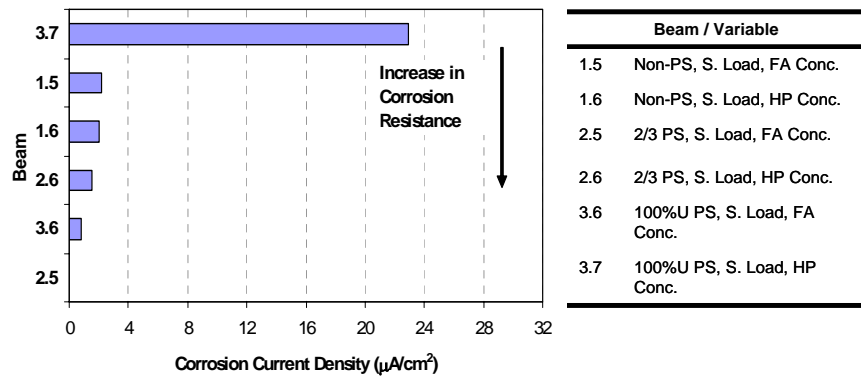


**Figure 6.27 Final Corrosion Rate Measurements Using 3LP Equipment for Phase II Autopsy Beams<sup>6,7</sup>**

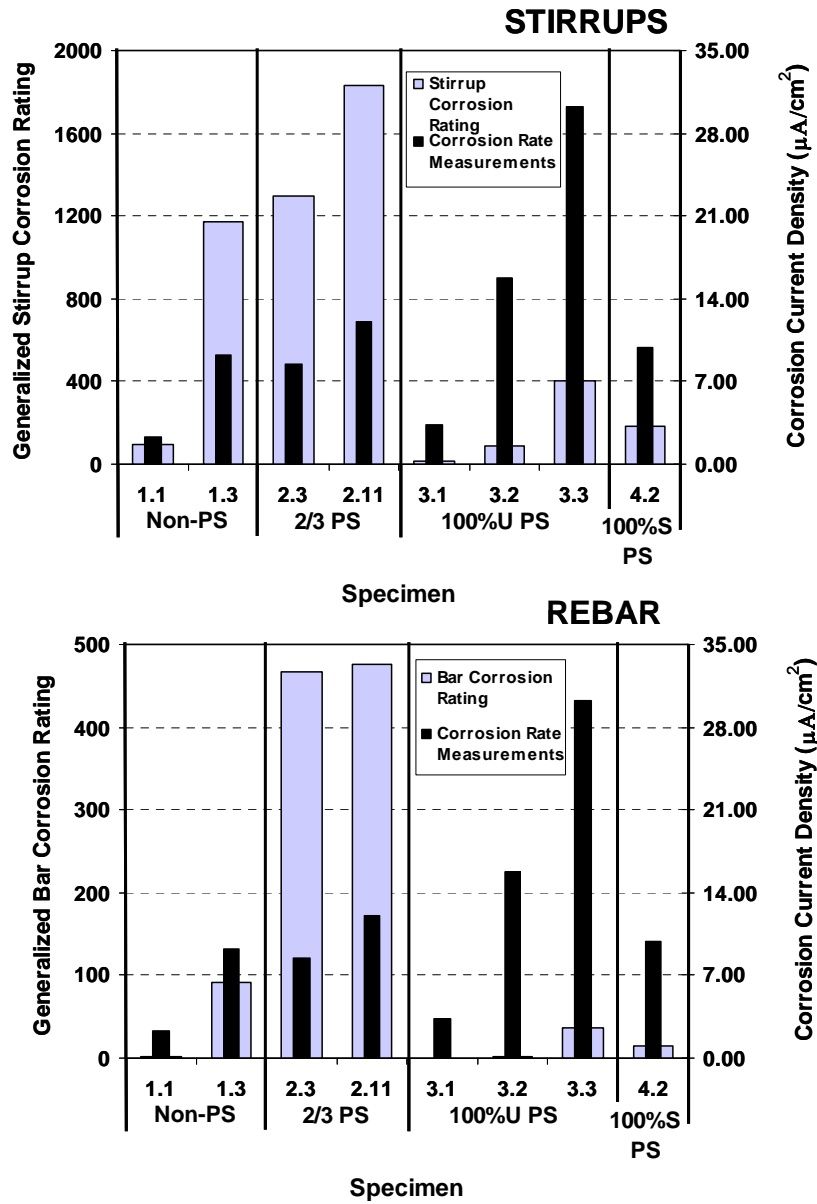


Figure 6.28 Corrosion Rate Measurements (using 3LP equipment) after 47 Months of Exposure versus Stirrup and Rebar Corrosion Ratings for Phase I Autopsy Specimens<sup>7</sup>

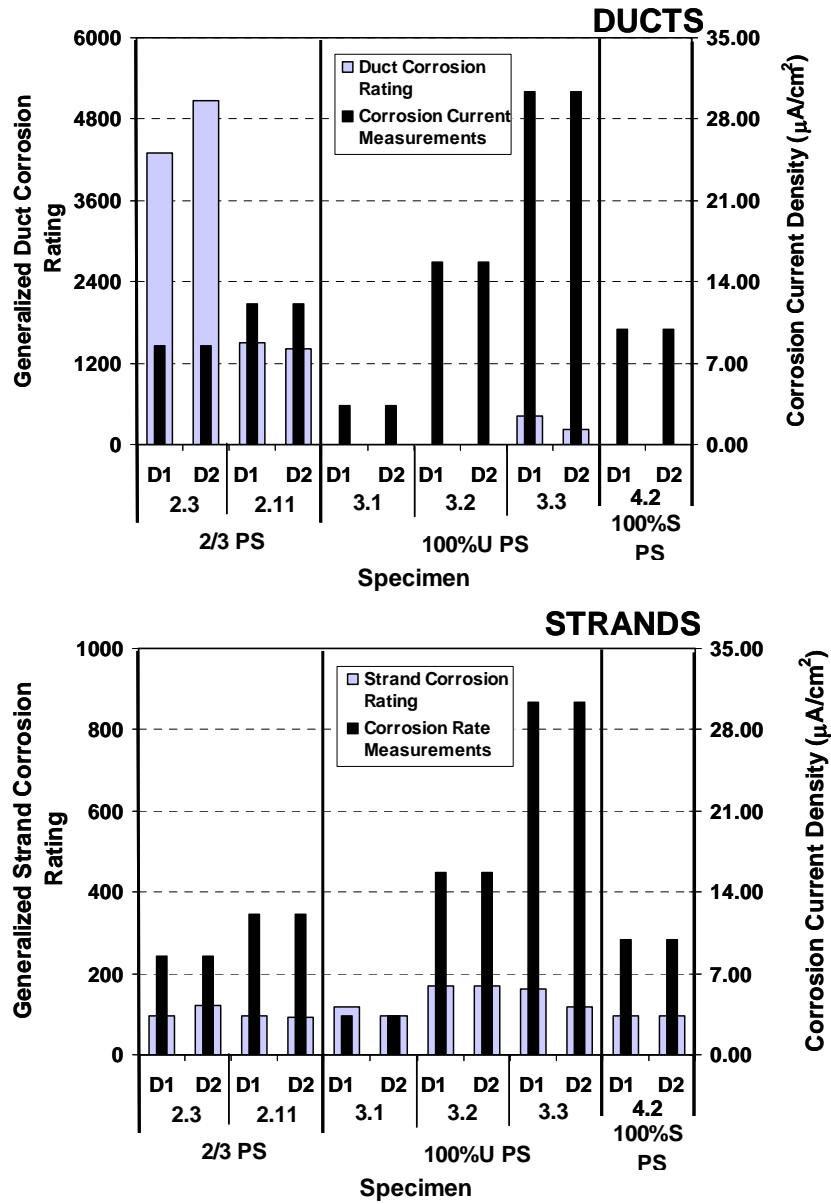


Figure 6.29 Corrosion Rate Measurements (using 3LP equipment) after 47 Months of Exposure versus Duct and Strand Corrosion Ratings for Phase I Autopsy Specimens<sup>7</sup>

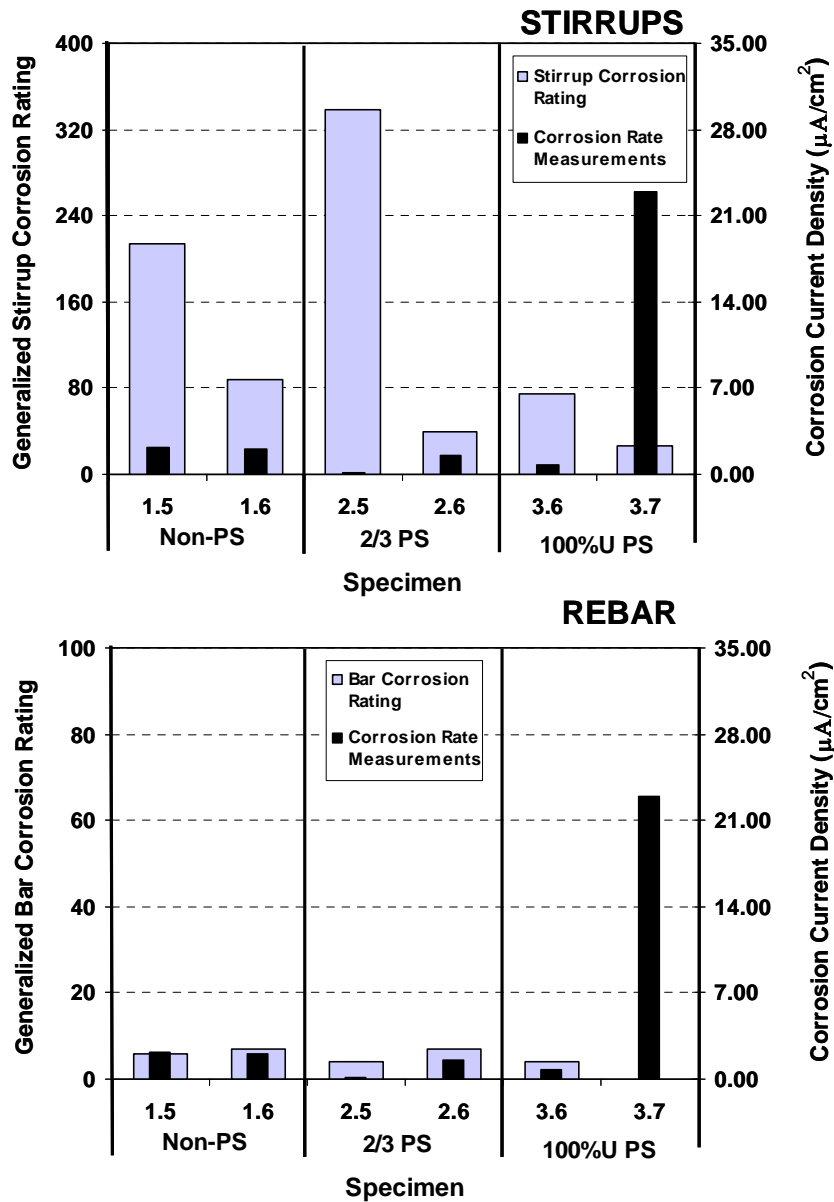
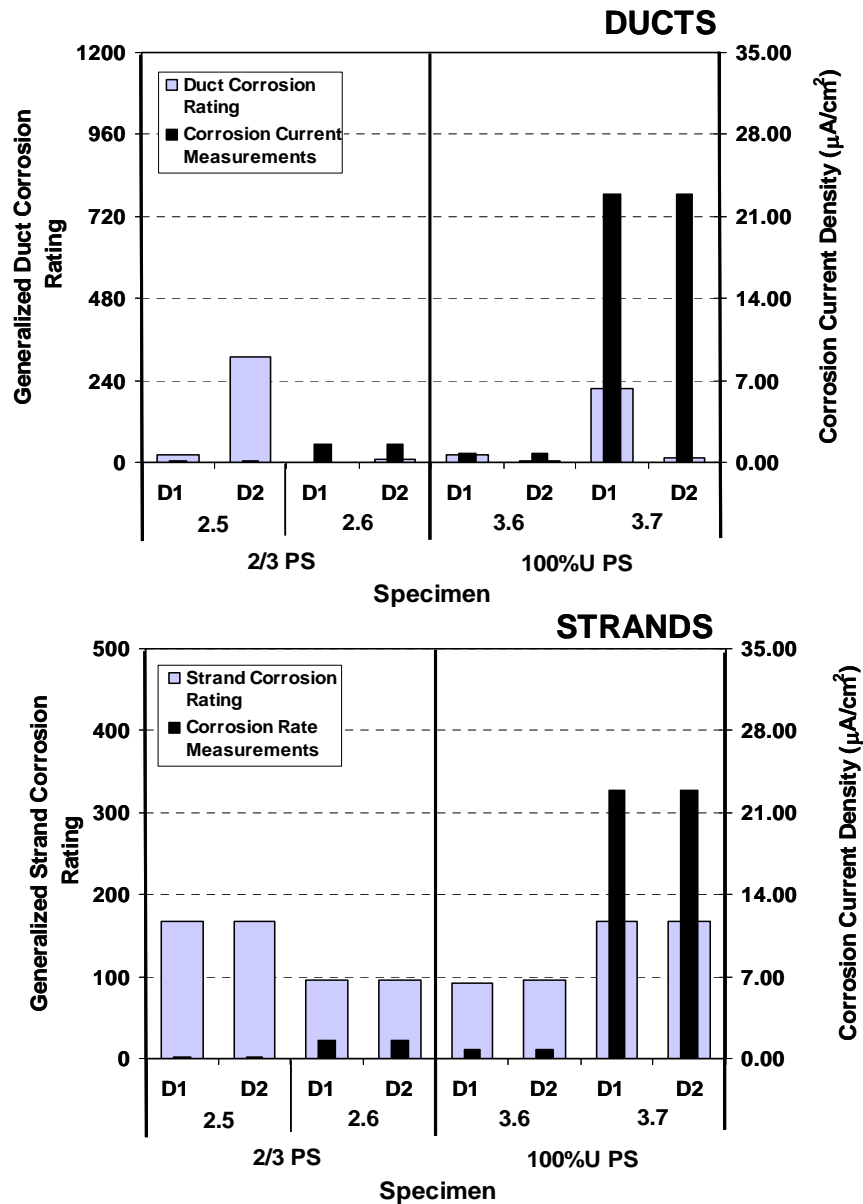


Figure 6.30 Corrosion Rate Measurements (using 3LP equipment) after 35 Months of Exposure versus Stirrup and Rebar Corrosion Ratings for Phase II Autopsy Specimens<sup>7</sup>





**Figure 6.31 Corrosion Rate Measurements (using 3LP equipment) after 35 Months of Exposure versus Duct and Strand Corrosion Ratings for Phase II Autopsy Specimens<sup>7</sup>**

Figures 6.28 through Figure 6.31 show very poor or inexistent correlation among corrosion rate readings and stirrup, rebar, duct and strand corrosion ratings.

### 6.8.3 Chloride Penetration versus Forensic Examination Results

Chloride penetration plots for samples taken within the ponded region (3-inch and 18-inch offset from centerline of beam), are shown in Figure 6.32 and Figure 6.33 for Phase I beams. In these graphs, the chloride content for the ponded blocks is compared to the chloride content for the beam specimens. As shown in these figures, the negative effect of cracking is evidenced since the ponded blocks were uncracked. While the chloride content in the beam specimens is very high, except in the case of Specimen 1.1, the corresponding chloride content in the ponded blocks is very low.

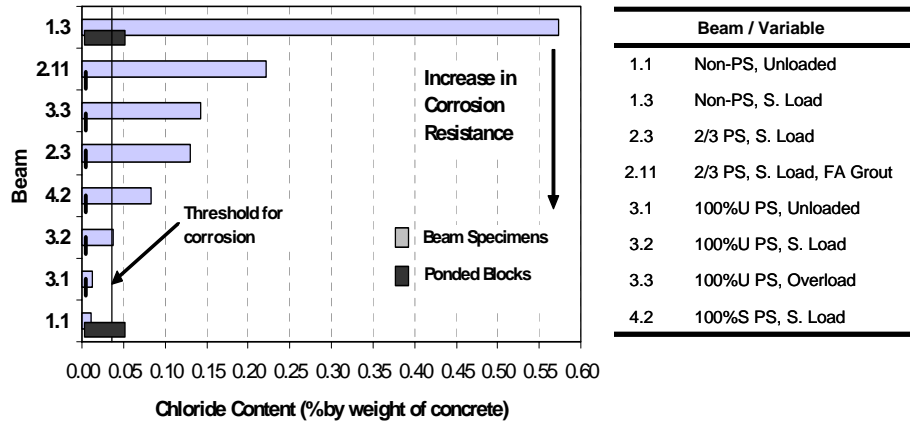


Figure 6.32 Beam Chloride Content at Bar Level – 3 in. Offset for Phase I Autopsy Beams<sup>6,7</sup>

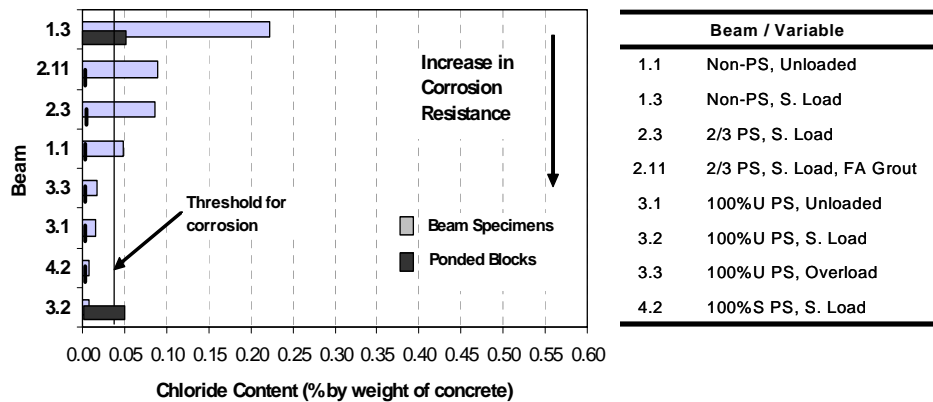


Figure 6.33 Beam Chloride Content at Bar Level – 18 in. Offset for Phase I Autopsy Beams<sup>6,7</sup>

Figure 6.34 and Figure 6.35 show the chloride penetration results for Phase II beams. Again, the chloride content for the blocks is shown. In this case, chloride contents were in all cases below the threshold of concern. However, it should be recognized that the chloride samples in the beams were taken at the location shown (3 in. or 18 in. offset), and therefore, they may not correspond to crack locations. Nevertheless, samples from the beam specimens showed in general higher chloride contents than those from the ponded blocks, which reflect again the negative effect of cracking on chloride penetration.

Figures 6.36 through Figure 6.39 show the comparison of acid-soluble chloride content at the bar level taken at three inches from the beam centerline versus stirrup, rebar, duct and strand corrosion ratings.

Overall, the chloride content measurements showed good correlation with stirrup, rebar and strand corrosion ratings in Phase I specimens, except for Specimen 1.3 that showed very high chloride content, and for Specimens 2.3 and 2.11 that showed lower chloride contents. However, chloride contents did not correlate well with duct corrosion ratings in all specimens. For Phase II beams there was no relationship between the chloride content at 3 in. offset and the actual corrosion ratings for most specimens, but this was due to the chloride contents for stirrups, bars, ducts and strands being very low. One of the reasons for these low chloride values was that samples were taken at specific distances from the beam centerline, and they may not have corresponded to crack locations.

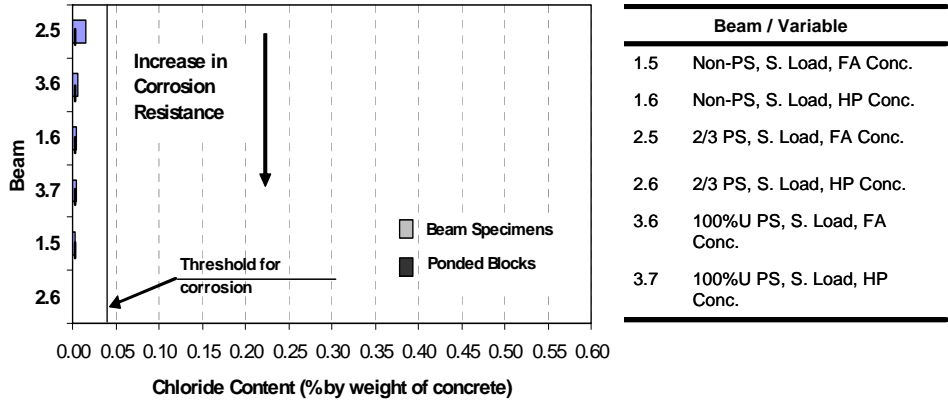


Figure 6.34 Beam Chloride Content at Bar Level – 3 in. Offset for Phase II Autopsy Beams<sup>7</sup>

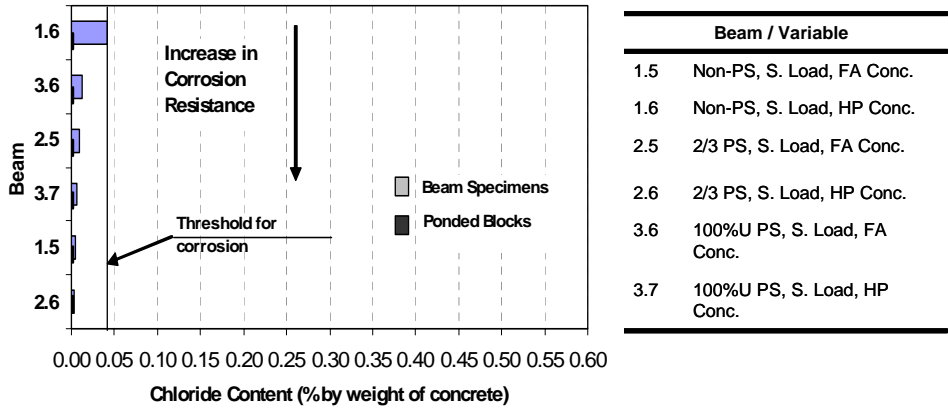


Figure 6.35 Beam Chloride Content at Bar Level – 18 in. Offset for Phase II Autopsy Beams<sup>7</sup>

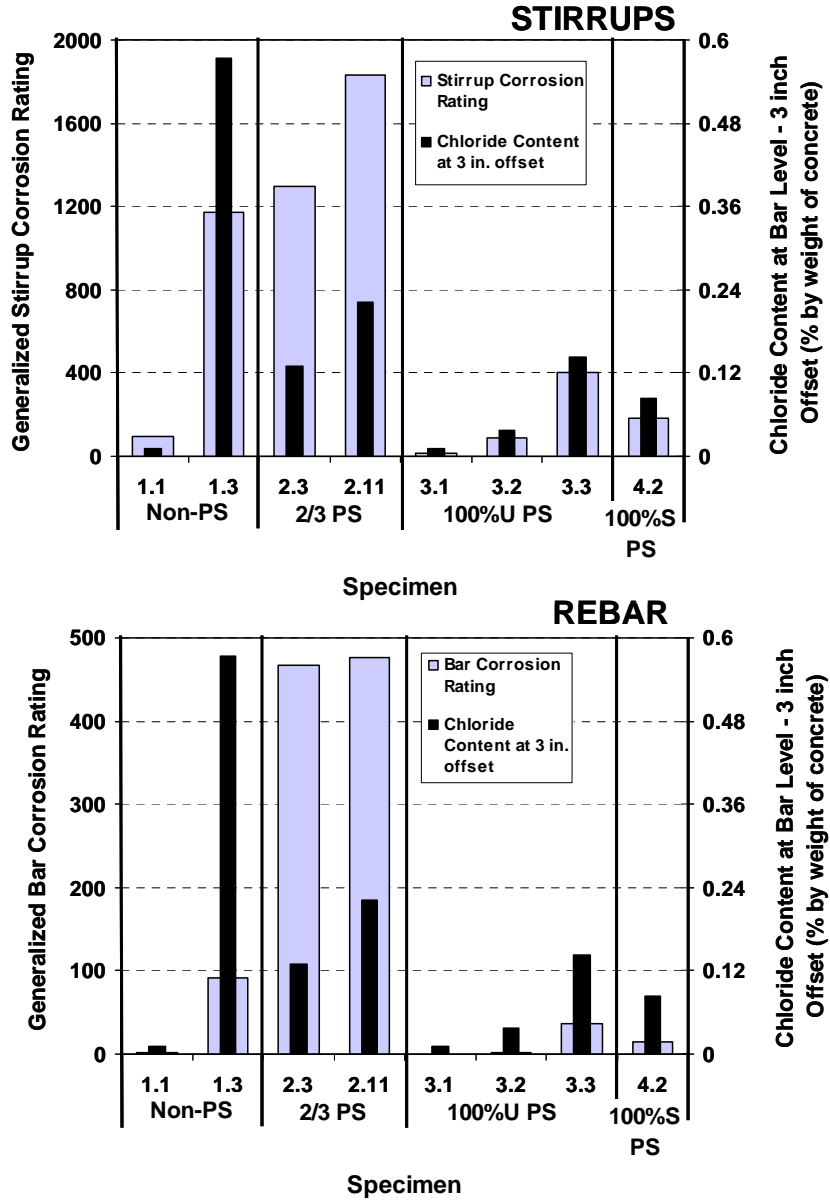


Figure 6.36 Acid-Soluble Chloride Content versus versus StIRRUPS and REBAR Corrosion Ratings for Phase I Autopsy Specimens<sup>7</sup>

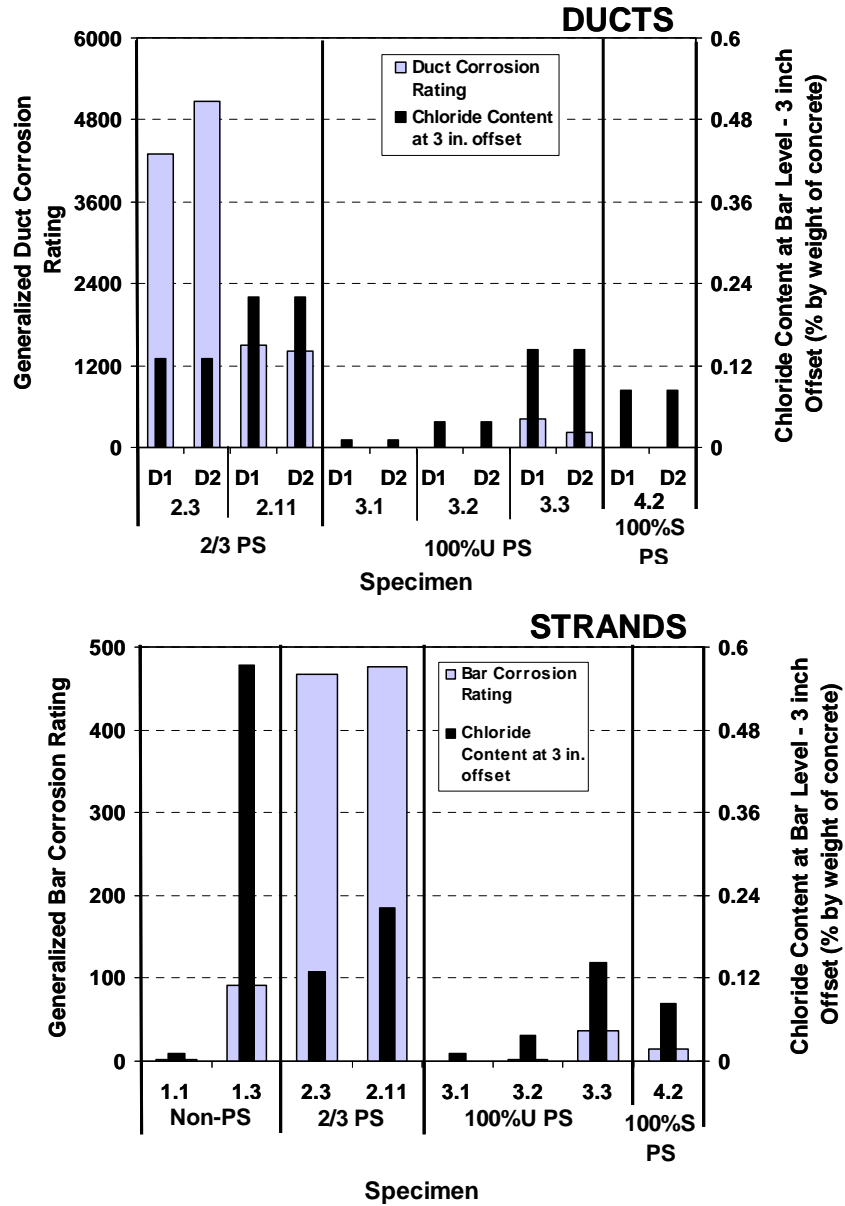


Figure 6.37 Acid-Soluble Chloride Content versus versus Duct and Strand Corrosion Ratings for Phase I Autopsy Specimens<sup>7</sup>

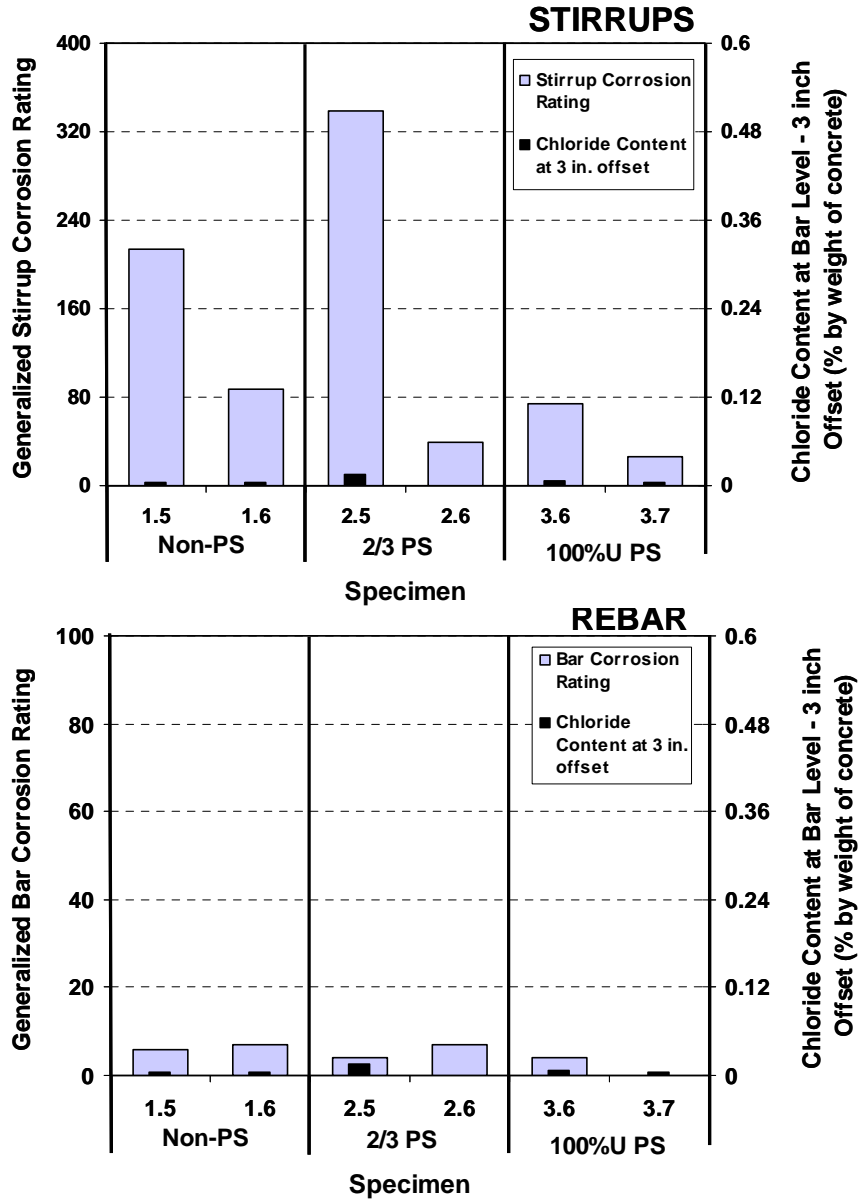


Figure 6.38 Acid-Soluble Chloride Content versus StIRRUPS and REBAR Corrosion Ratings for Phase II Autopsy Specimens<sup>7</sup>

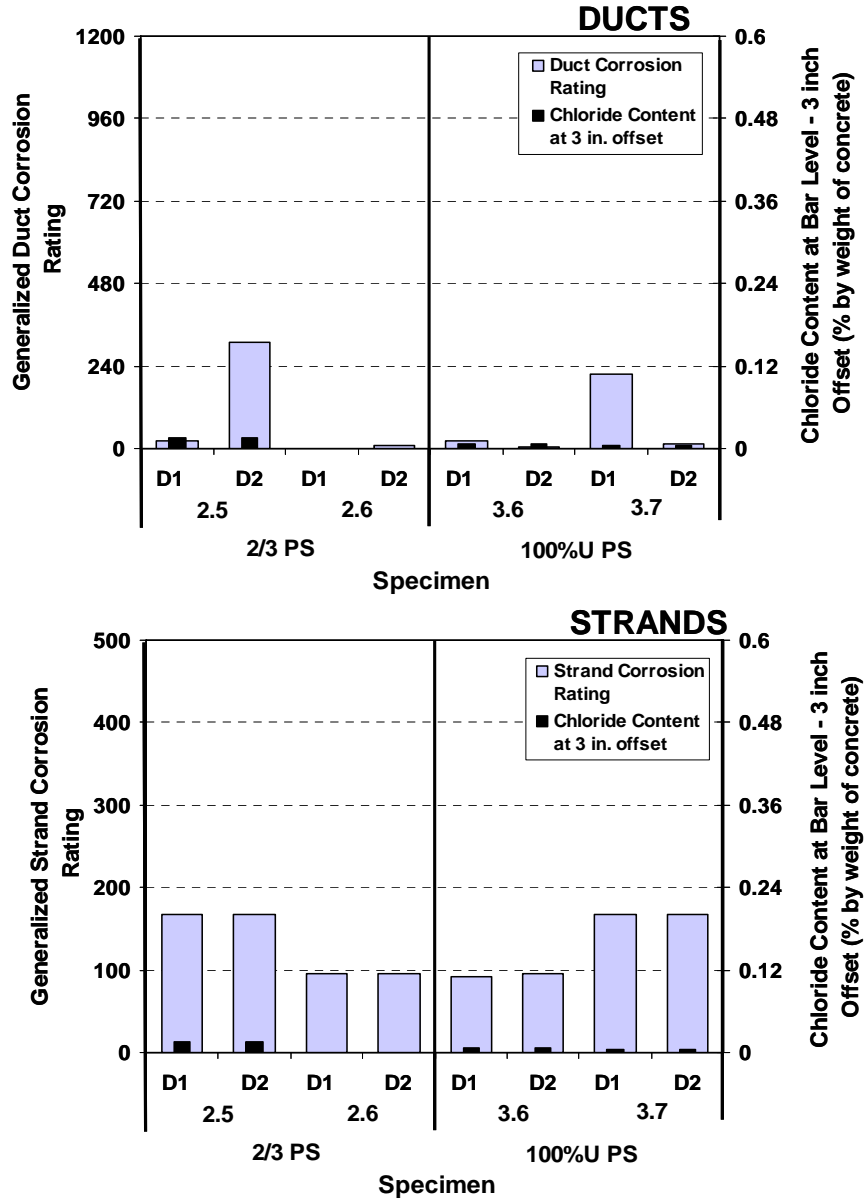


Figure 6.39 Acid-Soluble Chloride Content versus Duct and Strand Corrosion Ratings for Phase II Autopsy Specimens<sup>7</sup>

## 6.9 FINAL FULL AUTOPSIES

Exposure testing will continue for nearly half of the laboratory specimens, for several years, until signs of corrosion based on exposure testing results and visual inspection, are deemed enough to decide on final autopsy. Table 6.3 shows the specimens to be compared and the main variables to be analyzed.

**Table 6.3 Main Variables to be Analyzed During Final (Future) Autopsy of Beam Specimens<sup>7</sup>**

<b>Beams to be compared</b>	<b>Variable to be analyzed</b>
1.1, 1.2, 1.4 3.1, 3.5	loading / cracking
1.4, 2.4, 3.5, 4.1 2.1, 4.1 1.2, 2.1, 4.1 1.1, 3.1	level of prestress / cracking
1.9, 2.12	Duct type
3.4; 3.4, 3.5	splice damage
3.4, 3.5; 2.2; 2.8; 2.9; 3.1	splice type
2.9, 2.10	grout type / poor grouting procedure
2.7, 2.8, 2.9	strand type / strand coating damage
2.7, 2.9, 2.12	anchorage system / encapsulated system



## CHAPTER 7: SUMMARY AND CONCLUSIONS

Twelve out of the twenty-seven large-scale beam specimens were fully autopsied to evaluate the effect of post-tensioning on durability and to evaluate the relative performance of a large number of corrosion protection variables. Two additional specimens were partially autopsied. Full autopsies for the remaining specimens will be performed at a future date. Beams were fabricated in two phases in order to begin exposure testing on a portion of the specimens while the remaining specimens were being fabricated. In Phase I (16 beams), which started exposure testing in December 1997, researchers investigated the effect of prestress level and crack width and also included one of the high performance grout specimens. In Phase II (11 beams), which started exposure testing in December 1998, researchers investigated duct splices, grout type, concrete type, strand type, duct type, and end anchorage protection. After the first full autopsy performed at four and a half years for six Phase I beams, and three and a half years for six Phase II beams, and partial autopsies performed to two Phase I beams, preliminary conclusions were drawn.

### 7.1 OVERALL PERFORMANCE

The variables selected for evaluation in this beam testing program fall into four main categories: level of prestress and crack width, concrete type, prestressing strand coatings and post-tensioning hardware protection. In addition, different post-tensioning duct splices were also evaluated. After the initial autopsies of the fourteen beams, the use of large-scale beam specimens was found to be a very good method for determining the effect of most of these variables. Prestressing strand coatings, post-tensioned hardware protection, and plastic duct will be evaluated at a future date, since they are included in the remaining specimens under exposure testing. Based on the autopsy performed to date, the following conclusions are drawn:

- Galvanized duct performed poorly. No plastic duct was used in the specimens of the first set of full autopsies.
- Bleed water voids were present in the ducts even after “good grouting procedures.” Anti-bleed grout was not evaluated in the first set of full autopsies, but it is included in one of the remaining specimens for future autopsy.
- Voids from bleed water in grout were shown to be very detrimental to the duct.
- A clear trend was found with respect to cracking and mild steel corrosion. As cracking increased, stirrup and rebar corrosion increased. This trend was not clearly shown on strands, since strand ratings were all very low and close in value
- Mixed reinforcing (2/3 PS) beams showed the worst corrosion resistance. The best performance was obtained from 100%S PS specimens, followed by 100%U PS specimens
- Phase I beam results showed that there was a reduced risk of corrosion damage with increasing levels of prestress
- High performance concrete specimens (low permeability concrete,  $w/c=0.29$ ), appear to perform better than class C fly ash concrete specimens. However, both appear to be effective in minimizing the chloride penetration through concrete
- Industry standard duct splices as well as heat shrink duct splices do not seem to provide adequate corrosion protection
- Duct splice damage did not show a direct correlation with the severity of corrosion
- No difference was found between normal and fly ash grout. Low strand corrosion ratings on all specimens after autopsy, did not allow clear identification of the effect of different types of grout

## **7.2 LOAD/PRESTRESS LEVEL VERSUS CORROSION: THE EFFECT OF CRACKING**

The effect of cracking (width and number) on corrosion protection was an area of great emphasis in this experimental program. The effect of cracking was primarily investigated using standard variables and the sections that would be expected to crack under service loads. The range of crack widths investigated in this program were based on a survey of relevant literature performed by West<sup>2</sup> regarding critical crack widths for corrosion and recommended allowable crack widths. Consideration was also given to the applied moment-crack width behavior computed for the sections. Three different load levels were used: unloaded, service load, and temporary overloaded. The following conclusions are drawn:

- The specimen corrosion protection decreases as the applied load increases
- Corrosion protection decreases with increasing cracking
- An increase in transverse crack width produces a decrease in corrosion protection
- Longitudinal or splitting cracks in the concrete surface are a clear indication of very severe corrosion within the member.
- The chloride content in the concrete is significantly higher at crack locations, and increases as the crack width increases
- The specimen corrosion protection increases as the level of prestress increases
- Mixed reinforcement (2/3 PS) beams showed the worst corrosion performance. Increasing the post-tensioning level from 2/3 PS to 100% PS significantly increased the corrosion protection
- The corrosion protection of the 2/3 PS beam was much more similar to Non-PS beams, as opposed to 100% PS Beams
- There was not a clear difference in the corrosion resistance among the fully prestressed beams designed with the ultimate strength method as compared to those designed with allowable stress method.

## **7.3 FLY ASH IN CONCRETE**

Concrete plays an important role in corrosion protection of steel reinforcement. One of the objectives of this research program is to evaluate the effectiveness of high performance concrete as a function of cracking. Three different concrete mixes were selected for comparison. The reference mix was the standard concrete: TxDOT Class C concrete. The alternates were a TxDOT Class C concrete with 25% Class F Fly Ash and a High Performance Concrete (0.29 w/c, 25% fly ash + superplasticizer). The following conclusions are drawn:

- Both the high performance concrete and the fly ash concrete beams showed good corrosion protection by minimizing the chloride penetration through the concrete
- The high performance concrete tends to show a slightly better corrosion protection than the fly ash concrete, but the difference is not significant.
- No conclusions can be drawn on corrosion protection of the high performance concrete and the fly ash concrete with respect to the standard TxDOT concrete due to the unfortunate lack of directly comparable specimens at the time of the first autopsy.

## **7.4 DUCT SPLICES FOR GALVANIZED STEEL DUCT**

In most practical applications, the post-tensioning ducts must be spliced at some location. It was decided to compare industry standard (IS) splices to heat shrink (HS) splices and unspliced duct. The effect of damaged splices was also examined. The IS splice consisted of a 1 ft length of oversized duct placed over the contact butt splice of the ducts. Concrete is prevented from entering the splice by wrapping the ends with duct tape. The heat shrink splice consists of a 8 inch length of heat shrink tubing placed over the

contact butt splice of the ducts. The original diameter of the heat shrink tubing was 4 inches. No mechanical connection was made between the two ducts being connected. The conclusions are as follows:

- The industry standard splice allowed moisture and chlorides to enter through the sides of the splice and get trapped between the duct and the splice due to inefficiency of duct tape.
- The heat-shrink splice also allowed moisture to enter through the sides and get trapped due to insufficient adhesion between the splice and the duct. It also traps bleed water from the grout.
- Damage inflicted on the duct splices did not show a direct correlation with the severity of corrosion.
- Neither the industry standard splice nor the heat-shrink splice appears to be a satisfactory duct splice for the corrosion protection of a galvanized steel duct.

## **7.5 HIGH PERFORMANCE FLY ASH GROUTS**

Two high performance grouts (a fly ash grout and an antibleed grout) were selected for investigation, in comparison with TxDOT standard grout. The fly ash grout specimen was autopsied, and results are reported herein. The antibleed grout specimen will be autopsied at a future date. Antibleed grout had a water-cement ratio of 0.33 with 2% cement weight of antibleed admixture. Based on the information to date, the following conclusions are drawn:

- The fly ash grout aided in the corrosion protection of the galvanized steel ducts
- The fly ash grout, in comparison to TxDOT standard grout, did not show an increase in corrosion protection of the prestressing strand. This result may be due to the strand ratings being very low and close in value. Several more years of exposure testing may be required to yield more conclusive results

## **7.6 EXPOSURE TESTING RESULTS**

Half-cell potential readings were measured using a saturated calomel reference electrode at the end of each wet cycle (once every four weeks). All measurements were performed according to ASTM C876.<sup>19</sup> In general, half-cell potential readings are inadequate in determining the severity of corrosion activity, but prove to be successful for relative comparison of specimens. The conclusions are as follows:

- There is an exact correlation in specimen performance between the greatest negative potential at the end of testing for autopsy beams and the time to corrosion
- Both half cell potential readings and corrosion rating graphs show the loaded Non-PS and 2/3 PS beams were the most corroded.
- Half-cell potential readings did not show a distinct correlation in high performance and fly ash concrete specimens with the corresponding corrosion ratings.

Corrosion rate measurements were taken four times during the exposure duration. Two types of equipment were used in this experimental program: the Pr Monitor and the 3LP. Measurements of the Phase I beams were taken after seven, twelve, fifteen and forty-seven months of exposure. Measurements of the Phase II beams were taken after 37 months of exposure. A final attempt to take corrosion rate measurements of all beams was made immediately prior to the forensic examination. This attempt was unsuccessful due to complications with the 3LP equipment. Corrosion rate readings did not show good correlation with forensic examination results. The presence of zinc in the galvanized steel ducts may have played a role in the erroneous results.

Chloride content was found to be a useful method in determining the onset of corrosion. However, there was not a direct relationship between the acid soluble chloride content at the bar/duct level and the severity of corrosion at time of autopsy.



## **CHAPTER 8: RECOMMENDATIONS FOR FUTURE TESTING**

The following recommendations are given for consideration in similar experimental programs:

- A smaller concrete cover may be used to accelerate the time to initiation of corrosion.
- Epoxy coated mild steel could be used to clearly separate and accelerate the corrosion of the post-tensioning system.
- Connection wires used to take half-cell potential readings and corrosion rate measurements should be protected against the outdoor environment, to avoid possible deterioration and corrosion that would increase resistivity.
- Add more control specimens or examine fewer variables.



## CHAPTER 9: IMPLEMENTATION OF RESULTS

After final autopsies of twelve out of twenty-seven beam specimens and partial autopsies of two beam specimens, research results generated the following findings. Final autopsies of the remaining beam specimens will be more conclusive for strand duct and grout types, and also for the use of encapsulated anchorage systems.

### **Post-tensioning Ducts**

- Galvanized ducts should not be used in aggressive exposures.

### **Level of Prestress**

- Mixed reinforcement members should not be used in aggressive exposures unless special provisions are made to effectively seal cracks and concrete cover from exposure to chlorides.
- Fully prestressed members are recommended in aggressive environments to delay moisture and chloride ingress.
- Post-tensioning systems need additional protection above the current typical practice when in aggressive environments. In particular the use of galvanized duct appears unwise. The use of plastic ducts and encapsulated anchorage protection systems appear promising but while plastic duct was clearly superior in the macrocell specimens the use in the beam specimens cannot be conclusively evaluated until after final autopsies of the remaining beam specimens.

### **Duct Splices for Galvanized Ducts**

- Neither the standard industry practice of duct taped sleeves nor heat shrink splices should be considered as watertight
- Better systems than industry standard or heat-shrink splices for galvanized steel ducts should be investigated and developed if galvanized duct continues to be used in non-aggressive environments.

### **High Performance Fly Ash Grout**

- Standard Class C grout with fly ash is not recommended.
- The use of antibleed admixture appear promising but cannot be conclusively evaluated until after final autopsies of the remaining beam specimens.

### **Concrete type**

- High Performance Concrete is recommended in aggressive environments due to the significantly reduced permeability and crack control. Fly ash (Class C) concrete may also be considered when the environment is less aggressive.

### **Grouting Procedure**

- Stringent grouting procedures should be enforced during construction.

### **Plastic Chairs**

- Fully plastic chairs are recommended for use throughout the substructure to eliminate corrosion damage. Chairs or bolster strips that contain any steel should be avoided.





# Appendix Supplementary Material

## A. DETAIL BEAM CONSTRUCTION DRAWINGS

Complete construction details of the four sections (Non-PS, 2/3 PS, 100%U PS and 100%S PS) are shown in the following detailed drawings.

<u>Long Term Exposure Test – Linear Flexural Elements</u>																																											
<table style="width: 100%; border-collapse: collapse;"> <thead> <tr> <th style="text-align: left; border-bottom: 1px solid black;">Sheet:</th> <th style="text-align: left; border-bottom: 1px solid black;">Title:</th> </tr> </thead> <tbody> <tr><td>S1</td><td>Non-PS – Section</td></tr> <tr><td>S2</td><td>Non-PS – Stirrup Layout</td></tr> <tr><td>S3</td><td>100%S – Section</td></tr> <tr><td>S4</td><td>100%S – Stirrup Layout</td></tr> <tr><td>S5</td><td>100%S – Anchorage Zone</td></tr> <tr><td>S6</td><td>100%S – End Detail</td></tr> <tr><td>S7</td><td>100%U – Section</td></tr> <tr><td>S8</td><td>100%U – Stirrup Layout</td></tr> <tr><td>S9</td><td>100%U – Anchorage Zone</td></tr> <tr><td>S10</td><td>100%U – End Detail</td></tr> </tbody> </table>	Sheet:	Title:	S1	Non-PS – Section	S2	Non-PS – Stirrup Layout	S3	100%S – Section	S4	100%S – Stirrup Layout	S5	100%S – Anchorage Zone	S6	100%S – End Detail	S7	100%U – Section	S8	100%U – Stirrup Layout	S9	100%U – Anchorage Zone	S10	100%U – End Detail	<table style="width: 100%; border-collapse: collapse;"> <thead> <tr> <th style="text-align: left; border-bottom: 1px solid black;">Sheet:</th> <th style="text-align: left; border-bottom: 1px solid black;">Title:</th> </tr> </thead> <tbody> <tr><td>S11</td><td>2/3 PS – Section</td></tr> <tr><td>S12</td><td>2/3 PS – Stirrup Layout</td></tr> <tr><td>S13</td><td>2/3 PS – Anchorage Zone</td></tr> <tr><td>S14</td><td>2/3 PS – End Detail</td></tr> <tr><td>S15</td><td>Reaction Beam – Section</td></tr> <tr><td>S16</td><td>Reaction Beam – Stirrup Layout</td></tr> <tr><td>D1</td><td>Bar Details</td></tr> <tr><td>D2</td><td>Anchorage Hardware</td></tr> <tr><td>D3</td><td>PT Duct and Splice Details</td></tr> </tbody> </table>	Sheet:	Title:	S11	2/3 PS – Section	S12	2/3 PS – Stirrup Layout	S13	2/3 PS – Anchorage Zone	S14	2/3 PS – End Detail	S15	Reaction Beam – Section	S16	Reaction Beam – Stirrup Layout	D1	Bar Details	D2	Anchorage Hardware	D3	PT Duct and Splice Details
Sheet:	Title:																																										
S1	Non-PS – Section																																										
S2	Non-PS – Stirrup Layout																																										
S3	100%S – Section																																										
S4	100%S – Stirrup Layout																																										
S5	100%S – Anchorage Zone																																										
S6	100%S – End Detail																																										
S7	100%U – Section																																										
S8	100%U – Stirrup Layout																																										
S9	100%U – Anchorage Zone																																										
S10	100%U – End Detail																																										
Sheet:	Title:																																										
S11	2/3 PS – Section																																										
S12	2/3 PS – Stirrup Layout																																										
S13	2/3 PS – Anchorage Zone																																										
S14	2/3 PS – End Detail																																										
S15	Reaction Beam – Section																																										
S16	Reaction Beam – Stirrup Layout																																										
D1	Bar Details																																										
D2	Anchorage Hardware																																										
D3	PT Duct and Splice Details																																										
<table border="1" style="width: 100%; border-collapse: collapse;"> <tr> <td colspan="2" style="text-align: center;">Durability of P/T Bridge Substructures</td> </tr> <tr> <td colspan="2" style="text-align: center;">TITLE Drawing List</td> </tr> <tr> <td style="font-size: small;">DRAWN BY: JSW</td> <td style="font-size: small;">SCALE: n/a</td> </tr> <tr> <td style="font-size: small;">DATE: 9-Jun-97</td> <td style="font-size: small;">SHEET: 0</td> </tr> </table>		Durability of P/T Bridge Substructures		TITLE Drawing List		DRAWN BY: JSW	SCALE: n/a	DATE: 9-Jun-97	SHEET: 0																																		
Durability of P/T Bridge Substructures																																											
TITLE Drawing List																																											
DRAWN BY: JSW	SCALE: n/a																																										
DATE: 9-Jun-97	SHEET: 0																																										

**Figure A.1 Sheet 0: Drawing List<sup>2</sup>**

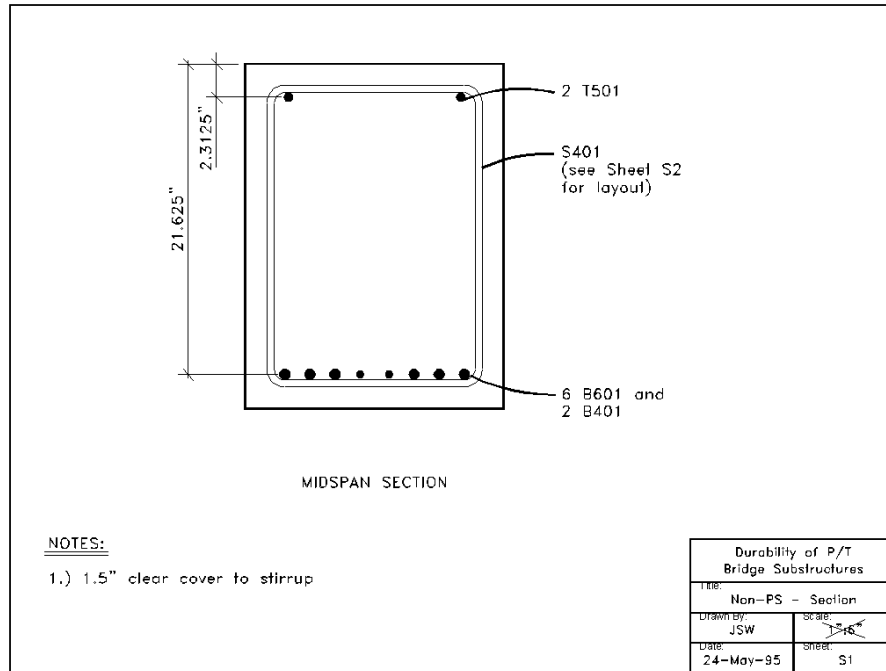


**Figure A.2 Sheet S1: Non-PS Section <sup>2</sup>**

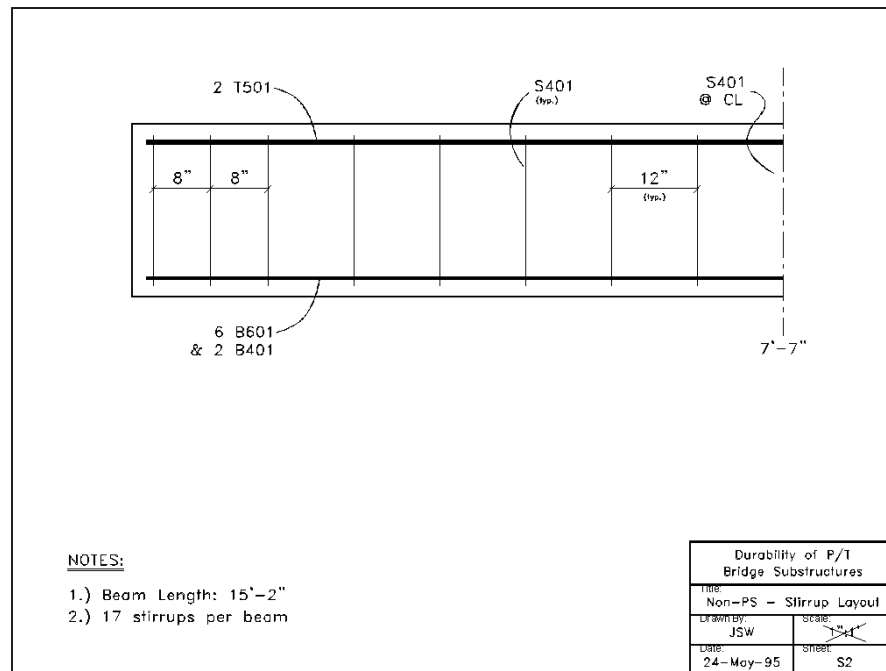


**Figure A.3 Sheet S2: Non-PS Stirrup Layout <sup>2</sup>**

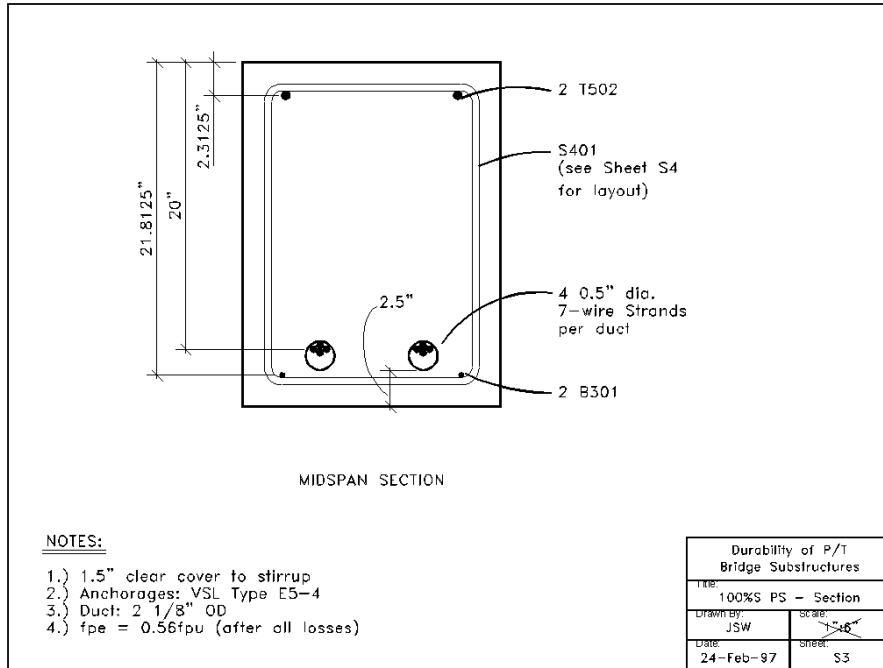


**Figure A.4 Sheet S3: 100%S PS Section<sup>2</sup>**

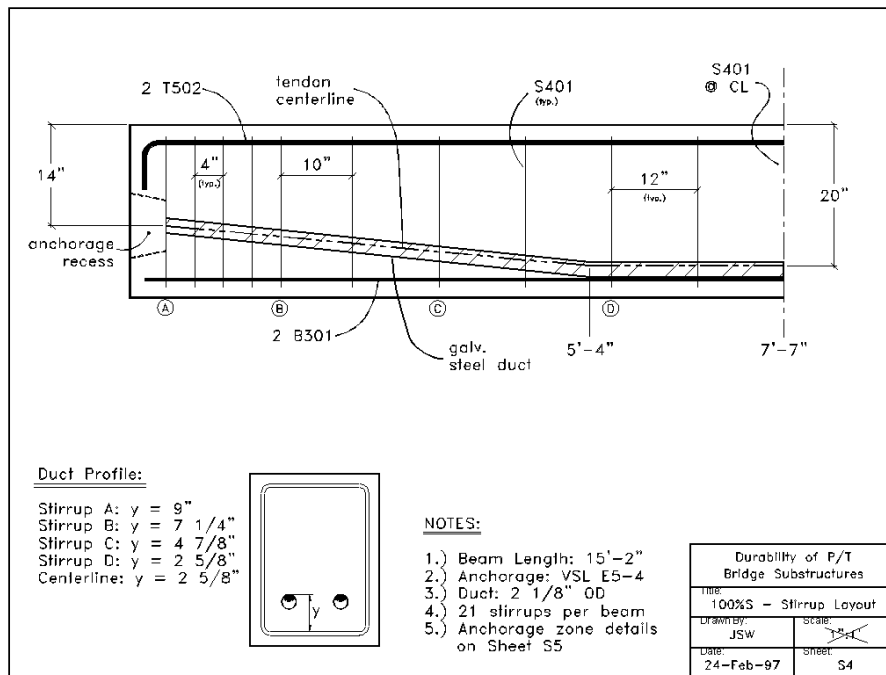


**Figure A.5 Sheet S4: 100%S Stirrup Layout<sup>2</sup>**

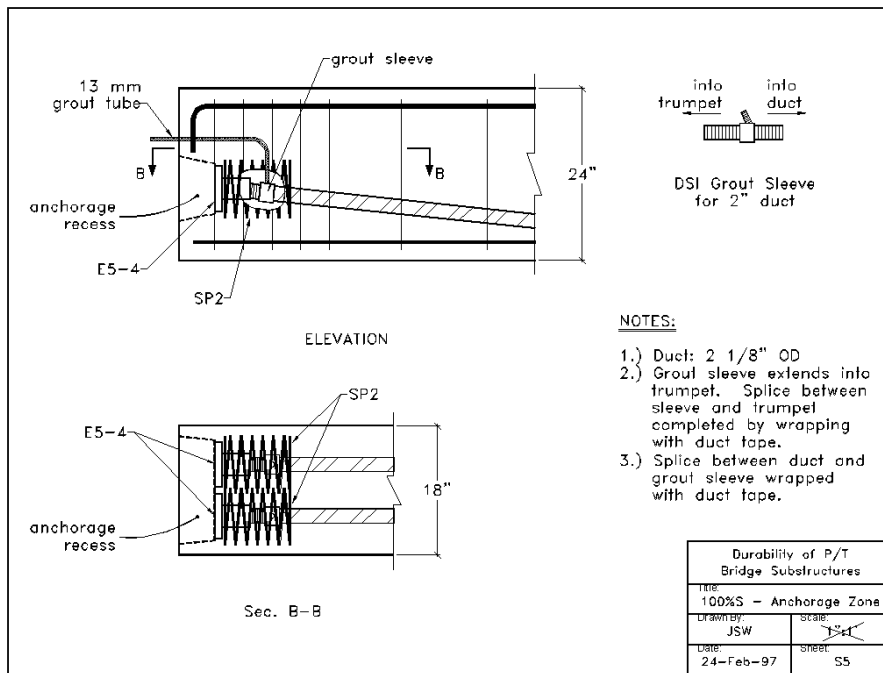


Figure A.6 Sheet S5: 100%S Anchorage Zone<sup>2</sup>

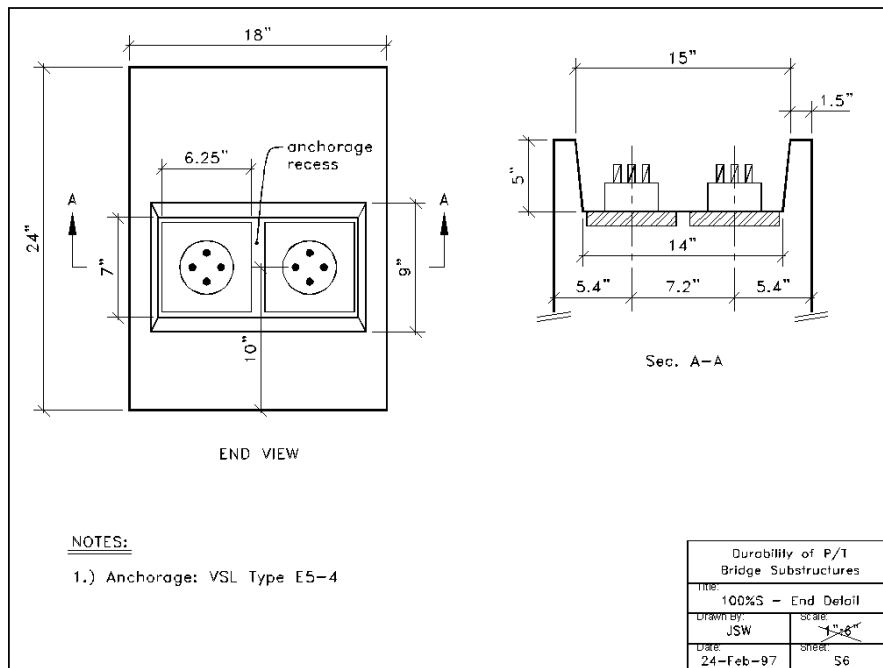
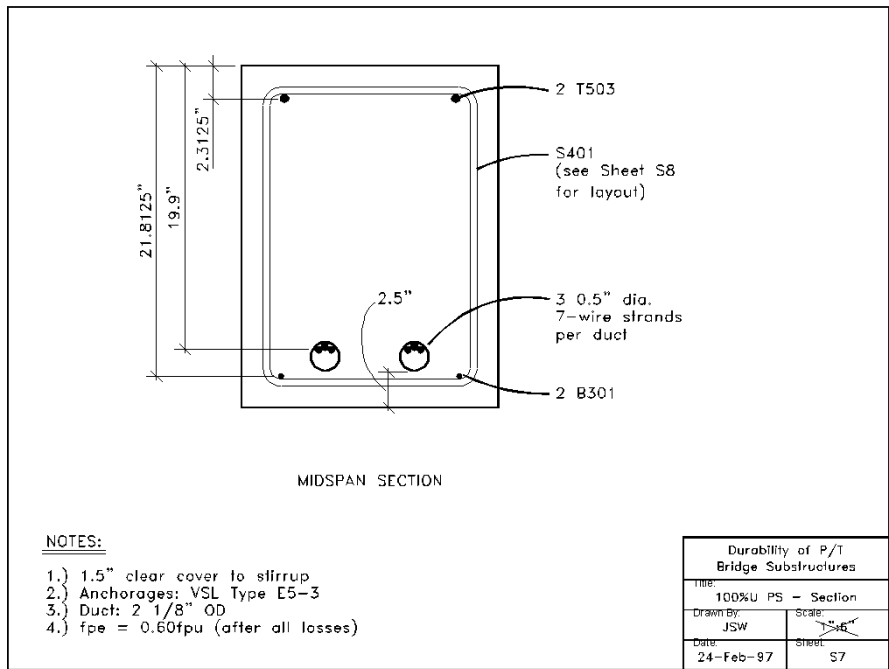
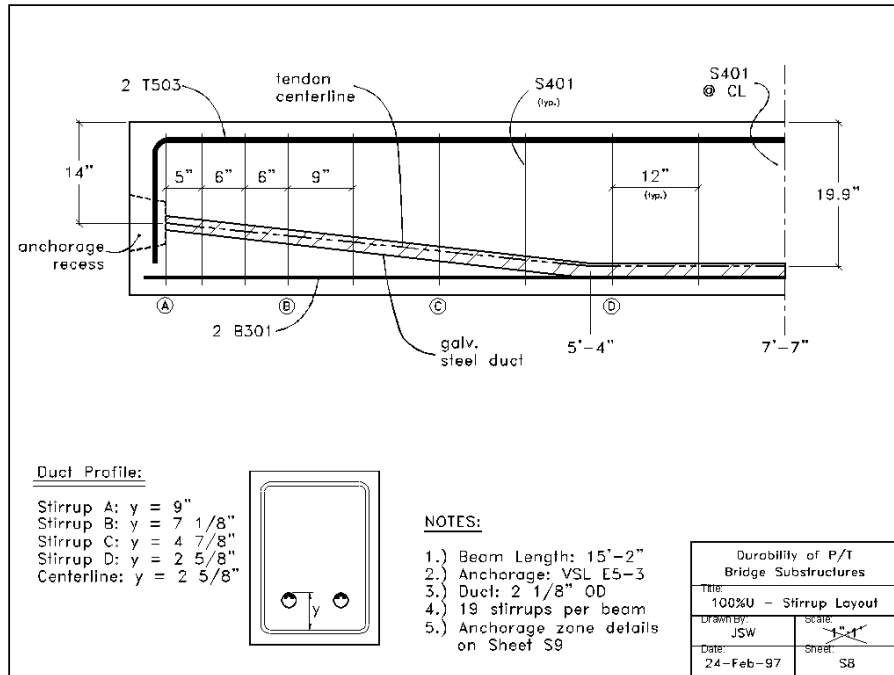


Figure A.7 Sheet S6: 100%S End Detail<sup>2</sup>



**Figure A.8 Sheet S7: 100%U PS Section <sup>2</sup>**



**Figure A.9 Sheet S8: 100%U Stirrup Layout <sup>2</sup>**

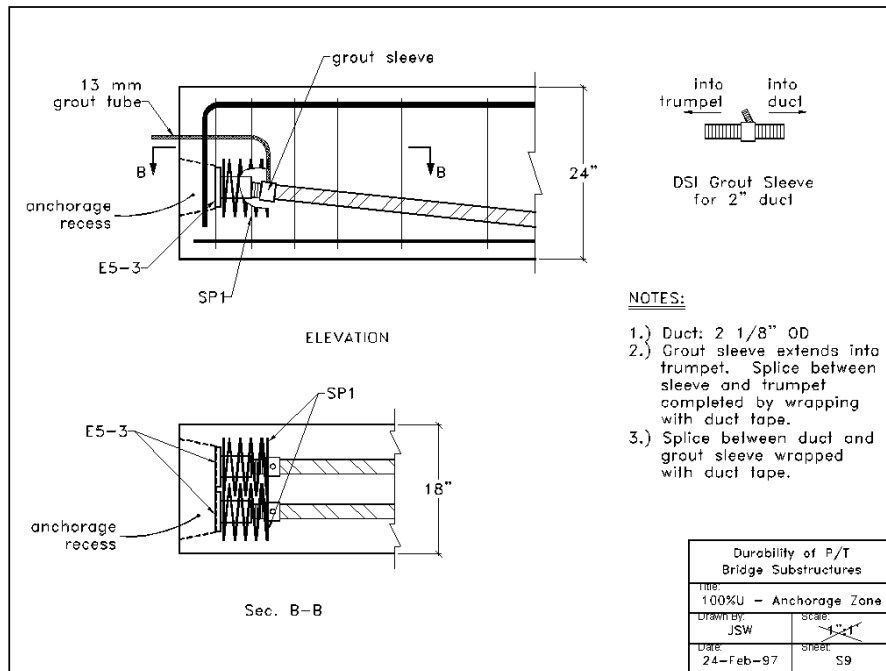


Figure A.10 Sheet S9: 100%U Anchorage Zone<sup>2</sup>

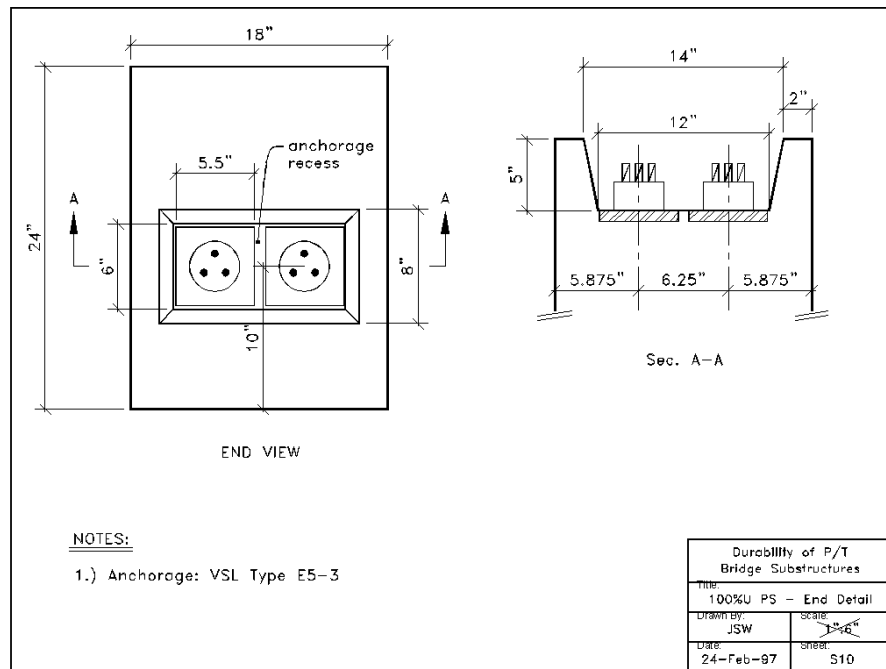
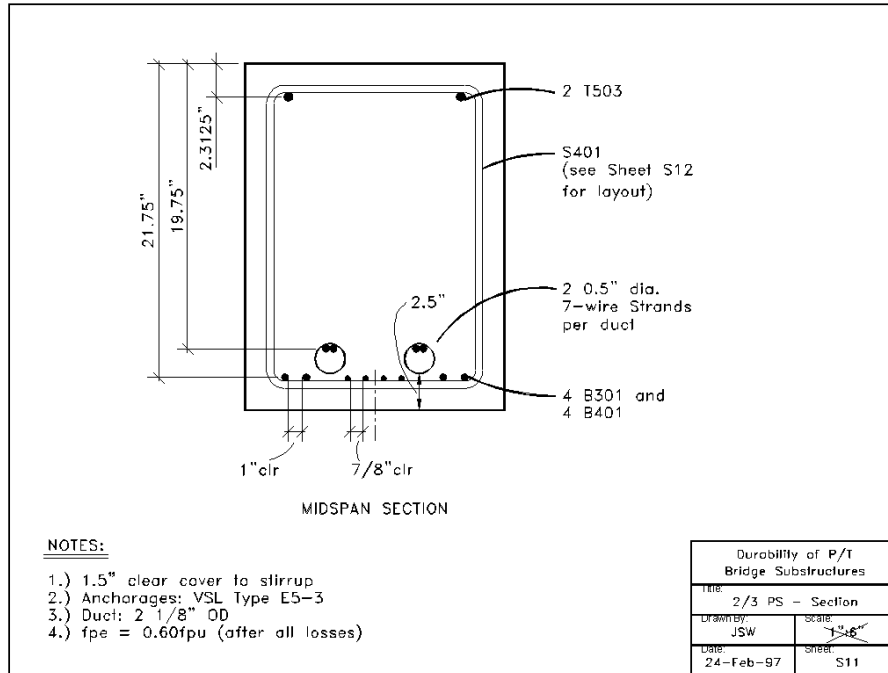
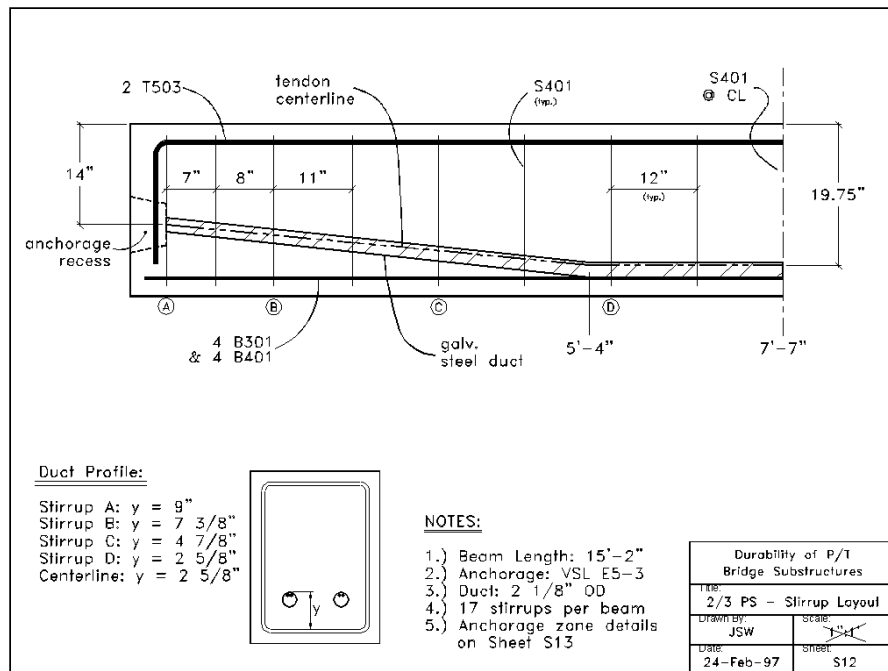


Figure A.11 Sheet S10: 100%U End Detail<sup>2</sup>



**Figure A.12 Sheet S11: 100%S End Detail<sup>2</sup>**



**Figure A.13 Sheet S12: 2/3 PS Stirrup Layout<sup>2</sup>**

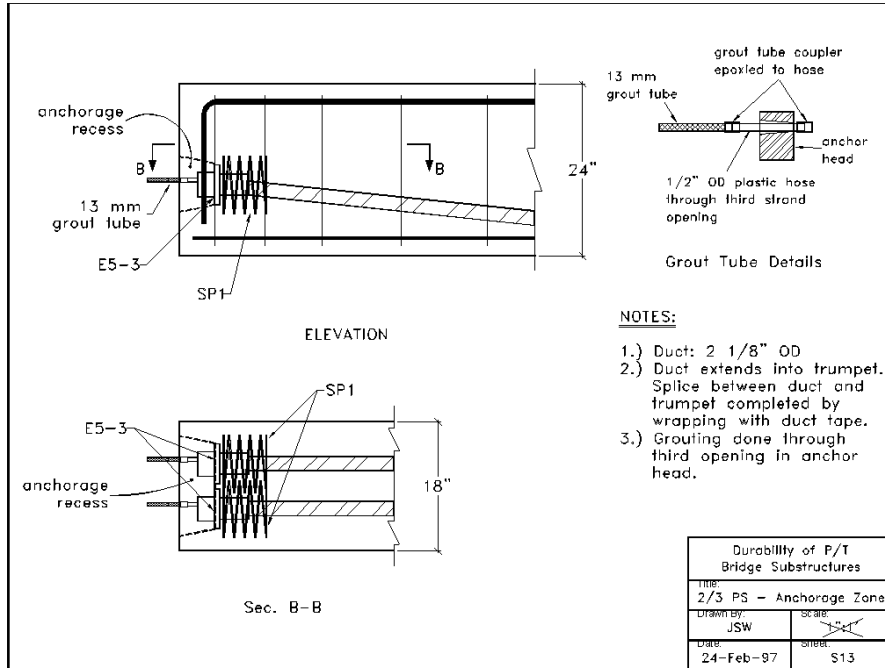


Figure A.14 Sheet S13: 2/3 PS Anchorage Zone<sup>2</sup>

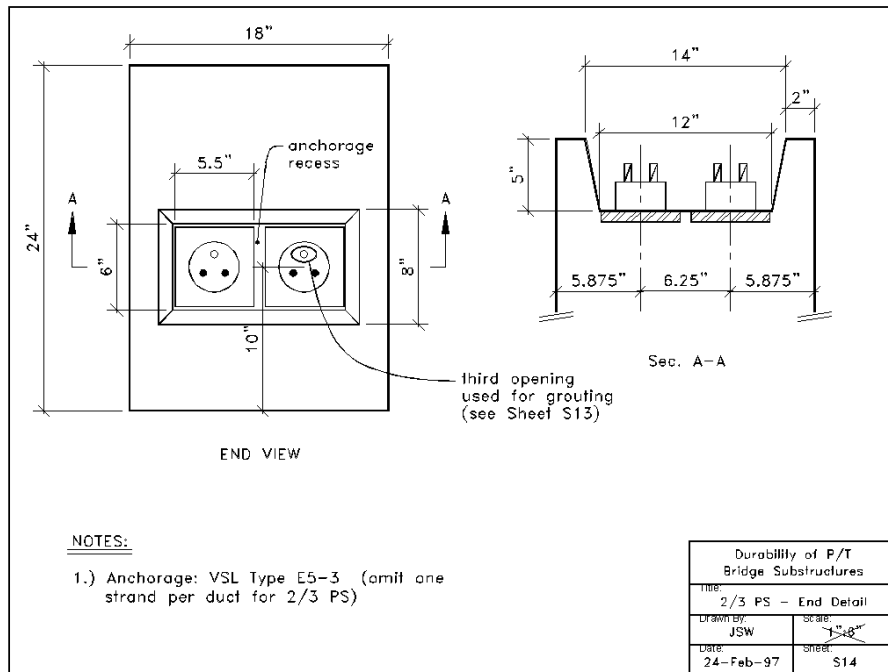
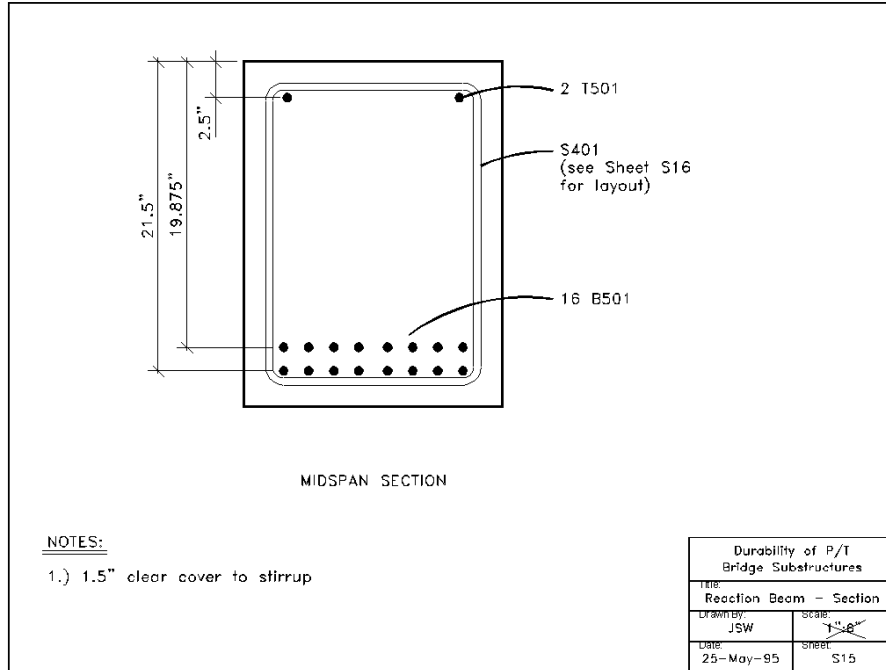
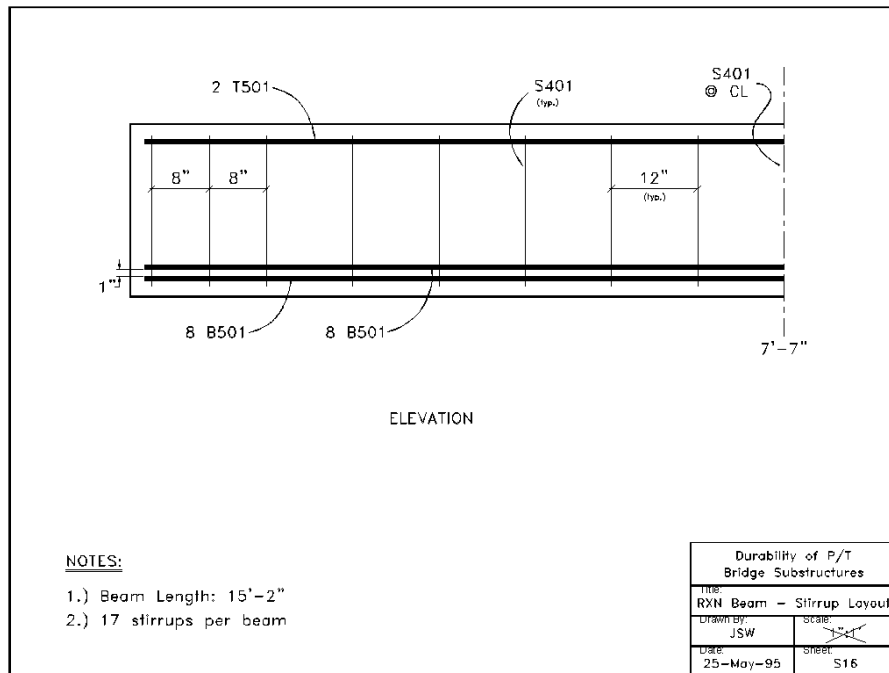


Figure A.15 Sheet S14: 2/3 PS End Detail<sup>2</sup>





**Figure A.16 Sheet S15: Reaction Beam Section<sup>2</sup>**



**Figure A.17 Sheet S16: Reaction Beam Stirrup Layout<sup>2</sup>**

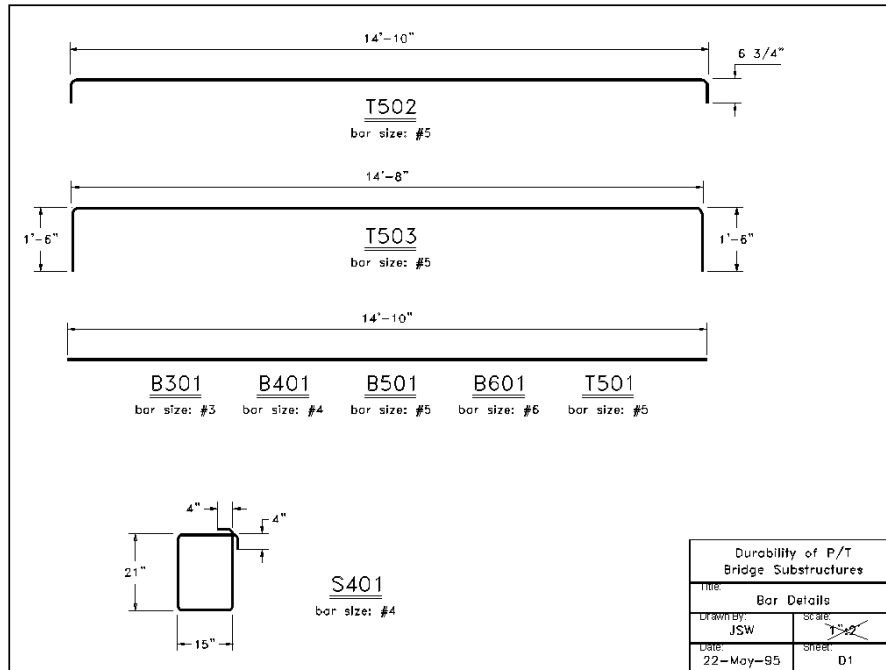


Figure A.18 Sheet D1: Bar Details <sup>2</sup>

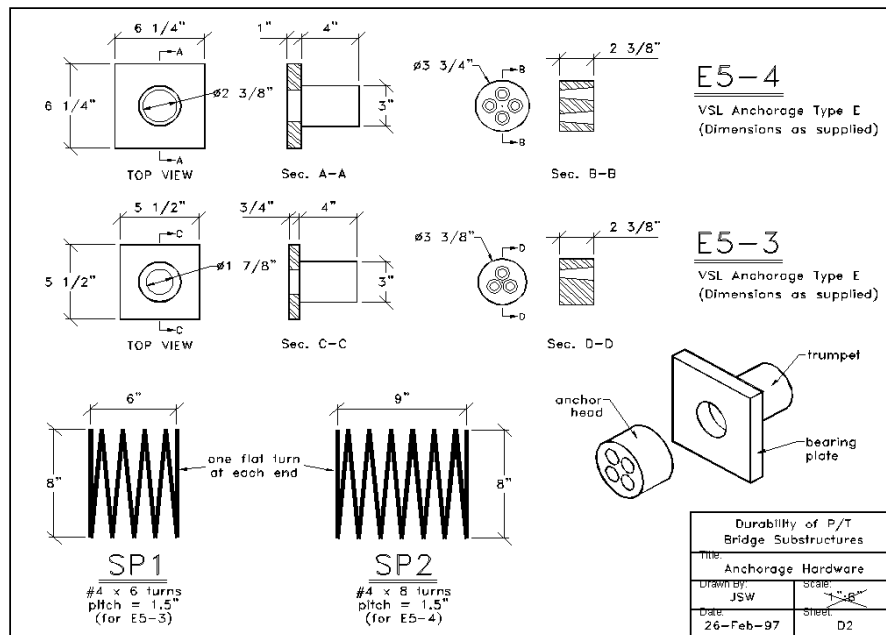
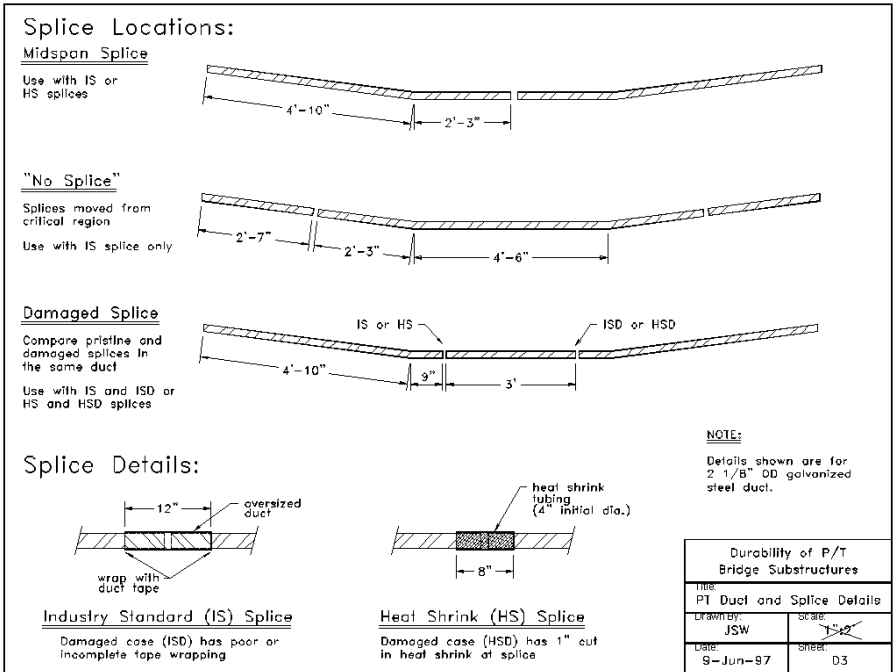


Figure A.19 Sheet D2: Anchorage Hardware <sup>2</sup>



**Figure A.20 Sheet D3: Post-Tensioning Duct and Splice Details<sup>2</sup>**

**B. SURFACE CRACK PATTERNS AND WIDTHS PRIOR TO AUTOPSY**

Crack patterns and widths for all Autopsy specimens immediately prior to concrete demolition and reinforcement removal, are shown in Figures B.1 through Figure B.12.

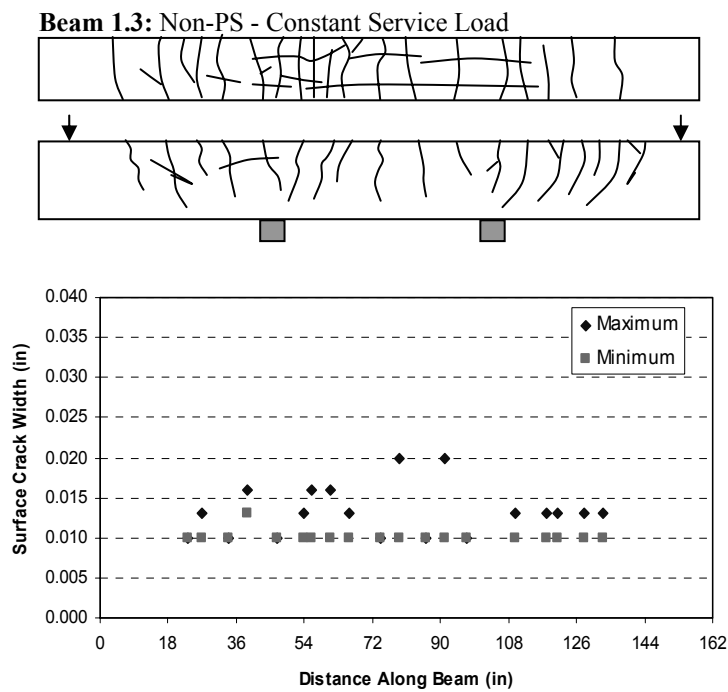


**Figure B.1 Final Crack Pattern and Measurements – Beam 1.3<sup>6,7</sup>**

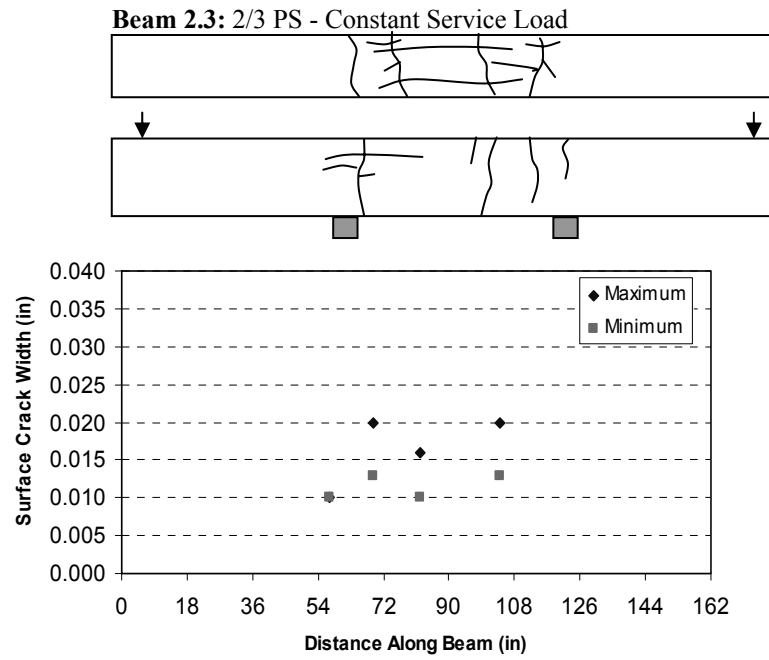


**Figure B.2 Final Crack Pattern and Measurements – Beam 2.3**<sup>6,7</sup>

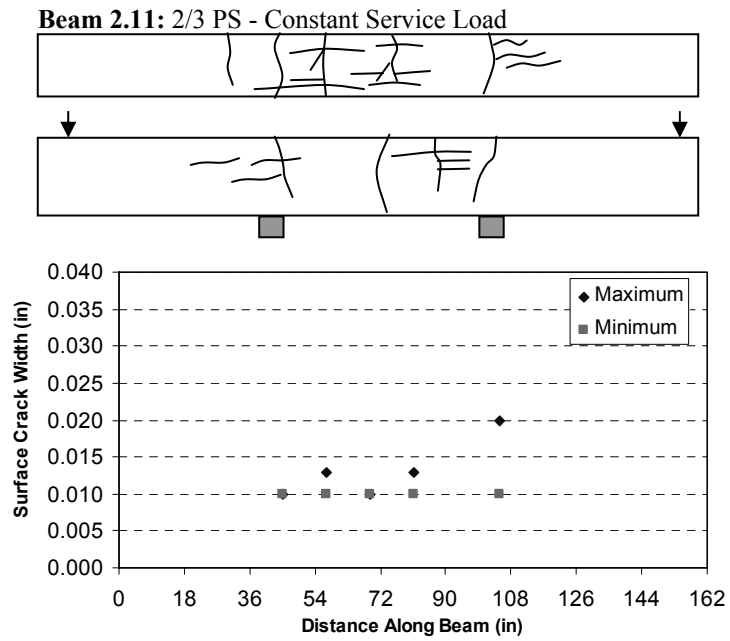


**Figure B.3 Final Crack Pattern and Measurements – Beam 2.11**<sup>6,7</sup>

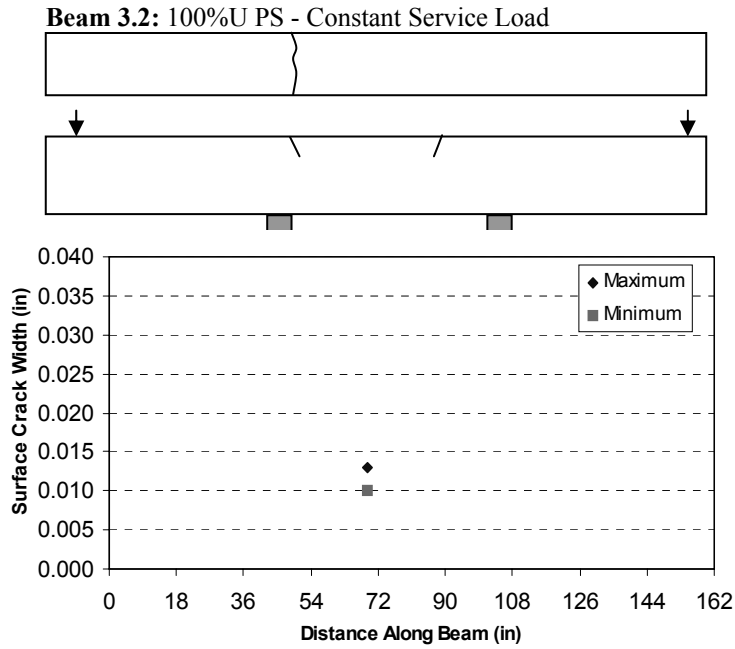


**Figure B.4 Final Crack Pattern and Measurements – Beam 3.2**<sup>6,7</sup>

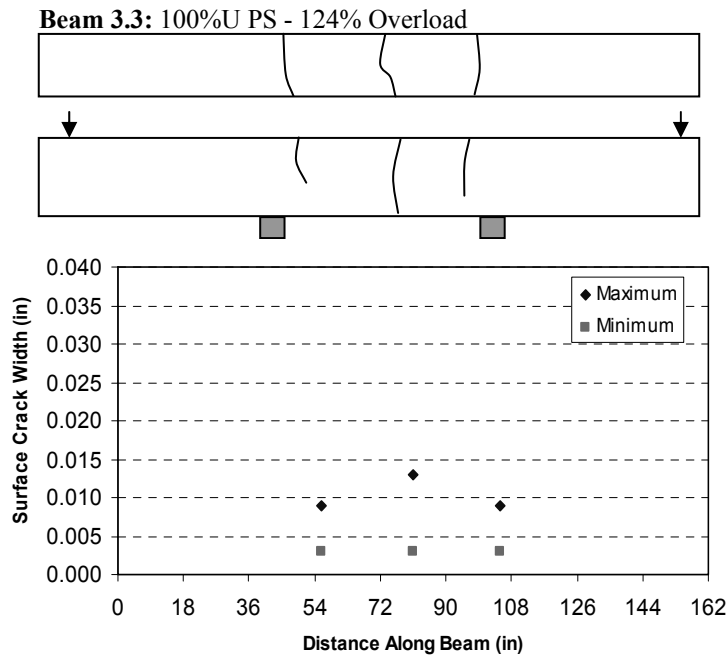


**Figure B.5 Final Crack Pattern and Measurements – Beam 3.3**<sup>6,7</sup>

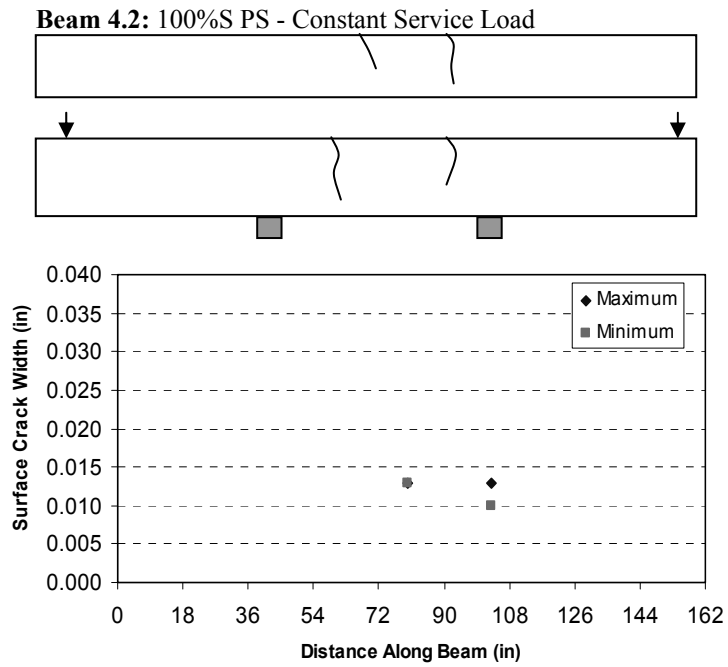


**Figure B.6 Final Crack Pattern and Measurements – Beam 4.2** <sup>6,7</sup>

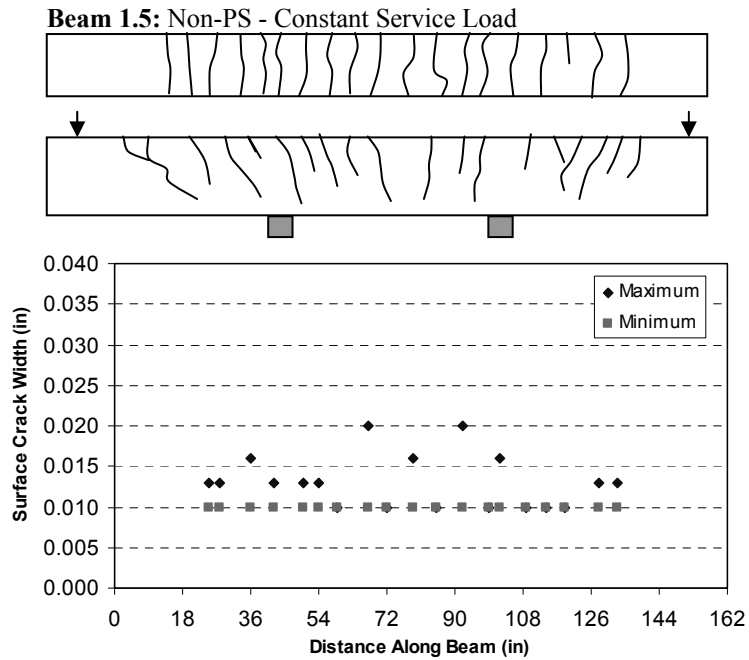


**Figure B.7 Final Crack Pattern and Measurements – Beam 1.5** <sup>6,7</sup>

**Beam 1.6: Non-PS - Constant Service**

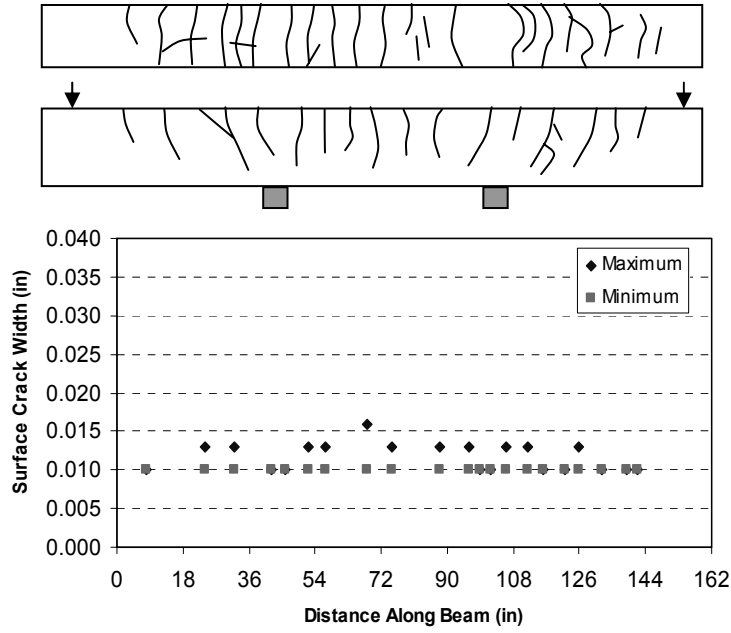


**Figure B.8 Final Crack Pattern and Measurements – Beam 1.6<sup>6,7</sup>**

**Beam 2.5: 2/3 PS - Constant Service Load**

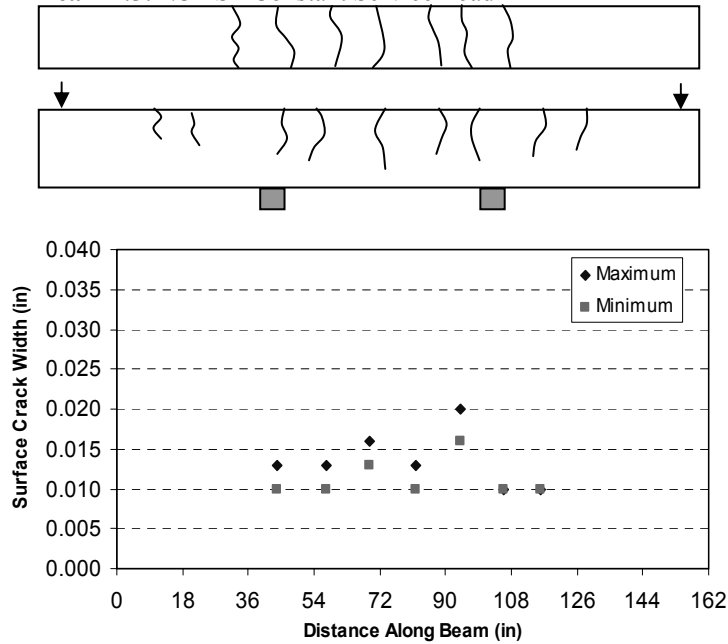


**Figure B.9 Final Crack Pattern and Measurements – Beam 2.5<sup>6,7</sup>**



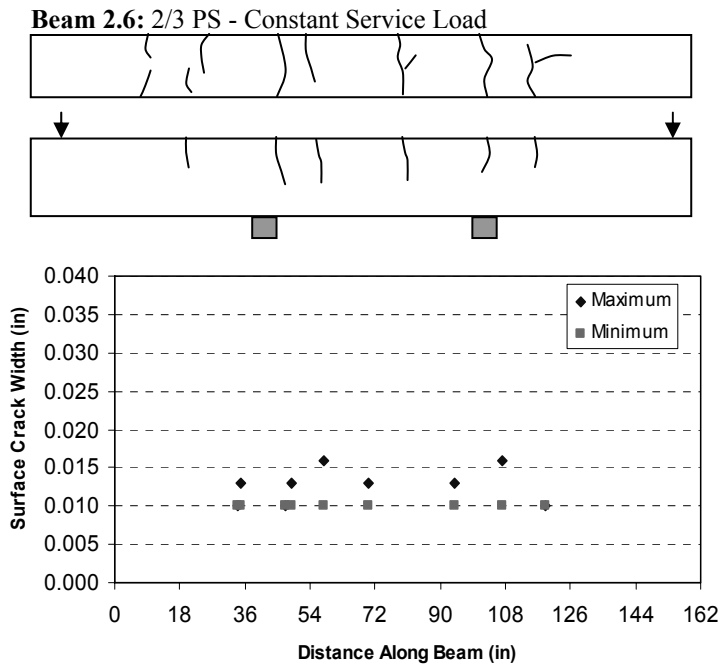


**Figure B.10 Final Crack Pattern and Measurements – Beam 2.6<sup>6,7</sup>**

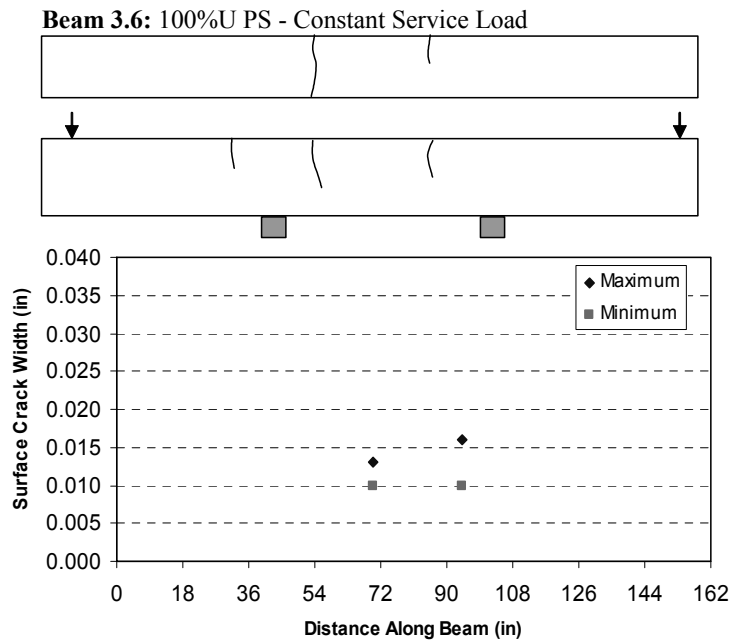


**Figure B.11 Final Crack Pattern and Measurements – Beam 3.6<sup>6,7</sup>**

**Beam 3.7: 100%U PS - Constant Service**

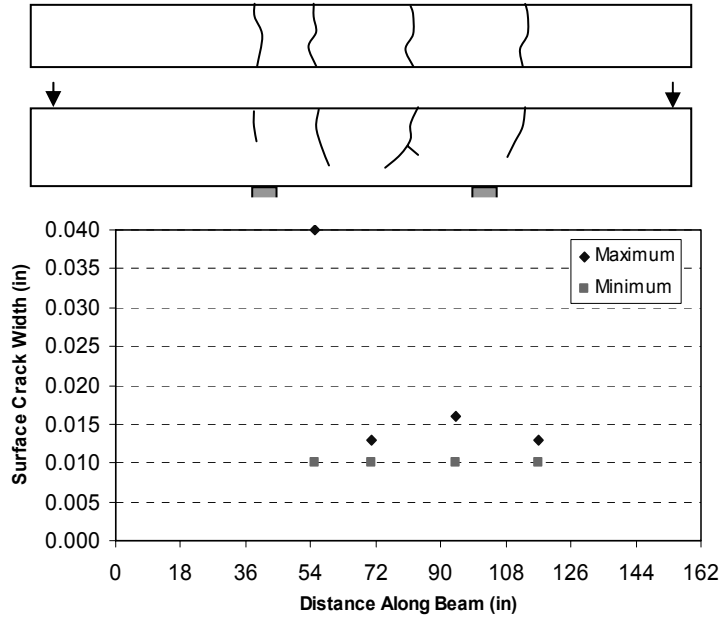


**Figure B.12 Final Crack Pattern and Measurements – Beam 3.7<sup>6,7</sup>**

### C. HALF-CELL POTENTIALS (LINE GRAPHS)

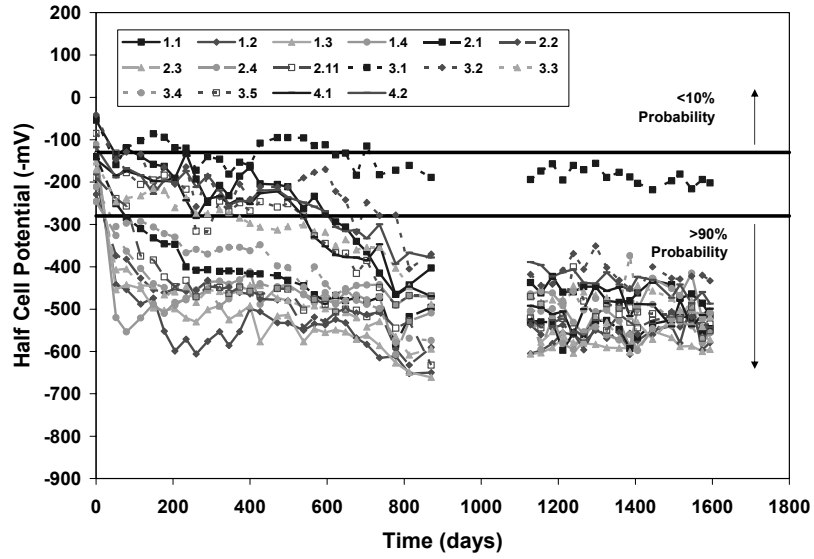


Figure C.1 Half-Cell Potential Readings for All Phase I Beams <sup>7</sup>

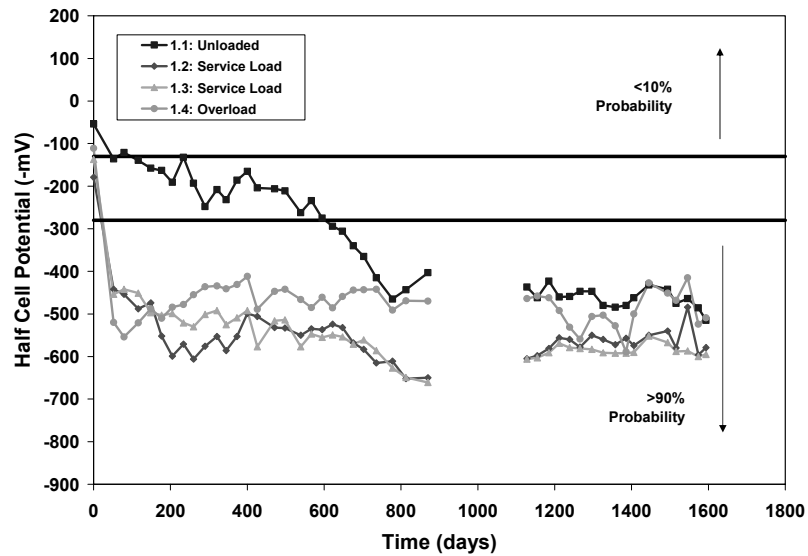
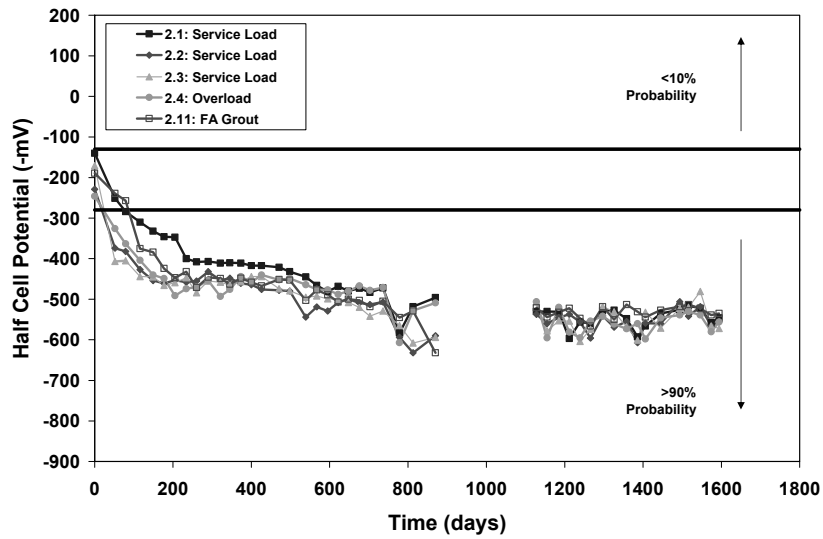
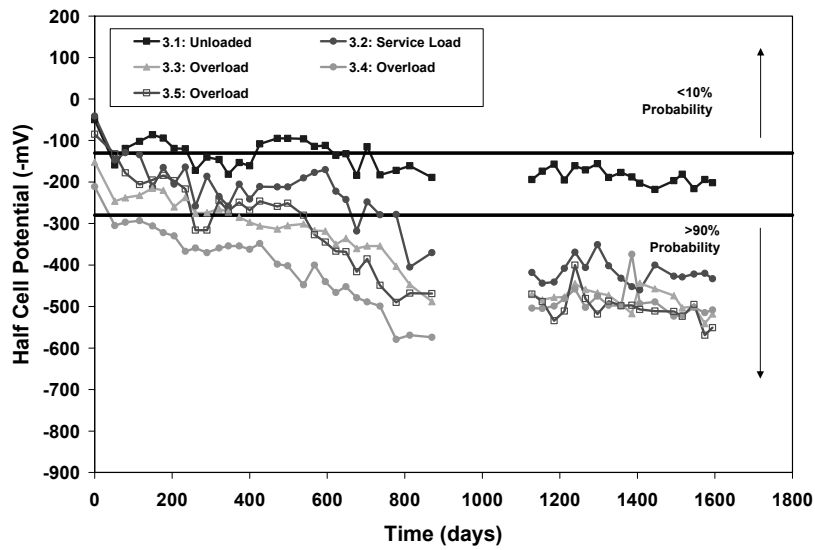


Figure C.2 Half-Cell Potential Readings for All Non-PS Phase I Beams <sup>7</sup>



**Figure C.3 Half-Cell Potential Readings for All 2/3 PS Phase I Beams <sup>7</sup>**



**Figure C.4 Half-Cell Potential Readings for All 100%U PS Phase I Beams <sup>7</sup>**

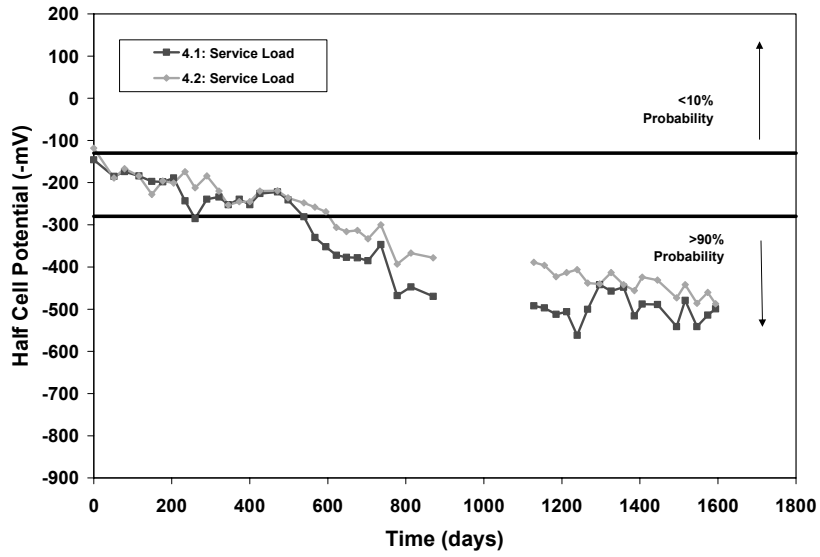


*Figure C.5 Half-Cell Potential Readings for All 100%S PS Phase I Beams<sup>7</sup>*

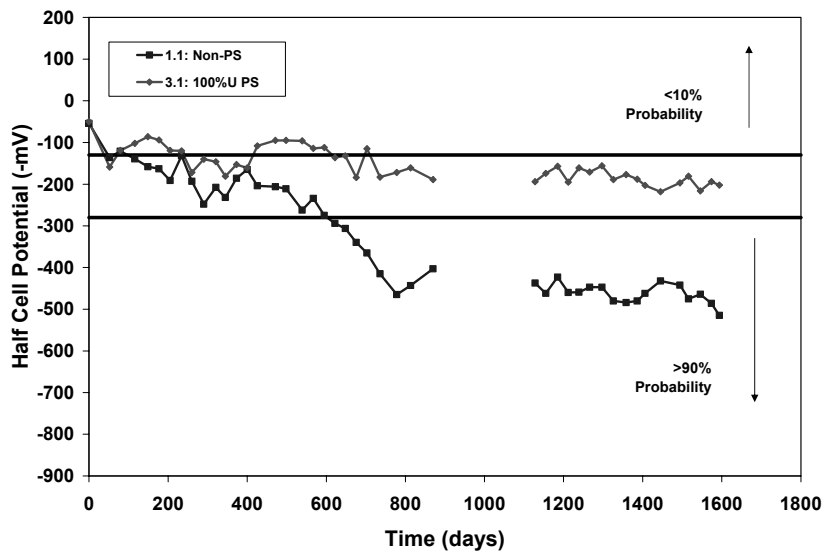


*Figure C.6 Half-Cell Potential Readings for All Unloaded Phase I Beams<sup>7</sup>*

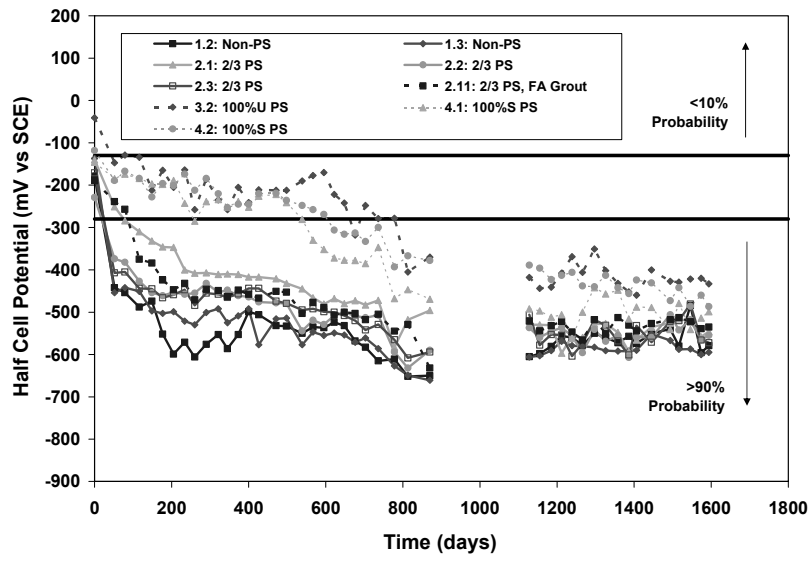


**Figure C.7 Half-Cell Potential Readings for All 100% Service Load Phase I Beams <sup>7</sup>**

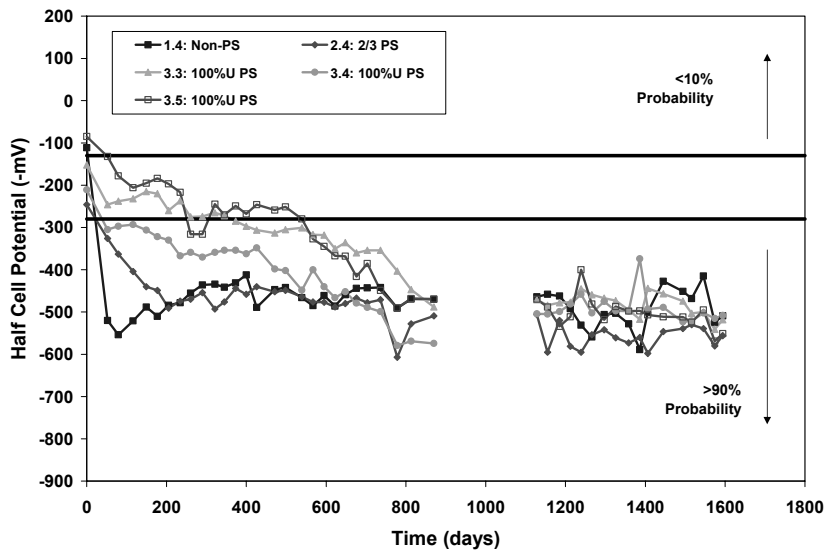


**Figure C.8 Half-Cell Potential Readings for All Overloaded Phase I Beams <sup>7</sup>**

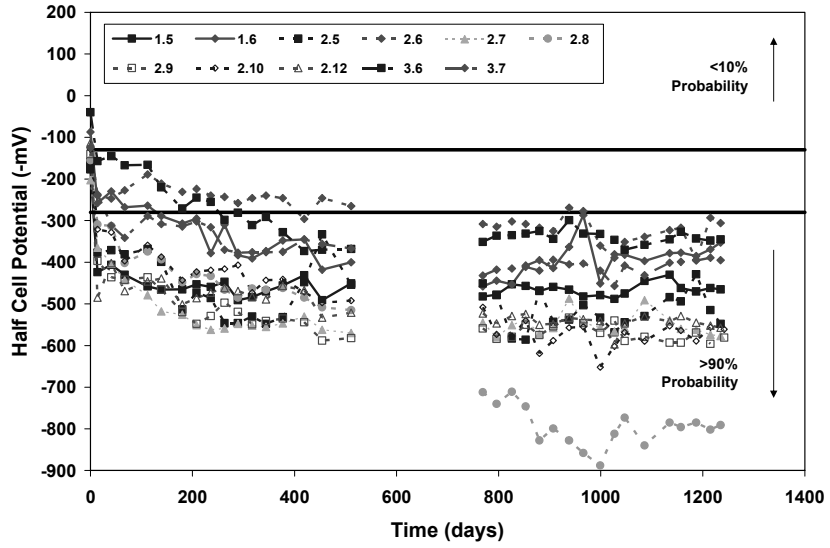


Figure C.9 Half-Cell Potential Readings for All Phase II Beams <sup>7</sup>

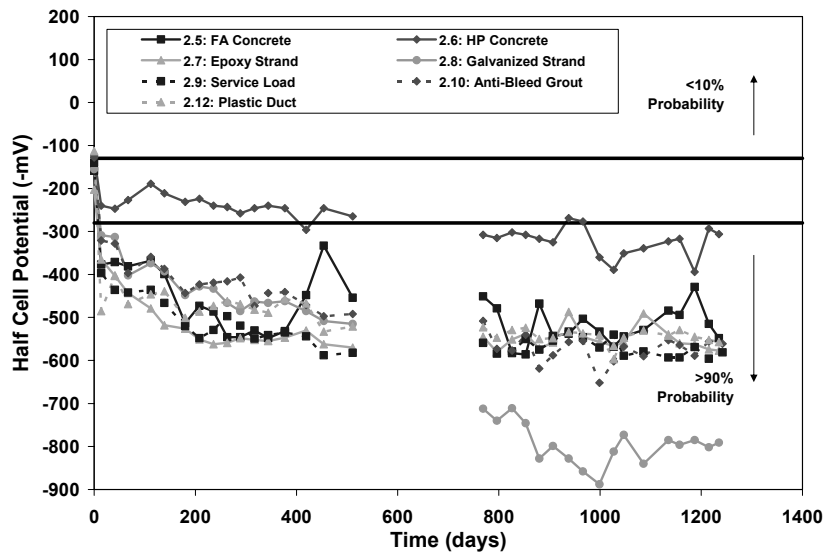
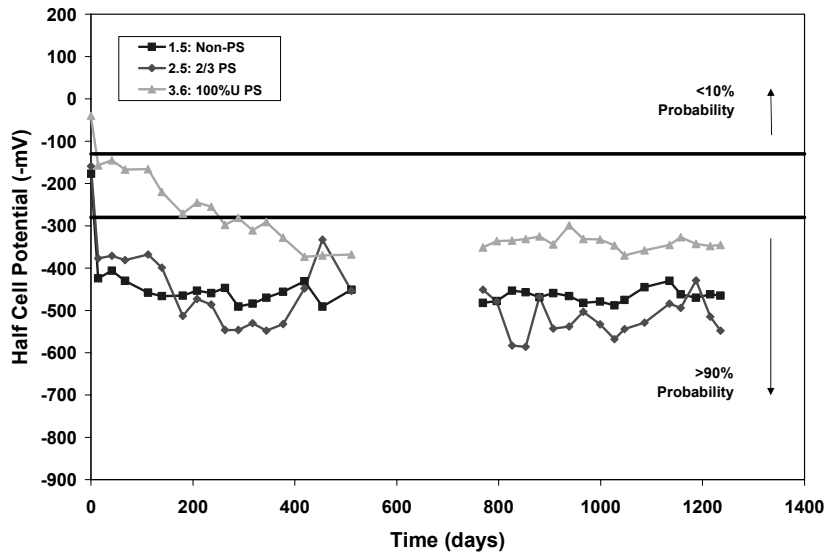
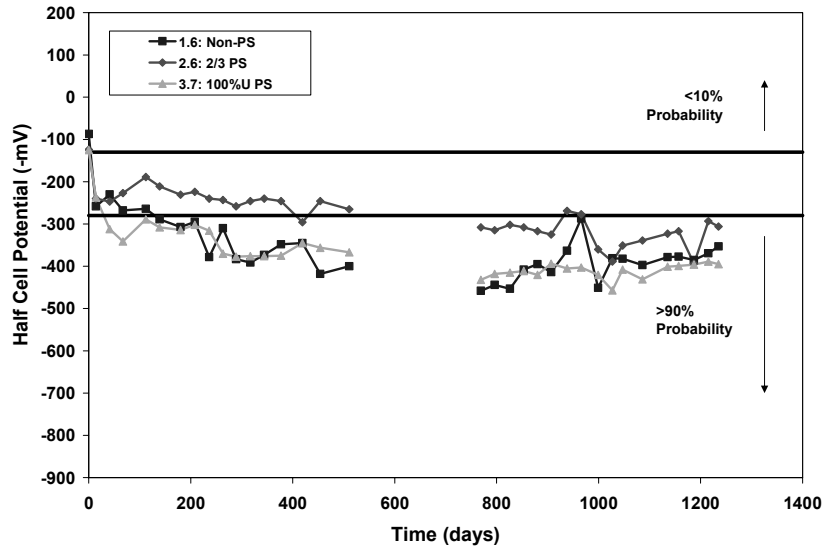


Figure C.10 Half-Cell Potential Readings for All 2/3 PS Phase II Beams <sup>7</sup>



*Figure C.11 Half-Cell Potential Readings for All Fly Ash Concrete Phase II Beams*<sup>7</sup>



*Figure C.12 Half-Cell Potential Readings for All High Performance Concrete Phase II Beams*<sup>7</sup>



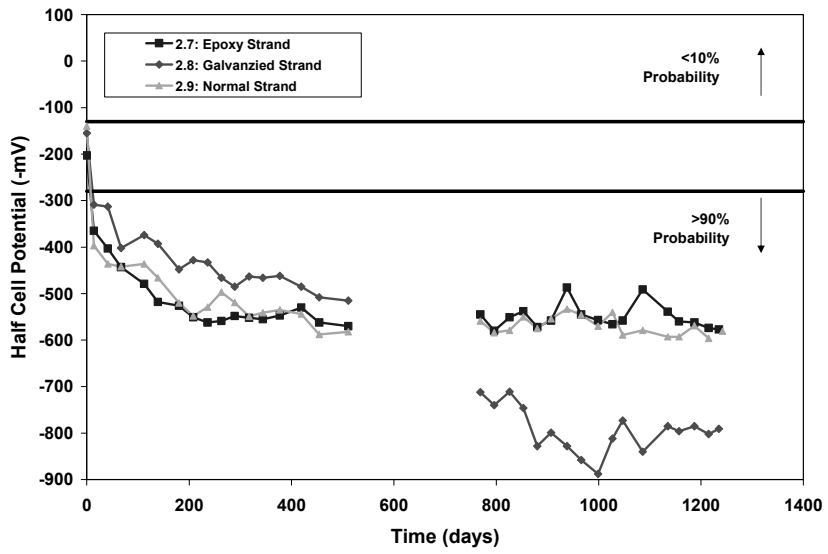


**Figure C.13 Half-Cell Potential Readings for All Varying Strand Type Phase II Beams<sup>7</sup>**

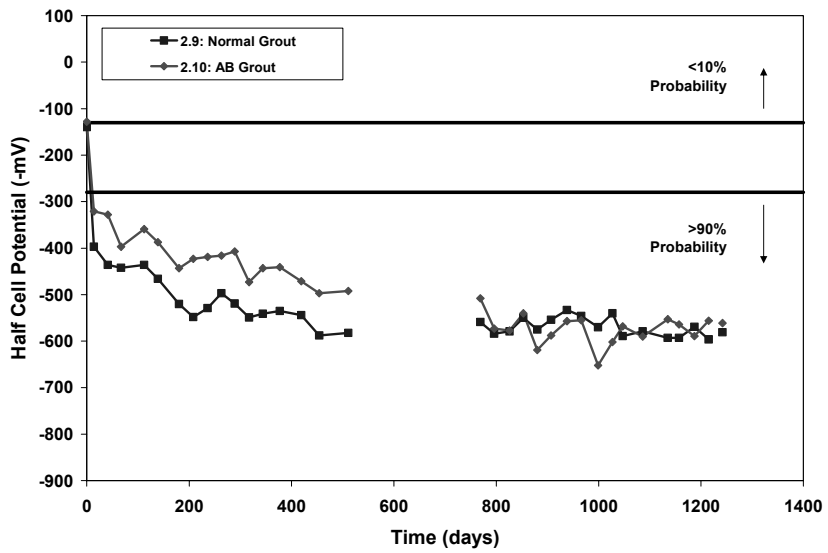


**Figure C.14 Half-Cell Potential Readings for All Varying Grout Type Phase II Beams<sup>7</sup>**

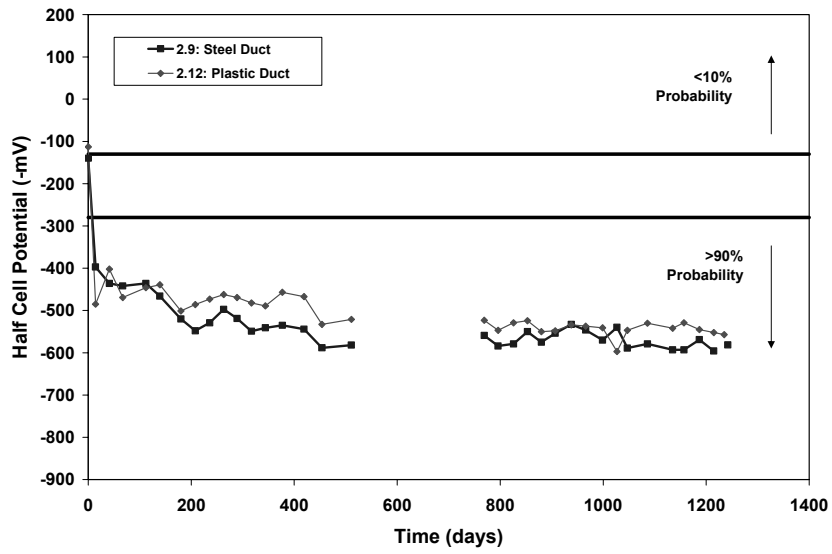


**Figure C.15 Half-Cell Potential Readings for All Varying Duct Type Phase II Beams<sup>7</sup>**

**D. HALF-CELL POTENTIALS (CONTOUR MAPS)**

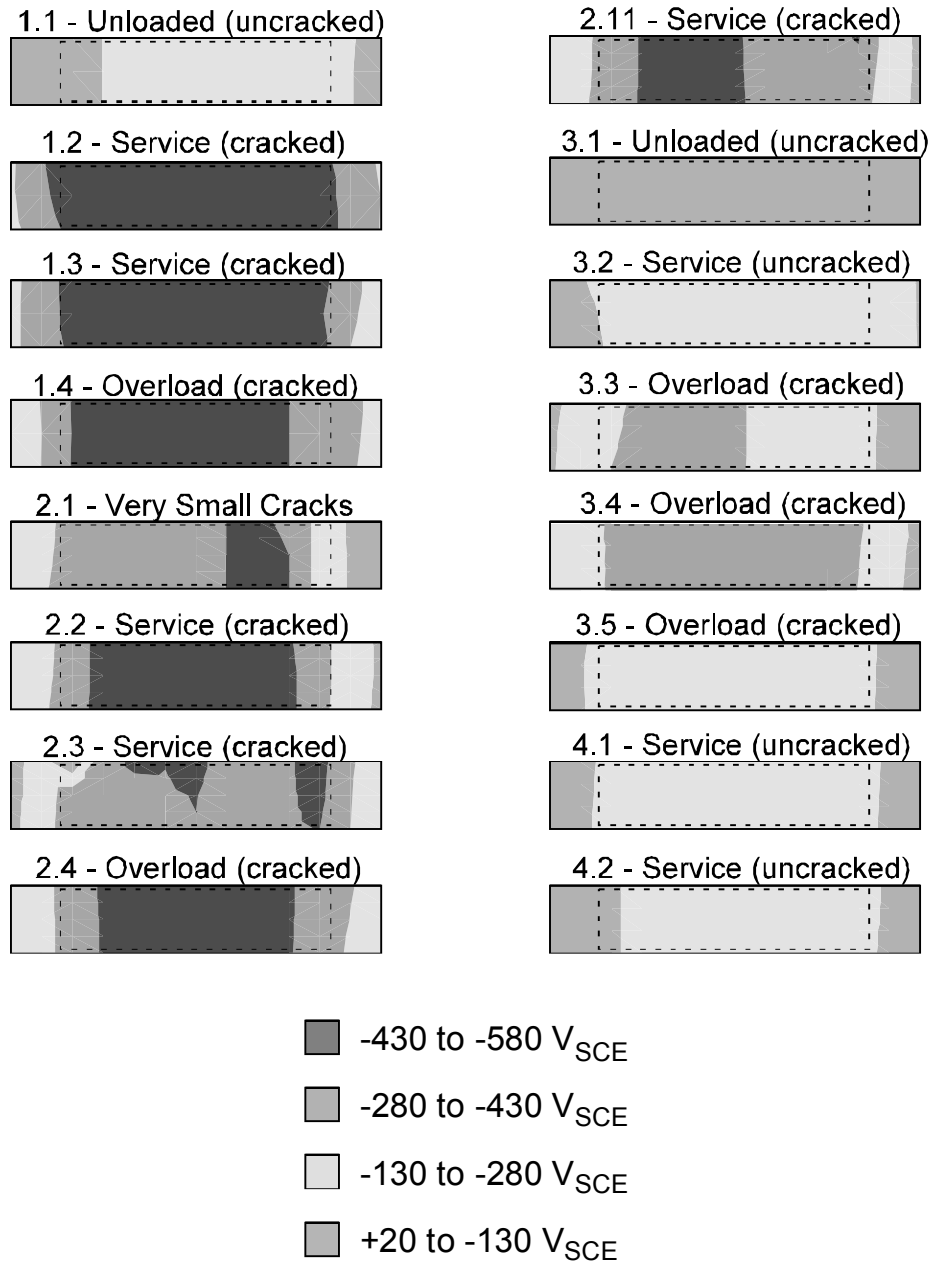


*Figure D.1 Contour Maps of Half-Cell Potential Readings at 498 Days<sup>3</sup>*

**E. HALF-CELL POTENTIALS (OUTLIERS)**

*Table E.1 Half-Cell Outliers – Phase I Beams<sup>6</sup>*

<b>Beam</b>	<b>Day of Reading</b>	<b>Initial Reading</b>	<b>Altered Reading</b>
1.1	736	-269	-415
	1297	-199	-447
	1326	-171	-480
1.2	1297	-255	-550
	1326	-261	-560
	1445	-312	-550
2.2	212	-304	-537
3.1	778	-403	-172
3.2	1297	-205	-351
	1326	-173	-402
4.1	1546	-791	-541

*Table E.2 Half-Cell Outliers – Phase II Beams<sup>6</sup>*

<b>Beam</b>	<b>Day of Reading</b>	<b>Initial Reading</b>	<b>Altered Reading</b>
2.8	938	-402	-828
	966	-389	-858
3.6	454	-262	-370
	1086	-515	-358
3.7	344	-470	-376

**F. CORROSION RATE READINGS**

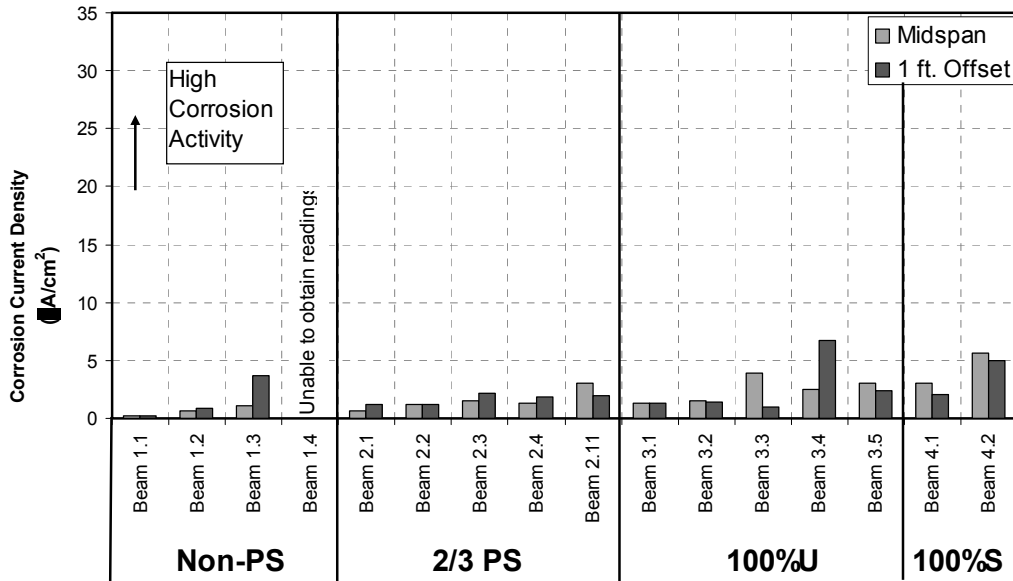


*Figure F.1 Phase I Beams - Measured Corrosion Rates (Seven Month Exposure Duration - PR Monitor Equipment) <sup>6</sup>*

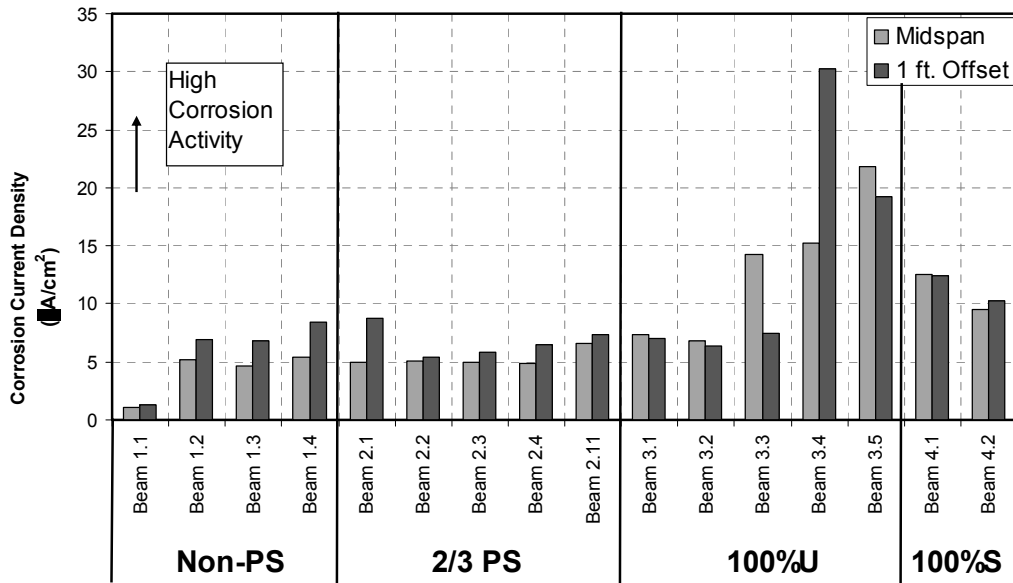


*Figure F.2 Phase I Beams - Measured Corrosion Rates (Twelve Month Exposure Duration - 3LP Equipment) <sup>6</sup>*

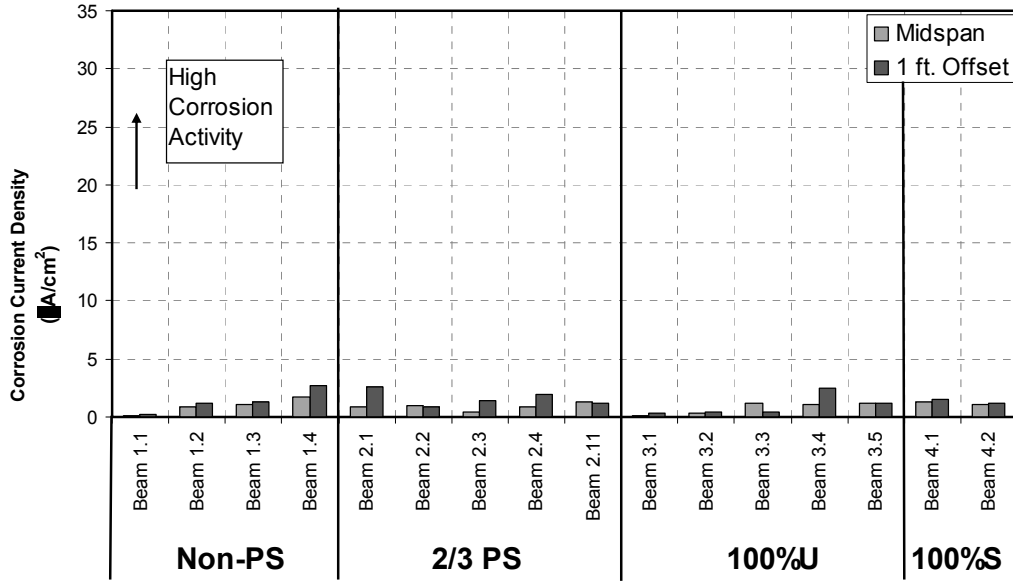


**Figure F.3 Phase I Beams - Measured Corrosion Rates (Fifteen Month Exposure Duration - PR Monitor Equipment) <sup>6</sup>**

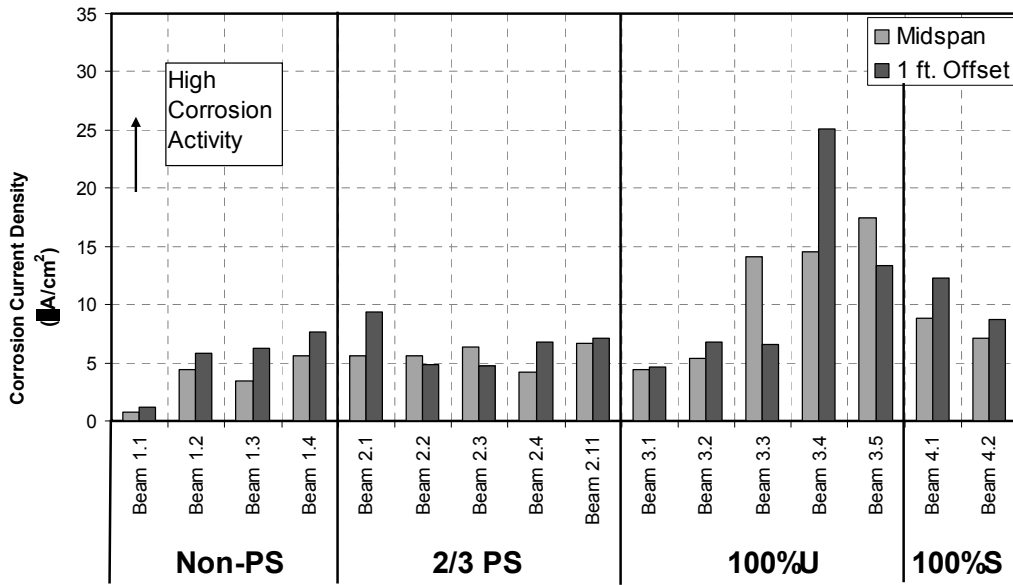


**Figure F.4 Phase I Beams - Measured Corrosion Rates (Fifteen Month Exposure Duration - 3LP Equipment) <sup>6</sup>**

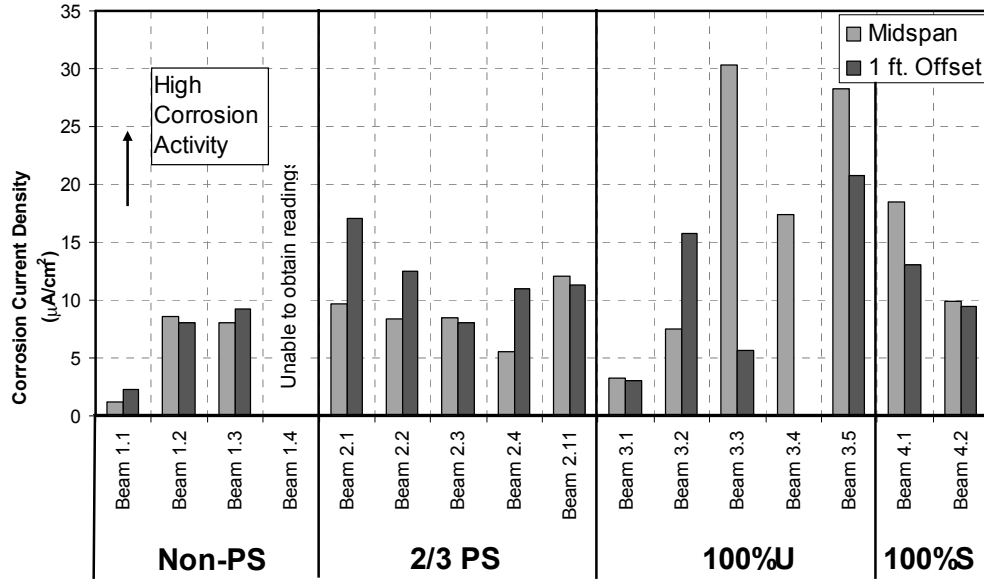


**Figure F.5 Phase I Beams - Measured Corrosion Rates (47 Month Exposure Duration – 3LP Equipment) <sup>6</sup>**

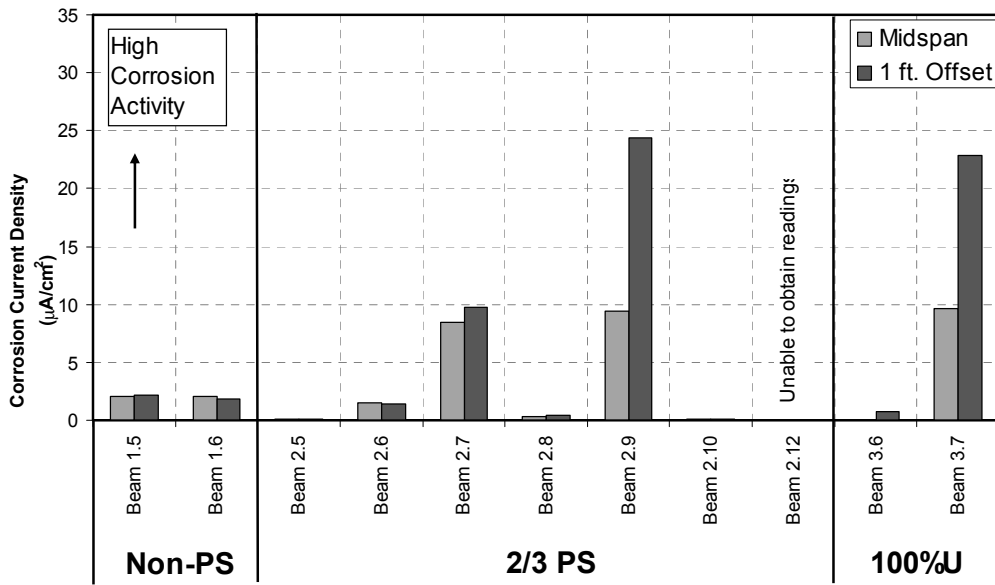


**Figure F.6 Phase II Beams - Measured Corrosion Rates (35 Month Exposure Duration – 3LP Equipment) <sup>6</sup>**

**G. BLOCK CHLORIDE PENETRATION GRAPHS**

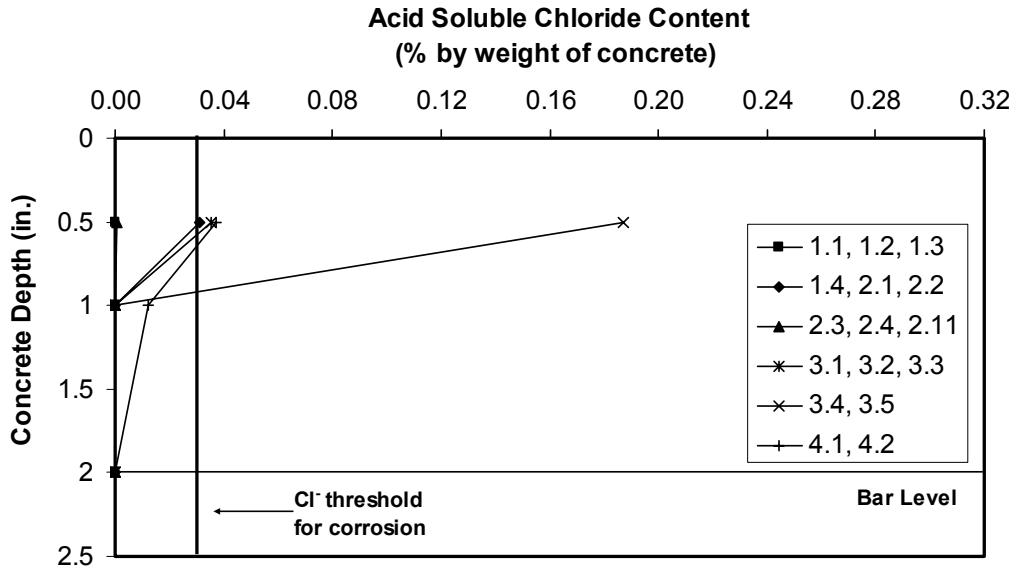


*Figure G.1 Block Chloride Penetration at 7 Months  
(Phase I Poned Block Specimens)<sup>6,7</sup>*

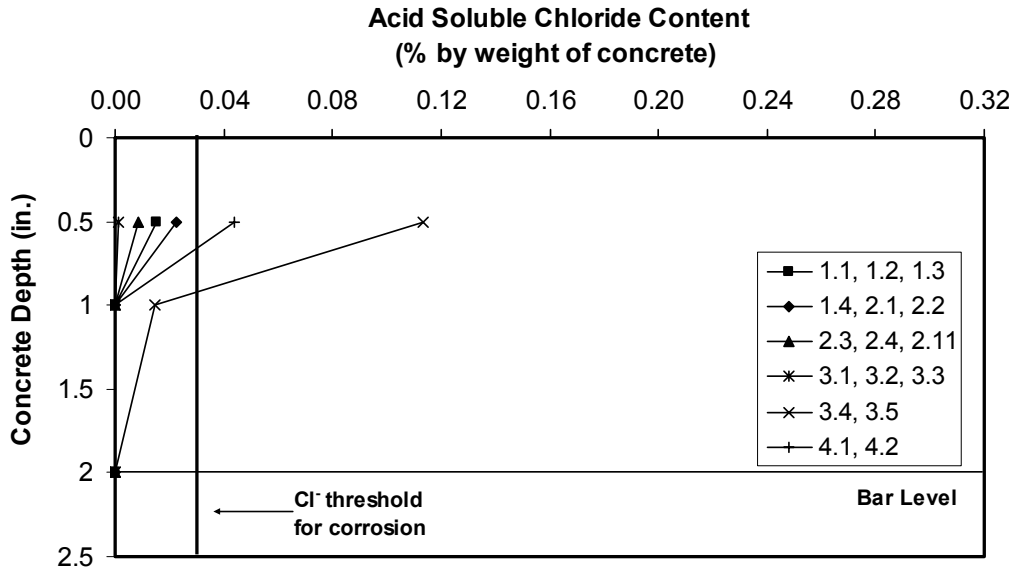


*Figure G.2 Block Chloride Penetration at 14 Months  
(Phase I Poned Block Specimens)<sup>6,7</sup>*



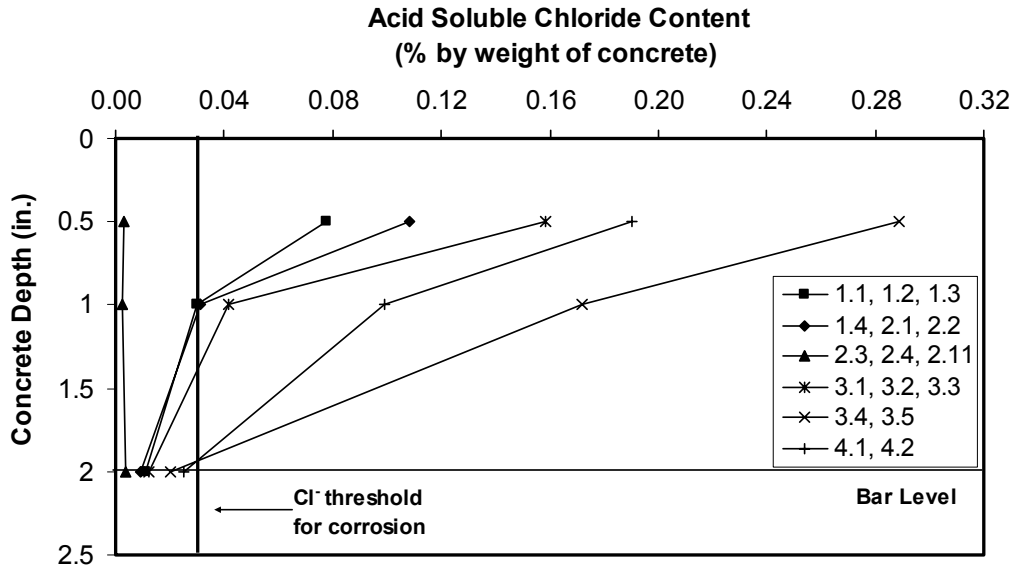


**Figure G.3 Block Chloride Penetration at 41 Months**  
(Phase I Ponded Block Specimens)<sup>6,7</sup>

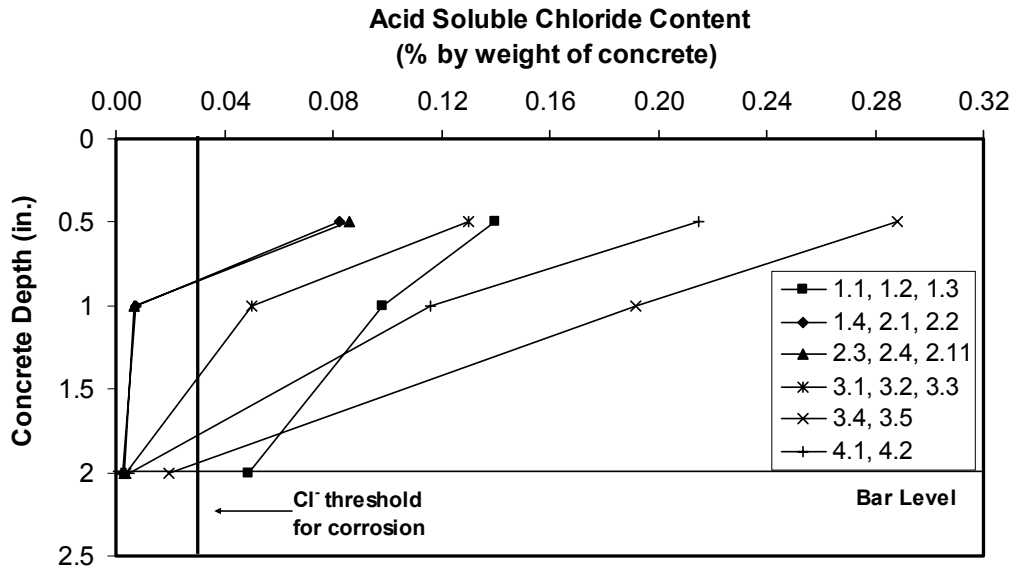


**Figure G.4 Block Chloride Penetration at 54 Months**  
(Phase I Ponded Block Specimens)<sup>6,7</sup>

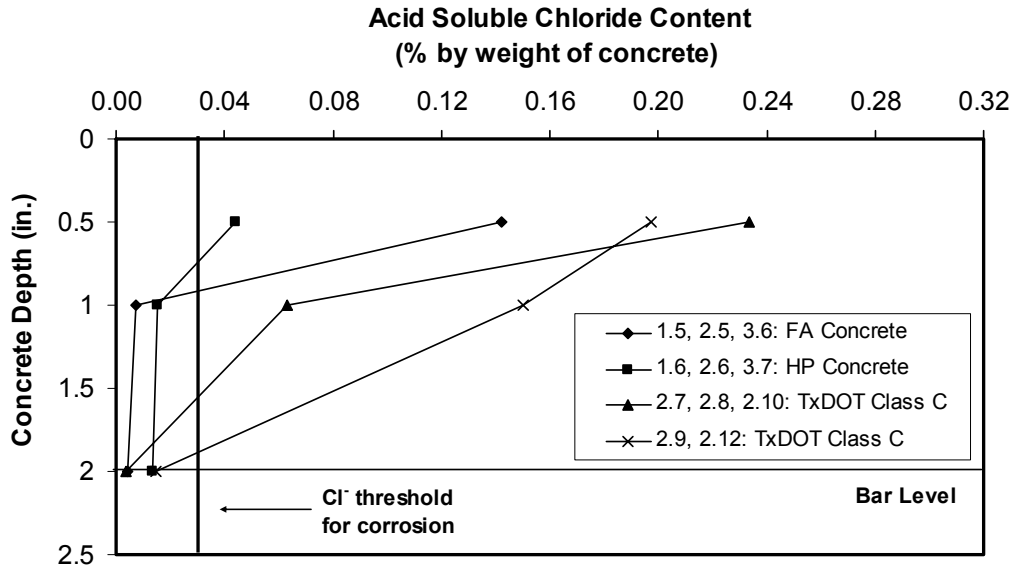


**Figure G.5 Block Chloride Penetration at 29 Months  
(Phase II Ponded Block Specimens)<sup>6,7</sup>**

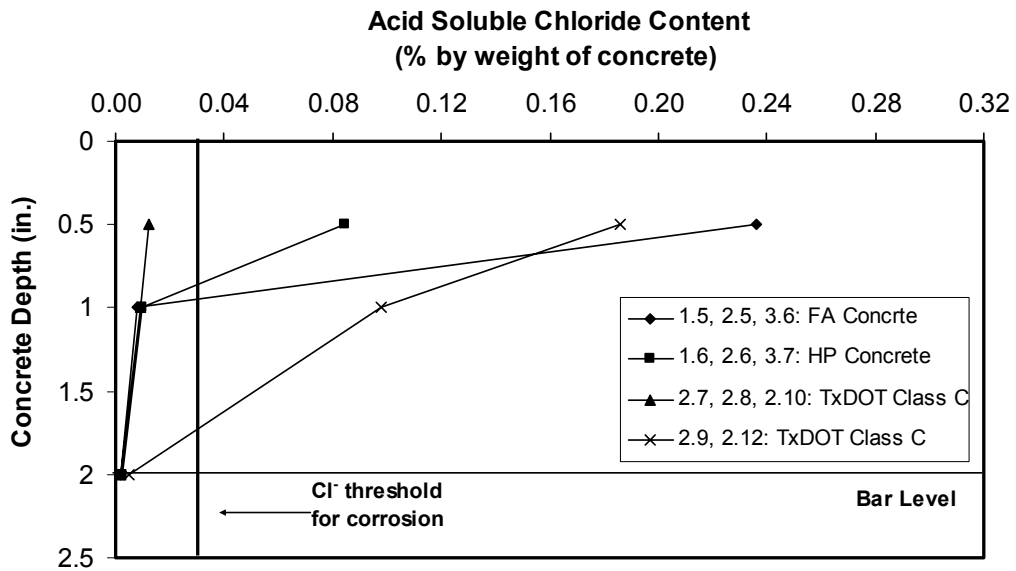


**Figure G.6 Block Chloride Penetration at 42 Months  
(Phase II Ponded Block Specimens)<sup>6,7</sup>**

**H. BEAM CHLORIDE PENETRATION GRAPHS**

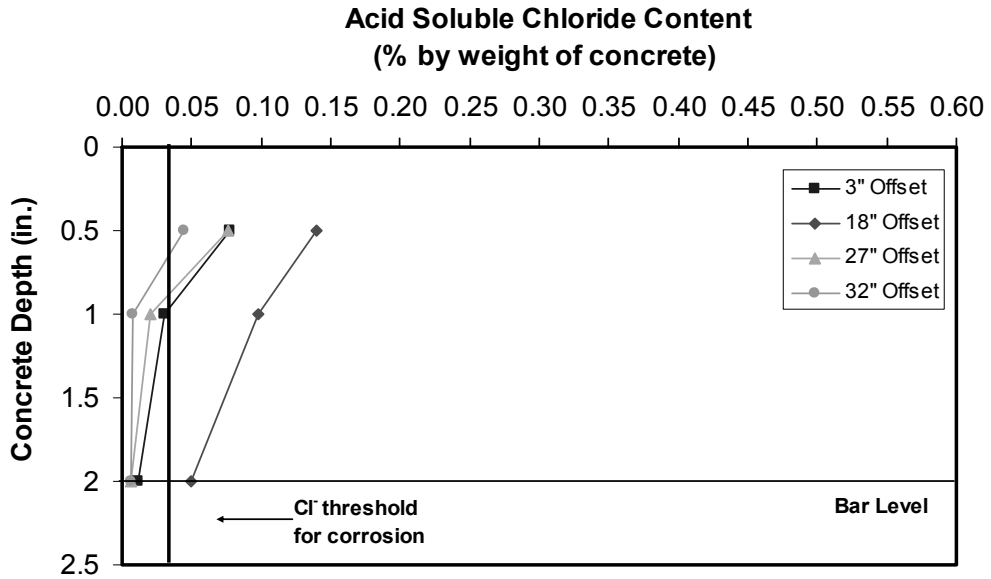


*Figure H.1 Chloride Penetration at 54 Months – Beam 1.1<sup>6,7</sup>*

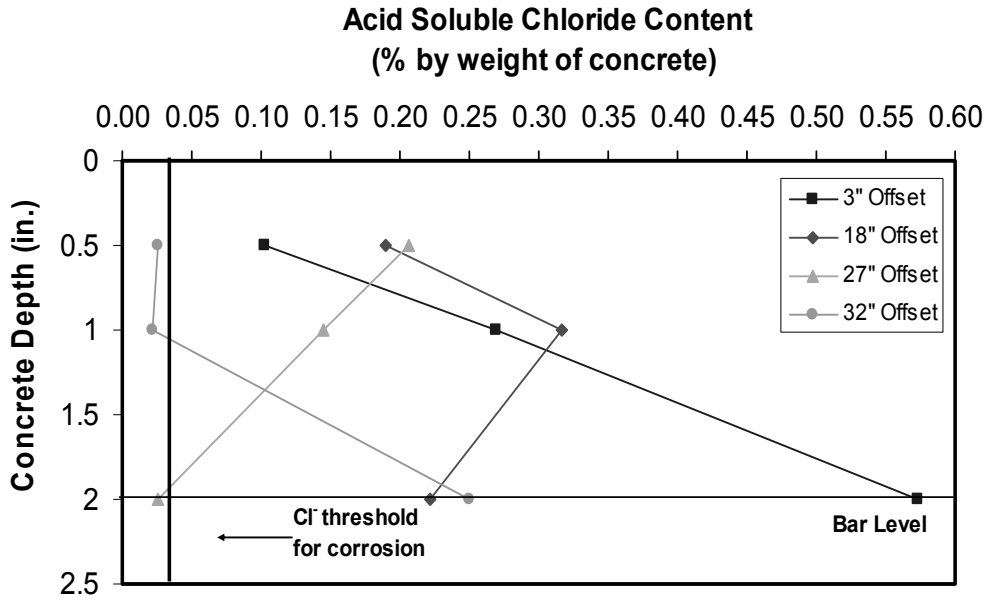


*Figure H.2 Chloride Penetration at 54 Months – Beam 1.3<sup>6,7</sup>*

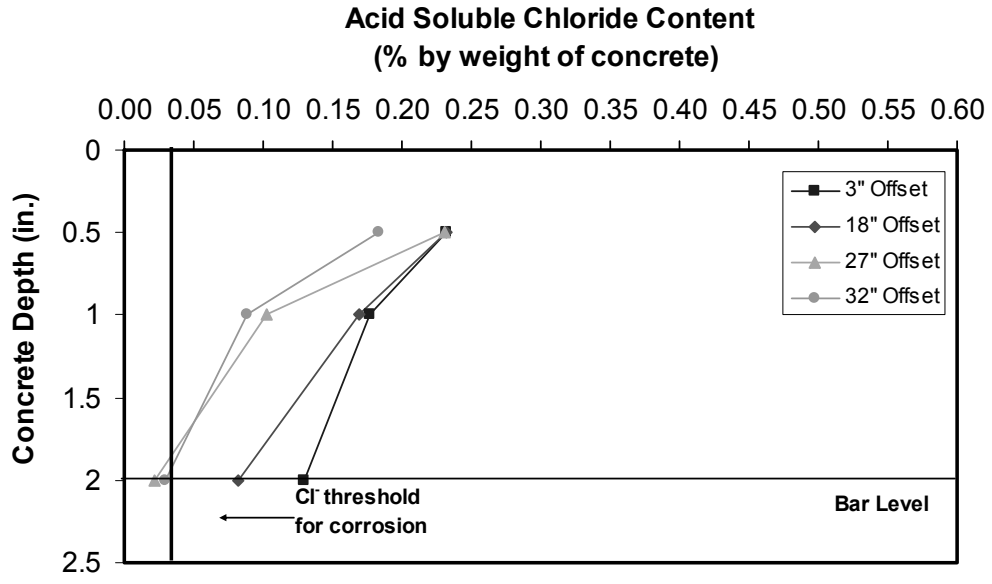


*Figure H.3 Chloride Penetration at 54 Months – Beam 2.3<sup>6,7</sup>*

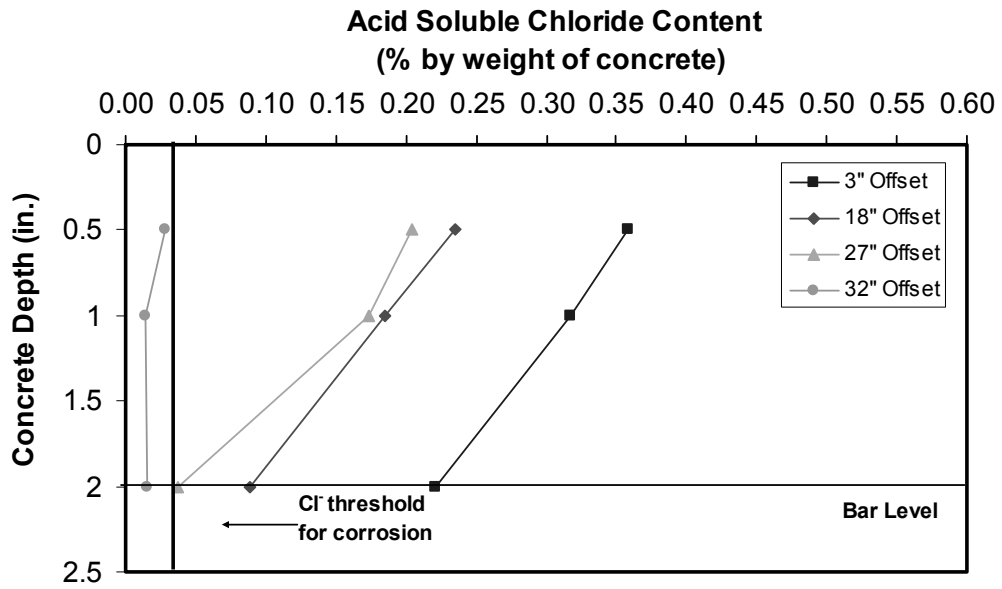


*Figure H.4 Chloride Penetration at 54 Months – Beam 2.11<sup>6,7</sup>*

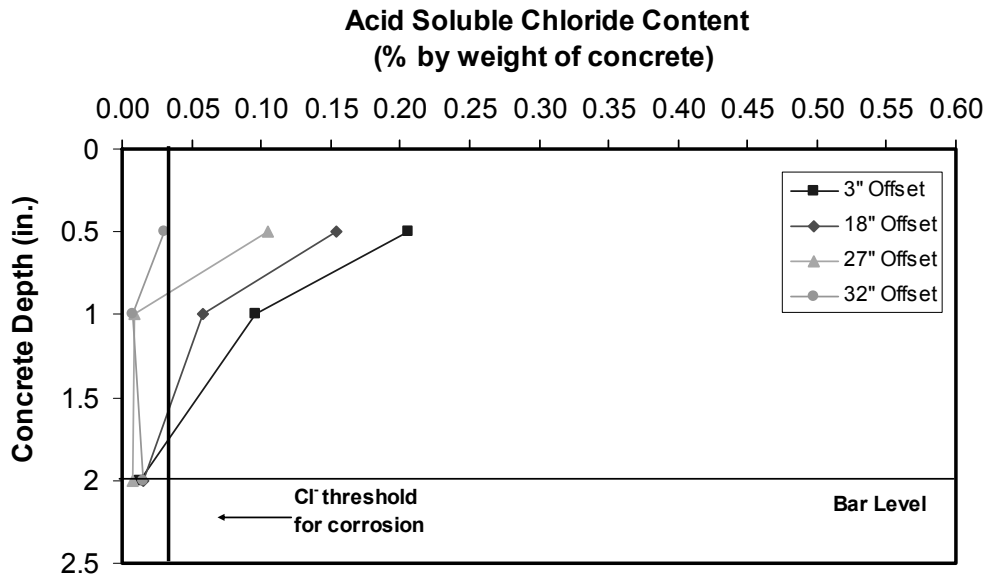


*Figure H.5 Chloride Penetration at 54 Months – Beam 3.1<sup>6,7</sup>*

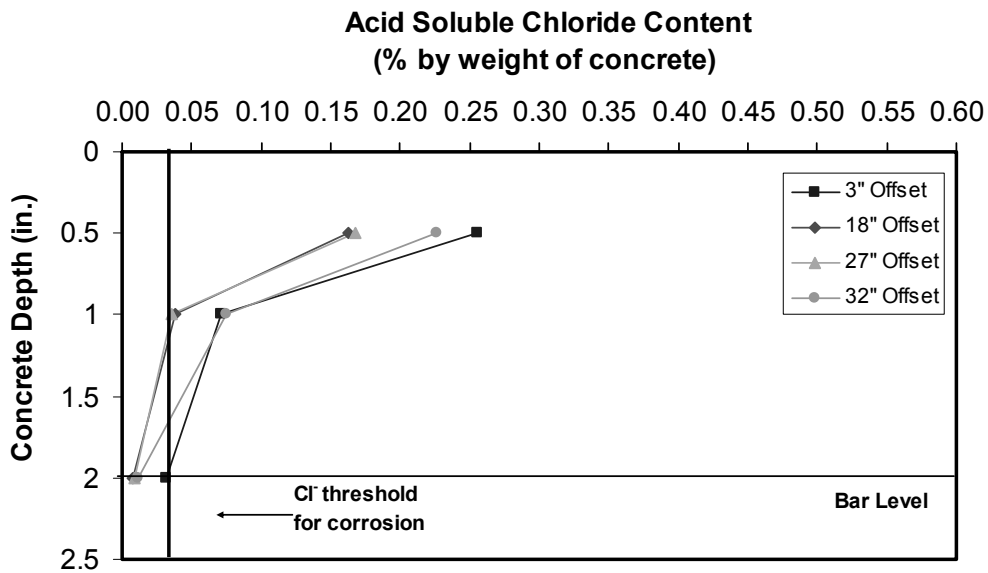


*Figure H.6 Chloride Penetration at 54 Months – Beam 3.2<sup>6,7</sup>*

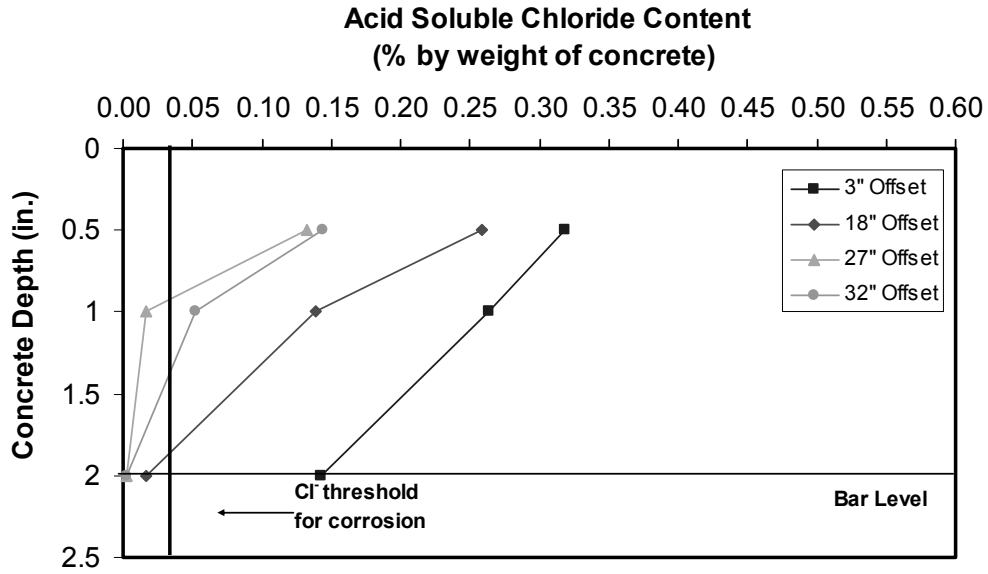


**Figure H.7 Chloride Penetration at 54 Months – Beam 3.3**<sup>6,7</sup>

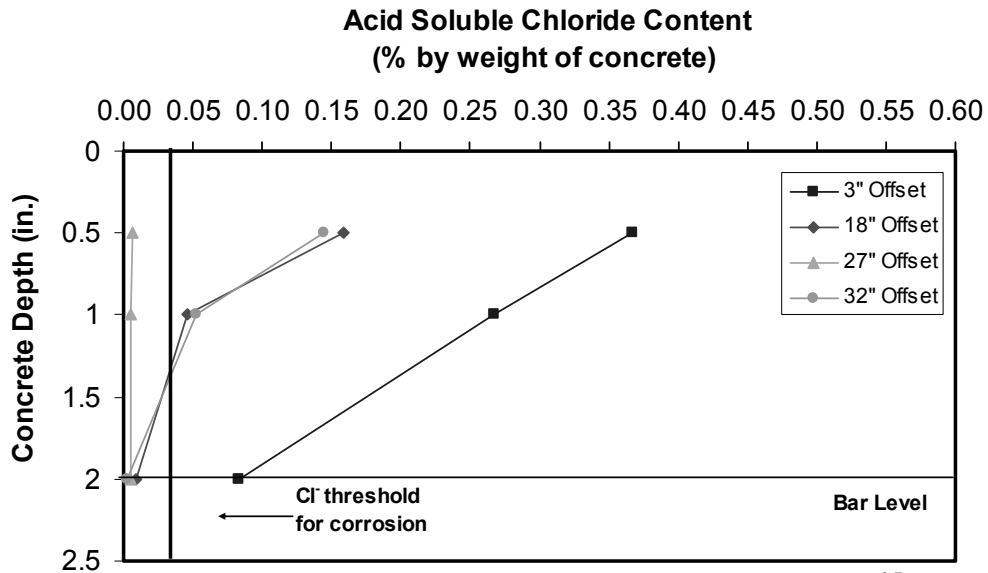


**Figure H.8 Chloride Penetration at 54 Months – Beam 4.2**<sup>6,7</sup>

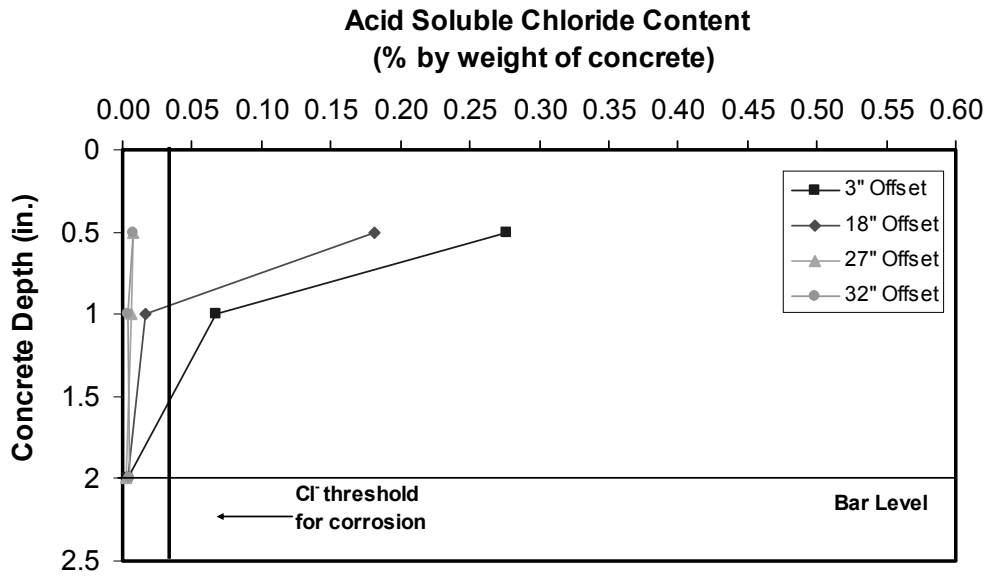


*Figure H.9 Chloride Penetration at 42 Months – Beam 1.5*<sup>6,7</sup>

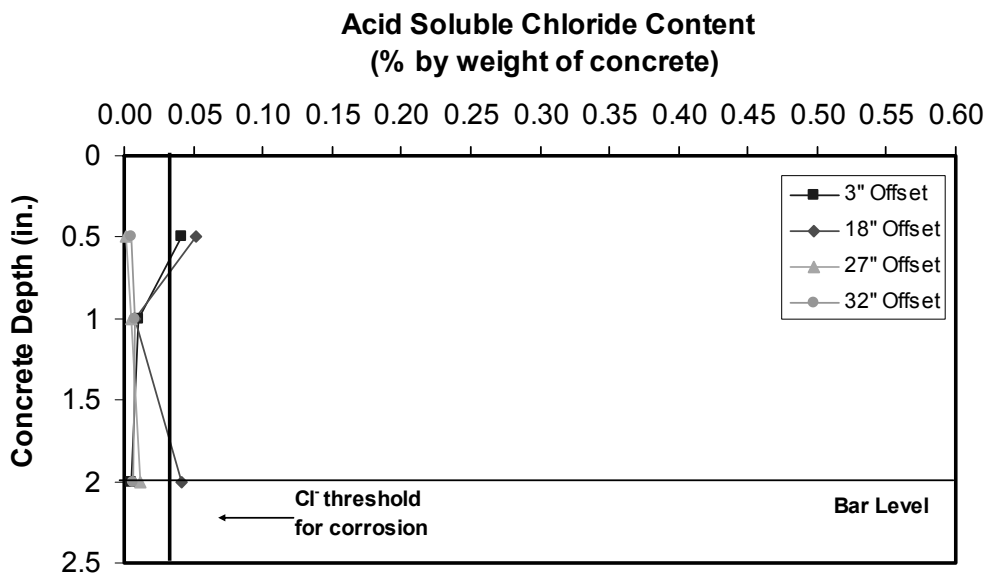


*Figure H.10 Chloride Penetration at 42 Months – Beam 1.6*<sup>6,7</sup>

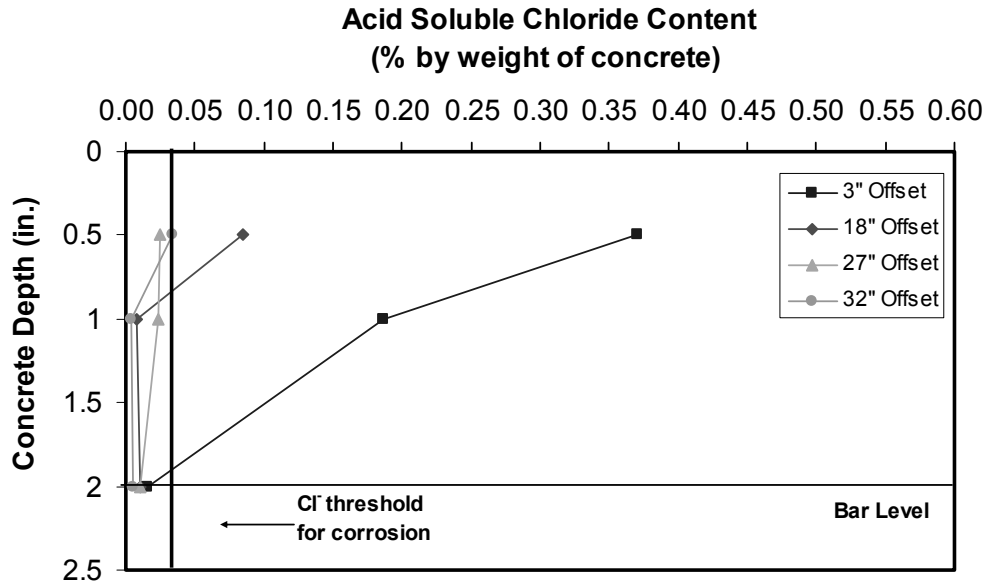


*Figure H.11 Chloride Penetration at 42 Months – Beam 2.5<sup>6,7</sup>*

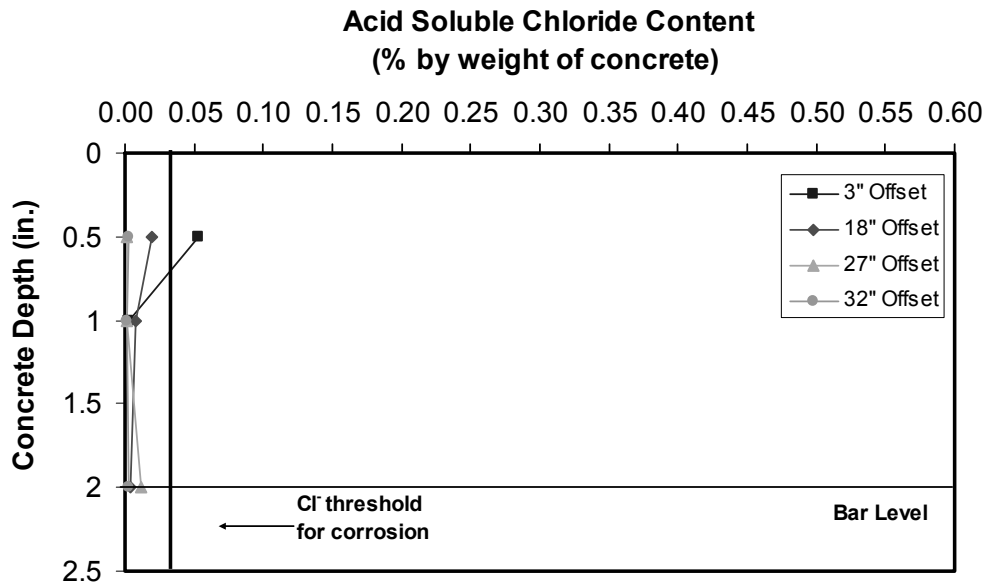


*Figure H.12 Chloride Penetration at 42 Months – Beam 2.6<sup>6,7</sup>*



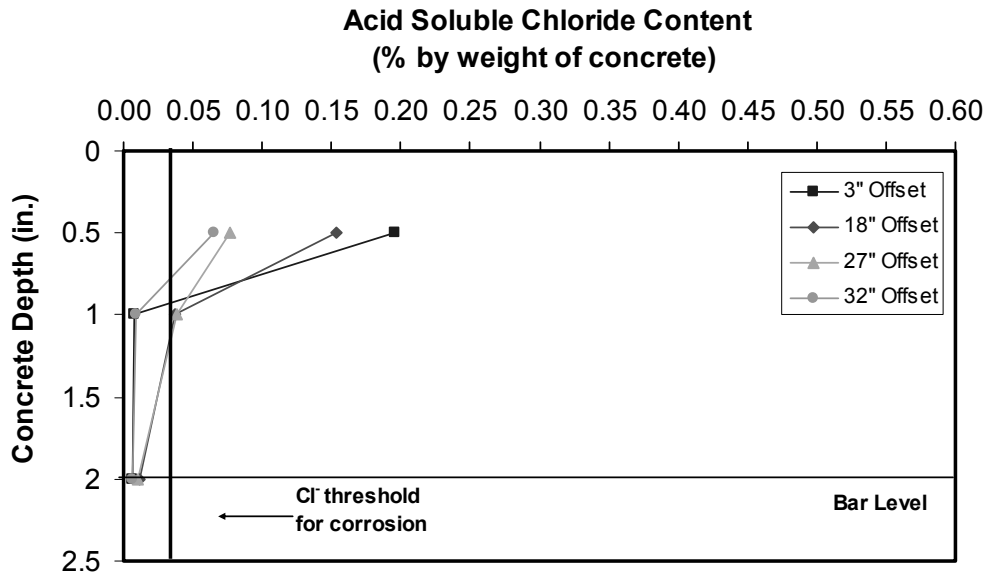


*Figure H.13 Chloride Penetration at 42 Months – Beam 3.6<sup>6,7</sup>*

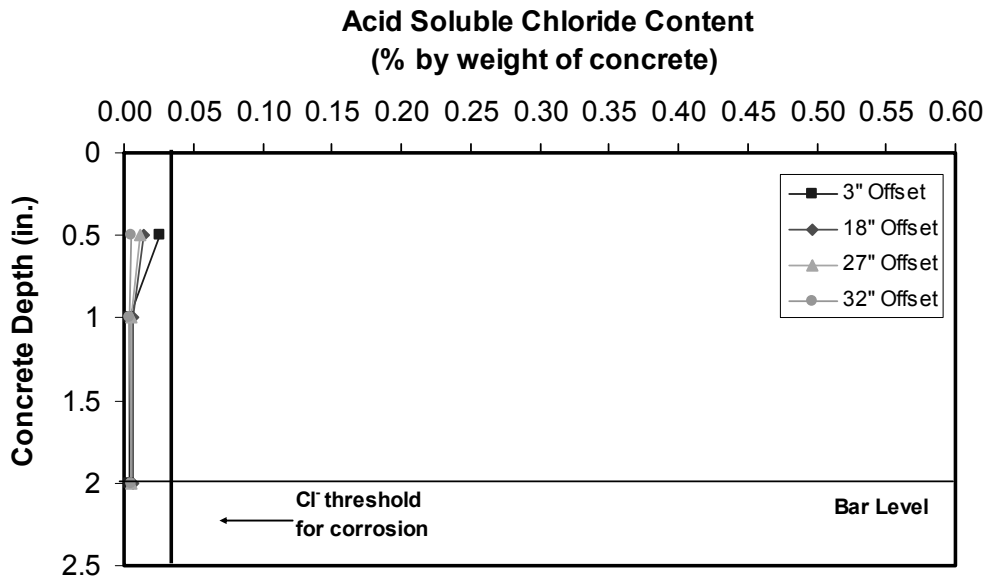


*Figure H.14 Chloride Penetration at 42 Months – Beam 3.7<sup>6,7</sup>*



## References

1. **Armstrong, S. D., Salas, R. M., Wood, B. A., Breen, J. E. and Kreger, M. E., (1997)** *“Behavior and Design of Large Structural Bridge Pier Overhangs,”* Research Report 1364-1, Center of Transportation Research, University of Texas at Austin, 1997.
2. **West, J. S., (1999)** *“Durability Design of Post-Tensioned Bridge Substructures,”* Doctor of Philosophy Dissertation, The University of Texas at Austin, May 1999.
3. **Schokker, A. J., (1999)** *“Improving Corrosion Resistance of Post-Tensioned Substructures Emphasizing High Performance Grouts,”* Doctor of Philosophy Dissertation, The University of Texas at Austin, May 1999.
4. **Koester, B. D. (1995)** *“Evaluation of Cement Grouts for Strand Protection Using Accelerated Corrosion Tests,”* Master of Science Thesis, The University of Texas at Austin, December 1995.
5. **Larosche, C. J. (1999)** *“Test Method for Evaluating Corrosion Mechanisms in Standard Bridge Columns,”* Master of Science Thesis, The University of Texas at Austin, August 1999.
6. **Kotys, A. L. (2003)** *“Durability Examination of Bonded Tendons in Concrete Beams under Aggressive Corrosive Environment.”* Master of Science Thesis, The University of Texas at Austin. May, 2003.
7. **Salas, R. M. (2003)** *“Accelerated Corrosion Testing, Evaluation and Durability Design of Bonded Post-Tensioned Concrete Tendons.”* Doctor of Philosophy Dissertation, The University of Texas at Austin, August 2003.
8. **Vignos, R. P. (1994)** *“Test Method for Evaluating the Corrosion Protection of Internal Tendons Across Segmental Bridge Joints.”* Master of Science Thesis, The University of Texas at Austin, May 1994.
9. **Hamilton, H. R. (1995)** *“Investigation of Corrosion Protection Systems for Bridge Stay Cables,”* Doctor of Philosophy Dissertation, The University of Texas at Austin, 1995.
10. **Schokker, A. J., Koester, B. D, Breen, J. E., and Kreger, M. E. (1999)** *“Development of High Performance Grouts for Bonded Post-Tensioned Structures,”* Research Report 1405-2, Center for Transportation Research, Bureau of Engineering Research, The University of Texas at Austin, December 1999.
11. **Schokker, A. J., West, J. S., Breen, J. E., and Kreger, M. E. (1999),** *“Interim Conclusions, Recommendations, and Design Guidelines for Durability of Post-Tensioned Bridge Substructures,”* Research Report 1405-5, Center for Transportation Research. The University of Texas at Austin, October 1999.
12. **West, J. S., Schokker, A. J., Larosche, C. J., Breen, J. E., Kreger, M. E. (1999),** *“Long-Term Post-Tensioned Beam and Column Exposure Test Specimens:*

- Experimental Program,*” Center for Transportation Research, Report 1405-3. The University of Texas at Austin, October 1999.
13. **AASHTO, (1998)** “*LRFD Bridge Design Specifications,*” 2<sup>nd</sup> Edition, American Association of State Highway and Transportation Officials, Washington, D.C., 1998.
  14. **ACI Committee 318, (1995)** “*Building Code Requirements for Structural Concrete,*” ACI 318-95, American Concrete Institute, Detroit, MI, 1995.
  15. **Breen, J. E., Burdet, O., Roberts, C., Sanders, D. and Wollman, G., (1994)** “*Anchorage Zone Reinforcement for Post-Tensioned Concrete Girders,*” NCHRP Report 356, Transportation Research Board, Washington, D.C., 1994, 204 pp.
  16. **ASTM G109, (1992)** “*Standard Test Method for Determining the Effects of Chemical Admixtures on the Corrosion of Embedded Steel Reinforcement in Concrete Exposed to Chloride Environments,*” ASTM G109-92, American Society for Testing and Materials, Philadelphia, PA., 1992.
  17. **AASHTO T259, (1980)** “*Standard Method of Test for Resistance of Concrete to Chloride Ion Penetration,*” AASHTO Designation T 259-80, American Association of State Highway and Transportation Officials, Washington, D.C., 1980.
  18. **Jones, D.A., (1992)** “*Principles and Prevention of Corrosion,*” Mac Millan Publishing Company, New York, 1992.
  19. **ASTM C876, (1991)** “*Standard Test Method for Half-Cell Potentials of Uncoated Reinforcing Steel in Concrete,*” ASTM C876-91, American Society for Testing and Materials, Philadelphia, PA., 1991.
  20. **Fontana, M.G., (1986)** “*Corrosion Engineering,*” 3<sup>rd</sup> Edition, McGraw-Hill, INC., New York, New York, 1986.
  21. **Jones, D.A., (1996)** “*Principles and Prevention of Corrosion,*” 2<sup>nd</sup> Edition, Prentice Hall, Inc., Upper Saddle River, NJ, 1996.
  22. **Flis, J., Sehal, A., Li, D., Kho, Y., Sabol, S., Pickering, H., Osseo-Asare, K., and Cady, P. D., (1992)** “*Condition Evaluation of Concrete Bridges Relative to Reinforcement Corrosion, Volume 2: Method for Measuring the Corrosion Rate of Reinforcing Steel,*” SHRP-S/FR-92-104, Strategic Highway Research Program, Washington, D.C., 1992.
  23. **Andrade, C., Castelo, V., Alonso, C. and Gonzalez J. A., (1986)** “*The Determination of Corrosion Rate of Steel Embedded in Concrete by the Polarization Resistance and AC Impedance Methods,*” Corrosion Effect of Stray Currents and the Techniques for Evaluation Corrosion of Rebars in Concrete, ASTM STP 906, V. Chaker, Editor, American Society for Testing and Materials, Philadelphia, PA., 1986.
  24. **CONCORR, Inc., (1996)** “*FHWA-SHRP Showcase: Assessment of Physical Condition of Concrete Bridge Components,*” Federal Highway Administration, Washington, D.C., 1996.
  25. **Cady, P., and Gannon, E., (1992)** “*Condition Evaluation of Concrete Bridges Relative to Reinforcement Corrosion, Volume 8: Procedure Manual,*” SHRP-S/FR-92-330, Strategic Highway Research Program, Washington, D.C., 1992.

26. **AASHTO T260, (1994)** “*Standard Method of Test for Sampling and Testing for Chloride Ion in Concrete Ram Materials,*” AASHTO Designation T 260-94, American Association of State Highway and Transportation Officials, Washington, D.C., 1994.
27. **ACI Committee 222, (1996)** “*Corrosion of Metals in Concrete,*” ACI 222 R-96, American Concrete Institute, Detroit, Michigan, 1996.
28. **West, J. S., Vignos, R. P., Breen, J. E., and Kreger, M. E. (1999),** “Corrosion Protection for Bonded Internal Tendons in Precast Segmental Construction,” Research Report 1405-4, Center for Transportation Research, The University of Texas at Austin, Austin, Texas, October, 1999.
29. **Salas, R. M., West, J. S., Kotys, A. L., Breen, J. E., and Kreger, M. E. (2002),** “Final Evaluation of Corrosion Protection for Bonded Internal Tendons in Precast Segmental Construction,” Research Report 1405-6, Center for Transportation Research, The University of Texas at Austin, Austin, Texas, October, 2002.
30. **Poston, R.W., (1984)** “Improving Durability of Bridge Decks by Transverse Prestressing,” Doctor of Philosophy Dissertation, The University of Texas at Austin, 1984.
31. **Sanson, A. S., (1992)** “*Evaluation of Degree of Rusting on Prestressed Concrete Strand,*” PCI Journal, Vol. 37, No. 3, May-June 1992.